

DESIGN OF POLYMERIZABLE LIQUID CRYSTAL MONOMERS FOR
NEW SIDE CHAIN LIQUID CRYSTALLINE POLYMERS (SCLCPs) AND
THEIR PROPERTIES

NOORDINI BINTI MOHAMAD SALLEH

FACULTY OF SCIENCE
UNIVERSITY OF MALAYA
KUALA LUMPUR

2014

**DESIGN OF POLYMERIZABLE LIQUID CRYSTAL
MONOMERS FOR NEW SIDE CHAIN LIQUID CRYSTALLINE
POLYMERS (SCLCPs) AND THEIR PROPERTIES**

NOORDINI BINTI MOHAMAD SALLEH

**THESIS SUBMITTED IN FULFILLMENT OF
THE REQUIREMENTS FOR THE DEGREE OF
DOCTOR OF PHILOSOPHY**

**DEPARTMENT OF CHEMISTRY
FACULTY OF SCIENCE
UNIVERSITY OF MALAYA
KUALA LUMPUR**

2014

UNIVERSITI MALAYA
ORIGINAL LITERARY WORK DECLARATION

Name of Candidate: **NOORDINI BINTI MOHAMAD SALLEH** (I.C. No: 840318035062)

Registration/Matric No: **SHC100013**

Name of Degree: **DOCTOR OF PHILOSOPHY**

Title of Project Paper/Research Report/Dissertation/Thesis ("this Work"):

**DESIGN OF POLYMERIZABLE LIQUID CRYSTAL MONOMERS FOR NEW SIDE CHAIN
LIQUID CRYSTALLINE POLYMERS (SCLCPs) AND THEIR PROPERTIES**

Field of Study: **PHYSICAL CHEMISTRY**

I do solemnly and sincerely declare that:

- (1) I am the sole author/writer of this Work;
- (2) This Work is original;
- (3) Any use of any work in which copyright exists was done by way of fair dealing and for permitted purposes and any excerpt or extract from, or reference to or reproduction of any copyright work has been disclosed expressly and sufficiently and the title of the Work and its authorship have been acknowledged in this Work;
- (4) I do not have any actual knowledge nor do I ought reasonably to know that the making of this work constitutes an infringement of any copyright work;
- (5) I hereby assign all and every rights in the copyright to this Work to the University of Malaya ("UM"), who henceforth shall be owner of the copyright in this Work and that any reproduction or use in any form or by any means whatsoever is prohibited without the written consent of UM having been first had and obtained;
- (6) I am fully aware that if in the course of making this Work I have infringed any copyright whether intentionally or otherwise, I may be subject to legal action or any other action as may be determined by UM.

Candidate's Signature

Date

Subscribed and solemnly declared before,

Witness's Signature

Date

Name:

Designation:

ABSTRAK

Sejenis monomer baru yang mengandungi cincin naftalena dalam mesogen dengan hubungan ester dan pelbagai jenis monomer yang terdiri daripada teras 1,4-benzena dengan asas Schiff dan hubungan ester yang boleh dijadikan polimer telah direka dan dihasilkan. Monomer-monomer yang berasaskan Schiff dan ester telah digunakan untuk mensintesis polimer dengan rantaian sisi cecair kristal (SCLCPs) melalui pempolimeran rantai radikal dan pempolimeran radikal melalui pemindahan atom (ATRP). Struktur kimia kesemua monomer dan polimer telah disahkan oleh spektroskopi ^1H NMR, ^{13}C NMR dan FTIR. Berat molekul dan polidispersiti polimer seperti yang diukur oleh GPC adalah dalam lingkungan 10,200 hingga 123,000 g / mol dan 1.16 hingga 2.79, masing-masing. Analisis GPC polimer menunjukkan kesan kaedah pempolimeran kepada polidispersiti di mana polimer yang dihasilkan oleh ATRP menunjukkan nilai polidispersiti yang kecil berbanding dengan polimer yang dihasilkan oleh pempolimeran rantai radikal.

Hasil daripada POM menunjukkan monomer yang mengandungi cincin naftalena dalam mesogen mempamerkan fasa nematik pada suhu 101.9°C dan fasa smektik pada 83.8°C manakala DSC mencadangkan kehadiran pelbagai meso-fasa yang luas antara 50°C dan 104°C . Analisis SAXS menunjukkan isyarat penyebaran mendadak dalam q kawasan rendah (2.2 nm^{-1}) menunjukkan tekstur fasa smektik. Polimer-polimer mereka juga mempamerkan kedua-dua fasa nematik dan smektik terdapat pada suhu 163°C dan 149°C masing-masing dikesan oleh DSC. Bagi monomer-monomer dengan asas Schiff dan hubungan ester, fasa nematik pada julat suhu 40.0°C hingga 195.7°C telah diperhatikan di bawah POM yang turut disokong oleh keputusan DSC. PXRD analisis juga menunjukkan ciri khas nematic daripada puncak yang luas di rantau $15\text{-}30^\circ$ dengan jarak- d $3\text{-}5 \text{ \AA}$. Polimer-polimer mereka juga mempamerkan meso-fasa nematik pada julat suhu antara 128.5°C dan 232.0°C .

Daripada analisis TGA, kesemua polimer mempunyai kestabilan terma di bawah 389°C yang sangat baik untuk praktikal pemprosesan atau untuk kegunaan dalam peranti. Puncak penyerapan polimer-polimer daripada spektroskopi UV-Vis ini adalah di antara 300-400 nm, manakala puncak pendarfluor adalah di antara 380-560 nm. Penyerapan maksima UV-Vis dan photoluminescence spektrum dipengaruhi oleh kumpulan elektron penderma yang terletak di sebelah rantaian polimer. Kesemua polimer mempunyai ciri-ciri polimer pancaran. Nilai HOMO dan LUMO yang diperolehi daripada polimer adalah sekitar -5.59 dan -2.59 masing-masing, iaitu hampir dengan bahan-bahan yang digunakan dalam lapisan lubang-mengangkut. Nilai jurang jalur bagi polimer-polimer (3.03-3.18 eV) mendedahkan bahawa polimer-polimer yang baru disintesis ini boleh menjadi bahan yang berpotensi dalam aplikasi photovoltaic.

Sifat-sifat reologi polimer menunjukkan bahawa modulus ricih dinamik dalam fasa smektik cenderung ke tahap luar di rantau kekerapan yang rendah. Kelikatan ricih stabil dalam fasa smektik dan nematik dipamerkan oleh kelakuan penipisan ricih terhadap kadar ricih. Sementara itu, tingkah laku Newtonian pada kadar ricih yang rendah, diikuti dengan terikan kelakuan pada kadar ricih yang lebih tinggi diperhatikan dalam fasa isotropik.

ABSTRACT

A new polymerizable monomer containing naphthalene ring in the mesogen with an ester linkage and various types of polymerizable monomers consisting of 1,4-disubstituted phenyl cores with a Schiff base and ester linkages have been designed and synthesized. These new Schiff base and ester based monomers were used to synthesize side chain liquid crystalline polymers (SCLCPs) via radical chain polymerization and atom transfer radical polymerization (ATRP). The chemical structure of monomers and polymers were confirmed by ^1H NMR, ^{13}C NMR and FTIR spectroscopies. The molecular weight and polydispersity of polymers as measured by GPC are in the range of 10,200 to 123,000 g/mol and from 1.16 to 2.79, respectively. The GPC analysis of the polymers also revealed the effects of polymerization method on polydispersity whereby polymers synthesized by ATRP showed narrow polydispersities compared to those synthesized by radical chain polymerization.

Results from POM showed monomer containing naphthalene ring in the mesogen exhibited a nematic phase at 101.9°C and a smectic phase at 83.8°C while DSC suggested presence of a wide mesophase range between 50°C and 104°C. SAXS analysis showed a sharp scattering signal in the low q region (2.2 nm^{-1}) indicating a typical smectic phase texture. Their polymers also exhibited both nematic and smectic phases appearing at 163°C and 149°C respectively as detected by DSC. As for the monomers with a Schiff base and ester linkages, a nematic phase at a temperature range of 40.0°C to 195.7°C was observed under POM which was further supported by DSC results. PXRD analysis also showed a typical nematic characteristic of a broad peak in the region 15-30° with d -spacing of 3-5 Å. Their polymers also exhibited nematic mesophase at a temperature range between 128.5°C and 232.0°C.

From TGA analysis, all the resulting polymers were thermally stable below 389°C which is really excellent for the practical processing or for the possible use in devices.

The absorption peaks from UV-Vis spectroscopy of these polymers varied from 300 to 400 nm, while the fluorescence peaks varied from 380 to 560 nm. The absorption maxima of UV-Vis and photoluminescence spectra were influenced by the electron donating substituent located at the side chain of polymers. All polymers have the characteristic of emissive polymers. The obtained HOMO and LUMO values of polymers are around -5.59 and -2.59 respectively which are close to that of the materials currently use in hole-transporting layers. The band gap values of polymers (3.03-3.18 eV) revealed that the newly synthesized SCLCPs could be potential candidate in photovoltaic applications.

The rheological properties of the polymers showed that the dynamic shear moduli in a smectic phase tended to level off in the low frequency region. The steady shear viscosities of the smectic and nematic phase exhibited a shear thinning behavior over the shear rate tested. Meanwhile, a Newtonian behavior at low shear rate, followed by a strain hardening behavior at higher shear rate was observed in the isotropic phase.

ACKNOWLEDGMENTS

I would like to express my sincere appreciation and gratitude to my supervisors, Dr. Md. Rezaul Karim Sheikh and Prof. Dr. Rosiyah Yahya for their sincere guidance, advice and stimulating suggestions and encourage in all the time of my research and writing of this thesis.

I would also like to convey my appreciation to the technical staff especially to Mr. Zulkifli Abu Hasan for the continuous help in setting up the lab equipment and all the Chemistry Department staff who are directly or indirectly involved in my research work. I want to thank my colleagues and friends, especially Md. Rabiul Karim, Wisam Naji, Azhar Kamil and Ahmad Danial for all their help, support, discussion and valuable suggestions.

I also truly appreciate the help and technical lab support given by my friends, Farhana, Murni, Mazwani, Raden, Idayu, Mas Mira and the rest of the polymer group members for their constructive comments and help.

Many thanks also to University of Malaya for the research grants PS490/2010B and RG151/11AFR and for the SLAB Scheme and Ministry of Higher Education for the financial support.

Finally, I owe special gratitude to my husband, Muhammad Thoriq, my son, Ahmad Hamizan, family and friends which supported me throughout my project. Without their support, I think I might not be able to complete my thesis as well.

TABLE OF CONTENTS

| | |
|----------------------------------------------------------|------|
| ABSTRAK | ii |
| ABSTRACT | iv |
| ACKNOWLEDGMENTS | vi |
| TABLE OF CONTENTS | vii |
| LIST OF FIGURES | x |
| LIST OF TABLES | xv |
| LIST OF SCHEMES | xvi |
| LIST OF ABBREVIATIONS AND SYMBOLS | xvii |
| LIST OF APPENDICES | xx |
| CHAPTER 1 : INTRODUCTION | 1 |
| 1.1. Liquid crystal | 1 |
| 1.2. Historical development of liquid crystals | 2 |
| 1.3. Classification of liquid crystals | 5 |
| 1.4. Calamatic liquid crystals | 6 |
| 1.4.1. Nematic phase | 8 |
| 1.4.2. Smectic phase | 9 |
| 1.5. Liquid Crystalline Polymers (LCPs) | 11 |
| 1.6. Radical polymerization (RP) | 12 |
| 1.6.1. Radical chain polymerization | 13 |
| 1.6.2. Atom transfer radical polymerization (ATRP) | 18 |
| 1.7. Motivation | 21 |
| 1.8. Research objective | 22 |
| 1.9. Thesis outline | 23 |
| CHAPTER 2 : LITERATURE REVIEW | 25 |
| 2.1. Naphthalene based liquid crystal | 25 |
| 2.2. Schiff base ester based liquid crystal | 26 |
| 2.3. Structure-mesomorphic properties relationship | 29 |

| | | |
|-----------------------------------------|--------------------------------------------------------------|----|
| 2.4. | Side Chain Liquid Crystalline Polymers (SCLCPs)..... | 37 |
| 2.5. | Applications of SCLCPs | 42 |
| CHAPTER 3 : EXPERIMENTAL..... | | 49 |
| 3.1. | Materials..... | 49 |
| 3.2. | Synthesis of liquid crystal monomers | 50 |
| 3.2.1. | Synthesis of monomer M1 | 50 |
| 3.2.2. | Synthesis of monomer M2 and M3..... | 53 |
| 3.2.3. | Synthesis of monomer M4 and M5..... | 59 |
| 3.2.4. | Synthesis of monomer M6 and M7 | 62 |
| 3.2.5. | Synthesis of monomer M8 and M9..... | 66 |
| 3.3. | Synthesis of SCLCPs..... | 71 |
| 3.3.1. | Synthesis of polymers HP1M1 to HP3M1 by ATRP..... | 71 |
| 3.3.2. | Synthesis of HP1M2 to HP2M9 by radical polymerization..... | 72 |
| 3.4. | Characterization methods and instrumentation | 74 |
| 3.4.1. | Nuclear Magnetic Resonance Spectroscopy (NMR) | 74 |
| 3.4.2. | Fourier Transform Infrared Spectroscopy (FTIR) | 74 |
| 3.4.3. | Differential Scanning Calorimetry (DSC) | 75 |
| 3.4.4. | Polarized Optical Microscopy (POM) | 75 |
| 3.4.5. | Small Angle X-ray Scattering (SAXS) | 75 |
| 3.4.6. | Powder X-Ray Diffraction (PXRD)..... | 76 |
| 3.4.7. | Gel Permeation Chromatography (GPC) | 76 |
| 3.4.8. | Thermogravimetric Analysis (TGA)..... | 77 |
| 3.4.9. | UV-Visible (UV-Vis) and Photoluminescence Spectrometry | 77 |
| 3.4.10. | Electrochemical measurements | 77 |
| 3.4.11. | Rheological measurements..... | 78 |
| CHAPTER 4 : RESULTS AND DISCUSSION..... | | 79 |
| 4.1. | LC monomers | 79 |
| 4.2. | SCLCPs | 84 |

| | | |
|-------------------------------------------------------------|--------------------------------------------------------------|-----|
| 4.3. | Structural determination | 89 |
| 4.3.1. | ¹ H NMR spectra | 89 |
| 4.3.2. | ¹³ C NMR and DEPT spectra | 94 |
| 4.3.3. | Fourier Transform Infrared spectroscopy (FTIR) | 100 |
| 4.4. | Solubility behavior | 101 |
| 4.5. | Thermal properties and mesomorphic behavior of monomers..... | 102 |
| 4.5.1. | Effect of mesogen structure | 103 |
| 4.5.2. | Effect of lateral substitution on mesogenic unit..... | 111 |
| 4.5.3. | Effect of polymerizable terminal group on the mesophase..... | 116 |
| 4.6. | Thermal properties and mesomorphic behavior of SCLCPs..... | 119 |
| 4.6.1. | Effect of the nature of polymer backbone..... | 120 |
| 4.6.2. | Effect of molecular weight and polydispersity | 122 |
| 4.7. | Thermal degradation properties of SCLCPs | 127 |
| 4.8. | Optical properties of SCLCPs | 130 |
| 4.9. | Electrochemical properties | 135 |
| 4.10. | Rheological properties of SCLCPs | 139 |
| CHAPTER 5 : CONCLUSIONS & SUGGESTIONS FOR FUTURE STUDIES .. | | 151 |
| 5.1. | Conclusions | 151 |
| 5.2. | Suggestions for future studies | 154 |
| REFERENCES..... | | 155 |
| APPENDICES..... | | 172 |

LIST OF FIGURES

| | |
|-------------------------------------------------------------------------------------------------------------------------------------------|----|
| Figure 1.1 : Molecular ordering of crystal, liquid crystal and liquid states. | 1 |
| Figure 1.2 : The classification of liquid crystals. | 6 |
| Figure 1.3 : General structure of typical liquid crystal. | 8 |
| Figure 1.4 : Schematic representation of molecular order in nematic and isotropic phases [18]. | 9 |
| Figure 1.5 : POM images of schlieren texture of nematic mesophase. Adopted from [17]. | 9 |
| Figure 1.6 : Schematic representation of molecular order in Smectic A and Smectic C phases. Adopted from [20]. | 10 |
| Figure 1.7 : POM textures of (a) focal-conic fan texture of SmA mesophase (b) schlieren texture of SmC mesophase. Adopted from [21]. | 11 |
| Figure 1.8 : Schematic representation of (a) MCLCPs (b) SCLCPs. | 12 |
| Figure 2.1 : A series of azomesogens with lateral units [51]. | 25 |
| Figure 2.2 : A series of Schiff's base cinnamates. Adopted from [52]. | 26 |
| Figure 2.3: Naphthyl azomesogens with lateral chloro group. Adopted from [51]. | 26 |
| Figure 2.4: <i>p-n</i> -octadecanoyloxybenzylidene- <i>p</i> -substituted-anilines. Adopted from [60]. | 27 |
| Figure 2.5 : Schiff base ester compounds with halogen end group. Redrawn from [65-67]. | 28 |
| Figure 2.6 : Schiff base ether with dimethyl amino unit. Adopted from [55]. | 29 |
| Figure 2.7 : Schiff base ester compounds with various end group. Adopted from [56]. | 29 |
| Figure 2.8 : Series of synthesized liquid crystals. Adopted from [69]. | 30 |
| Figure 2.9 : Compounds under investigations. Adopted from [70]. | 31 |
| Figure 2.10 : Pyridine-containing liquid crystalline compounds. Adopted from [71]. | 32 |
| Figure 2.11: Studied compound. Adopted from [72]. | 33 |

| | |
|------------------------------------------------------------------------------------------------|----|
| Figure 2.12 : Series A and series B compounds. Adopted from [54]. | 34 |
| Figure 2.13 : Azo benzothiazole compounds. Adopted from [76]. | 35 |
| Figure 2.14 : A series of ferroelectric LCs. Redrawn from [79]. | 35 |
| Figure 2.15 : α -methylstilbene-tolane liquid crystals. Adopted from [80]. | 36 |
| Figure 2.16 : A series of azo-ester with lateral units. Adopted from [81]. | 37 |
| Figure 2.17 : Copolymers under investigation. Adopted from [89]. | 38 |
| Figure 2.18 : Synthesized SCLCPs. Adopted from [90]. | 39 |
| Figure 2.19 : SCLCPs polyacrylate and polymethacrylates. Adopted from [98]. | 40 |
| Figure 2.20: SCLCPs with achiral and chiral units on the side chain. Adopted from [99]. | 40 |
| Figure 2.21 : Monomers and polymers structure. Adopted from [21]. | 41 |
| Figure 2.22 : Homopolymers and diblock-copolymers with QQP units. Adopted from [100]. | 42 |
| Figure 3.1 : ^1H NMR spectra of monomer M1. | 53 |
| Figure 3.2 : ^1H NMR spectra of monomer M2. | 58 |
| Figure 3.3 : ^1H NMR spectra of monomer M3. | 59 |
| Figure 3.4 : ^1H NMR spectra of monomer M4. | 61 |
| Figure 3.5 : ^1H NMR spectra of monomer M5. | 62 |
| Figure 3.6 : ^1H NMR spectra of monomer M6. | 65 |
| Figure 3.7 : ^1H NMR spectra of monomer M7. | 66 |
| Figure 3.8 : ^1H NMR spectra of monomer M8. | 69 |
| Figure 3.9 : ^1H NMR spectra of monomer M9. | 70 |
| Figure 4.1 : Reaction involved in the preparation of monomer M1. | 80 |
| Figure 4.2 : Reaction mechanism of acid-catalyzed esterification reaction. Adopted from [140]. | 81 |
| Figure 4.3 : Reaction involved in the preparation of monomers, M2 to M9. | 82 |

| | |
|----------------------------------------------------------------------------------------------------------------------------------------------------------------------------------------------------------------------------------------------------------------------------------------------------------------------------------|-----|
| Figure 4.4: Reaction mechanism of Schiff base formation. Redrawn from [142]. | 82 |
| Figure 4.5 : Reaction mechanism of Steglich esterification by DCC. Adopted from [143]. | 83 |
| Figure 4.6 : Function of DMAP in the esterification reaction. Adopted from [143]. | 84 |
| Figure 4.7 : GPC chromatograms of polymer HP1M6. | 87 |
| Figure 4.8: ¹ H NMR spectrum of (a) monomer M1 (b) polymer HP1M1. | 90 |
| Figure 4.9 : ¹ H NMR spectrum of (a) monomer M3 (b) polymer HP2M3. | 92 |
| Figure 4.10 : ¹ H NMR spectrum of (a) monomer M8 (b) polymer HP1M8. | 94 |
| Figure 4.11: ¹³ C NMR and DEPT 135° spectra of monomer M1. | 96 |
| Figure 4.12 : ¹³ C NMR spectrum of monomer M3. | 98 |
| Figure 4.13 : ¹³ C NMR spectrum of monomer M8 and the molecular structure. | 100 |
| Figure 4.14 : FTIR spectra of monomer M3 and polymer HP1M3. | 101 |
| Figure 4.15 : DSC thermograms of M1, M4 and M8 monomers. | 104 |
| Figure 4.16 : Molecular structures and molecular lengths of the monomers (a) M1 (b) M4 (c) M8. The molecular lengths of the compounds were estimated from the most extended conformation with optimized energy level by energy-minimized space filling model (MM2 energy parameters derived from ChemBio3D Ultra 10.0 software). | 106 |
| Figure 4.17 : POM textures of monomer M1. (a) 101.9°C (b) 85.1°C (c) 83.8°C (d) Crystalline at room temperature. | 107 |
| Figure 4.18 : POM textures of monomer M4 at (a) 108°C (b) 106°C (c) 104°C (d) 106°C. | 108 |
| Figure 4.19 : POM textures of monomer M8 at (a) 46°C (b) 40°C. | 109 |
| Figure 4.20 : Small angle X-ray scattering of monomer M1. | 110 |
| Figure 4.21 : PXRD patterns for monomers (a) M4 and (b) M8. | 111 |
| Figure 4.22 : DSC thermograms of monomer M3 and monomer M5. | 112 |
| Figure 4.23: Molecular structures of monomers (a) M3 and (b) M5. | 113 |

| | |
|------------------------------------------------------------------------------------------------------------------------------------------------------------------------------------------------------------|-----|
| Figure 4.24: POM textures of monomer M3. (a) 195.7°C (b) 193.9°C (c) 192.5°C (d) 190.9°C (e) 186.6°C (f) 177.8°C (g) 53.1°C (h) crystalline at room temperature..... | 115 |
| Figure 4.25: POM textures of monomer M5. (a) 94.5°C (b) crystalline at room temperature..... | 115 |
| Figure 4.26 : PXR D spectra for monomers (a) M3 and (b) M5..... | 116 |
| Figure 4.27 : DSC thermograms of monomer M2 and monomer M3. | 118 |
| Figure 4.28 : POM textures of monomer M2. (a) 207.9°C (b) 66.5°C (c) 61.8°C (d) crystalline at room temperature..... | 119 |
| Figure 4.29 : DSC thermograms for the polymers, HP1M1, HP2M1 and HP3M1. | 123 |
| Figure 4.30 : POM textures of polymer HP1M1. (a) 165.7°C (b) 162°C (c) 108°C. ... | 124 |
| Figure 4.31 : POM textures of polymers. (a) HP2M2 (b) HP2M1 (c) HP1M2 (d) HP2M8..... | 125 |
| Figure 4.32 : Schematic representation of the polydomain structure produced by spatial distribution of dislocation lines of $S=+1/2$ (open circles) and $S=-1/2$ (filled circles). Adopted from [171]..... | 126 |
| Figure 4.33 : PXR D patterns of representative polymers, HP1M1 and HP2M2. | 127 |
| Figure 4.34 : TG and DTG traces of polymer HP2M3. | 128 |
| Figure 4.35 : UV-Vis absorption spectra of polymers, HP1M2, HP1M5, HP1M6 and HP1M8..... | 132 |
| Figure 4.36 : Photoluminescence spectra of polymers, HP1M2, HP1M5, HP1M6 and HP1M8..... | 134 |
| Figure 4.37 : UV-vis spectrum of polymer HP1M2 in THF solution..... | 136 |
| Figure 4.38 : CV of polymer HP1M2 in chloroform solution. The inset is the CV curve of ferrocene standard, swept in the same conditions as that for polymer HP1M2..... | 137 |
| Figure 4.39 : Strain amplitude sweep of polymer HP2M1 and polymer HP3M1 at 170°C. | 140 |

| | |
|-----------------------------------------------------------------------------------------------------------------------------------|-----|
| Figure 4.40 : Plots of $\log \eta$ vs $\log \gamma$ for polymer HP2M1 and polymer HP3M1 at various temperatures. | 141 |
| Figure 4.41 : Plots of $\log G'$ vs $\log \omega$ and $\log G''$ vs $\log \omega$ for polymer HP2M1 at various temperatures. | 143 |
| Figure 4.42 : Plots of $\log \eta^* $ vs $\log \omega$ for polymer HP2M1 at various temperatures. | 144 |
| Figure 4.43 : Strain amplitude sweep of polymer HP1M5 at 160°C. | 145 |
| Figure 4.44 : Plots of $\log \eta$ vs $\log \gamma$ for polymer HP1M5 at various temperatures. | 146 |
| Figure 4.45 : Plots of $\log G'$, G'' and $ \eta^* $ vs $\log \omega$ for polymer HP1M5 at (a) 110°C (b) 90°C. | 147 |
| Figure 4.46 : Plots of $\log G'$ vs $\log \omega$ and $\log G''$ vs $\log \omega$ for polymer HP1M5 at various temperatures. | 149 |
| Figure 4.47 : Plots of $\log \eta^* $ vs $\log \omega$ for polymer HP1M5 at various temperatures. | 150 |

LIST OF TABLES

| | |
|-------------------------------------------------------------------------------------------------------------|-----|
| Table 1.1 : Thermal initiators..... | 14 |
| Table 3.1: Amounts of reactants used in the radical polymerization experiments | 73 |
| Table 4.1 : Synthesized LC monomers | 79 |
| Table 4.2 : SCLCPs synthesized by ATRP | 85 |
| Table 4.3 : SCLCPs synthesized by radical chain polymerization | 86 |
| Table 4.4 : GPC results of synthesized side chain liquid crystalline polymers | 88 |
| Table 4.5 : Phase behavior and thermal properties of the monomers by Differential Scanning Calorimetry..... | 102 |
| Table 4.6 : Phase behavior and thermal properties of SCLCPs | 120 |
| Table 4.7 : TGA data of polymers | 129 |
| Table 4.8 : Absorption and PL emission spectral data of synthesized polymers in THF solutions | 131 |
| Table 4.9 : Electrochemical data of selected polymers..... | 137 |

LIST OF SCHEMES

| | |
|------------------------------------------------------------------|----|
| Scheme 1.1: Radical attachment on α -carbon | 15 |
| Scheme 1.2 : Radical attachment on β -carbon..... | 15 |
| Scheme 1.3 : Head-to-Tail arrangement of monomer unit | 16 |
| Scheme 1.4 : Random arrangement of monomer unit..... | 17 |
| Scheme 1.5 : Combination termination..... | 17 |
| Scheme 1.6 : Disproportionation termination | 17 |
| Scheme 1.7 : General mechanism of ATRP. Adopted from [37]. | 21 |
| Scheme 3.1 : Synthetic route of monomer M1. | 53 |
| Scheme 3.2 : Synthetic route of compound 3, 4 and 5..... | 55 |
| Scheme 3.3 : Synthetic route of monomer M2 and monomer M3..... | 56 |
| Scheme 3.4 : Synthetic route of monomer M4 and monomer M5..... | 60 |
| Scheme 3.5 : Synthetic route of monomer M6 and monomer M7..... | 63 |
| Scheme 3.6 : Synthetic route of monomer M8 and monomer M9..... | 67 |
| Scheme 3.7: General synthetic route for polymerization..... | 74 |

LIST OF ABBREVIATIONS AND SYMBOLS

| | |
|-----------------------------|-----------------------------------------------------|
| ATR | Attenuated Total Reflectance |
| ATRP | Atom Transfer Radical Polymerization |
| BPO | Benzoyl Peroxide |
| CDCl ₃ | Deuterated chloroform |
| CV | Cyclic Voltammetry |
| DCC | <i>N,N'</i> -dicyclohexylcarbodiimide |
| DCM | Dichloromethane |
| DEPT | Distortionless Enhancement by Polarization Transfer |
| DMAP | <i>p</i> -Dimethylaminopyridine |
| DMF | <i>N,N</i> -dimethylformamide |
| DMSO | Dimethylsulfoxide |
| DMSO- <i>d</i> ₆ | Deuterated dimethylsulfoxide |
| DSC | Differential Scanning Calorimetry |
| EBriB | Ethyl 2-Bromoisobutyrate |
| FTIR | Fourier Transform Infrared Spectroscopy |
| G' | Storage modulus |
| G'' | Loss modulus |

| | |
|-----------|-----------------------------------------------------|
| GPC | Gel Permeation Chromatography |
| HOMO | Highest Occupied Molecular Orbital |
| LC | Liquid crystal |
| LUMO | Lowest Unoccupied Molecular Orbital |
| LVE | Linear viscoelastic |
| M_n | Weight average molecular weight |
| M_w | Weight average molecular weight |
| M_z | Z average molecular weight |
| M_{z+1} | Z+1 average molecular weight |
| NMR | Nuclear Magnetic Resonance Spectroscopy |
| NOE | Nuclear overhauser enhancement |
| PDI | Polydispersity index |
| PMDETA | <i>N,N,N',N',N''</i> -pentamethyldiethylenetriamine |
| POM | Polarized Optical Microscopy |
| ppm | Parts per million |
| PXRD | Powder X-ray Diffraction |
| RP | Radical polymerization |
| SAXS | Small Angle X-ray Scattering |
| SCLCPs | Side chain liquid crystal polymers |

| | |
|-------|------------------------------|
| T_g | Glass transition temperature |
| T_i | Isotropic temperature |
| T_m | Melting temperature |
| TGA | Thermogravimetric analysis |
| THF | Tetrahydrofuran |

LIST OF APPENDICES

| | |
|-----------------------------------------------|-----|
| APPENDIX A : ^1H NMR Figures..... | 172 |
| APPENDIX B : ^{13}C NMR Figures..... | 175 |
| APPENDIX C : DSC Figures | 180 |
| APPENDIX D : GPC Figures | 181 |
| APPENDIX E : TGA Figures | 182 |
| APPENDIX F : Research Output..... | 183 |

CHAPTER 1 : INTRODUCTION

1.1. Liquid crystal

Liquid crystalline materials have received significant attention in the past several decades. The term ‘liquid crystals’ was first used by Lehmann in 1980, to designate a state of matter between those of solid crystalline and those of isotropic liquid phases. Liquid crystals exhibit the intermediate phases where they can diffuse freely like liquids and yet retain some physical properties characteristic of solid crystalline [1]. In the crystal state, there is a long-range order in position and orientation, while in the liquid state there is no long-range ordering in either. Figure 1.1 shows a molecular ordering of the crystal, liquid crystal and liquid states.

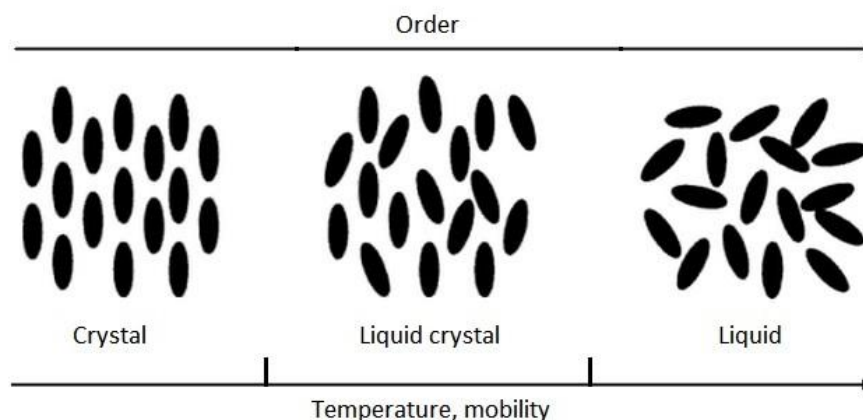


Figure 1.1 : Molecular ordering of crystal, liquid crystal and liquid states.

In the crystal state, molecules are highly ordered and have little translational freedom. They are closely packed, held together by strong cohesive forces and cannot move randomly. Crystalline solids are basically anisotropic. As the temperature of matter increases the thermal movement of molecules becomes so intense that the crystal lattice is dissolved and begins to move more freely in a rotational motion. At this temperature, an anisotropic solid becomes an isotropic liquid. In the liquid state however, the molecules are no longer arranged in a regular order and not as rigidly fixed

PPas in the crystalline state. They have some freedom of motion and no intrinsic order. The molecules diffuse randomly with the molecular axes tumbling wildly and promoting fluidity [2, 3]. On the other hand, the molecules in a liquid crystal state have an arrangement in between that of a solid crystal and a liquid. They can be considered to be crystals which have lost some of their positional orders, while maintaining full orientational order as a liquid. The molecules tend to arrange themselves with a degree of order far exceeding that found in ordinary liquids and approaching that of solid crystals. Typically, liquid crystals are long and thin molecules. Hence, even if the molecular positions are random, their orientation can be aligned in a regular pattern giving rise to the ordered structure of a liquid crystal. They flow like liquids, but they have many optical and material properties such as permittivity, refractive index, elasticity and viscosity, which are anisotropic. Since the order is not as firmly fixed as that in a solid crystal, they can be easily modified with corresponding changes in the optical properties [4]. One can therefore define liquid crystals as a condensed fluid phase with spontaneous anisotropy. Liquid crystals are also called mesophases or mesomorphic phases because of their intermediate nature [5].

1.2. Historical development of liquid crystals

The development of liquid crystals is thought to have been started nearly 150 years ago although its significance was not fully realized until more than a hundred years later. In the period 1834 to 1861, a group of researchers [6] who studied biological samples derived from nerve tissue observed that the nerve fiber formed a fluid substance when left in water and which exhibited a strange behavior under polarized light. Not realizing this was a new phase, they attributed it to the first observation of liquid crystals. Further investigations of this phenomenon were carried out in 1877 by the German physicist Otto Lehmann, who designed and developed polarized

microscopes. He observed that one substance would change from a clear liquid to a cloudy liquid before it crystallized. However, he thought that this was simply an imperfect transition from liquid to crystalline phase. The observation of the colored phenomena occurring in melts of cholesteryl acetate and cholesteryl benzoate by the botanist Reinitzer in 1888 is conventionally regarded as the date of discovery of liquid crystals. He observed the “double melting” behavior of cholesteryl benzoate. This material melted at 145.5°C into a cloudy fluid, which suddenly became clear transparent liquid upon further heating to 178.5°C. This discovery represented the first recorded documentation of the liquid crystal phase. He was also the first to suggest that this cloudy fluid was a new phase of matter. Consequently, he has been given the credit for the discovery of liquid crystals.

Puzzled with his discovery, Reinitzer asked the advice of Otto Lehmann who was an expert in crystal optics. Lehmann concluded that the cloudy liquid had a unique kind of order. On the contrary, the transparent fluid at higher temperatures had the disordered state of all common liquids. Eventually, he named the cloudy liquid “liquid crystal”, sharing the important properties of both. The properties of normal liquid are isotropic but not so in the case of liquid crystal. They are strongly dependent on direction even if the substance itself is fluid. Thus a new type of liquid crystalline states of matter was discovered. The first synthetic liquid crystal, *p*-azoxyanisole was prepared by Gatterman and Ritschke in 1890. Ten years later they studied the liquid crystalline properties of *p*-methoxycinnamic acid and in 1902 the first smectogen, *p*-azoxybenzoate was synthesized by Meyer and Dahlem. In 1992, G. Friedel divided liquid crystals into nematic, smectic and cholesteric types based on the level of order the molecules possessed in the bulk material.

From the beginning of the twentieth century until 1935, Daniel Vorlander had synthesized the most liquid crystals. However, liquid crystals were not popular among

scientists and the material remained a pure scientific curiosity for about 80 years [7]. In the late 1940s, George William Gray began investigating liquid crystal materials in England. His group synthesized many new materials that exhibited the liquid crystalline state and developed a better understanding of how to design molecules that exhibited the state [8]. In 1965, Glenn H. Brown organized the first international conference on liquid crystals, in Kent, Ohio, with the participation of about 100 of the world's top liquid crystal scientists. This conference marked the beginning of a worldwide effort to conduct research in this field, which soon led to the development of practical applications for these unique materials [9]. A microscopic theory of liquid crystals was formulated by Maier and Saupe [10], Frank and later Leslie and Ericksen developed continuum theories for static and dynamic systems of liquid crystal. In 1968, a group of researchers from the Radio Corporation of America (RCA) demonstrated display devices based on liquid crystals. This opened the eyes of the liquid crystal community to the potential of liquid crystals for application in electronic devices [6]. The interest in liquid crystals has grown ever since due to the great variety of phenomena exhibited by liquid crystals and the enormous commercial interest in liquid crystal displays.

In 1970, electro-optical liquid crystal display devices have become well established. Hilsum [11] published an article on the discovery of the cyanobiphenyls which were widely used to produce display devices. The advent of cyanobiphenyls made the materials available for the manufacture of high quality and reliable liquid crystal displays. Later, cyclohexane analogs of the biphenyls [12] and pyrimidine analogs [13] became available hence widening the choice of physical properties to device engineers. These materials still constitute the simple common displays found in calculators or mobile phones. In 1991, when liquid crystal displays were already well established, Pierre-Gilles de Gennes received the Nobel Prize for his findings on the fascinating analogies between liquid crystals and superconductors as well as magnetic materials.

The modern development of liquid crystal science has been greatly influenced by the work of Pierre-Gilles de Gennes [14]. Today, liquid crystals play a dominant role in display technology.

1.3. Classification of liquid crystals

Liquid crystals are divided into two main groups: thermotropic and lyotropic liquid crystals, based on how the liquid crystalline phase has been obtained. Thermotropic liquid crystals exhibit a variety of phases as temperature is changed. The mesophase can be obtained either by heating a solid crystal or by cooling an isotropic liquid. The liquid crystal phases are stable for a certain temperature interval. The terms that are always used in discussing the thermal properties of these types of liquid crystals are melting point, clearing point, enantiotropic and monotropic. Melting point is the transition temperature from the crystal to the mesophase while the transition temperature from the mesophase to the isotropic liquid is called the clearing point. The mesophase which is obtained on both heating and cooling is known as the enantiotropic phase. Meanwhile, the mesophase obtained only during cooling from its isotropic liquid is called the monotropic phase, and is a metastable mesophase since the mesophase transition occurs below melting point [3].

Lyotropic liquid crystals are formed by dissolving certain molecules in solution. The phases of these materials are determined mainly by the composition of the mixture at a certain temperature. The concentration in lyotropic liquid crystals plays the role that temperature does in thermotropic liquid crystals. Lyotropic liquid crystals will not be covered in this thesis. There are two classes of thermotropic liquid crystals based on molecular mass. Low molecular mass thermotropic liquid crystals consist of mesogenic and oligomeric materials. They are divided into three main types by their molecular shape. They are i) calamatic liquid crystals containing rod-like groups, ii) discotic liquid

crystals containing disk-like groups and iii) bent-shaped liquid crystals. Only calamatic liquid crystals will be covered in this thesis. Meanwhile, high molecular mass liquid crystals are known as liquid crystalline polymers. The classification of liquid crystals is shown in Figure 1.2.

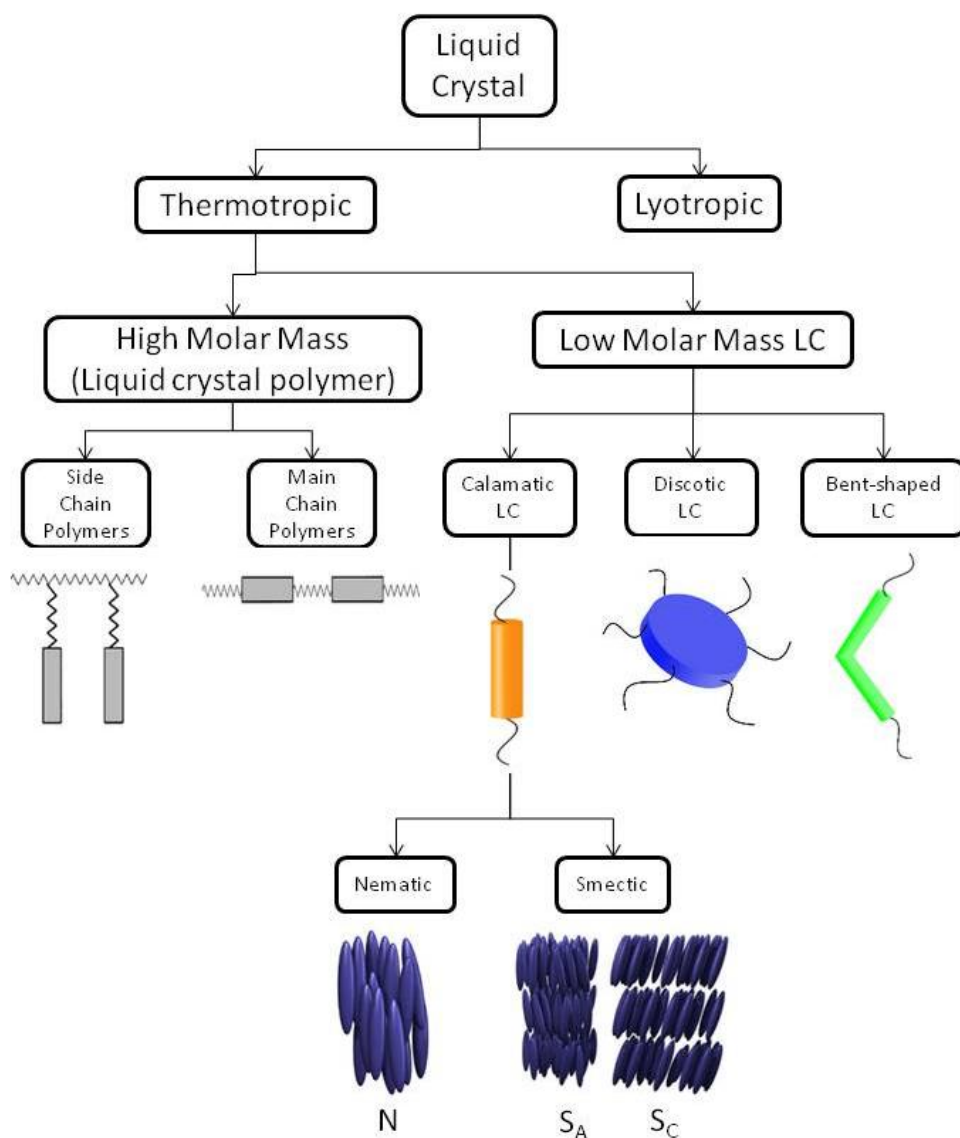


Figure 1.2 : The classification of liquid crystals.

1.4. Calamatic liquid crystals

Rod-like molecules are a common type of molecules that form the thermotropic mesophase. These molecules possess an elongated shape where the molecular length (l) is significantly greater than the molecular breadth (b). These elongated molecules

possess strong attractive forces and have little tendency to collide with each other as they tend to point in the same direction. This helps to stabilize the whole structure of the compound. Figure 1.3 presents the general structure of typical liquid crystals.

Generally, the molecules must have a rigid structure known as a mesogen and flexible chain known as a spacer unit, to exhibit liquid crystal phases. The core units normally consist of benzene, naphthalene, saturated cyclohexane, unsaturated phenyl, biphenyl and terphenyl in various combinations. Heterocyclic compounds such as pyridine, pyrimidine and benzothiazole have also been used as a core unit. These core units are connected to one another by a linking group, Y. Examples of linking groups are stilbene (-CH=CH-), ester (-COO-), Schiff base (-CH=N-), azo (-N=N-), acetylene (-C≡C-), and diacetylene (-C≡C-C≡C-). The rigidity of the mesogen is highly dependent on this group. In addition, the names of liquid crystals are often fashioned after the linking group (e.g. Schiff base liquid crystal). The flexible spacers, R are usually alkyl (C_nH_{2n+1}) and alkoxy (C_nH_{2n+1}O) groups. The flexibility allows one molecule to place itself easily between other molecules when it moves around. Both flexibility and rigidity must be in balance in order to exhibit liquid crystal properties [15].

M and Z are generally small lateral and terminal substituents respectively, consisting of halogens, methoxy, methyl or cyano groups at different positions on the mesogen structure. The incorporation of the substituent on the rigid core will highly affect the mesophase behavior of the liquid crystals. In order to produce polymerizable liquid crystals, a polymerizable group (R') such as acrylate and methacrylate groups is inserted in one of the terminal sides. The presence of this group also has some effect on the thermal transition behavior of these liquid crystals [2] as will be discussed in detail in Chapter 4 (section 4.5.3). Calamatic liquid crystals generally exhibit two types of mesophases: nematic and smectic.

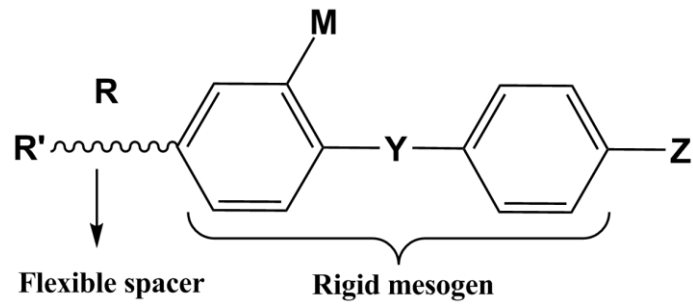


Figure 1.3 : General structure of typical liquid crystal.

1.4.1. Nematic phase

The nematic phase (N) has a high degree of long-range orientational order of molecules, but no long-range translational order. This is the least ordered mesophase which is the closest to the isotropic liquid state. As shown in Figure 1.4, the molecules are spontaneously oriented with their long axes approximately parallel to one another, which is totally different from the case of isotropic liquid. In this case, the long axes of the molecules point on the average in the same direction, which is defined by a unit vector commonly known as ‘the director’ (\mathbf{n}) [16].

The term “nematic” is derived from the Greek word for “thread” which relates to the thread-like texture formed by defects between ordered regions visible under the polarizing optical microscopy (POM). As shown in Figure 1.5, a randomly oriented nematic liquid crystal fluid will make these beautiful patterns when seen under crossed polarizers. Some regions are dark when the molecules are aligned in the direction of the light path while some regions are bright when aligned perpendicular to the light path [17].

Nematic liquid crystals are widely used in LCD devices due to their high fluidity and the substantial effects of their electric and magnetic fields. In addition, they can be easily aligned and reoriented by the application of relatively small electric and magnetic fields [3].

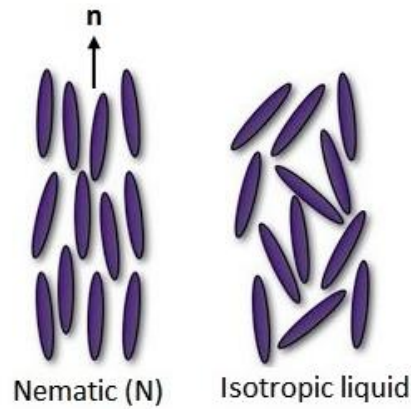


Figure 1.4 : Schematic representation of molecular order in nematic and isotropic phases [18].

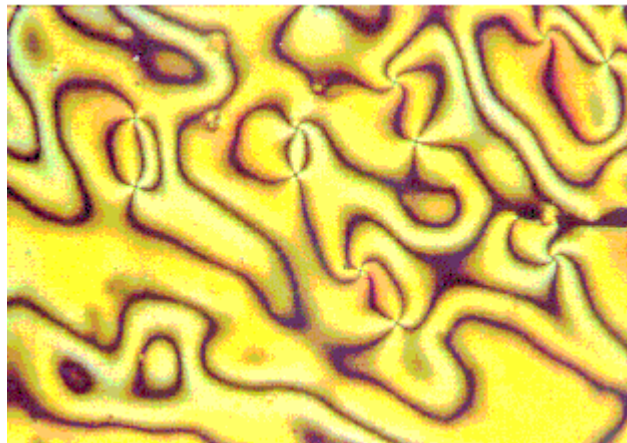


Figure 1.5 : POM images of schlieren texture of nematic mesophase. Adopted from [17].

1.4.2. Smectic phase

Smectic phases are higher order liquid crystal phases which combine orientational order with positional order. Unlike the nematic phase, the density is not uniform as there is some correlation between the molecules' centre of mass. However, the molecules in the layered structure have some degree of freedom to move because the interlayer forces are weak in comparison to the intra-layer forces between the molecules. The word "smectic" originates from the Latin "smecticus", meaning cleaning, or having soap-like properties. Due to the layered structure, smectics phases are usually more viscous than conventional nematics and tend to appear at lower temperatures [19]. There are a number of different smectic phases and these are

characterized by a variety of molecular arrangements within and between the layers. Smectic liquid crystals can be classified depending on whether the director is parallel to or tilted with respect to the layer normal. The total number of smectic mesophases cannot be specified, but the more commonly encountered are smectic A (SmA) and smectic C (SmC).

In the SmA phase, the director, \mathbf{n} , points in the same direction as the layer normal, \mathbf{z} (Figure 1.6). This mesophase has fluid properties but it is more viscous than the nematic mesophase. This type of properties is due to the strong lateral forces and weak interlayer attractions between the molecules which allow the layers to slide over one another easily [16]. The SmC phase has the same layer structure as the SmA, but the director, \mathbf{n} , is at a constant tilt angle measured normally to the layer normal, \mathbf{z} (Figure 1.6). Both SmA and SmC phases have unstructured layers and they possess one-dimensional (1D) layer periodicity [3]. SmA appears as focal-conic fan texture whereas SmC is observed as schlieren texture under POM as shown in Figure 1.7.

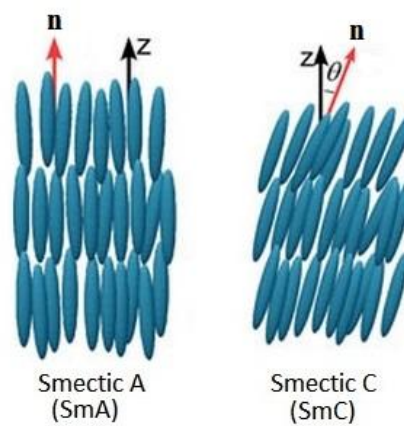


Figure 1.6 : Schematic representation of molecular order in Smectic A and Smectic C phases. Adopted from [20].

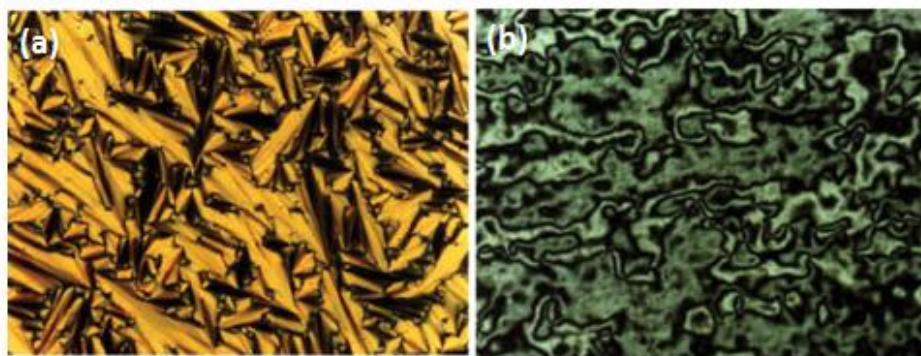


Figure 1.7 : POM textures of (a) focal-conic fan texture of SmA mesophase (b) schlieren texture of SmC mesophase. Adopted from [21].

1.5. Liquid Crystalline Polymers (LCPs)

Liquid crystalline polymers (LCPs) are a kind of polymer that shows liquid crystal phases. They are composed of low molecular mass liquid crystals, which can be either rod-like, or disc-like, or rod- and disc-like together in one. LCPs can be divided into two classes of compounds, main chain liquid crystalline polymers (MCLCPs) and side-chain liquid crystalline polymers (SCLCPs) depending on the way the mesogenic units are incorporated into the polymers. In MCLCPs, the mesogenic units are connected in the backbone whereas in SCLCPs, the mesogenic units are attached laterally to the backbone as illustrated in Figure 1.8. Both of them can form thermotropic or lyotropic mesophases. In this thesis, only thermotropic SCLCPs will be discussed. Almost all the polymers exhibited thermotropic liquid crystalline properties as the liquid crystalline state are induced thermally. The liquid crystalline state can be achieved by raising the temperature of a solid and/or lowering the temperature of a liquid.

SCLCPs generally consist of three structural components: polymer backbone, mesogenic groups and flexible spacer. The flexible spacer plays a critical role in determining the properties of the polymer by decoupling the opposing tendency of the liquid crystal groups to self-assemble from the polymer backbones to adopt random coil conformations [22]. The nature of their mesophase depends rather

sensitively on these components. The nematic, smectic and cholesteric types of mesophases are observed with rod-like repeating units [16].

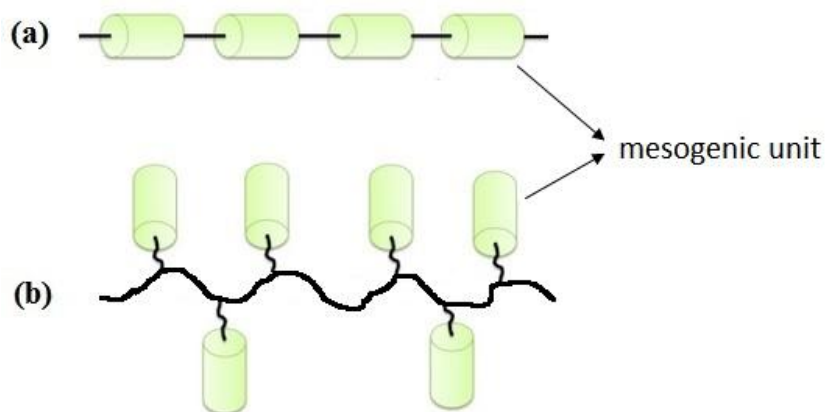


Figure 1.8 : Schematic representation of (a) MCLCPs (b) SCLCPs.

1.6. Radical polymerization (RP)

Radical polymerization is the major polymerization method used for preparing high molecular weight polymers in both industrial and academic laboratories. Conventional RP has been used for the production of ~50% of all commercial polymers such as low density polyethylene, polystyrene, polyacrylates, polyacrylamides and fluorinated polymers. However, copolymers and polymers with controlled architecture cannot be produced by conventional RP due to the very short lifetime of the growing chains (~1 s). The active species in RP are free radicals and typically sp^2 hybridized intermediates and therefore showed poor stereoselectivity. On the other hand, polymers synthesized by RP have shown good regio- and chemoselectivity due to the high degree of head-to-tail structures in the chain and the formation of high molecular weight polymers [23].

In 1956, Micheal Szwarc discovered living polymerization which opened an avenue to the production of well-defined polymers with precisely designed molecular architectures and nano-structured morphologies. Some examples of living polymerizations are anionic, cationic, ring-opening metathesis polymerization and free

radical polymerization. In 1996, Matyjaszewski [24] used the term controlled/living radical polymerization (CRP) for free radical polymerization. CRP methods, including nitroxide-mediated stable free radical polymerization (NMP), radical addition fragmentation chain transfer polymerization (RAFT), and atom transfer radical polymerization (ATRP) are based on establishing a rapid dynamic equilibrium between a minute amount of growing free radicals and a large concentration of the dormant species.

CRP and RP proceed via the same radical mechanism and exhibit similar chemo-, regio- and stereo-selectivities. They can also be used to polymerize a similar range of monomers. In this thesis, the discussion will focus on radical chain polymerization and atom transfer radical polymerization (ATRP) reactions only.

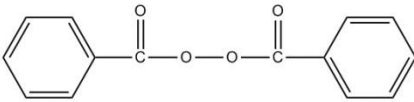
1.6.1. Radical chain polymerization

Radical chain polymerization is commonly used to polymerize acrylate, methacrylate and chloroacrylate monomers. It involves three fundamental steps: initiation, propagation and termination. The details of these three individual events are highly dependent on the exact mechanism of polymerization. The active intermediates that are produced may be categorized as being radicals, anions, cations, or coordinated species. In this thesis, the discussion will be narrowed down to the aspects of free radical chain polymerization reactions only. The common feature of the many monomers that can be transformed into long chain macromolecules is the conversion of unsaturated carbon-carbon bond into a saturated moiety. However, it should be noted that these reactions are not limited to simply carbon-carbon bond polymerization but includes, in principle and in fact, many other reactions as well [25].

The most widely used mode of generating radicals to initiate free radical polymerization is the thermal, homolytic dissociation of initiators. Several of these

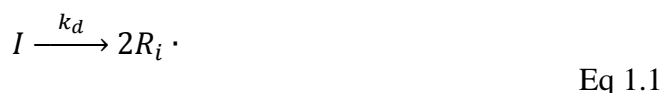
common initiators and some suitable temperature ranges where they could be used are listed in Table 1.1 [25, 26].

Table 1.1 : Thermal initiators

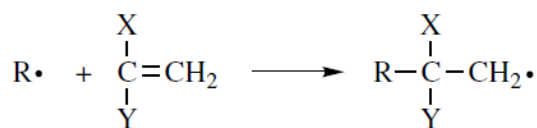
| Name | Structure | Polymerization Temperature Range / °C |
|------------------------------------|---------------------------------------------------------------------------------------------------------------|---------------------------------------|
| hydrogen peroxide | $\text{H}-\text{O}-\text{O}-\text{H}$ | 30-80 |
| potassium persulfate | $\text{KO}-\text{S}(\text{O})_2-\text{O}-\text{O}-\text{S}(\text{O})_2-\text{OK}$ | 30-80 |
| benzoyl peroxide |  | 40-100 |
| <i>t</i> -butyl hydroperoxide | $\text{CH}_3-\text{C}(\text{CH}_3)_2-\text{O}-\text{O}-\text{H}$ | 50-120 |
| <i>t</i> -butyl peroxide | $\text{CH}_3-\text{C}(\text{CH}_3)_2-\text{O}-\text{O}-\text{C}(\text{CH}_3)_2-\text{CH}_3$ | 80-150 |
| 2,2'-azobisisobutyronitrile (AIBN) | $\text{CH}_3-\text{C}(\text{CH}_3)(\text{CN})-\text{N}=\text{N}-\text{C}(\text{CH}_3)(\text{CN})-\text{CH}_3$ | 50-70 |

The first five initiators in the list of Table 1.1 are peroxy compounds, and their most notable feature is the relatively weak oxygen-oxygen bond, which is susceptible to homolytic cleavage. On the other hand, 2,2'-azobisisobutyronitrile (AIBN) dissociates, not due to the presence of a weak bond, but rather because the driving force for homolysis is the formation of the highly stable nitrogen molecule and the resonance-stabilized cyano propyl radical. The initiator used throughout this work is a peroxide type initiator, specifically benzoyl peroxide. This is chosen due to it being readily available, its suitable polymerization temperature range as well as its solubility in the organic solvents.

The initiation step consists of the homolytic dissociation of an initiator species I to yield a pair of radicals $R_i \cdot$ where k_d is the rate constant for the catalyst dissociation. This step is followed by the addition of this radical to the first monomer molecule to produce the chain initiating radical $R_iM \cdot$ where k_i is the rate constant for the initiation step. The general form of the initiation step in the reaction is given by Eq 1.1 and Eq 1.2:

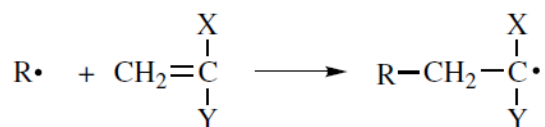


Scheme 1.1 and Scheme 1.2 are the possible modes of propagation for the polymerization of the acrylic and/or methacrylic monomers in this work:



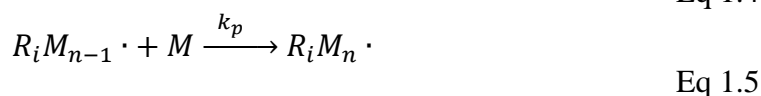
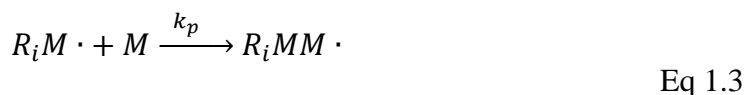
Scheme 1.1: Radical attachment on α -carbon

and/or

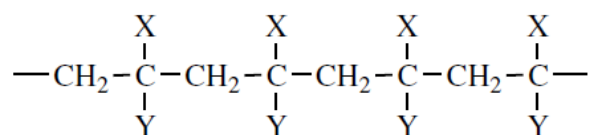


Scheme 1.2 : Radical attachment on β -carbon

The propagation step proceeds by the addition of a free monomer unit M to the radical $R_iM \cdot$ to produce a longer radical chain with two monomer units, and so on, where k_p is the rate constant for propagation. Propagation with growth of the chain to high polymer proportions takes place very rapidly. The general form of the propagation step in the reaction is given by Eq 1.3 through Eq 1.5:



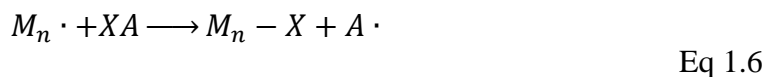
If each successive addition of monomer molecules to the propagating radical occurs in the same manner as in Scheme 1.1 or Scheme 1.2, the polymer chain will have an arrangement of monomer units in which the substituents are on alternate carbon atoms as implied by Scheme 1.3. This type of addition is also known as the Head-to-Tail or 1,3-*placement* configuration of monomer units which are overwhelmingly predominant due to steric effects. It should also be noted that the propagating radical of Scheme 1.2 and Scheme 1.3 is favored due to the resonance stabilization effects of the pendant groups on the α -carbon.



Scheme 1.3 : Head-to-Tail arrangement of monomer unit

However, a Head-to-Head and Tail-to-Tail configuration can occur along the polymer chain as shown in Scheme 1.4. This type of addition is usually referred to as the 1,2-*placement* configuration of monomer units. Due to the steric hindrance of the Head-to-Head and Tail-to-Tail configuration, this occurrence is usually much less than 10% [25, 26].

Additionally, a chain transfer reaction may be involved alongside the three main steps of the polymerization mentioned thus far. This occurs when a radical species reacts with a non-radical species. The general form is given in Eq 1.6:



where XA may be a monomer, initiator, solvent, modifier or other substance (even the polymer chain itself, either intermolecularly or intramolecularly) and X is the atom or species transferred. The effect of this side reaction is the premature termination of a growing polymer by the transfer of hydrogen or other atom or species to it from some XA compound present in the system. The polymerization can proceed basically as before, and the rate does not necessarily decrease if one assumes that the new radical $A \cdot$ will again reinitiate more monomers. However, the occurrence of chain transfer reactions during polymerization causes the polymer molecular weight to be lower than predicted and wastes initiators (i.e. an initiator molecule is consumed, but no new chains are begun). Sometimes this process is called induced decomposition of the initiator. It is a common side reaction for peroxy initiators, but happens less often with azo initiators [26, 27].

1.6.2. Atom transfer radical polymerization (ATRP)

Atom transfer radical polymerization (ATRP) is another polymerization technique used in this study to synthesis SCLCPs. ATRP is a robust and versatile technique for the synthesis of well-defined polymers with various architectures and narrow polydispersities [28-31]. It is a multicomponent system consisting of an alkyl halide as an initiator, a redox-active transition metal in its lower oxidation state (Mt^m) as a catalyst, a ligand, $X-Mt^{m+1}$ species as a deactivator, monomer and solvent.

The main role of the alkyl halide (R-X) species is to quantitatively generate growing chains. The structure of alkyl group (R) should be similar to the structure of growing chain. For example, 1-phenylethyl derivatives resemble growing polystyrene chains and 2-halopropionates model growing acrylate chains. Group X must rapidly and selectively migrate between the growing chain and transition metal. Bromine and chlorine seem to work best. However, pseudohalogens such as thiocyanates have also been used especially in the polymerization of acrylates and styrenes.

Transition metal and ligand (Mt^mL_n) are the key to successful ATRP. The good catalyst must have high selectivity in the atom transfer process and high lability in the resulting $X-Mt^{m+1}$ species. The metal should participate in one electron transfer redox cycle which would result in the oxidative addition/reduction elimination process. In addition, the metal should have high affinity for atom X but a low affinity for hydrogen and alkyl radicals. Otherwise, a transfer reaction and the formation of organometallic may be observed which reduces the selectivity of propagation and livingness of the process. The catalyst must have an equilibrium position and dynamics of exchange between dormant and active species. The inner coordination sphere of Mt^m must be expanded to accommodate a new ligand. For example, the expansion from tetra to penta coordinated structure ($Cu^I/2bipy$ to $X-Cu^{II}/2bipy$) must be possible. Recently, the most efficient redox-active transition metal complex has been a copper complex with various nitrogen-based ligands. The ligands affect the redox chemistry by their electronics effects, control the selectivity by steric or electronic effects and also solubilize the catalytic systems [32].

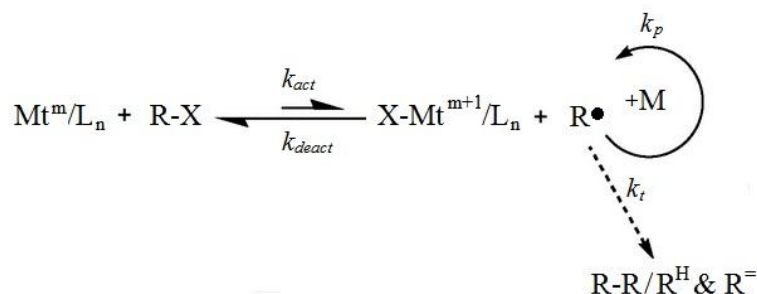
The deactivator ($X-Mt^{m+1}$ species) is an important part of the catalytic system because it can reduce the rate of polymerization, polydispersity and may also be involved in the side reactions. The addition of a small quantity of deactivator (5%) at the very beginning of polymerization can reduced the proportion of dead chains and

generates a persistent radical effect. The CuX_2 species is one example of a deactivator which is relatively a strong Lewis acid and may catalyze heterolytic cleavage of the C-X bond. However, this reaction depends on the ligand, the nature of X, the nature of the α -substituents at the terminal C-atom and the solvent. CuX_2 may also react with radicals not only via transfer of halogen atoms but also by the formation of the short-lived Cu^{III} species which decomposes by hydrogen abstraction. Thus, it is important to control the concentration of the deactivator to avoid a low polymerization rate and side reactions.

ATRP can be used for many vinyl monomers such as styrene, methacrylate, acrylate, acrylonitrile and diene [33-35]. However, the currently available catalytic system is not efficient enough to polymerize less reactive monomers which produce non-stabilized and very reactive radicals such as ethylene, vinyl chloride and vinyl acetate. Another class of monomers which cannot be polymerized by ATRP are acids. This is due to the rapid formation of Cu^{II} carboxylates which are inefficient deactivators and cannot be reduced to active Cu^{I} species. There are also some limitations in the monomer structure as well. For instance, the polymerization of *p*-methoxystyrene is accompanied by severe side reactions and the structure of oligomers formed suggests an involvement of cationic intermediates. This results in homolytic and heterolytic cleavage of the R-X bond.

Another important component in conducting ATRP is the solvent. Typically, polymerizations are carried out in relatively non-polar solvents such as benzene, *p*-dimethoxybenzene or diphenyl ether. However, more polar solvents such as ethylene carbonate, propylene carbonate and water have been successfully used [30, 36]. The selection of solvent should be dictated by the potential for chain transfer which is the limiting factor for the desired molecular weight. In addition, the solvent interactions with the catalytic system should be considered. During the ATRP reaction, the polymerization system must be free from oxygen. Small amounts of oxygen can be

Scavenged by the catalyst which is present at a much higher concentration than the growing radicals. Thus, it reduces the catalyst concentration and may produce an excess of deactivator [37].



Scheme 1.7 : General mechanism of ATRP. Adopted from [37].

The general mechanism of ATRP is given in Scheme 1.7. Mechanistically, ATRP is based on an inner sphere electron transfer process, which involves a reversible alkyl halide or pseudohalide transfer between a dormant species (R-X) and a transition metal complex (Mt^m/L_n) resulting in the formation of propagating radicals ($\text{R}\cdot$) and the metal complex in the higher oxidation state (e.g. $\text{X-Mt}^{m+1}/\text{L}_n$). The radical is quickly deactivated by a higher-oxidation state transition metal complex (deactivator) and the dormant chain is created. These processes occur with a rate constant of activation, k_{act} , and deactivation k_{deact} , respectively. Polymer chains grow by the addition of monomers to the periodically generated radicals in a manner similar to a conventional radical polymerization, with the rate constant of propagation, k_p . Termination reactions (k_t) also occur in ATRP, mainly through radical coupling and disproportionation [24, 37-39].

1.7. Motivation

The present work is directed to the synthesis of a new polymerizable monomer containing naphthalene ring in the mesogen with an ester linkage and various types of polymerizable monomers consisting of 1,4-disubstituted phenyl cores with a Schiff base

and ester linkages. The synthesis is targeted to produce high molecular weight and narrow polydispersity SCLCPs so as to improve their thermal and mechanical properties. Although Schiff base ester liquid crystals have been extensively investigated for different applications, research on SCLCPs having a Schiff base ester moiety as the side group is still limited. Schiff base is chosen as it contains -CH=N- group which exhibit optical and electrochemical properties. To the best of my knowledge and according to the literature survey, SCLCPs bearing a Schiff base ester mesogen as the side group have not yet been reported.

The synthesized monomers were used to synthesize SCLCPs via radical polymerization. The effects of mesogen, lateral and terminal substitution on mesomorphic properties of monomers were studied. The effect of the nature of polymer backbone, molecular weight and polydispersity of the polymers were also investigated. The thermal stability, optical properties, electrochemical properties and rheological properties of the polymers were investigated.

1.8. Research objective

The scope of this work covers the synthesis and characterization aspects of new monomers for side chain liquid crystalline polymers (SCLCPs) thus far unreported in the literature. Based on the research outline as mentioned in Section 1.8, the research objectives can be summarized as to:

1. synthesize several types of new liquid crystal polymerizable monomers and high molecular weight SCLCPs by radical polymerization for improved thermal and mechanical properties.
2. characterize and study the properties of the prepared monomers and polymers by several analytical techniques such as:
 - i. nuclear magnetic resonance spectroscopy (NMR)

- ii. fourier transform infrared spectroscopy (FTIR)
- iii. gel permeation chromatography (GPC)
- iv. differential scanning calorimetry (DSC)
- v. polarized optical microscopy (POM)
- vi. powder X-ray diffraction (PXRD)
- vii. small angle X-ray scattering (SAXS)
- viii. thermal gravimetric analysis (TGA)
- ix. UV-Vis and fluorescence spectroscopy
- x. cyclic voltametry (CV)
- xi. rheology

1.9. Thesis outline

Chapter 1 presents an introduction and background of liquid crystals. Motivations, research objectives and scope of work are also presented.

Chapter 2 describes the literature background of side chain liquid crystalline polymers and their potential properties. A brief theoretical introduction on polymerization kinetics is also included.

Chapter 3 describes the experimental procedures used throughout this work, starting from the material preparations, moving on to the synthesis aspect of the experiments, and finally the characterization methods. Details of the optimum conditions for the handling of instruments are included as well.

Chapter 4 discusses the general results from the characterization techniques used throughout this work. The monomers and their polymers were characterized by ^1H NMR with the spectral assignments corroborated by ^{13}C NMR and FTIR spectroscopies. The solubility behavior of the synthesized compounds was observed using different solvents. The molecular weight and polydispersity of the polymers were

measured by GPC. The liquid crystalline properties of monomers as well as polymers were studied by POM, DSC and confirmed by PXRD and SAXS. The structural and mesomorphic properties relationship on the monomers and polymers were investigated. Glass transition temperature (T_g) and thermal gravimetric analysis were performed by DSC and TGA analyzers respectively. The effect of molecular weight, polydispersity and the nature of polymer backbone on the T_g of the polymers were also investigated. The last part of Chapter 4 discusses the optical, electrochemical and rheological properties of the synthesized polymers.

Finally, Chapter 5 presents concluding remarks of the research output and recommended future steps with respect to the objectives of this thesis.

The Appendix provides supplementary data related to the experimental work and results discussion.

CHAPTER 2 : LITERATURE REVIEW

2.1. Naphthalene based liquid crystal

A vast number of mesogenic naphthalene derivatives are reported [8, 40-48] as naphthalene derivatives exhibit rich mesomorphism if properly designed. Prajapati and co-workers [49, 50] reported the synthesis of mesogenic homologous series of azomesogens with lateral methyl and chloro groups (Figure 2.1). Compounds in series A showed lower nematic to isotropic (N-I) transition temperature (111-186°C) compared to parent unsubstituted compounds in series B (135-218°C) due to the presence of lateral chloro group *ortho* to the -COO- central linkage. The compound with the lateral methyl group (compounds in series C) also showed low thermal stabilities (86-147°C) and exhibited only a nematic phase. The effect was more pronounced compared to the lateral chloro group due to the polar nature of the chloro group.

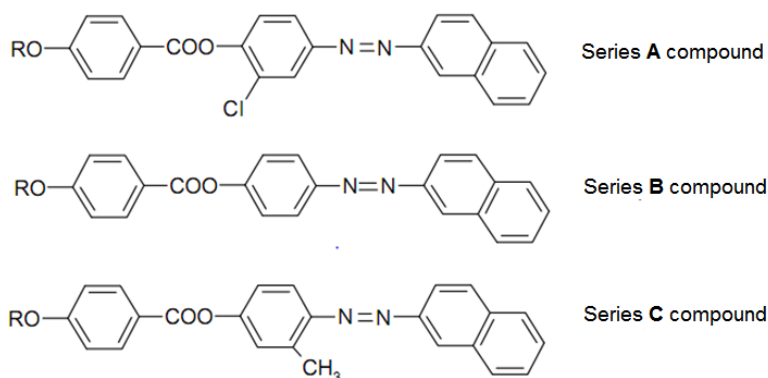
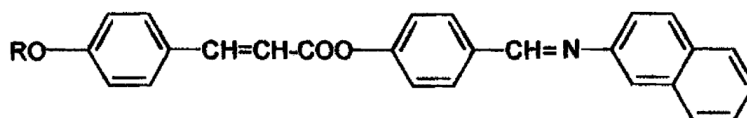


Figure 2.1 : A series of azomesogens with lateral units [51].

They also reported mesogenic homologous series of Schiff's base cinnamates [52] comprising a naphthalene moiety (Figure 2.2) and investigated the effect of an ethylene linking group and naphthalene moiety on the mesomorphic properties. They found that all the synthesized compounds of this homologous series exhibited mesomorphism. The

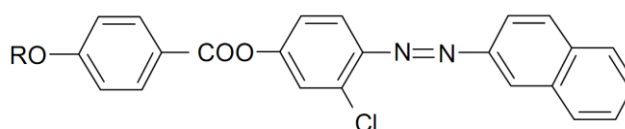
naphthalene moiety at the terminal position broadens the mesophase transition temperature due to high polarizability of the molecule. The presence of naphthalene moiety decreases the smectic mesophase range but increases the nematic mesophase range due to the thickening effect.



$$R = -C_nH_{2n+1}, n = 1 \text{ to } 8, 10, 12, 14 \text{ and } 16$$

Figure 2.2 : A series of Schiff's base cinnamates. Adopted from [52].

In another work, Prajapati and co-workers [51] reported the synthesis of a mesogenic homologous series of naphthyl azomesogens with lateral chloro group (Figure 2.3) to study the effect on mesomorphism. They found that the lateral chloro group decrease the nematic mesophase range and the nematic-isotropic (N-I) transition temperature of the studied compounds. The presence of the lateral chloro group on central benzene ring has increased the breadth of the molecule.



$$R = -C_nH_{2n+1}, n = 1 \text{ to } 8, 10, 12, 14 \text{ and } 16$$

Figure 2.3: Naphthyl azomesogens with lateral chloro group. Adopted from [51].

2.2. Schiff base ester based liquid crystal

Extensive studies of Schiff base core system had been conducted ever since discovery of 4-methoxybenzylidene-4'-butylaniline (MBBA) by Kelker and Scheurle [53] and the application of its room temperature nematic phase in displays sparked a renewed interest in liquid crystals. The ester and Schiff base linking groups are known

as side-step units which depart the molecule one step aside at such units but a linear contour of the molecule can be maintained [2]. This Schiff base ester structure still maintains molecular linearity providing higher stability and enabling mesophase formation.

Schiff base is a very interesting organic precursor for material science particularly in the preparation of liquid crystalline substance, thermochromic as well as photochromic materials which may possess potential applications in the measurement of radiation intensity and in optical display system [6]. Nowadays, a lot of studies have been conducted on Schiff base esters due to their interesting properties and wide temperature range [54-60].

Yeap et al. [60] synthesized a series of Schiff base esters, with para-substituents R (where R= *p*-CN, *p*-NO₂, *p*-OH and *p*-COOH) at the aniline fragment (Figure 2.4) to study their mesomorphic properties. The compounds containing R=*p*-CN and R=*p*-OH exhibited smectic phases whereas the compound with R=*p*-COOH showed nematic and smectic mesophases. However, the compound containing R=*p*-CN did not show any mesophase characteristic. Most of the studies by Yeap and co-workers [61-64] were focused on the series of Schiff base esters containing aniline derivatives. They revealed that Schiff base ester linking units were the useful structural components for generating mesomorphism in two and three aromatic rings thermotropic liquid crystals.

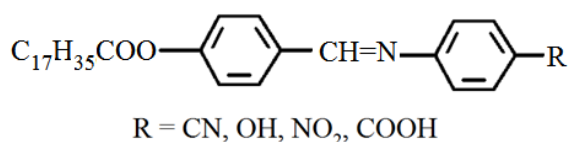


Figure 2.4: *p*-*n*-octadecanoyloxybenzylidene-*p*-substituted-anilines. Adopted from [60].

Ha et al. [65-67] continued the effort of Yeap and co-workers by carrying on the synthesis and characterization of a new series of Schiff base esters possessing terminal halogen X (where X= -Cl, -Br and -I) on the 4-X-benzylidene-4'-*n*-

alkanoyloxyanilines (Figure 2.5). Most of the compounds contained even number of carbons at the end groups of the molecules ($C_{n-1}H_{2n-1}COO-$, $n= 2, 4, 6, 8, 10, 12, 14, 16$). They found that the length of terminal alkanoyloxy chains influenced the mesomorphic properties of the compounds. The C2 and C4 members did not possess any mesogenic properties while C6 to C16 derivatives possessed monotropic and enantiotropic smectic phases. The terminal halogen promoted the formation of smectic phase due to their polarity.

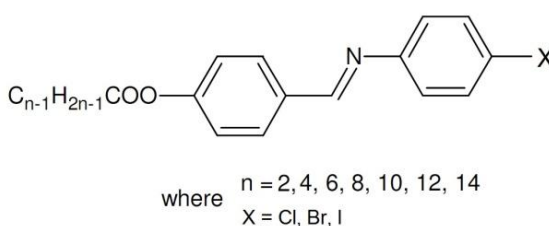
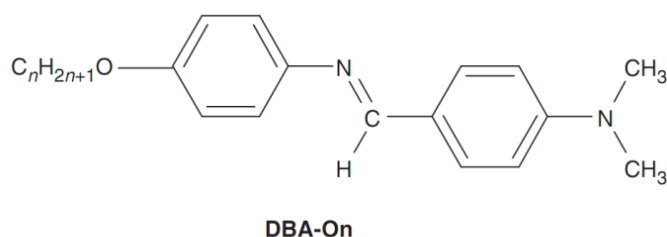


Figure 2.5 : Schiff base ester compounds with halogen end group. Redrawn from [65-67].

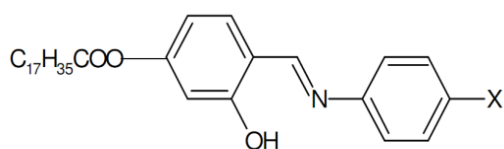
In another work, Ha et al. [55] synthesized a series of Schiff base ethers comprising a dimethylamino group at one terminal position and an even number of carbons at the end groups of the molecules (Figure 2.6). They found that the *n*-ethyloxy, *n*-propyloxy and *n*-octadecyloxy were not mesogenic whereas the *n*-butyloxy to *n*-hexadecyloxy derivatives exhibited nematic mesophase. The formation of less-ordered mesophase was due to the presence of a dimethylamino unit which acts as a charge transfer donor in the formation of conjugative interactions. This unit has contributed to the molecule's polarizability which affected its intermolecular interactions.



Where $n = 2, 3, 4, 5, 6, 7, 8, 9, 10, 12, 14, 16, 18$

Figure 2.6 : Schiff base ether with dimethyl amino unit. Adopted from [55].

Ha and co-workers [56, 68] also synthesized a series of Schiff base esters with stearoyl moieties with different end groups X (where X = -H, -F, -Cl, -Br, -OCH₃, -CH₃ and -C₂H₅) (Figure 2.7). They found that the compounds with halogen and methoxy substituents exhibited mesomorphic properties whereas the compounds with less polar substituents (X = -CH₃ and -C₂H₅) were non-mesogenic materials. The compound with methoxy end group possessed a nematic mesophase while the compounds with halogen end group possessed a smectic mesophase. The incorporation of a lateral hydroxyl group on each compound has enhanced the molecular ordering leading led to higher clearing points.



SB-X

where X = H, F, Cl, Br, OCH₃, CH₃, C₂H₅

Figure 2.7 : Schiff base ester compounds with various end group. Adopted from [56].

2.3. Structure-mesomorphic properties relationship

An understanding of the structure-mesomorphic properties relationship of mesogenic units is important in selecting molecular modification for the synthesis of new mesogens with the desirable properties for future applications. According to Gray [8], the relationship between structure and mesomorphic behavior has been studied to

determine: (i) whether a compound possessed any mesomorphic properties or not, (ii) which chemical constitution of a compound possesses smectic, nematic or cholesteric mesophase, and (iii) the changes in the mesomorphic transition temperatures which occur when the chemical constitution of a compound is altered.

Effect of mesogenic core on mesomorphic properties

Fornasieri et al. [69] prepared three series of calamatic liquid crystals consisting of a mesogenic core attached to a perfluorinated chain via thioester linkage and a hydrocarbon chain with terminal double bond. A monophenyl, biphenyl or phenyl benzoate group was incorporated as a rigid core together with a hydrocarbon chain length varying with 1 and 9 carbons (Figure 2.8) to study their effect on the mesomorphic properties. They concluded that increasing the length of the alkyl chain strongly reduced the mesomorphic behavior, while increasing the number of aromatic rings in the core structure increased transition temperatures. The monophenyl allyloxy derivative showed interesting smectogenic enantiotropic character near room temperature. The biphenyl compounds shift the mesophase to higher temperatures but the temperature range remained unchanged, whereas the compounds with the phenyl benzoate group stabilized the mesophase at wider temperature range (181°C). All compounds showed unique enantiotropic behavior.

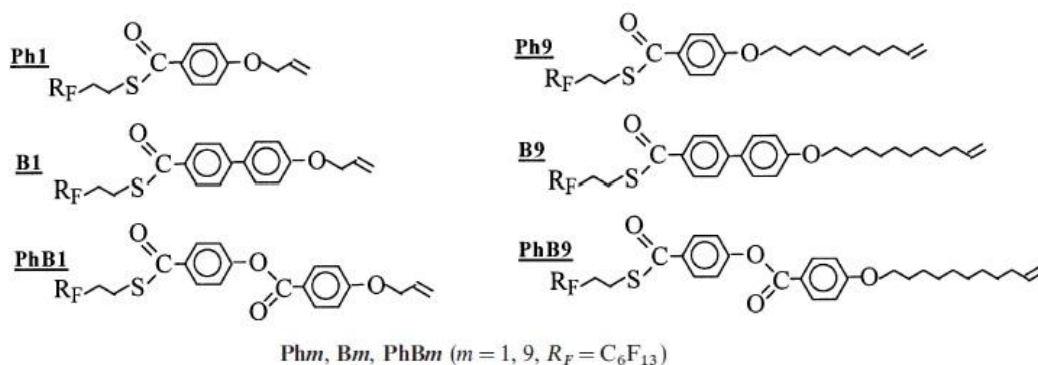


Figure 2.8 : Series of synthesized liquid crystals. Adopted from [69].

Mori [70] studied mesomorphic properties of three-ring systems such as 2,5-dibenzoyloxytropones, 5-benzoylamino-2-benzoyloxy-tropones and 2,5-dibenzoylamino-tropones with 4-alkoxy, 3,4-dialkoxy, and 3,4,5-trialkoxy groups on the benzoyl groups together with those of the corresponding benzenoids (Figure 2.9). Derivatives with two monoalkoxybenzoyl groups exhibited nematic and smectic A and C mesophases. Troponoid tetracatenars with two dialkoxybenzoyl groups had hexagonal columnar phases except for troponoids tetracatenar **2** with two ester-connecting groups, whereas the corresponding benzenoids tetracatenars (**11**, **14**, **17**) with two dialkoxybenzoyl groups were non-mesomorphic. All troponoid hexacatenars with two trialkoxybenzoyl groups formed hexagonal columnar phases. With the exception of benzenoid hexacatenars with two ester-connecting groups, the benzenoid hexacatenars showed hexagonal and tetragonal columnar phases.

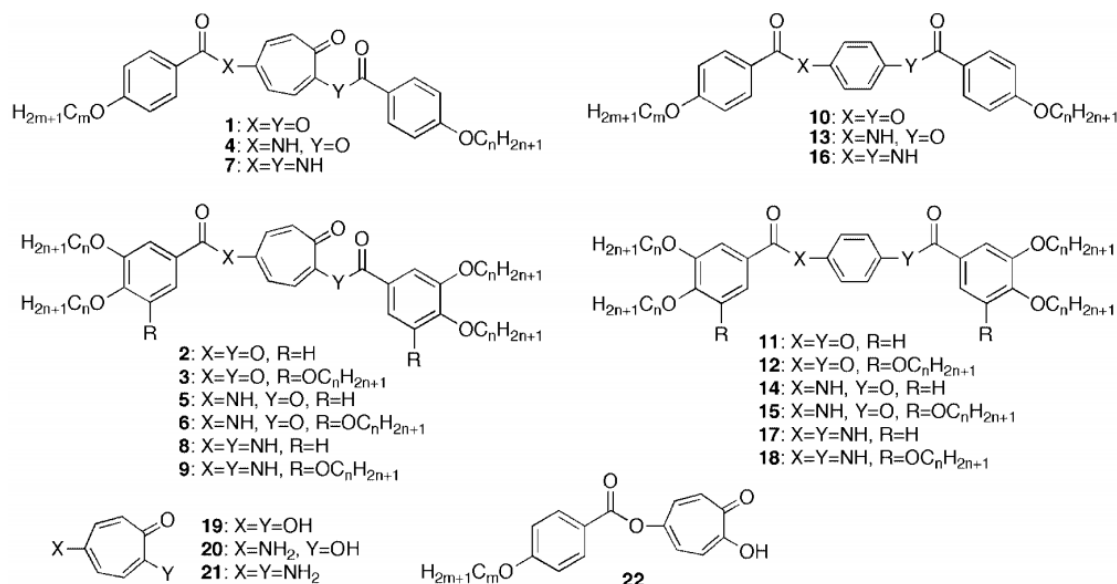


Figure 2.9 : Compounds under investigations. Adopted from [70].

Chia et al. [71] synthesized two homologous series of pyridine-containing liquid crystalline compounds, 2-(4-alkoxyphenyl)-5-phenylpyridines (*n*O-PPyP, *n* = 3–7) and 2-(6-alkoxynaphthalen-2-yl)-5-phenylpyridines (*m*O-NpPyP, *m* = 3–7) (Figure 2.10).

They found that the pyridine moiety in the mesogen favors the appearance of smectic behavior, reduces the thermal stabilities of the crystal and introduces an attractive force and causes the appearance of nematic phase. In the series of *mO*-NpPyP, $m = 3-7$, all compounds exhibited an enantiotropic nematic phase with an additional narrow monotropic smectic A phase observed in 8O-NpPyP. The replacement of phenyl core with a naphthalene moiety provides a much better nematogen.

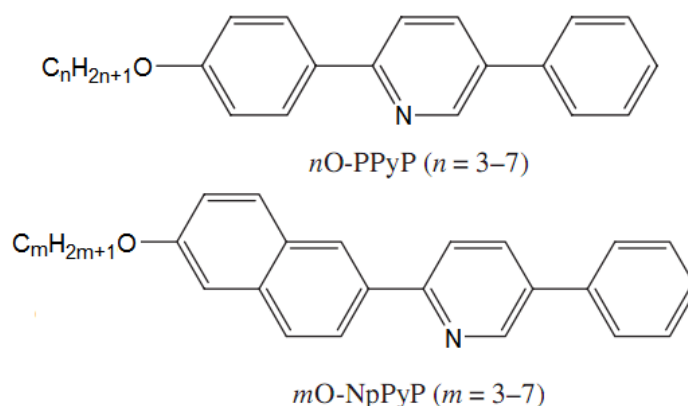


Figure 2.10 : Pyridine-containing liquid crystalline compounds. Adopted from [71].

Effect of terminal group on mesomorphic properties

Matsunaga et al. [72] studied the effects of terminal substituents of 4-(4-X-substituted benzylideneamino)phenyl-4-Y-substituted benzoates on mesomorphic properties (Figure 2.11). X and Y were chosen from methoxy, nitro, chloro, bromo, dimethylamino, methyl, fluoro and trifluoromethyl groups. They found that the order of group (X or Y) efficiency in promoting the nematic-isotropic transition temperature is markedly affected by the nature of the group (X or Y) located at the other end. The methoxy and methyl series gives $NO_2 > CH_3O > N(CH_3)_2 > Cl = Br > CH_3 > F > CF_3$, whereas the trifluoromethyl series gives $N(CH_3)_2 > CH_3O > CH_3 > Cl = Br > NO_2 > F$, suggesting that the dipole-dipole interaction contributes significantly to the stabilization of the nematic phase.

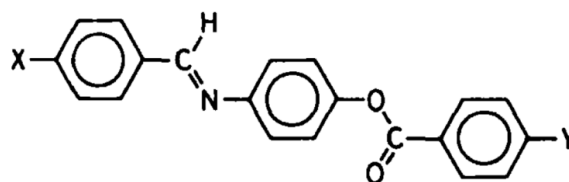
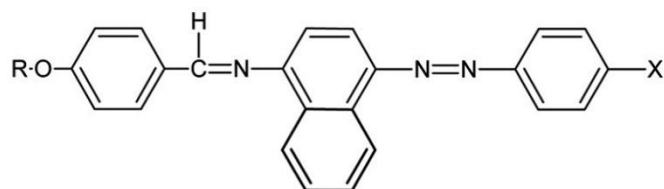


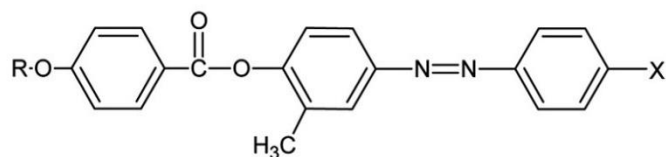
Figure 2.11: Studied compound. Adopted from [72].

Neubert et al. [73, 74] investigated the effect of terminal chains on the mesomorphic properties of 4,4'-disubstituted diphenyldiacetylenes. The synthesized compounds showed wide nematic ranges, higher clearing temperatures, low viscosities and low enthalpies of melting. In another work [75], they studied the effect on mesomorphic of triple bond in a terminal chain of 4,4'-disubstituted phenyl benzoates and phenyl thiobenzoates. They found that the insertion of a triple bond into the 1,2-position of a terminal chain on the phenyl benzoates and phenyl thiobenzoates did not improve liquid crystalline properties. Fewer mesophases having shorter temperature ranges and lower transition temperatures were observed. However, the thioesters showed better mesomorphic properties and nematic phases were favored over smectic phases.

Thaker et al. [54] synthesized two new series of azo-Schiff base (series A) and azo-ester (series B) liquid crystals (Figure 2.12) to study the influence of central linkages, terminal and lateral group on the mesomorphism and thermal stability of these compounds. They reported that all synthesized compounds possessed mesomorphic properties. In series A, compounds A₁ and A₃ exhibited only nematic mesophase, while compounds A₂, A₄, A₅, A₆, A₇, A₈, A₉, and A₁₀ exhibited a smectic and nematic mesophases. In series B, compounds B₁ to B₉ exhibited only nematic mesophase whereas compounds B₁₀ and B₁₁ exhibited smectic and nematic mesophases. Compound B₁₂ exhibited only a nematic mesophase.



Series A



Series B

| Compounds | R = n-Alkoxy | X | Compounds | R = n-Alkoxy | X |
|-----------------|--------------|-------------------|-----------------|--------------|-------------------|
| A ₁ | Octyloxy | -H | B ₁ | Octyloxy | -H |
| A ₂ | Octyloxy | -CH ₃ | B ₂ | Octyloxy | -CH ₃ |
| A ₃ | Octyloxy | -OCH ₃ | B ₃ | Octyloxy | -OCH ₃ |
| A ₄ | Octyloxy | -Cl | B ₄ | Octyloxy | -Cl |
| A ₅ | Octyloxy | -Br | B ₅ | Octyloxy | -Br |
| A ₆ | Hexadecyloxy | -H | B ₆ | Octyloxy | -NO ₂ |
| A ₇ | Hexadecyloxy | -CH ₃ | B ₇ | Hexadecyloxy | -H |
| A ₈ | Hexadecyloxy | -OCH ₃ | B ₈ | Hexadecyloxy | -CH ₃ |
| A ₉ | Hexadecyloxy | -Cl | B ₉ | Hexadecyloxy | -OCH ₃ |
| A ₁₀ | Hexadecyloxy | -Br | B ₁₀ | Hexadecyloxy | -Cl |
| | | | B ₁₁ | Hexadecyloxy | -Br |
| | | | B ₁₂ | Hexadecyloxy | -NO ₂ |

Figure 2.12 : Series A and series B compounds. Adopted from [54].

Very recently, Karim et al. [76] studied the effect of different substituents R (where R = -H, -CH₃, -OCH₃, and -OC₂H₅) at the sixth position on benzothiazole chromophore (Figure 2.13) on mesomorphic, thermal and optical properties. All synthesized compounds showed mesomorphic behaviors and exhibited lamellar structure. The compound with -H substituent revealed only smectic mesophase whereas the compounds with -CH₃, -OCH₃, and -OC₂H₅ groups exhibited nematic and smectic mesophases. They thus concluded that the formation of the mesophases was greatly influenced by the sixth position electron pushing substituents on the benzothiazole ring as well as the terminal methacrylate group. The optical study on these compounds showed that the compound with a methoxy substituent exhibited higher fluorescent emission compared to other compounds.

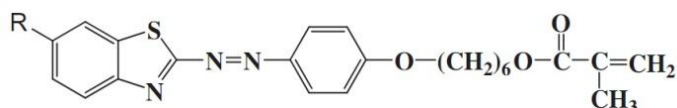


Figure 2.13 : Azo benzothiazole compounds. Adopted from [76].

Effect of lateral substitution on mesomorphic properties

The effect of a lateral methoxy [77], methyl [78], fluorine and bromine [79] group on the mesomorphic properties in a series of ferroelectric liquid crystals with a 2-alkoxypropionate unit have been done by Kašpar and co-workers (Figure 2.14). They concluded that the phase transition temperature to the SmC* phase decreases in a sequence H > F > Cl > Br > CH₃ > CH₃O whereas the values of the spontaneous polarization increase in a sequence CH₃O < H < F < CH₃ < Cl < Br. The introduction of a lateral unit on the mesogenic core lowered all phase transition temperatures and affected the spontaneous polarization values of the chiral compounds compared with the non-substituted chiral compound.

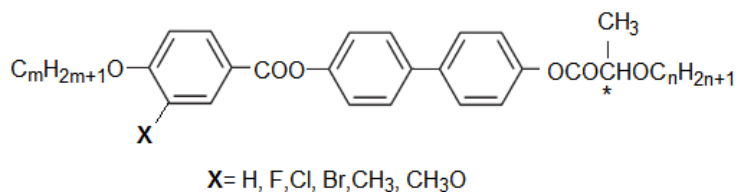
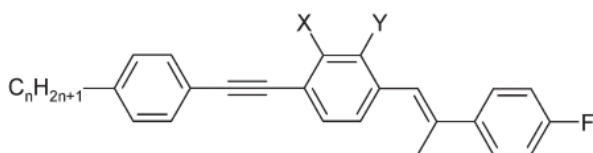


Figure 2.14 : A series of ferroelectric LCs. Redrawn from [79].

Other researchers, Chang and co-workers [80] studied the effect of a lateral methyl substitution on α -methylstilbene-tolane liquid crystals (Figure 2.15). They found that the compounds with a lateral methyl group at the 3 position of the middle phenyl ring displayed low melting points, wide nematic range and had small enthalpy of fusion.



$$n = 2-6; X \text{ and } Y = \text{H or } \text{CH}_3$$

Figure 2.15 : α -methylstilbene-tolane liquid crystals. Adopted from [80].

Recently, Dave et al. [81, 82] prepared two new homologous series (series I and II) consisting of central azo-ester linkage and methyl group at the central as well as terminal benzene rings with spacer lengths varying from $n=1$ to 8, 10, 12, 14, 16 (Figure 2.16(a) and Figure 2.16(b)) to study their mesomorphic properties. The odd-even effect was observed for the series II compounds in the initial carbon members up to C6 derivative. The introduction of methyl group in lateral position at terminal and central benzene core in series I and II decreased nematic to isotropic (N-I) thermal stabilities of smectic and nematic mesophases compared to series A compounds (Figure 2.16(c)) prepared by Doshi and Ganatra [83]. However, the thermal stability of the compounds in series B (Figure 2.16(d)) prepared by Thaker et al. [54] was higher than that of the compounds in series II. This was because the introduction of one more lateral methyl group in the central benzene core had a more pronounced effect in the reduction of N-I thermal stability. From this study, they suggested that the introduction of a lateral unit on the mesogenic core lowered the thermal stability of the compounds.

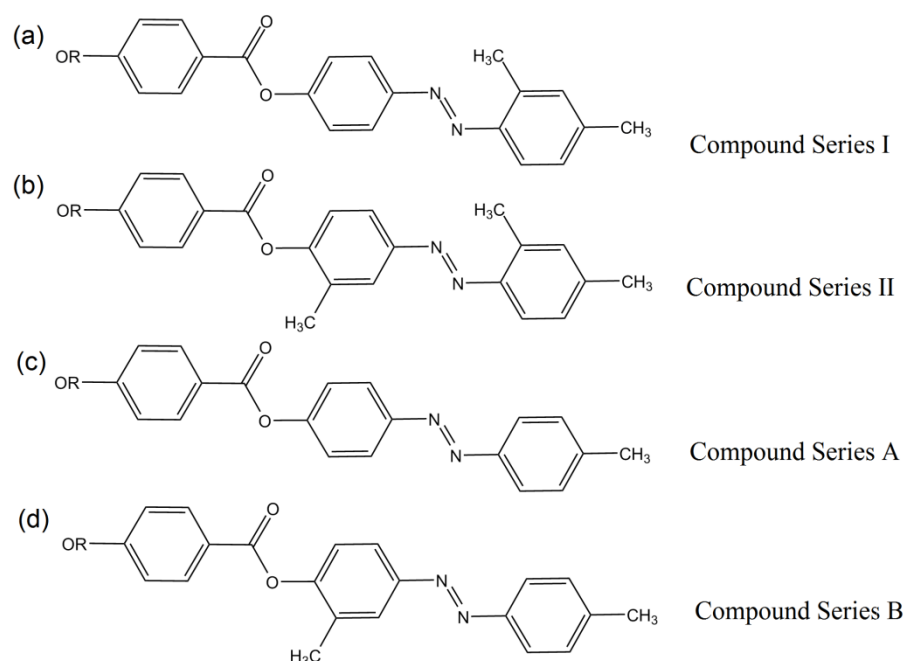


Figure 2.16 : A series of azo-ester with lateral units. Adopted from [81].

2.4. Side Chain Liquid Crystalline Polymers (SCLCPs)

SCLCPs generally consist of three structural components: polymer backbone, mesogenic groups and flexible spacer. The flexible spacer plays a critical role in determining the properties of the polymer by decoupling the opposing tendency of the liquid crystal groups to self-assemble from the polymer backbones to adopt random coil conformations [22]. The nature of their mesophase depends rather sensitively on these components. The nematic, smectic and cholesteric types of mesophases are observed with rod-like repeating units [16].

Effect of flexible spacer on mesomorphic properties

The property of SCLCPs is determined by the polymer backbone, spacer length and mesogenic unit. The incorporation of the flexible spacers leads to the formation of liquid crystalline phases [84]. In addition, more flexible polymers should have a stronger tendency to form more stable mesophases. Numerous studies have been carried out by Akiyama et al. [85-88] on the effects of spacer length on SCLCPs properties.

They concluded that the spacer introduced between a polymer backbone and a mesogenic core decoupled its motion and enhanced the dynamic ordering of the mesogenic group. Therefore, the ability of the mesogenic side chains to form more ordered mesophases was increased.

De Tang et al. [89] studied the effect of flexible spacer on the liquid crystalline properties of ABA-type triblock copolymers containing azobenzene groups (Figure 2.17). The monomers, *n*-[4-(4-ethoxyphenylazo)phenoxy]alkyl methacrylates with varying methylene groups (*n* = 0, 2, 6) were used to synthesize a series of azobenzene-containing amphiphilic triblock copolymers PA*n*C-PEG-PA*n*C by ATRP. The *T_g* of these copolymers decreased with increasing *n*. Copolymer without methylene spacer (PA0C-PEG-PA0C) did not show any mesophase while both PA2C-PEG-PA2C and PA6C-PEG-PA6C exhibited a nematic mesophase.

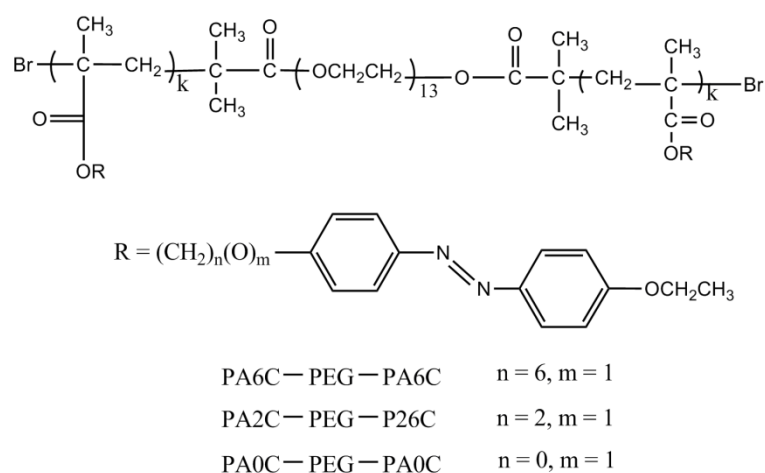


Figure 2.17 : Copolymers under investigation. Adopted from [89].

Palani and co-workers [90] synthesized two series of alkoxyethyl-1H-[1,2,3]-triazol-1-yl containing SCLCPs by free radical polymerization (Figure 2.18). They investigated the effect of insertion of polar alkoxy group on terminal triazole ring and spacer length between mesogen on phase transition temperature and mesomorphic property of the polymers. They found that the *T_m* and *T_g* of the polymers were decreased

clearing temperatures compared to analogous polymethacrylates. In addition, the flexible polyacrylate chain promoted the formation of smectic phases.

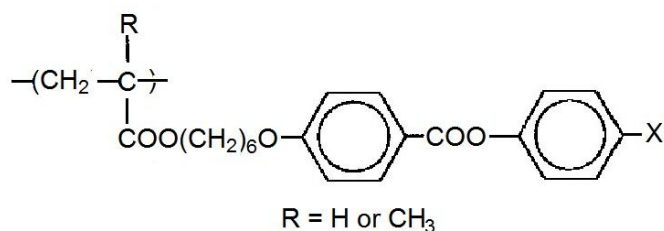


Figure 2.19 : SCLCPs polyacrylate and polymethacrylates. Adopted from [98].

Zhang et al. [99] synthesized thermotropic SCLCPs containing mesogenic units with different flexible groups and a chiral methyl group by grafting upon a polysiloxane backbone (Figure 2.20). A wide mesomorphic region was observed for all polymers. The polymers exhibited colorful cholesteric Grand-Jean textures when the content of the chiral unit was higher than 15 mol% for polymer P1, and higher than 10 mol% for polymers P2 and P3. Other polymers exhibited nematic thread-like textures and all polymers were thermally stable over 300°C.

Polymers P1, P2, P3

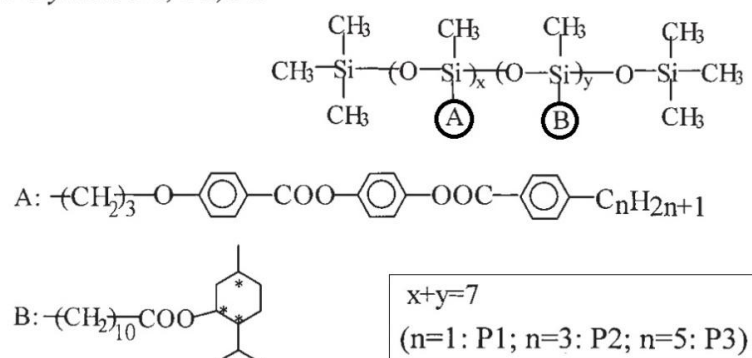


Figure 2.20: SCLCPs with achiral and chiral units on the side chain. Adopted from [99].

Ritter et al. [21] prepared two chiral SCLCPs polyacrylates having a biphenyl-phenyl system as a mesogenic core unit (Figure 2.21). In this work, they used an

undecyl spacer to connect the mesogenic group to the backbone and both polymers exhibited enantiotropic SmA* mesophase while the monomers showed both SmC* and SmA* phases. In the case of the monomers, the conclusion is that the carbonyloxy linking group is superior to the oxy group in stabilizing a liquid-crystals phase of the monomers. Both polymers exhibited a T_g above room temperature. The thermal transition temperature and the T_g of the polymers are strongly dependent on backbone flexibility and the chiral terminal chain.

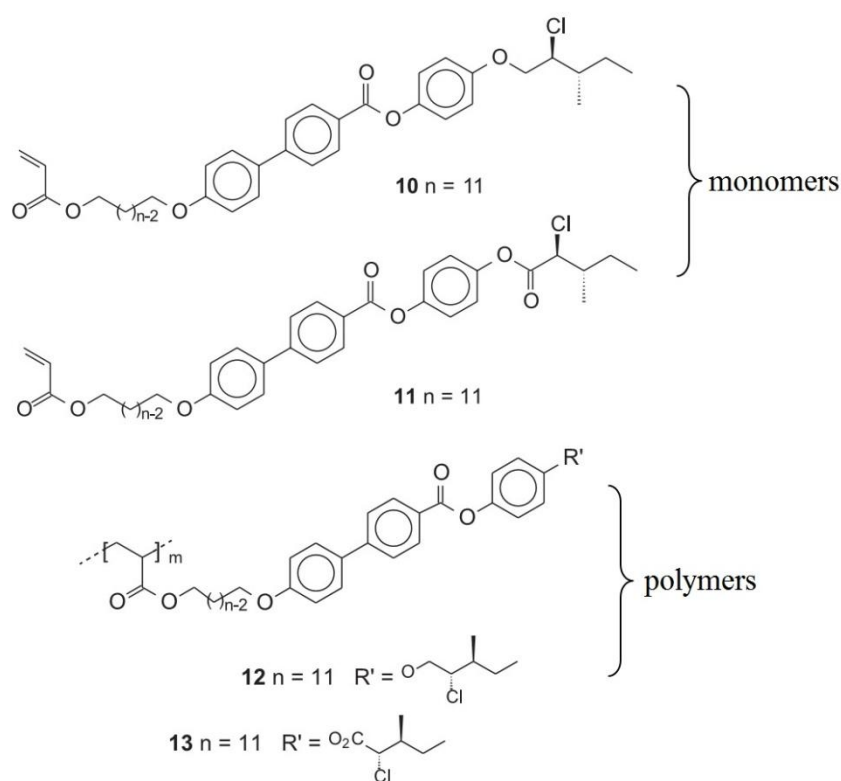


Figure 2.21 : Monomers and polymers structure. Adopted from [21].

Wang and co-workers [100] prepared a series of novel SCLCPs consisting of laterally attached photoluminescent *p*-quinquephenyl (QQP) pendants with different flexible terminal- and/or side alkoxy chains via ATRP (Figure 2.22). All the homopolymers and copolymers exhibited nematic mesophase which were influenced by the long peripheral flexible chains ($-\text{OC}_8\text{H}_{17}$) on both longitudinal terminal and lateral sides of the rigid pendant rods. Besides mesomorphic properties, they also studied the

photophysical properties of the synthesized polymers. They found that all polymers had almost identical maximum UV-Vis absorption and possessed blue photoluminescence emission wavelengths originating from their similar rod-like conjugated units in dilute solutions and solid films.

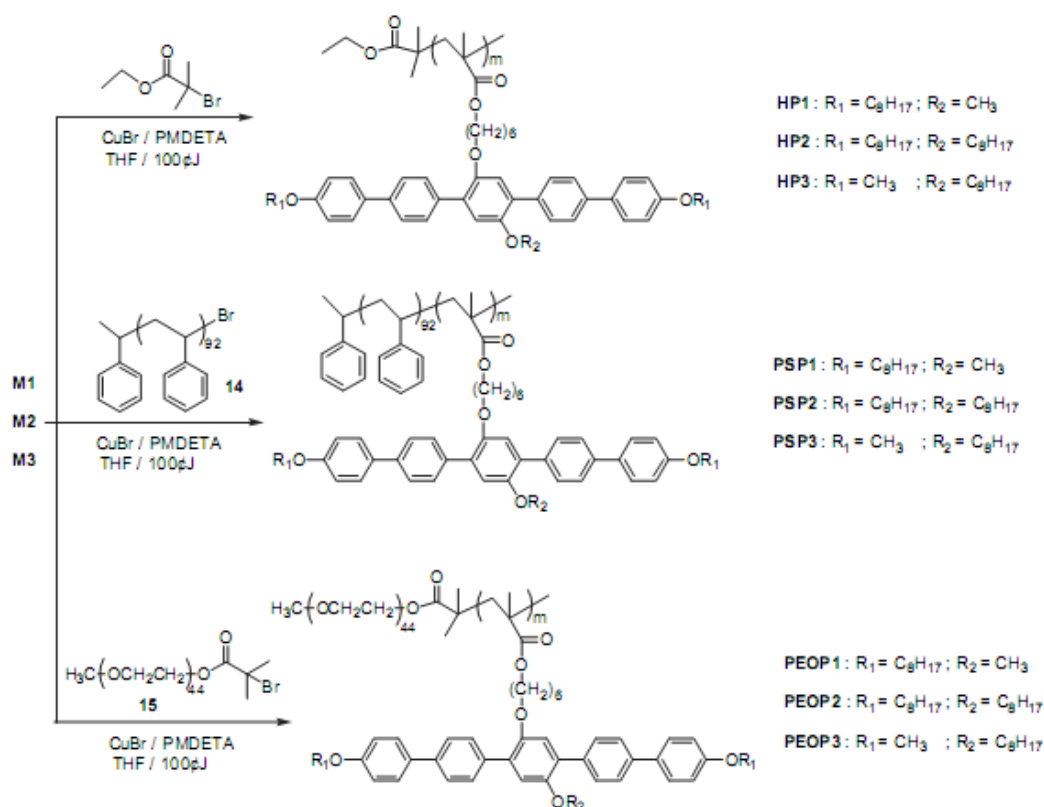


Figure 2.22 : Homopolymers and diblock-copolymers with QQP units. Adopted from [100].

2.5. Applications of SCLCPs

Side chain liquid crystalline polymers (SCLCPs) which represent a combination of liquid crystalline behavior and polymeric properties have been the subject of intensive research in the last decade. They exhibit unique properties such as high heat resistance, flame retardance, chemical resistance, heat aging resistance, low viscosity and comparatively low cost. SCLCPs have received increasing attention from the scientific, technological and also commercial points of view due to their wide range of potential applications in the fields such as optical data storage, non-linear optics, stationary

phases for gas chromatography, supercritical-fluid chromatography and high performance liquid chromatography, solid polymer electrolytes, separation membranes and display materials [101].

Optical data storage

SCLCPs as a reversible optical data storage material were first demonstrated by Shibaev et al. [102]. SCLCPs have an advantage as image storage materials because the T_g of the polymers can be frozen-in. Thus, the stored image can be kept below T_g for a long time. The polymers have good film-forming properties which allow cell-free performance of the image storage materials. In addition, the low fluidity of the polymers is favorable for long-term stability of the stored image.

SCLCPs containing azobenzene chromophores are widely used in reversible optical data storage [103-107]. An azobenzene group can exist in two configurations: the *trans* or E form and the *cis* or Z form. In the thermodynamically stable *trans* configuration, azobenzene groups are mesogenic, forming nematic phases, whereas the isomeric *cis* configuration is thermodynamically unstable with respect to the *trans* state. Therefore, a thermal relaxation process occurs in the dark state. By irradiating with a proper wavelength, it is possible to induce *trans-cis-trans* isomerization cycles driving optical anisotropy at a molecular level [108].

The effect of polarity of the azobenzene group in SCLCPs for reversible optical storage has been studied by Ho et al. [109]. They reported that saturated levels of birefringent were increased when the dipole moment of the azo moiety in the azo polymers increased. The writing and relaxation behaviors were found to be related to the dipole moment of azo moiety, the T_g and the molecular weight of the polymer. They concluded that the azo moiety with donor-acceptor arrangement (pseudo stilbene-type azobenzene) gave the best optical properties. It offered the fast *trans-cis-trans*

isomerization and strong dipolar interactions which were important for optically induced ordering and stability.

Hvilsted et al. [110] synthesized azobenzene side chain liquid crystalline polyesters and studied their outstanding optical storage properties. The important storage features reported by the authors were no pre-alignment of thin polyester films prior to the writing process and the sensitivity in a broad laser wavelength window (415-532 nm). The information was recorded by polarization holography and the polyesters films showed high diffraction efficiency and high storage density. The non-destructive read out was performed with a red light at 600-750 nm wavelength. The information could be erased by heating the polyester film to 80°C or irradiating it with UV-light. These new materials were also reported to have outstanding temperature resistance and the holograms in them were preserved after long exposure to 180°C.

Non-linear optic (NLO) materials

SCLCPs containing non-linear optic (NLO) pendant groups have been used for applications in non-linear optics devices. This is due to the large polarizabilities which result from the complex excitation of delocalized π -electron systems under appropriate electromagnetic fields as opposed to inorganic condensed-matter systems of these materials. An organic molecule must contain one or more acceptor and donor groups in appropriate positions to a π -delocalized moiety to allow asymmetric charge transfer in the excited electronic state. Also, the molecule must not possess any inversion symmetry. The organic and macromolecular systems based on aromatic Schiff bases consisting of suitably substituted electron donor and acceptor functional groups have been reported by Mandal et al. [111-113]. The organic compound with this structural feature usually possesses facile intra-molecular charge transfer which contributes to its second-order molecular hyperpolarizability, β . The pendant groups containing Schiff

base compound with large ground-state dipole moment, μ lead to a higher degree of molecular alignment upon poling, forming a macroscopic non-centrosymmetric system.

Kumar and Tripathy [114] have also agreed that to yield large macroscopic nonlinearities, the molecular units must have large second order and NLO hyperpolarizabilities. By using quantum chemistry software, they concluded that for second order hyperpolarizability, an NLO moiety should have these criteria: i) delocalized moiety such as stilbene, azo, azomethines and others, ii) electron withdrawing and donating group, iii) wavelength tenability and iv) functionality which could form crosslinks or polymerized upon heating or exposure to UV or had an active molecule surface. The linear optical properties of the synthesized materials were measured by UV-Visible spectroscopy and ellipsometry. The second and third order NLO properties of the polymeric materials were evaluated by second harmonic generation (SHG) and electric field induced phase changes by interferometry. In addition, a stable second order non-linear coefficient was obtained by crosslinked systems.

SCLCPs as the stationary phase in chromatography

In 1963, Kelker reported the usage of liquid crystals as the stationary phase in gas chromatography (GC). Liquid crystal stationary phases yield separation based on differences in solute molecular shape. Polymeric liquid crystals offer significant improvements in column efficiency and are thermally stable over low molar mass liquid crystals. Polysiloxanes are particularly useful as stationary phases. These polymers are known as mesomorphic polysiloxanes (MEPSIL) and their application as GC stationary phases has been studied by Janini et. al [115-117] and other researchers [118-121].

Markides et al. [122] reported that smectic liquid crystalline polysiloxanes offered unique selectivities when used as stationary phases in GC. The retention could be

correlated to solute molecular size and shape. They synthesized polysiloxanes containing biphenylcarboxylate ester moieties with different lengths of flexible spacers. These compounds showed smectic characteristics from 100°C to 300°C with unsurpassed selectivity for the separation of various isomeric polycyclic aromatic compounds.

Fang et al. [123] synthesized a new type of fullerene containing polysiloxane to be used as stationary phases for capillary GC. This compound enhanced column efficiency, wide operational temperature and high thermostability, and exhibited unique selectivity for many organic substances such as alkanes, alcohols, ketones and aromatic compounds. The new stationary phase was suitable for the separation of high boiling compounds and some alcoholic or aromatic positional isomers. Many other researchers have done studies on fullerene containing polysiloxanes as stationary phases for capillary GC [124-126].

After 1988, even more studies were conducted on SCLCPs as the stationary phase in supercritical-fluid chromatography (SFC) [127-129] and high performance liquid chromatography (HPLC) [130, 131]. In HPLC, the liquid crystals are needed to be chemically bonded to the solid support to achieve the stability required for a long column lifetime. The liquid crystal bonded phases have been evaluated by using cyclic aromatic hydrocarbon as the probe samples in reversed-phase HPLC. The results indicated that these phases had better planarity and shape recognition than commercially available octadecylsilica phases [132].

Klein and Springer [133] synthesized a series of side chain polyacrylates containing methoxyphenyl benzoate moieties with aliphatic spacers ($n=2-6$) and these polymers were coated onto silica gels. These SCLCPs modified silica gels were used as stationary phases in HPLC. Steroids and dinitrobenzene isomers were used as sample substances for testing the chromatographic properties of these stationary phases. They concluded

that separations based on the mesophase structure could be observed in analogy to gas chromatography.

Display technology

Over the last 30 years liquid crystals have been widely used in many commercial applications as functional organic materials in electro-optical display devices and office equipment such as watches, radio clocks, calculators, notebooks, computers and others. Specifically, liquid crystals dominate the display market in portable instruments. Liquid crystal displays (LCDs) have replaced cathode ray tubes (CRTs) in a segment of the computer monitor market. The shares of the total market for displays have increased with the invention and developments in technologies such as Light-Emitting Polymers (LEPs), Field Emission Displays (FEDs) and plasma displays.

Gray and Kelly [134] described the use of nematic liquid crystals in Twisted Nematic Liquid Crystal Display (TN-LCD) due to the large production of LCDs utilizing this type of device. They studied the correlation between the electro-optical performances of these devices. The invention and synthesis of nematic liquid crystals with a continually improved property spectrum in order to meet constantly changing specifications was illustrated using the TN-LCD.

SCLCPs have also been used in display technology. SCLCPs materials seem to have the following possibilities: i) to be free-standing flat display, ii) to be paper-like display, iii) to be meter-size display and iv) to deposit electrodes directly on these polymers thereby obviating the need for conventional glass supporting substrates [135]. Finkelmann [136] first demonstrated that a cholesteric SCLCP could be heated above T_g , to a temperature at which it was selectively reflective to a desired wavelength of light, and then quenched below T_g , thus locking in both the helical structure of cholesteric mesophase and the required optical characteristics. This technique led to the

production of cast films or coatings for use in applications such as optical filters, reflectors or linear polarizers.

Svensson et al. [137] synthesized ferroelectric copolysiloxanes with a different molar mass to study the mechanical measurements and electro-optical switching behavior. They reported the effects of polymer molecular weight on the switching dynamics. The removal of low molecular weight components slowed down the electro-optic response time, but has no effect on mechanical properties. However, and more surprisingly, a further doubling of molecular weight did not increase the electro-optic switching time, but obviously produced a marked improvement in the mechanical properties.

CHAPTER 3 : EXPERIMENTAL

3.1. Materials

The chemicals used for the synthesise work were: 6-Hydroxy-2-napthaonic acid (Sigma-Aldrich, 98%), Acrylic acid (Sigma-Aldrich, 99%), Methacrylic acid (Sigma-Aldrich, 99%), Boric acid (Sigma-Aldrich, 99.5%), Sulphuric acid (R&M Chemicals, 98%), Hydrochloric acid (R&M Chemicals, 95%), Benzoyl peroxide (BPO) (Merck, 98%), Ethyl 2-Bromoisobutyrate (EBriB) (TCI, Japan, 98%), Copper(I) bromide (Sigma-Aldrich, 95%), (6-Chlorohexanol (Merck, 98%), 1,6-Dibromohexane (Merck, 98%), *N,N'*-dicyclohexylcarbodiimide (DCC) (Merck, 98%), Hydroquinone (Merck, 98%), *p*-Anisidine (Merck, 98%), *p*-Butoxyphenol (TCI, Japan, 95%), *p*-Dimethylaminopyridine (DMAP) (Merck, 95%), *p*-Hydroxy benzoic acid (Sigma-Aldrich, 98%), *p*-Hydroxybenzaldehyde (Merck, 98%), *p*-Phenoxyaniline (Merck, 98%), *p*-Toluenesulfonic acid (Merck, 95%), *N,N,N',N',N''*-pentamethyldiethylenetriamine (PMDETA) (Sigma-Aldrich, 98%), Potassium carbonate (R&M Chemicals), Potassium hydrogen carbonate (R&M Chemicals), Potassium hydroxide (R&M Chemicals), Sodium hydroxide (R&M Chemicals), Vanillin (Merck, 95%). They were used without further treatment.

All of the solvents such as acetonitrile, anisole, dichloromethane, diethyl ether, *n*-hexane, isopropanol, petroleum ether (40–60°C), tetrahydrofuran (THF) and toluene were reagent grades and purchased from Merck, Friendemann Schmidt Chemicals and J. T. Baker. Acetone, *N,N*-dimethylformamide (DMF), methanol, and ethanol were distilled to keep anhydrous before used.

Copper (I) bromide catalyst was purified successively by stirring in acetic acid and ethanol, and then dried. Benzoyl peroxide (BPO) was recrystallized twice from absolute ethanol and dried under vacuum at 40°C before used.

3.2. Synthesis of liquid crystal monomers

In this work, several polymerizable liquid crystal monomers with similar general structure but with variations in mesogenic structure, lateral substituent and polymerizable terminal substituent were synthesized. The procedure, synthetic route as well as chemical structure identification by ^1H NMR and ^{13}C NMR were listed for all the synthesized compounds and monomers.

3.2.1. Synthesis of monomer M1

4-butoxyphenyl 6-hydroxynaphthalene-2-carboxylate (1)

In a 250 ml two-necked reaction flask equipped with a magnetic stirrer, *p*-butoxyphenol (5.0 g, 0.03 mol) and 6-hydroxy-2-naphthoic acid (4.5 g, 0.023 mol) were added in 50 ml dried toluene. Concentrated sulphuric acid (0.2 g, 0.002 mol) and boric acid (1.32 g, 0.002 mol) were added subsequently. The mixture was then refluxed for 48 hours using Dean-Stark trap to remove the produced water. After completion of the reaction, the solvent was removed under reduced pressure and the product was washed with a mixture of petroleum ether (40-60°C) and *n*-hexane (1:1). Acetonitrile was then added into the reaction mixture and heated to dissolve the product. The insoluble solid was then removed by hot filtration. The filtrate was then kept at 0°C for 12 hours and the solid was filtered. The solid was again dissolved in hot toluene and filtered to remove unreacted 6-hydroxy-2-naphthoic acid. The filtrate was then kept at 0°C for 12 hours and the product was filtered to get white crystal product. The product was dried at 40°C under vacuum with 40% yield. $T_m=180^\circ\text{C}$.

^1H NMR, δ (ppm, DMSO- d_6 , 400 MHz) 10.3 (H, s, Np-OH), 8.7 (H, s, Np-H), 7.8-8.1 (3H, m, Np-H), 7.2 (4H, m, Ph-H), 7.0 (2H, m, Ph-H), 3.9 (t, 2H, -OCH₂-), 1.65-1.72 (m, 2H, -CH₂-), 1.39-1.48 (m, 2H, -CH₂-), 0.89-0.94 (m, 3H, -CH₃). ^{13}C NMR, δ (ppm, DMSO- d_6 , 400 MHz) 165.2 (-OC=O), 158.2 (aromatic C-O(CH₂)₆), 156.2

(aromatic $-C-OC_4H_9$) 141.0 (aromatic $-C-OC=O$), 136.2, 131.6, 127.0, 126.2 (aromatic C), 130.3, 126.3, 122.5 (aromatic C *ortho* to $-OC=O$), 125.1 (aromatic C-COO), 120.0, 106.5 (aromatic C *ortho* to $-OH$), 115.1, (aromatic C *ortho* to $-OC_4H_9$), 68.1 (aromatic $-OCH_2-$), 30.5, 18.5 ($-CH_2-$), 13.4 ($-CH_3$).

Synthesis of 4-butoxyphenyl 6-(6-bromohexyloxy)-2-naphthoate (2)

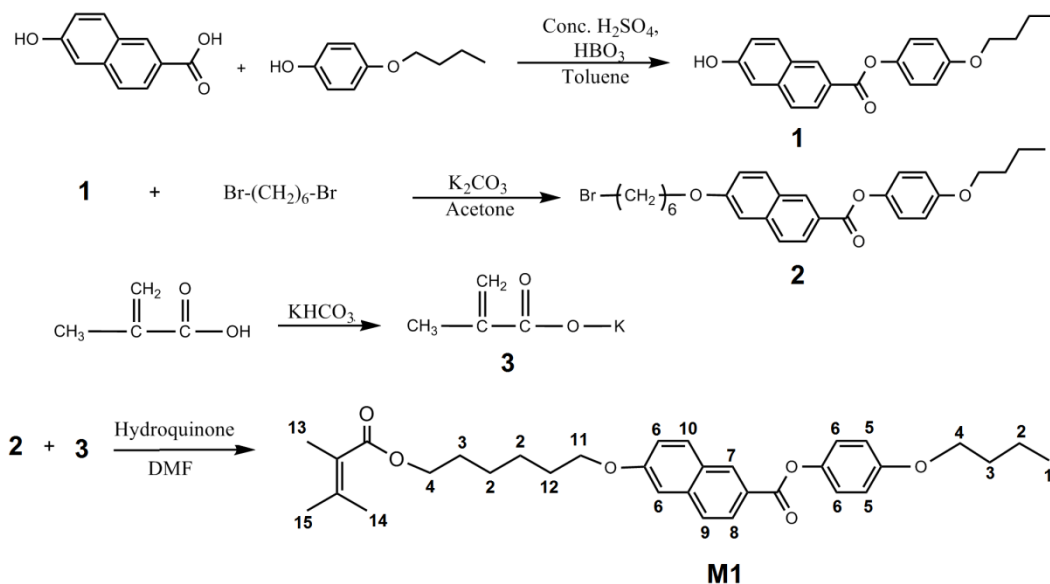
In a 250 ml two-necked reaction flask equipped with a magnetic stirrer, a mixture of compound 1 (6.46 g, 0.02 mol), 1,6-dibromohexane (48.79 g, 0.20 mol), potassium carbonate (2.76 g, 0.02 mol) and distilled acetone (50 ml) was refluxed under stirring for 24 hours. After the reaction was stopped, the reaction mixture was filtered and the precipitate washed thoroughly with acetone. The acetone was then removed under reduced pressure. After removing solvent, a mixture of petroleum ether (40–60°C) and *n*-hexane (1:1) was added. The precipitate was filtered off and recrystallized twice from ethanol with hot filtration. The resulting white solid products were dried under vacuum at 50°C. The product yield of compound 2 was 80%. T_m : 80°C.

1H NMR, δ (ppm, $CDCl_3$, 400 MHz) 8.69 (s, 1H, Np-H), 8.13-8.16 (dd, 1H, Np-H), 7.78-7.93 (dd, 2H, Np-H), 7.14-7.24 (m, 4H, Ar-H), 6.93-7.00 (m, 2H, Ph-H), 4.11-4.14 (t, 2H, $-OCH_2-$), 3.97-4.00 (t, 2H, $-CH_2-Br$), 3.43-3.47 (t, 2H, Ar- CH_2-), 1.86-1.97 (m, 4H, $-CH_2-$), 1.76-1.83 (m, 2H, $-CH_2-$) 1.4-1.5 (m, 6H, $-CH_2-$), 0.89-0.94 (m, 3H, $-CH_3$). ^{13}C NMR, δ (ppm, DMSO- d_6 , 400 MHz) 165.2 ($-OC=O$), 158.2 (aromatic C- $O(CH_2)_6$), 156.2 (aromatic $-C-OC_4H_9$) 141.0 (aromatic $-C-OC=O$), 136.2, 131.6, 127.0, 126.2 (aromatic C), 130.3, 126.3, 122.5 (aromatic C *ortho* to $-OC=O$), 125.1 (aromatic C-COO), 120.0, 106.5 (aromatic C *ortho* to $-O(CH_2)_6$), 115.1, (aromatic C *ortho* to $-OC_4H_9$), 68.1 (aromatic $-OCH_2-$), 33.8 ($-BrCH_2-$), 32.7, 31.4, 29.0, 27.9, 25.4, 19.3($-CH_2-$), 13.9 ($-CH_3$).

Synthesis of 4-butoxyphenyl 6-(6-(methacryloyloxy)hexyl)-2-naphthoate (Monomer M1)

In a 250 ml two-necked reaction flask, methacrylic acid (0.29 g, 3.35 mmol) was added slowly to potassium hydrogen carbonate (0.335 g, 3.35 mmol) at room temperature to form potassium methacrylate. A solution of compound 2 (1.08 g, 2.24 mmol) and hydroquinone (0.0027 g, 0.025 mmol) in DMF (50 ml) was added slowly into the previously prepared potassium methacrylate solution. The reaction mixture was heated at 100°C for 24 hours with continuous stirring. After completion of the reaction, the solvent was removed under vacuum followed by addition of 100 ml water at room temperature. The solid was again filtered and dissolved in dichloromethane. The organic phase was washed twice by 5% NaOH solution and twice by distilled water, followed by solvent removal under reduced pressure. The solid was filtered and recrystallized twice from ethanol. The resulting white solid products were dried under vacuum at 40°C. The product yield of **M1** was 35%.

¹H NMR, δ (ppm, CDCl₃, 400 MHz) 8.61 (s, H, Np-H), 8.05-8.08 (dd, 1H, Np-H), 7.70-7.81 (dd, 2H, Np-H), 7.05-7.15 (m, 4H, Ar-H), 6.85-6.89 (m, 2H, Ph-H), 6.03 (H, s, =CH₂), 5.46 (m, H, =CH₂) 4.09-4.12 (t, 2H, -OCH₂-), 4.02-4.06 (t, 2H, Ph-CH₂-), 3.88-3.92 (t, 2H, Ar-CH₂-), 1.86-1.87 (t, 3H, -CH₃) 1.78-1.85 (m, 2H, -CH₂-), 1.63-1.74 (m, 4H, -CH₂-) 1.4-1.5 (m, 6H, -CH₂-), 0.89-0.94 (t, 3H, -CH₃). ¹³C NMR, δ (ppm, DMSO-*d*₆, 400 MHz) 167.0, 165.5 (-OC=O), 159.4 (aromatic C-O(CH₂)₆), 156.9 (aromatic -C-OC₄H₉) 144.5.0 (aromatic -C-OC=O), 137.7, 136.5, 126.0, 125.9 (aromatic C), 131.6, 124.3, 123.5 (aromatic C *ortho* to -OC=O), 123.1 (aromatic C-COO), 120.4, 107.1 (aromatic C *ortho* to -O(CH₂)₆), 125.0 (CH₂=C-), 115.4 (aromatic C *ortho* to -OC₄H₉), 68.2, 68.0 (aromatic -OCH₂-), 64.7 (-CH₂-OCO), 31.2, 29.0, 28.5, 25.7, 19.2, 19.3 (-CH₂-), 18.4, 14.1 (-CH₃).



Scheme 3.1 : Synthetic route of monomer **M1**.

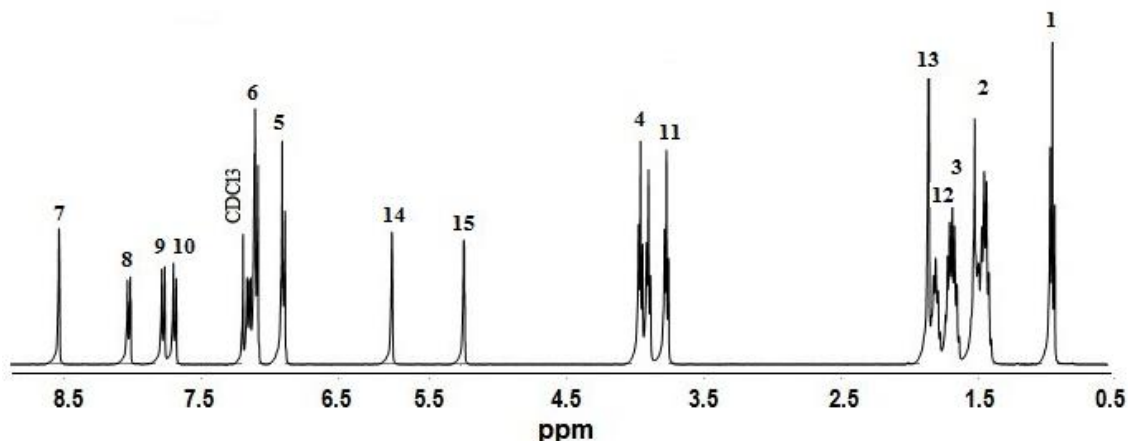


Figure 3.1 : ^1H NMR spectra of monomer **M1**.

3.2.2. Synthesis of monomer **M2** and **M3**

Synthesis of 4-(6-Hydroxyhexyloxy)benzoic acid (3)

In a 250 ml two-necked reaction flask equipped with a magnetic stirrer, *p*-hydroxy benzoic acid (10.0 g, 0.07 mol) was dissolved in a mixture of ethanol (30 ml) and water (20 ml) along with potassium hydroxide (11 g, 0.19 mol) and a pinch of potassium iodide. While stirring vigorously, 6-chlorohexanol (9.0 g, 0.07 mol) was added slowly to the mixture at room temperature. Then the mixture was refluxed while stirring for 24 hours. After completion of the reaction, the solvent was then removed under reduced

pressure and the solid residue was dissolved in water (120 ml) and washed with diethyl ether (3 x 30 ml). The aqueous layer was acidified with concentrated HCl until the pH was 2. The white solid was filtered, washed with water and recrystallized twice from ethanol. The product was dried under vacuum at 50°C and the product yield was 55%. $T_m = 139-140^\circ\text{C}$.

^1H NMR, δ (ppm, DMSO- d_6 , 400 MHz): 12.6 (s, 1H, -COOH), 7.81-7.90 (d, 2H, Ar-H), 6.79-7.03 (d, 2H, Ar-H), 4.35 (1H, -OH), 4.01 (m, 2H, -CH₂OPh), 1.7 (m, 2H, -OCH₂-), 1.3-1.45 (m, 8H, -CH₂). ^{13}C NMR, δ (ppm, DMSO- d_6 , 400 MHz): 166.9 (-COOH), 162.2 (aromatic C-(CH₂)₆), 131.2 (aromatic C *ortho* to -COOH), 122.7 (aromatic C-COOH), 114.1 (aromatic C *ortho* to -(CH₂)₆), 67.6 (-CH₂OH), 60.6 (-Ar-OCH₂-), 32.4, 28.5, 25.3, 25.2 (-CH₂-).

Synthesis of 4-(6-Acryloyloxyhexyloxybenzoic acid (4))

In a 250 ml two-necked reaction flask equipped with a magnetic stirrer, a mixture of compound 3 (2.5 g, 0.01 mol), acrylic acid (3 ml, 0.04 mol), *p*-toluenesulfonic acid (0.7 g, 0.004 mol), and hydroquinone (0.24 g, 0.002 mol) were dissolved in 50 ml toluene. The mixture was then refluxed for 6 hours using Dean-Stark trap to remove the reduced water. After completion of the reaction, the cooled reaction mixture was diluted with a 3 to 4 fold excess of diethyl ether, and washed with warm water to remove unreacted acrylic acid. The organic layer was dried over NaSO₄. After filtration, the solvent was removed under reduced pressure. The white solid was recrystallized from isopropanol and dried at 40°C under vacuum to give 82% yield of compound 4.

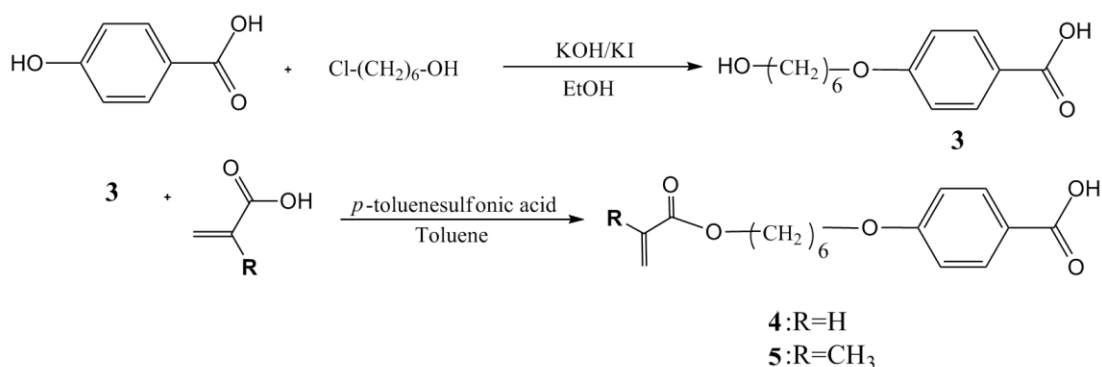
^1H NMR, δ (ppm, DMSO- d_6 , 400 MHz): 12.6 (s, 1H, -COOH), 7.80-8.04 (d, 2H, Ar-H), 6.93-7.12 (d, 2H, Ar-H), 6.24, 5.92 (d, 1H, CH₂=CH), 6.14 (q, 1H, CH), 4.0-4.11 (m, 4H, -OCH₂-), 1.68-1.73 (m, 2H, -OCH₂CH₂-), 1.59-1.65 (m, 2H, -CH₂), 1.37-1.43 (m, 4H, -(CH₂)₂-). ^{13}C NMR, δ (ppm, DMSO- d_6 , 400 MHz): 166.9 (-

COOH), 165.4 (–OC=O) 162.2 (aromatic C–(CH₂)₆), 131.2 (aromatic C *ortho* to –COOH), 128.3 (HC=C–), 127.9 (HC=C–), 122.7 (aromatic C–COOH), 114.1 (aromatic C *ortho* to –(CH₂)₆), 67.6 (–CH₂O–), 60.6 (–OCH₂–), 28.3, 27.9, 25.07, 25.03 (–CH₂–).

Synthesis of 4-(6-Methacryloyloxyhexyloxybenzoic acid (5))

A mixture of compound 3 (2.5 g, 0.01 mol), methacrylic acid (3 ml, 0.04 mol), *p*-toluenesulfonic acid (0.7 g, 0.004 mol), and hydroquinone (0.24 g, 0.002 mol) were dissolved in 50 ml toluene. The mixture was then refluxed for 4 hours in a two-necked reaction flask equipped with a magnetic stirrer using Dean-Stark trap to remove the reduced water. The rest of the succeeding steps were identical to the ones described for the synthesis of compound 4. The product yield of compound 5 was 82%.

¹H NMR, δ (ppm, DMSO-*d*₆, 400 MHz): 12.6 (1H, –COOH), 7.80-7.90 (d, 2H, Ar–H), 6.93-7.03 (d, 2H, Ar–H), 5.99, 5.64 (s, 1H, CH₂=C(CH₃)–), 3.98-4.35 (m, 4H, –OCH₂–), 1.89 (t, 3H, CH₂=C(CH₃)–), 1.68-1.85 (m, 2H, –OCH₂CH₂–), 1.59-1.66 (m, 2H, –CH₂), 1.38-1.43 (m, 4H, –(CH₂)₂–). ¹³C NMR, δ (ppm, DMSO-*d*₆, 400 MHz): 166.9 (–COOH), 166.5 (–OC=O) 162.2 (aromatic C–O(CH₂)₆), 135.9 (H₃C–C=C–), 131.2 (aromatic C *ortho* to –COOH), 125.4 (H₃C–C=C–), 122.5 (aromatic C–COOH), 114.5 (aromatic C *ortho* to –O(CH₂)₆), 67.6 (–CH₂O–), 64.1 (–Ar–OCH₂–), 28.3, 27.9, 25.1, 25.0 (–CH₂–), 17.9 (–CH₃).

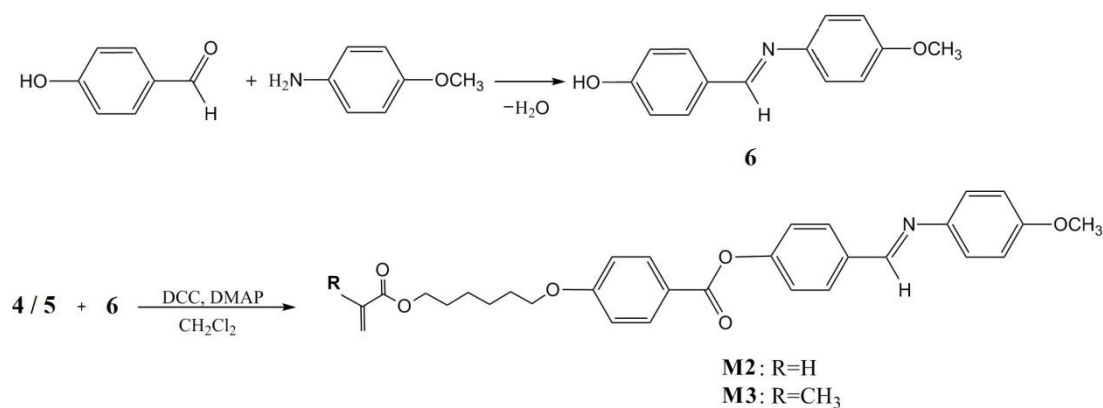


Scheme 3.2 : Synthetic route of compound 3, 4 and 5.

Synthesis of 4-[(E)-N-(4-methoxyphenyl)carboximidoyl]phenol (**6**)

In a 250 ml two-necked reaction flask equipped with a magnetic stirrer, a mixture of *p*-hydroxybenzaldehyde (2.4 g, 0.02 mol) and distilled ethanol (100 ml) was refluxed for 30 minutes. A solution of *p*-anisidine (2.5 g, 0.02 mmol) dissolved in methanol (20 ml) was then added through a dropping funnel attached to the reaction flask within 15 minutes. This was followed by the addition of 2-3 drops of glacial acetic acid. Refluxing of the mixtures was allowed to continue for 2 hours with magnetic stirring. After completion of the reaction, the solvent was removed by vacuum drying. The solid obtained was redissolved in ethanol, and then water was added drop-wise to the solution until crystals were formed. The resulting yellowish crystals were separated by simple filtration and dried under vacuum at 50°C. The product yield of compound **6** was 80%. T_m : 80°C.

^1H NMR, δ (ppm, DMSO- d_6 , 400 MHz): 10.03 (s, 1H, OH), 8.45 (1H, s, CH=N), 7.72-7.74 (d, 2H, Ar-H), 7.19-7.21 (d, 2H, Ar-H), 6.84-6.94 (dd, 4H, Ar-H), 2.49 (s, 3H, -OCH₃). ^{13}C NMR, δ (ppm, DMSO- d_6 , 400 MHz): 160.2 (aromatic C-OH), 157.8 (CH=N), 157.3 (aromatic C-OCH₃), 144.6 (aromatic C-N=CH), 130.2 (aromatic C *ortho* to -CH=N-), 127.7 (aromatic C-CH=N), 122.0 (aromatic C *ortho* to -N=CH-), 115.5 (aromatic C *ortho* to C-OH), 114.3 (aromatic C *ortho* to -OCH₃), 55.2 (O-CH₃).



Scheme 3.3 : Synthetic route of monomer **M2** and monomer **M3**.

Synthesis of 4-[(E)-N-(4-methoxyphenyl)carboximidoyl]phenyl 4-[[6-(prop-2-enoyloxy)hexyl]oxy]benzoate (M2)

Compound **4** (1.46 g, 0.005mol) and compound **6** (1.14 g, 0.005mol) were dissolved in minimal amounts of THF in a 250 ml Erlenmeyer conical flask. *p*-dimethylaminopyridine (DMAP) (0.061 g, 0.0005 mol) and *N,N'*-dicyclohexylcarbodiimide (DCC) (1.0 g, 0.005 mmol) dissolved in 80 ml of dichloromethane was then poured into the flask and the solution mixture was allowed to stir for 1 hour at 0°C. The mixture was stirred for another 24 hours at room temperature before the reaction was stopped. The solvent was then removed under reduced pressure. Ethanol and *n*-hexane mixture (1:1) was added to the dry residue. It was then kept at 0°C in a refrigerator for 12 hours to crystallize. To increase the purity, the product was re-crystallized again in ethanol. The resulting yellowish crystals were separated by simple filtration and dried under vacuum at 50°C. The product yield of **M2** was 55%.

¹H NMR, δ (ppm, DMSO-*d*₆, 400 MHz): 8.66 (s, 1H, CH=N), 8.00-8.09 (d, 4H, Ar-H), 7.29-7.41 (d, 4H, Ar-H), 6.97-7.12 (d, 4H, Ar-H), 6.28-6.33 (d, 1H, CH₂=CH), 6.13-6.20 (dd, 1H, CH), 5.91-5.93 (d, 1H, CH₂=CH), 4.01-4.12 (q, 4H, -OCH₂-), 3.77 (s, 1H, -OCH₃), 1.73-1.77 (m, 2H, -OCH₂CH₂-), 1.60-1.67 (m, 2H, -CH₂), 1.39-1.45 (m, 4H, -(CH₂)₂-). ¹³C NMR, δ (ppm, DMSO-*d*₆, 400 MHz): 166.5, 164.0 (-OC=O) 163.7 (-CH=N), 158.5 (aromatic C-O(CH₂)₆), 156.8, (aromatic C-OCH₃), 153.3 (aromatic C-OC=O), 144.6 (aromatic C-N=CH), 134.4(aromatic C-CH=N), 132.0, 122.2 (aromatic C *ortho* to -COO-), 129.9 (HC=C-), 128.6 (H₂C=C-), 129.4 (aromatic C *ortho* to -N=CH-), 122.2 (aromatic C *ortho* to -CH=N-), 122.2 (aromatic C *ortho* to -COO-), 121.2 (aromatic C-COO-), 114.4 (aromatic C *ortho* to -OCH₃), 114.2 (aromatic C *ortho* to C-O(CH₂)₆), 68.1 (-CH₂O-), 63.9 (-OCH₂-), 54.8 (-OCH₃), 28.3, 27.9, 25.1, 25.0(-CH₂-).

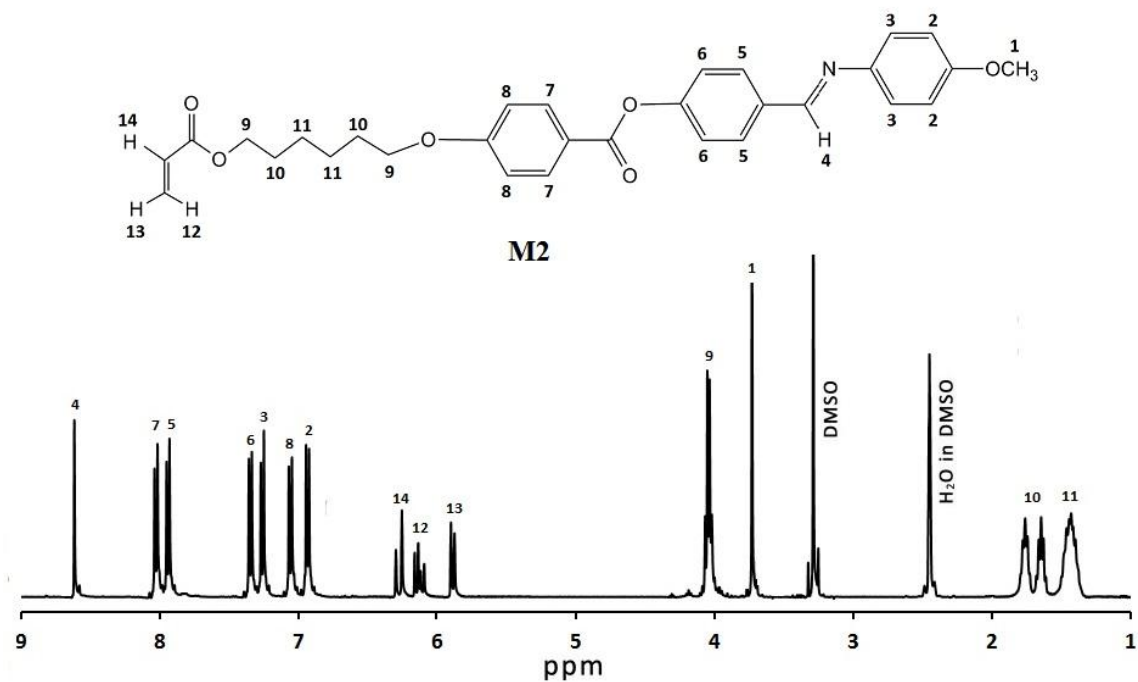


Figure 3.2 : ^1H NMR spectra of monomer **M2**.

Synthesis of 4-[(E)-N-(4-methoxyphenyl)carboximidoyl]phenyl 4-[(6-[(2-methylprop-2-enyl)oxy]hexyl)oxy]benzoate (**M3**)

Compound **5** (1.5 g, 0.005mol) and compound **6** (1.14 g, 0.005mol) were dissolved in minimal amounts of THF in a 250 ml Erlenmeyer conical flask. The rest of the succeeding steps were identical to the ones described for the synthesis of monomer **M2**. The product yield of monomer **M3** was 60%.

^1H NMR, δ (ppm, $\text{DMSO-}d_6$, 400 MHz): 8.72 (s, 1H, CH=N), 7.85-8.18 (d, 4H, Ar-H), 7.32-7.56 (d, 4H, Ar-H), 6.99-7.21 (d, 4H, Ar-H), 6.07, 5.71 (s, 1H, $\text{CH}_2=\text{C}(\text{CH}_3)-$), 4.08-4.19 (q, 4H, $-\text{OCH}_2-$), 3.39 (s, 1H, $-\text{OCH}_3$), 1.89 (s, 3H, $\text{CH}_2=\text{C}(\text{CH}_3)-$), 1.73-1.77 (m, 2H, $-\text{OCH}_2\text{CH}_2-$), 1.60-1.67 (m, 2H, $-\text{CH}_2$), 1.39-1.45 (m, 4H, $-(\text{CH}_2)_2-$). ^{13}C NMR, δ (ppm, $\text{DMSO-}d_6$, 400 MHz): 166.5, 163.9 ($-\text{OC}=\text{O}$) 163.2 (CH=N), 157.9 (aromatic C-O(CH_2)₆), 157.2 (aromatic C-OCH₃), 152.7 (aromatic C-OC=O), 143.9 (aromatic C-N=CH), 135.9 ($\text{H}_3\text{C}-\text{C}=\text{C}-$), 133.9 (aromatic C-CH=N), 132.0 (aromatic C ortho to $-\text{COO}-$), 129.5 (aromatic C ortho to $-\text{N}=\text{CH}-$), 125.4 ($\text{H}_2\text{C}=\text{C}-$), 122.4 (aromatic C ortho to $-\text{CH}=\text{N}-$), 122.3 (aromatic C ortho to

COO), 120.5 (aromatic C–COO–), 114.6 (aromatic *C ortho* to –OCH₃), 114.3 (aromatic *C ortho* to C–O(CH₂)₆), 67.8 (–Ar–OCH₂–), 64.1 (–CH₂O–), 55.2 (–OCH₃), 28.3, 27.9, 25.1, 25.0 (–CH₂–) 17.9 (–CH₃).

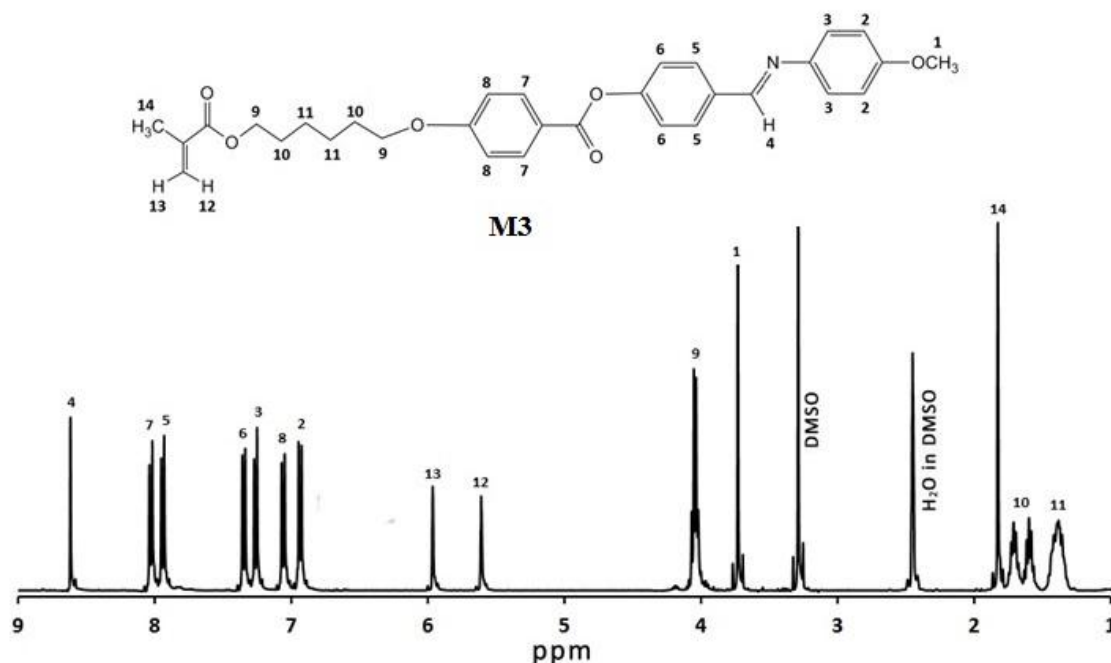


Figure 3.3 : ¹H NMR spectra of monomer **M3**.

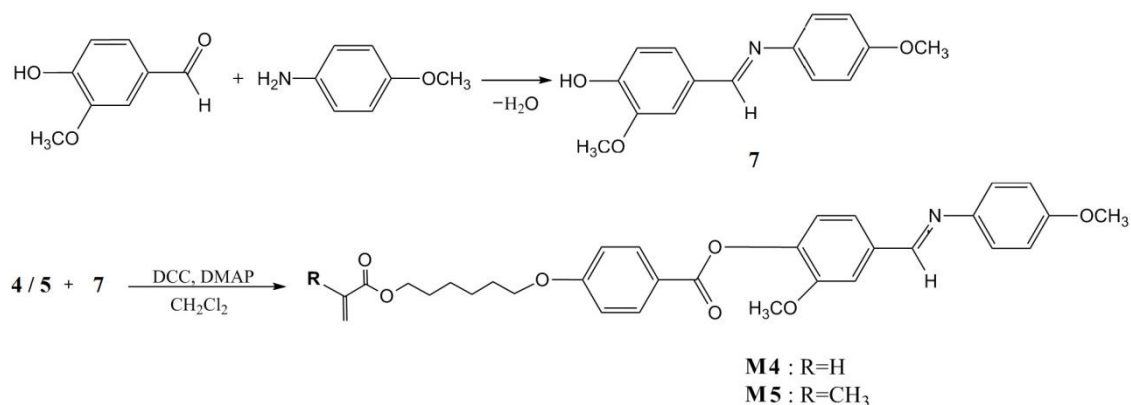
3.2.3. Synthesis of monomer **M4** and **M5**

Synthesis of 2-methoxy-4-[(*E*)-*N*-(4-methoxyphenyl)carboximidoyl]phenol (**7**)

A mixture of vanillin (3.16 g, 0.02 mol) and distilled ethanol (100 ml) was refluxed for 30 minutes in a two-necked reaction flask equipped with a magnetic stirrer. The rest of the succeeding steps were identical to the ones described for the synthesis of compound **6**. The product yield of compound **7** was 80%. *T*_m: 70°C

¹H NMR, δ (ppm, Acetone-*d*₆, 400 MHz): 8.45 (s, 1H, CH=N), 8.20 (s, 1H, OH), 7.60 (d, 1H, Ar–H), 7.33–7.35 (dd, 1H, Ar–H), 7.20–7.23 (dd, 2H, Ar–H), 6.91–6.96 (m, 3H, Ar–H), 3.98 (s, 3H, –OCH₃), 3.84 (s, 3H, –OCH₃). ¹³C NMR, δ (ppm, CDCl₃, 400 MHz) 158.4 (CH=N), 158.0, 147.1 (aromatic C–OCH₃), 148.8 (aromatic C–OH), 145.2 (aromatic C–N=CH), 129.4 (aromatic C–CH=N), 125.0, 108.4 (aromatic *C ortho* to –

CH=N-), 122.1 (aromatic *C ortho* to -N=CH-), 114.4 (aromatic *C ortho* to -OCH₃), 114.2 (aromatic *C ortho* to C-OH), 56.1, 55.5 (-OCH₃).



Scheme 3.4 : Synthetic route of monomer **M4** and monomer **M5**.

Synthesis of 2-methoxy-4-[(*E*)-*N*-(4-methoxyphenyl)carboximidoyl]phenyl 4-[[6-(prop-2-enyloxy)hexyl]oxy]benzoate (**M4**)

Compound **4** (1.46 g, 0.005 mol) and compound **7** (1.28 g, 0.005 mmol) were dissolved in minimal amounts of THF in a 250 ml Erlenmeyer conical flask. The rest of the succeeding steps were identical to the ones described for the synthesis of monomer **M2**. The product yield of monomer **M4** was 63%.

¹H NMR, δ (ppm, DMSO-*d*₆, 400 MHz): 8.64 (s, 1H, CH=N), 8.04-8.06 (d, 2H, Ar-H), 7.70 (s, 1H, Ar-H), 7.51-7.53 (d, 1H, Ar-H), 7.29-7.35 (q, 3H, Ar-H), 7.09-7.11 (d, 2H, Ar-H), 6.97-6.99 (d, 2H, Ar-H), 6.29-6.33 (d, 1H, CH₂=CH), 6.12-6.19 (dd, 1H, CH), 5.91-5.93 (d, 1H, CH₂=CH), 4.01-4.12 (q, 4H, -OCH₂-), 3.83 (s, 1H, -OCH₃), 3.77 (s, 1H, -OCH₃), 1.73-1.77 (m, 2H, -OCH₂CH₂-), 1.60-1.67 (m, 2H, -CH₂), 1.39-1.45 (m, 4H, -(CH₂)₂-). ¹³C NMR, δ (ppm, DMSO-*d*₆, 400 MHz): 166.5, 163.4 (-OC=O) 163.2 (CH=N), 157.9 (aromatic C-O(CH₂)₆), 157.5, 151.3 (aromatic C-OCH₃), 143.9 (aromatic C-N=CH), 141.7 (aromatic -COC=O), 135.2 (aromatic C-CH=N), 132.0, 123.4 (aromatic *C ortho* to -COO-), 131.2 (HC=C-), 128.3 (H₂C=C-), 122.4 (aromatic *C ortho* to -N=CH-), 121.9, 110.9 (aromatic *C ortho* to -CH=N-),

120.3 (aromatic C–COO–), 114.6 (aromatic C *ortho* to –OCH₃), 114.4 (aromatic C *ortho* to C–O(CH₂)₆), 67.8 (–CH₂O–), 64.0 (–Ar–OCH₂–), 55.8, 55.2 (–OCH₃), 28.3, 28.0, 25.1, 25.0 (–CH₂–).

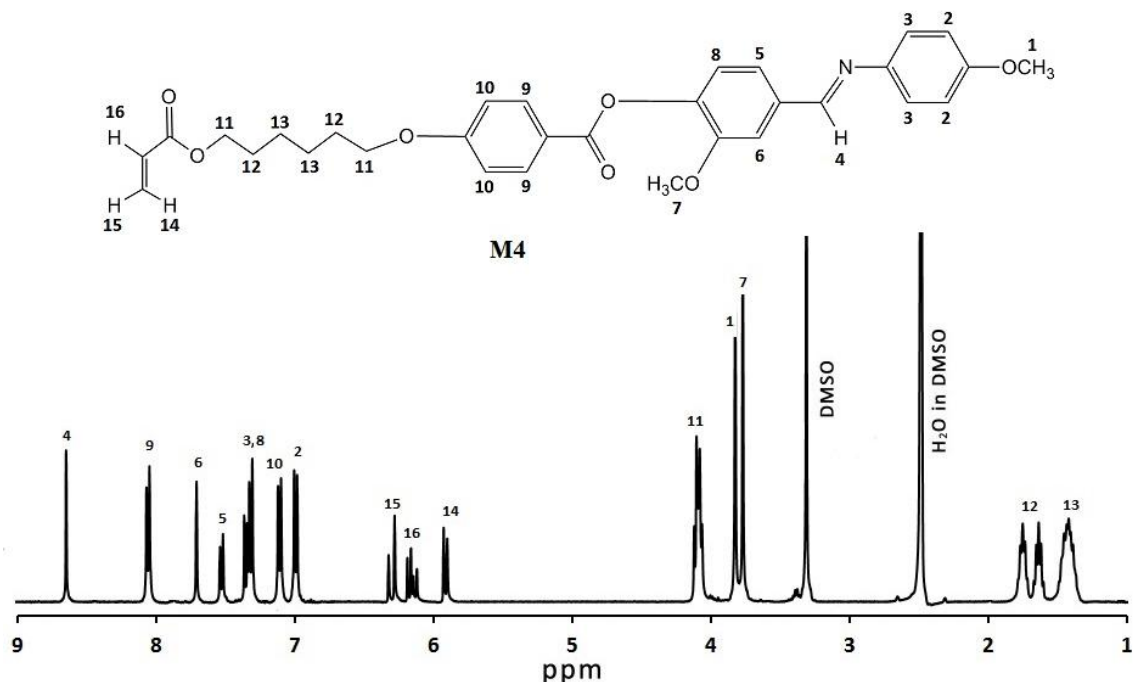


Figure 3.4 : ¹H NMR spectra of monomer **M4**.

Synthesis of 2-methoxy-4-[(E)-N-(4-methoxyphenyl)carboximidoyl]phenyl 4-((6-[(2-methylprop-2-enyl)oxy]hexyl)oxy)benzoate (**M5**)

Compound **5** (1.5 g, 0.005 mol) and compound **7** (1.28 g, 0.005 mmol) were dissolved in minimal amounts of THF in a 250 ml Erlenmeyer conical flask. The rest of the succeeding steps were identical to the ones described for the synthesis of monomer **M2**. The product yield of monomer **M5** was 67%.

¹H NMR, δ (ppm, DMSO-*d*₆, 400 MHz): 8.64 (s, 1H, CH=N), 8.04-8.06 (d, 2H, Ar-H), 7.70 (s, 1H, Ar-H), 7.51-7.53 (d, 1H, Ar-H), 7.29-7.35 (q, 3H, Ar-H), 7.09-7.11 (d, 2H, Ar-H), 6.97-6.99 (d, 2H, Ar-H), 6.00, 5.65 (s, 1H, CH₂=C(CH₃)–), 4.01-4.11 (q, 4H, –OCH₂–), 3.83 (s, 3H, –OCH₃), 3.77 (s, 3H, –OCH₃), 1.86 (s, 3H, CH₂=C(CH₃)–), 1.73-1.77 (m, 2H, –OCH₂CH₂–), 1.60-1.67 (m, 2H, –CH₂–), 1.39-1.45

(m, 4H, $-(\text{CH}_2)_2-$). ^{13}C NMR, δ (ppm, $\text{DMSO}-d_6$, 400 MHz): 166.5, 163.4 ($-\text{OC}=\text{O}$) 163.2 ($\text{CH}=\text{N}$), 157.9 (aromatic $\text{C}-\text{O}(\text{CH}_2)_6$), 157.5, 151.3 (aromatic $\text{C}-\text{OCH}_3$), 143.9 (aromatic $\text{C}-\text{N}=\text{CH}$), 141.7 (aromatic $-\text{C}-\text{OC}=\text{O}$), 135.9 ($\text{H}_3\text{C}-\text{C}=\text{C}-$), 135.2 (aromatic $\text{C}-\text{CH}=\text{N}$), 132.0, 123.4 (aromatic C *ortho* to $-\text{COO}-$) 125.4 ($\text{H}_2\text{C}=\text{C}-$), 122.4 (aromatic C *ortho* to $-\text{N}=\text{CH}-$), 121.9, 110.9 (aromatic C *ortho* to $-\text{CH}=\text{N}-$), 120.3 (aromatic $\text{C}-\text{COO}-$), 114.6 (aromatic C *ortho* to $-\text{OCH}_3$), 114.4 (aromatic C *ortho* to $\text{C}-\text{O}(\text{CH}_2)_6$), 67.8 ($-\text{CH}_2\text{O}-$), 64.1 ($-\text{Ar}-\text{OCH}_2-$), 55.8, 55.2 ($-\text{OCH}_3$), 28.3, 27.9, 25.1, 25.0 ($-\text{CH}_2-$), 17.9 ($-\text{CH}_3$).

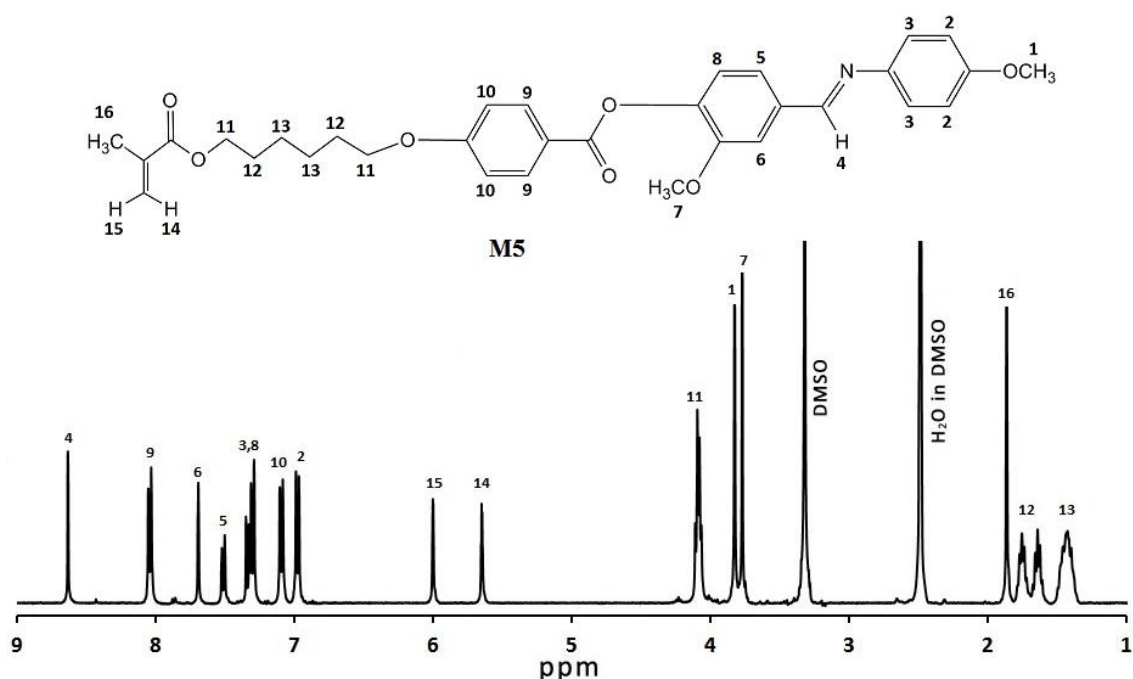


Figure 3.5 : ^1H NMR spectra of monomer **M5**.

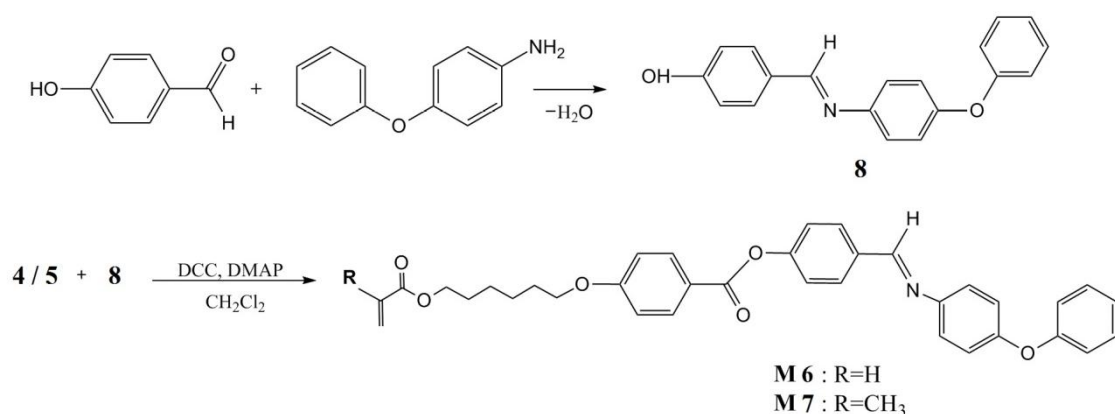
3.2.4. Synthesis of monomer **M6** and **M7**

Synthesis of 4-[(*E*)-*N*-(4-phenoxyphenyl)carboximidoyl]phenol (**8**)

A mixture of *p*-hydroxybenzaldehyde (2.4 g, 0.02 mol) and distilled ethanol (100 ml) was refluxed for 30 minutes in a two-necked reaction flask equipped with a magnetic stirrer. A solution of *p*-phenoxyaniline (3.8 g, 0.02 mol) dissolved in methanol (20 ml) was then added through a dropping funnel attached to the reaction flask within

15 minutes. The rest of the succeeding steps were identical to the ones described for the synthesis of compound **6**. The product yield of compound **8** was 80%. T_m : 80°C.

^1H NMR, δ (ppm, DMSO- d_6 , 400 MHz): 10.11 (s, 1H, OH), 8.52 (s, 1H, CH=N), 7.74-7.76 (d, 2H, Ar-H), 7.36-7.43 (t, 2H, Ar-H), 7.24-7.26 (d, 2H, Ar-H), 7.09-7.11 (t, 1H, Ar-H), 6.99-7.03 (m, 4H, Ar-H), 6.86-6.88 (d, 2H, Ar-H). ^{13}C NMR, δ (ppm, DMSO- d_6 , 400 MHz): 161.0 (aromatic C-OH), 159.9 (CH=N), 157.5, 154.8 (aromatic C-O-Ar), 148.0 (aromatic C-N=CH), 131.1 (aromatic C *ortho* to -CH=N-), 130.5, 123.8 (aromatic C), 128.0 (aromatic C-CH=N), 123.0 (aromatic C *ortho* to -N=CH-), 120.0, 118.8 (aromatic C *ortho* to C-O-Ar), 116.1 (aromatic C *ortho* to C-OH).



Scheme 3.5 : Synthetic route of monomer **M6** and monomer **M7**.

Synthesis of 4-[(E)-N-(4-phenoxyphenyl)carboximidoyl]phenyl 4-[[6-(prop-2-enoyloxy)hexyl]oxy]benzoate (**M6**)

Compound **4** (1.46 g, 0.005 mol) and compound **8** (1.44 g, 0.005 mol) were dissolved in minimal amounts of THF in a 250 ml Erlenmeyer conical flask. The rest of the succeeding steps were identical to the ones described for the synthesis of monomer **M2**. The product yield of monomer **M6** was 55%.

^1H NMR, δ (ppm, DMSO- d_6 , 400 MHz): 8.68 (s, 1H, CH=N), 7.99-8.09 (dd, 4H, Ar-H), 7.39-7.43 (m, 4H, Ar-H), 7.34-7.37 (d, 2H, Ar-H), 7.14-7.17 (t, 1H, Ar-H), 7.11-7.12 (d, 2H, Ar-H), 7.05-7.08 (d, 2H, Ar-H), 7.03-7.05 (d, 2H, Ar-H), 6.29-6.33 (d, 1H, CH₂=CH), 6.12-6.19 (dd, 1H, CH), 5.91-5.91 (d, 1H, CH₂=CH), 4.06-4.11 (q, 4H, -OCH₂-), 1.73-1.77 (m, 2H, -OCH₂CH₂-), 1.60-1.67 (m, 2H, -CH₂), 1.39-1.45 (m, 4H, -(CH₂)₂-). ^{13}C NMR, δ (ppm, DMSO- d_6 , 400 MHz): 166.0, 164.5 (-OC=O) 163.8 (CH=N), 159.4 (aromatic C-O(CH₂)₆), 157.4, 155.4 (aromatic C-O-Ar), 153.5 (aromatic -COO), 147.2 (aromatic C-N=CH), 134.3 (aromatic C-CH=N), 132.6 (aromatic C *ortho* to -COO-), 130.6 (aromatic C *ortho* to -CH=N-), 130.3 (aromatic C), 131.9 (HC=C-), 128.9 (H₂C=C-), 123.9 (aromatic C), 123.3, (aromatic C *ortho* to -COO-), 123.0 (aromatic C *ortho* to -N=CH-), 121.0 (aromatic C-COO-), 119.9, 118.9 (aromatic C *ortho* to C-O-Ar), 115.2 (aromatic C *ortho* to C-O(CH₂)₆), 68.4(-CH₂O-), 64.5 (-Ar-OCH₂-), 28.8, 28.5, 25.6, 25.7(-CH₂-).

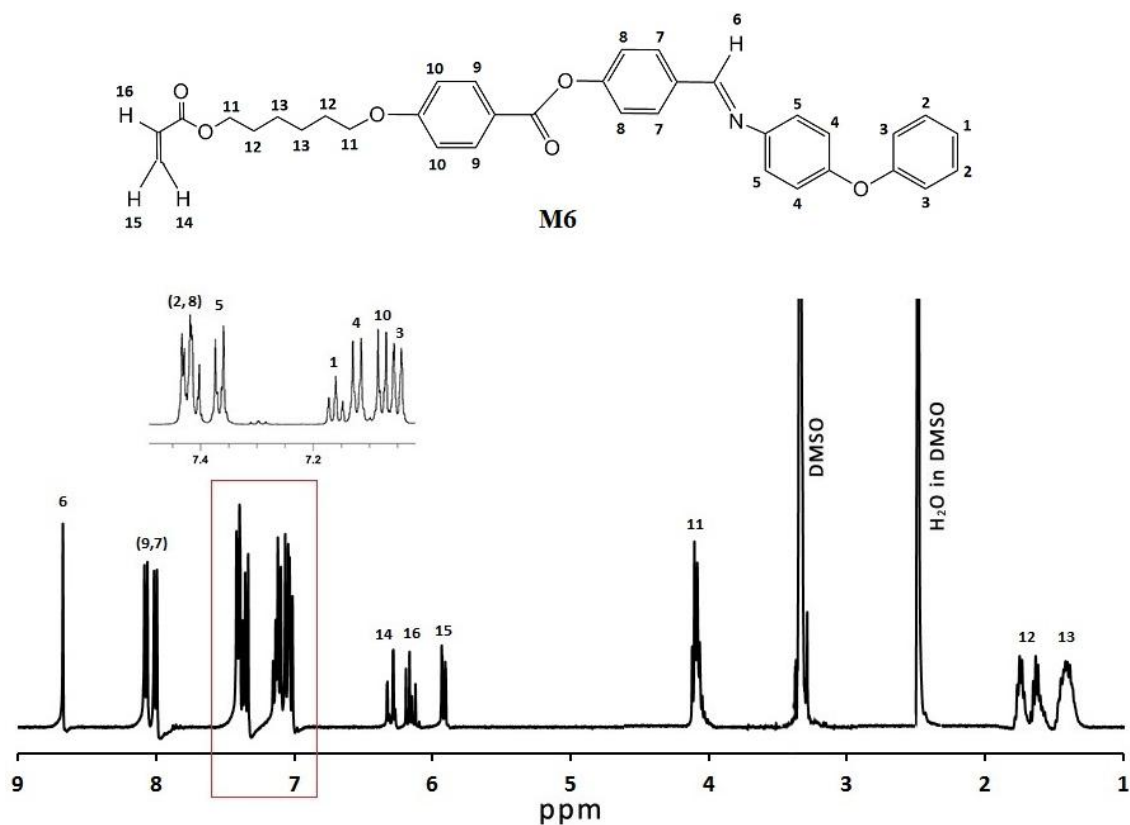


Figure 3.6 : ^1H NMR spectra of monomer **M6**.

Synthesis of 4-[(E)-N-(4-phenoxyphenyl)carboximidoyl]phenyl 4-([6-[(2-methylprop-2-enyl)oxy]hexyl]oxy)benzoate (**M7**)

Compound **5** (1.5 g, 0.005 mol) and compound **8** (1.44 g, 0.005 mol) were dissolved in minimal amounts of THF in a 250 ml Erlenmeyer conical flask. The rest of the succeeding steps were identical to the ones described for the synthesis of monomer **M2**. The product yield of monomer **M7** was 60%.

^1H NMR, δ (ppm, $\text{DMSO-}d_6$, 400 MHz): 8.68 (s, 1H, CH=N), 7.99-8.09 (dd, 4H, Ar-H), 7.39-7.43 (m, 4H, Ar-H), 7.34-7.37 (d, 2H, Ar-H), 7.14-7.17 (t, 1H, Ar-H), 7.11-7.12 (d, 2H, Ar-H), 7.05-7.08 (d, 2H, Ar-H), 7.03-7.05 (d, 2H, Ar-H), 6.00 (s, 1H, $\text{CH}_2=\text{C}(\text{CH}_3)-$), 5.65 (s, 1H, $\text{CH}_2=\text{C}(\text{CH}_3)-$), 4.06-4.11 (q, 4H, $-\text{OCH}_2-$), 1.86 (s, 3H, $\text{CH}_2=\text{C}(\text{CH}_3)-$), 1.73-1.77 (m, 2H, $-\text{OCH}_2\text{CH}_2-$), 1.60-1.67 (m, 2H, $-\text{CH}_2$), 1.39-1.45 (m, 4H, $-(\text{CH}_2)_2-$). ^{13}C NMR, δ (ppm, $\text{DMSO-}d_6$, 400 MHz): 167.1, 164.5 ($-\text{OC}=\text{O}$), 163.8 (CH=N), 159.4 (aromatic $\text{C}-\text{O}(\text{CH}_2)_6$), 157.4, 155.4 (aromatic $\text{C}-\text{O}$

Ar), 153.5 (aromatic $-\text{COO}$), 147.2 (aromatic $\text{C}=\text{N}=\text{CH}$), 136.5 ($\text{H}_3\text{C}-\text{C}=\text{C}-$), 134.3 (aromatic $\text{C}-\text{CH}=\text{N}$), 132.6 (aromatic C *ortho* to $-\text{COO}-$), 130.6 (aromatic C *ortho* to $-\text{CH}=\text{N}-$), 126.0 ($\text{H}_2\text{C}=\text{C}-$), 130.3, 123.9 (aromatic C), 123.3 (aromatic C *ortho* to $-\text{COO}-$), 123.0 (aromatic C *ortho* to $-\text{N}=\text{CH}-$), 121.0 (aromatic $\text{C}-\text{COO}-$), 119.9, 118.9 (aromatic C *ortho* to $\text{C}-\text{O}-\text{Ar}$), 115.2 (aromatic C *ortho* to $\text{C}-\text{O}(\text{CH}_2)_6$), 68.4($-\text{CH}_2\text{O}-$), 64.7 ($-\text{Ar}-\text{OCH}_2-$), 28.8, 28.5, 25.6, 25.7($-\text{CH}_2-$), 18.5 ($-\text{CH}_3$).

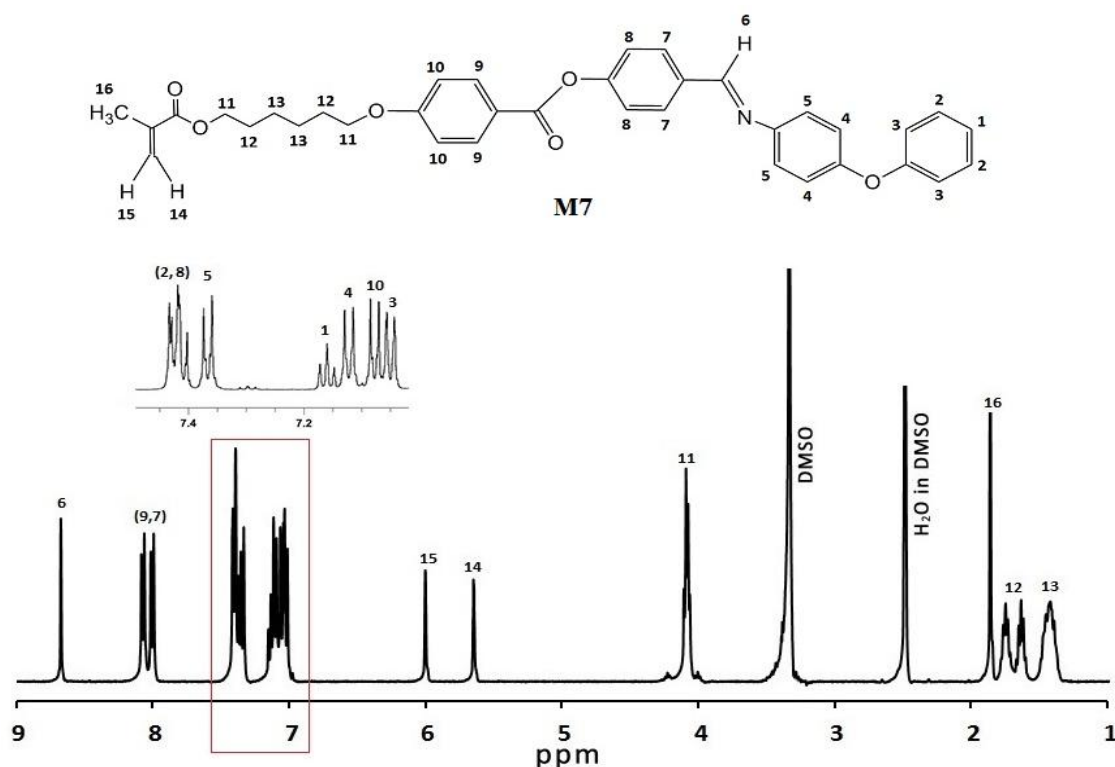


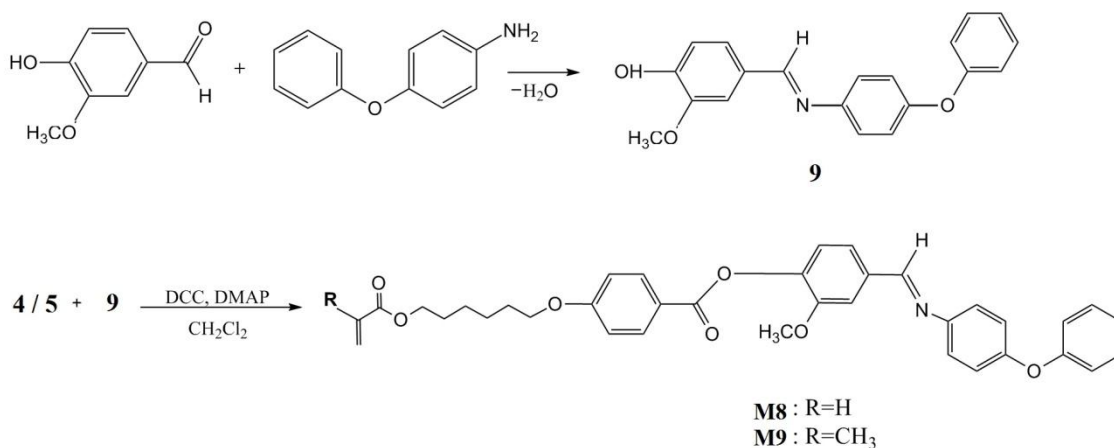
Figure 3.7 : ^1H NMR spectra of monomer M7.

3.2.5. Synthesis of monomer M8 and M9

Synthesis of 2-methoxy-4-[(E)-N-(4-phenoxyphenyl)carboximidoyl]phenol (9)

A mixture of vanillin (3.16 g, 0.02 mol) and distilled ethanol (100 ml) was refluxed for 30 minutes in a two-necked reaction flask equipped with a magnetic stirrer. The rest of the succeeding steps were identical to the ones described for the synthesis of compound **8**. The product yield of compound **9** was 80%. T_m : 80°C.

^1H NMR, δ (ppm, Acetone- d_6 , 400 MHz): 9.72 (s, 1H, OH), 8.42 (s, 1H, CH=N), 7.5 (d, 1H, Ar-H), 7.36-7.40 (t, 2H, Ar-H), 7.29-7.32 (dd, 1H, Ar-H), 7.24-7.26 (d, 2H, Ar-H), 7.12-7.14 (t, 1H, Ar-H), 6.99-7.03 (m, 4H, Ar-H), 6.86-6.88 (d, 2H, Ar-H), 3.83 (s, 3H, $-\text{OCH}_3$). ^{13}C NMR, δ (ppm, DMSO- d_6 , 400 MHz): 159.4 (CH=N), 157.6, 155.2 (aromatic C-O-Ar), 149.0 (aromatic C-OH), 147.6 (aromatic C-OCH₃), 147.2 (aromatic C-N=CH), 129.2 (aromatic C-CH=N), 129.8, 123.2 (aromatic C), 125.2 (aromatic C-CH=N), 122.3 (aromatic C *ortho* to -N=CH-), 119.8, 118.6 (aromatic C *ortho* to C-O-Ar), 114.3 (aromatic C *ortho* to C-OH), 108.4 (aromatic C *ortho* to -CH=N-), 56.1 ($-\text{OCH}_3$).



Scheme 3.6 : Synthetic route of monomer **M8** and monomer **M9**.

Synthesis of 2-methoxy-4-[(E)-N-(4-phenoxyphenyl)carboximidoyl]phenyl 4-[[6-(prop-2-enoyloxy) hexyl]oxy]benzoate (**M8**)

Compound **4** (1.46 g, 0.005 mol) and compound **9** (1.6 g, 0.005 mol) were dissolved in minimal amounts of THF in a 250 ml Erlenmeyer conical flask. The rest of the succeeding steps were identical to the ones described for the synthesis of monomer **M2**. The product yield of monomer **M8** was 58%.

^1H NMR, δ (ppm, DMSO- d_6 , 400 MHz): 8.66 (s, 1H, CH=N), 8.04-8.06 (d, 2H, Ar-H), 7.72 (s, 1H, Ar-H), 7.53-7.55 (dd, 1H, Ar-H), 7.40-7.43 (q, 2H, Ar-H), 7.33-7.38 (q, 3H, Ar-H), 7.14-7.17 (t, 1H, Ar-H), 7.11-7.12 (d, 2H, Ar-H), 7.05-7.08 (d, 2H, Ar-H), 7.03-7.05 (d, 2H, Ar-H), 6.29-6.33 (d, 1H, CH₂=CH), 6.12-6.19 (dd, 1H, CH), 5.91-5.92 (d, 1H, CH₂=CH), 4.08-4.12 (q, 4H, -OCH₂-), 3.8 (s, 3H, -OCH₃), 1.73-1.77 (m, 2H, -OCH₂CH₂-), 1.60-1.67 (m, 2H, -CH₂-), 1.39-1.45 (m, 4H, -(CH₂)₂-).

^{13}C NMR, δ (ppm, DMSO- d_6 , 400 MHz): 166.5, 163.4 (-OC=O) 163.2 (CH=N), 159.1 (aromatic C-O(CH₂)₆), 156.7, 154.9 (aromatic C-O-Ar), 151.3 (aromatic C-OCH₃), 146.6 (aromatic C-N=CH), 142.0 (aromatic C-OCO-), 135.0 (aromatic C-CH=N), 132.0 (aromatic C *ortho* to -CH=N-), 130.0 (aromatic C *ortho* to -COO-), 131.3 (HC=C-), 128.3 (H₂C=C-), 123.4 (aromatic C *ortho* to -OCO), 122.7, 122.2 (aromatic C), 120.3 (aromatic C-COO-), 119.3 (aromatic C *ortho* to -N=CH-), 118.4 (aromatic C *ortho* to C-O-Ar), 114.7 (aromatic C *ortho* to C-O(CH₂)₆), 111.1 (aromatic C *ortho* to -OCH₃), 67.8 (-Ar-OCH₂-), 64.0 (-CH₂O-), 55.8 (-OCH₃), 28.3, 28.0, 25.1, 25.0 (-CH₂-).

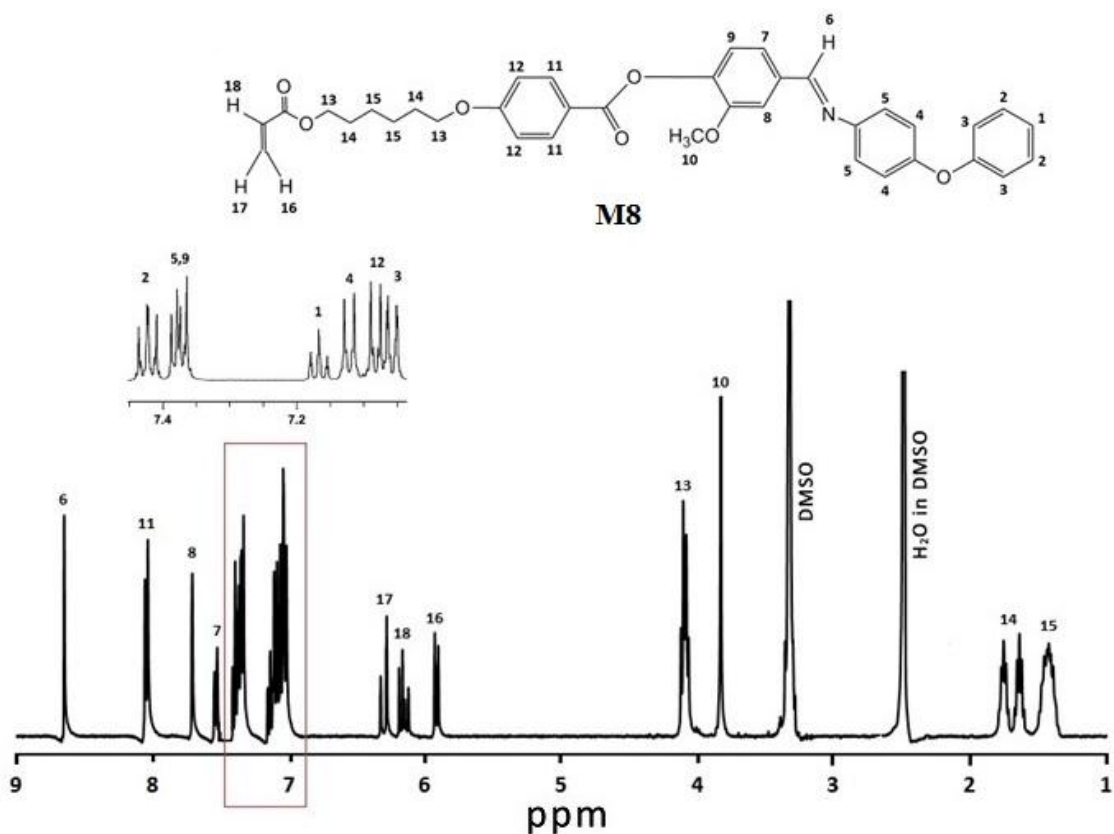


Figure 3.8 : ^1H NMR spectra of monomer **M8**.

Synthesis of 2-methoxy-4-[(E)-N-(4-phenoxyphenyl)carboximidoyl]phenyl 4-([6-[(2-methylprop-2-enyl)oxy]hexyl]oxy)benzoate (**M9**)

Compound **5** (1.5 g, 0.005 mol) and compound **9** (1.6 g, 0.005 mol) were dissolved in minimal amounts of THF in a 250 ml Erlenmeyer conical flask. The rest of the succeeding steps were identical to the ones described for the synthesis of monomer **M2**. The product yield of monomer **M9** was 72%.

^1H NMR, δ (ppm, $\text{DMSO-}d_6$, 400 MHz): 8.66 (s, 1H, CH=N), 8.04-8.06 (d, 2H, Ar-H), 7.72 (s, 1H, Ar-H), 7.53-7.55 (dd, 1H, Ar-H), 7.40-7.43 (q, 2H, Ar-H), 7.33-7.38 (q, 3H, Ar-H), 7.14-7.17 (t, 1H, Ar-H), 7.11-7.12 (d, 2H, Ar-H), 7.05-7.08 (d, 2H, Ar-H), 7.03-7.05 (d, 2H, Ar-H), 6.00 (s, 1H, $\text{CH}_2=\text{C}(\text{CH}_3)-$), 5.65 (s, 1H, $\text{CH}_2=\text{C}(\text{CH}_3)-$), 4.06-4.11 (q, 4H, $-\text{OCH}_2-$), 3.8 (s, 3H, $-\text{OCH}_3$), 1.86 (s, 3H, $\text{CH}_2=\text{C}(\text{CH}_3)-$), 1.73-1.77 (m, 2H, $-\text{OCH}_2\text{CH}_2-$), 1.60-1.67 (m, 2H, $-\text{CH}_2$), 1.39-1.45 (m, 4H, $-(\text{CH}_2)_2-$). ^{13}C NMR, δ (ppm, $\text{DMSO-}d_6$, 400 MHz): 166.5, 163.4 ($-\text{OC}=\text{O}$) 163.2 (CH=N), 159.1

(aromatic C–O(CH₂)₆), 156.7, 154.9 (aromatic C–O–Ar), 151.3 (aromatic C–OCH₃), 146.6 (aromatic C–N=CH), 142.0 (aromatic C–OCO–), 135.9 (H₃C–C=C–), 135.0 (aromatic C–CH=N), 132.0 (aromatic C *ortho* to –CH=N–), 130.0 (aromatic C *ortho* to –COO–), 125.4 (H₂C=C–), (aromatic C *ortho* to –OCO), 122.7, 122.2 (aromatic C), 120.3 (aromatic C–COO–), 119.3 (aromatic C *ortho* to –N=CH–), 118.4 (aromatic C *ortho* to C–O–Ar), 114.6 (aromatic C *ortho* to C–O(CH₂)₆), 111.1 (aromatic C *ortho* to –OCH₃), 67.8 (–Ar–OCH₂–), 64.1 (–CH₂O–), 55.8 (–OCH₃), 28.3, 27.9, 25.1, 25.0 (–CH₂–), 18.5 (–CH₃).

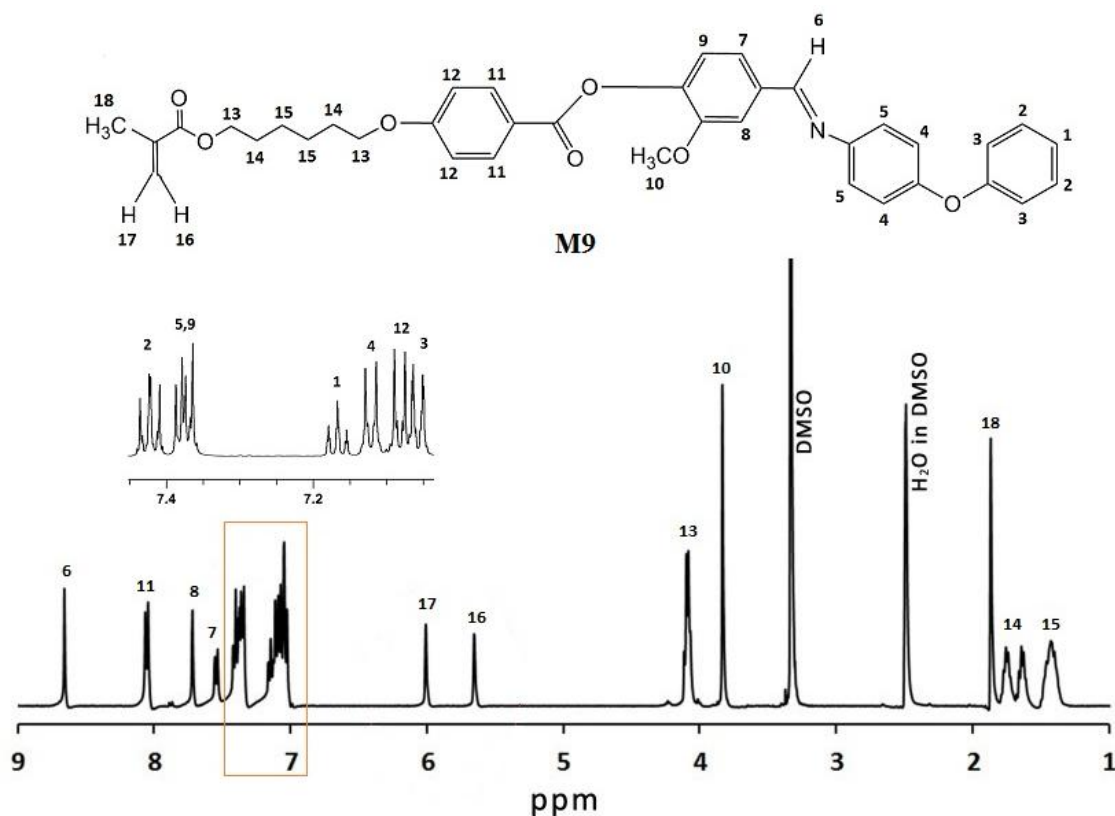


Figure 3.9 : ¹H NMR spectra of monomer **M9**.

3.3. Synthesis of SCLCPs

3.3.1. Synthesis of polymers **HP1M1** to **HP3M1** by ATRP

Polymers (**HP1M1** – **HP3M1**) were synthesized by living ATRP using ethyl 2-bromoisobutyrate (EBriB), CuBr and N,N,N',N',N''-pentamethyldiethylenetriamine (PMDETA) as an initiator, catalyst and ligand respectively.

Polymer **HP1M1**

In a 50 ml three-necked reaction flask equipped with a magnetic stirrer, CuBr (0.0068 g, 0.05 mmol), and monomer **M1** (0.5 g, 1.3 mmol) were added. The flask was then sealed with a rubber septum, degassed and back-filled with nitrogen gas three times. 2 ml deoxygenated anisole was added via syringe, followed by deoxygenated PMDETA (0.0110 g, 0.064 mmol). The solution turned light green as the CuBr/PMDETA complex was formed. After the majority of the metal complex had formed, ethyl 2-bromoisobutyrate (EBriB) (0.0062 g, 0.032 mmol) was added to the reaction flask. When the reaction is ready to be started, the reaction vessel was immersed in the preheated silicone oil bath. Once the stable target temperature of 90°C has been achieved, the starting time of the polymerization reaction was taken to be from this point onwards. The polymerization was carried out for 7 hours.

After the reaction was stopped, the entire reaction solution was passed through a neutral Al₂O₃ column with THF as an eluent to remove the catalyst, CuBr. The product was concentrated under reduced pressure. The concentrated product was dissolved in minimal amounts of THF (about 1 ml) in a small vial and was added dropwise into a 250 ml beaker containing 5 to 10 fold excess of methanol (the non-solvent) and magnetically stirred for 30 minutes. Then, the polymer was filtered and re-dissolved in minimal amount of THF. This polymer solution was re-precipitated in the same 250 ml beaker containing 10 to 20 fold excess of a fresh batch of non-solvent by drop-wise

addition under vigorous stirring conditions. This was repeated until the polymer contained no trace of monomer and dried overnight at 40°C under vacuum. The product yield of polymer **HP1M1** was 30%.

Polymer **HP2M1**

Polymer **HP2M1** was synthesized according to the procedure described for polymer **HP1M1** except for the amount of catalyst, CuBr (0.0053 g, 0.037 mmol), ligand, PMDETA (0.0081 g, 0.046 mmol) and initiator, EBriB (0.0041 g, 0.0211 mmol). The product yield of polymer **HP2M1** was 35%.

Polymer **HP3M1**

Polymer **HP3M1** was synthesized according to the procedure described for polymer **HP1M1** except for the amount of catalyst, CuBr (0.0040 g, 0.028 mmol), ligand, PMDETA (0.0055 g, 0.031) and initiator, EBriB (0.0031 g, 0.0159 mmol). The product yield of polymer **HP2M1** was 28%.

3.3.2. Synthesis of HP1M2 to HP2M9 by radical polymerization

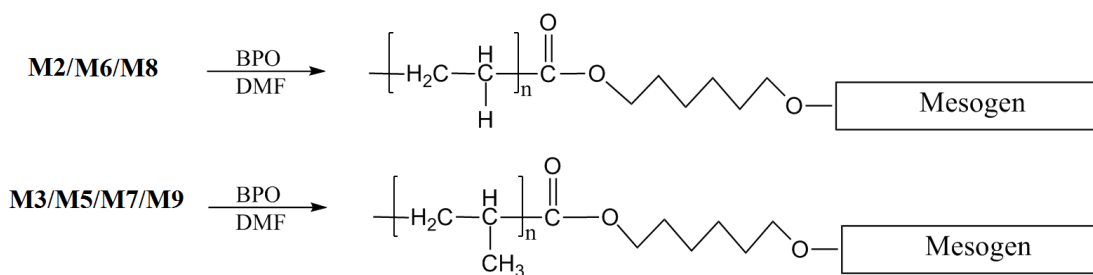
Polymers **HP1M2** to **HP2M9** were synthesized by conventional solution radical polymerization using benzoyl peroxide (BPO) as an initiator. The amounts of monomers, initiator and solvent used in this polymerization are listed in Table 3.1. A silicone oil bath was preheated to 90°C and the materials (monomers and initiator) were weighed. Predetermined amounts of monomers, initiator and dry DMF (refer to Table 3.1) were charged into the Schlenk polymerization tube and sealed with rubber septum. The polymerization tube containing all the reactants and magnetic stirrer was connected to a silicone oil trap bubbler to ensure no outside air re-enters the system during N₂ purge. The solution of monomers and solvent will be N₂ purged for at least 30 minutes

before the reaction started. The polymerization tube was held suspended mid-air from the preheated silicone oil at a distance far enough to avoid heating in the polymerization tube. When the reaction is ready to be started, the reaction vessel was immersed in the preheated silicone oil bath. Once the stable target temperature of 90°C has been achieved, the starting time of the polymerization reaction was taken to be from this point onwards. The N₂ purged was stopped after 2 hours of the reaction and polymerization tube was sealed.

Table 3.1: Amounts of reactants used in the radical polymerization experiments

| Monomer | Polymer | Monomer (g) | BPO (g) | DMF (ml) |
|-----------|--------------|-------------|---------|----------|
| M2 | HP1M2 | 0.5 | 0.30 | 3.5 |
| | HP2M2 | 0.5 | 0.03 | 2.5 |
| M3 | HP1M3 | 0.5 | 0.30 | 3.5 |
| | HP2M3 | 0.5 | 0.03 | 2.5 |
| M5 | HP1M5 | 0.5 | 0.30 | 3.5 |
| M6 | HP1M6 | 0.5 | 0.30 | 3.5 |
| | HP2M6 | 0.5 | 0.03 | 2.5 |
| M7 | HP1M7 | 0.5 | 0.30 | 3.5 |
| | HP2M7 | 0.5 | 0.03 | 2.5 |
| M8 | HP1M8 | 0.5 | 0.30 | 3.5 |
| M9 | HP1M9 | 0.5 | 0.30 | 3.5 |
| | HP2M9 | 0.5 | 0.03 | 2.5 |

After completion of the reaction, the entire reaction solution was poured out into a 250 ml beaker containing 5 to 10 fold excess of methanol (the non-solvent) including the magnetic stirrer and stirred for 30 minutes. Then, the polymer was filtered and re-dissolved in minimal amounts of THF (about 1 ml) in a small vial. This polymer solution was re-precipitated in the same 250 ml beaker containing 10 to 20 fold excess of a fresh batch of non-solvent by drop wise addition under vigorous stirring conditions. This was repeated until the polymer contained no trace of monomer and dried overnight at 40°C under vacuum. The general synthetic route for the polymerization is shown in Scheme 3.7.



Scheme 3.7: General synthetic route for polymerization.

3.4. Characterization methods and instrumentation

3.4.1. Nuclear Magnetic Resonance Spectroscopy (NMR)

NMR is a powerful and non-destructive technique for determination of molecular structure [138]. ^1H NMR and ^{13}C NMR measurements were performed with JEOL JNM-LA 400 MHz spectrometer, JEOL ECA 400 MHz spectrometer and Bruker AVN 600 MHz. All compounds were dissolved in an appropriate deuterated solvent to give a viscous solution in an NMR tube and concentrations were maintained at 2.5% (w/v) and 15% (w/v) for the ^1H NMR and ^{13}C NMR analyses respectively. The chloroform peaks for the ^1H NMR and ^{13}C NMR were set at 7.26 ppm and 77.0 ppm respectively. The dimethyl sulfoxide (DMSO) peaks were set at 3.34 ppm and 2.4 ppm for ^1H NMR and 40.6 ppm for ^{13}C NMR.

3.4.2. Fourier Transform Infrared Spectroscopy (FTIR)

The FTIR spectra were recorded with a Spotlight 400 PerkinElmer spectrometer with 16 scans using attenuated total reflectance (ATR) method. The wavelength was recorded from region 650 to 4000 cm^{-1} at room temperature. Polymer samples were placed over the ATR crystal and maximum pressure was applied using the slip-clutch mechanism. All of the data processing was done using the instrument's built in Spectrum v6.3.1.0132 software.

3.4.3. Differential Scanning Calorimetry (DSC)

Thermal transition temperature of the synthesized monomers and polymers were obtained using a PerkinElmer Hyper DSC instrument. The DSC analysis procedure used consisted of first heating from 30°C to 250°C, then cooling it to 30°C at a rate 10°C min⁻¹, and holding for 1 minute before cooling and next heating cycle to erase any previous thermal history. Accurately known sample weights of about 3 to 4 mg were used for all the experiments. The instrument was calibrated with standard sample of indium and all of the data collected were analyzed by Pyris v9.1.0.0203 software. The results of the second heating scan have been reported throughout to ensure that all of the samples had equivalent thermal histories.

3.4.4. Polarized Optical Microscopy (POM)

The thermotropic liquid crystalline behavior was characterized by using a Mettler Toledo FP82HT hot stage and viewed with an Olympus BX51 microscope fitted with crossed polarizing filters. The microscope was connected to an Olympus camera for image capture, with magnification factors of 10 and 20. A small amount of the sample was placed on a glass slide and covered with a cover slip. The material was heated until it reached isotropic temperature and the mesophase image formed was taken upon slow cooling at the rate of 1°C min⁻¹ for better texture.

3.4.5. Small Angle X-ray Scattering (SAXS)

Small angle X-ray scattering (SAXS) experiments were performed with Nano-Viewer equipped with a CCD camera (Rigaku Corp. Japan). The X-ray experiment was performed by using the Cu K_α radiation beam ($\lambda = 1.541 \text{ \AA}$) which was converged and monochromatized by a Confocal Max Flax (CMF) mirror. X-ray generator was a Rigaku Micro7 rotating anode generator (40 kV, 30 mA). The diameter of the X-ray

beam controlled by a 3-slit optical system was set to 250 μm . The pellet sample was wrapped with aluminium foil and placed to the instrument. The temperature of a pellet sample was controlled with a hot stage (Mettler Toledo Inc. Switzerland) with accuracy of $\pm 0.1^\circ\text{C}$.

3.4.6. Powder X-Ray Diffraction (PXRD)

Powder X-ray diffraction (PXRD) was performed on a PANalytical Empyrean, using the Ni-filtered Cu-K α radiation. A HTK 16N temperature chamber (with nitrogen inert atmosphere) and a TCU 2000N temperature controller unit (Anton Paar) were used. A very fine sample powder was covered on a platinum plate in the chamber and the diffraction patterns were recorded during the first heating process at definite temperatures with a rate of $10^\circ\text{C}/\text{min}$.

3.4.7. Gel Permeation Chromatography (GPC)

Molecular weight determinations were performed using a gel permeation chromatography (GPC) instrument (Waters 2414 refractive index detector coupled with a Waters 717 plus Autosampler and Waters 600 Controller) with polystyrene standards as reference and tetrahydrofuran (THF) as the eluent at flow rate of 1 ml per minute. A weight of 5 to 10 mg of the polymer sample was dissolved in 5 mL of tetrahydrofuran. The samples were filtered through a Waters GHP Acrodisc® that has a minispikes diameter of 13 mm and a pore size of $0.45 \mu\text{m}$ (to protect the chromatography instrument from undissolved particulates) into a sample vial of about 1 ml capacity. The total run time for each sample was set to 55 minutes and the injection volume was 100 μl for each vial. All of the data processing was done using the instrument's built in Empower v2.0 software.

3.4.8. Thermogravimetric Analysis (TGA)

Thermal data were obtained using a PerkinElmer Pyris-Diamond TG/DTA thermo-balance. Thermogravimetric analysis was performed in N₂ at a heating rate of 20°C min⁻¹ from 50°C to 900°C with a digital resolution of 2550 points. Sample weights of about 5 mg were used for all the experiments. All of the data processing was done using the instrument's built in Pyris v9.1.0.0203 software.

3.4.9. UV-Visible (UV-Vis) and Photoluminescence Spectrometry

UV-vis absorption spectra were recorded with a Cary 60 UV-Vis spectrophotometer. The polymer solution (1x10⁻⁶ M) in THF was prepared and fresh THF was used as a blank. The solution was placed into 4 sided clear quartz cuvette and the sample was measured from 200 nm to 500 nm with medium scan rate. The photoluminescence emission spectra were obtained on a Cary Eclipse spectrophotometer and the sample was measured from 200 nm to 600 nm.

3.4.10. Electrochemical measurements

The electrochemical measurements were carried out using a potentiostat / galvanostat (AUTOLAB/PGSTAT 302N) which was run by General Purpose Electrochemical System software (GPES) installed in computer. Ag/AgCl, platinum wire, and platinum coil served as reference electrode, counter electrode and working electrode, respectively. All the measurements were performed at room temperature in the potential range from -1.0 V to +2.0 V with a scan rate of 50 mV s⁻¹ and 0.1 M tetrabutylammonium perchlorate (Bu₄N(ClO₄)) was used as supporting electrolyte in chloroform. The potentials were measured against Ag/AgCl reference electrode and ferrocene was used as the internal standard.

3.4.11. Rheological measurements

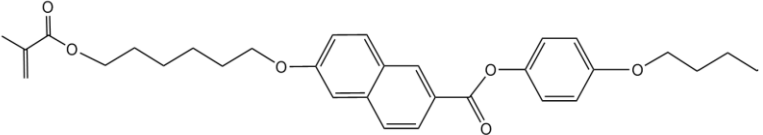
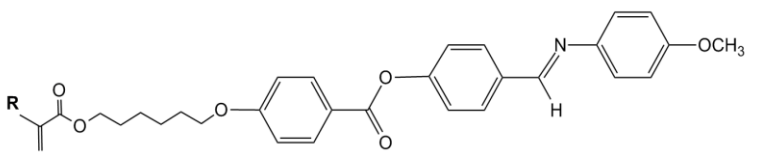
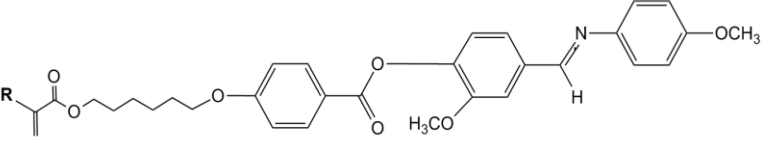
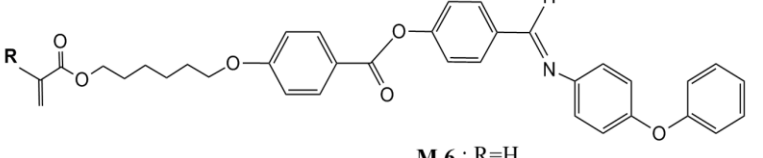
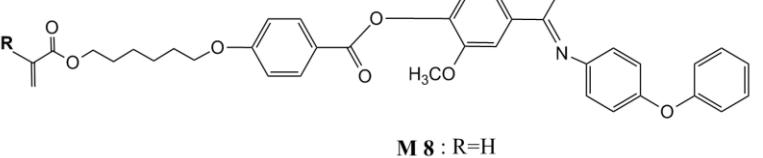
The rheological behavior of the polymers was investigated using a Rheometer Physica MCR301 with 15 mm parallel plates. Prior to any test the zero-gap between the parallel plates was calibrated at 5°C above their clearing temperature. In the measurements, the sample was placed between preheated fixtures and 15 min were allowed to reach thermal equilibrium, before the gap was set to 0.2 mm. For temperature changes, the control system needed about 5 min to reach a target equilibrium temperature with an error of 1~2°C. For dynamic oscillatory shearing the linear viscoelastic region of 1% strain was first obtained by strain sweep tests and no pre-shear was applied.

CHAPTER 4 : RESULTS AND DISCUSSION

4.1. LC monomers

Table 4.1 shows the LC monomers that have successfully synthesized.

Table 4.1 : Synthesized LC monomers

| Molecular structure | Monomer | Yield (%) |
|----------------------------------------------------------------------------------------------------------------------------------------------------------------------------|-----------|-----------|
|  <p style="text-align: center;">M1</p> | M1 | 35 |
|  <p style="text-align: center;">M 2 : R=H M 3 : R=CH₃</p> | M2 | 55 |
| | M3 | 60 |
|  <p style="text-align: center;">M 4 : R=H M 5 : R=CH₃</p> | M4 | 63 |
| | M5 | 67 |
|  <p style="text-align: center;">M 6 : R=H M 7 : R=CH₃</p> | M6 | 55 |
| | M7 | 60 |
|  <p style="text-align: center;">M 8 : R=H M 9 : R=CH₃</p> | M8 | 58 |
| | M9 | 72 |

Monomer **M1** has been designed with the ester functionality as the central linkage. The acid-catalyzed esterification reaction has been used to connect the naphthalene ring and the phenolic compound to form a rigid mesogen for the liquid crystal monomer as shown in Figure 4.1.

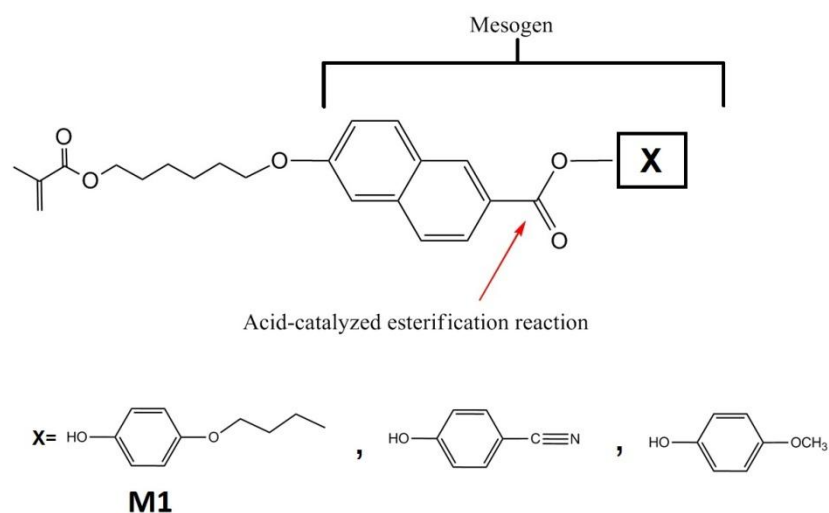


Figure 4.1 : Reaction involved in the preparation of monomer **M1**.

Acid-catalyzed esterification reaction

In the acid-catalyzed esterification reaction, mineral acids such as H_2SO_4 , HCl or HI have been used to catalyze the esterification reaction. However, the esterification of phenols with both aliphatic and aromatic carboxylic acids is difficult to achieve under normal condition. Thus, a combination of H_3BO_3 and H_2SO_4 can be used to catalyze the esterification reaction [139]. The catalysts essentially promote the protonation of the carbonyl oxygen on the carboxylic group, thereby activating nucleophilic attack by an alcohol to form a tetrahedral intermediate. Disproportionation of this intermediate complex ultimately yields the ester [140] as illustrated in Figure 4.2.

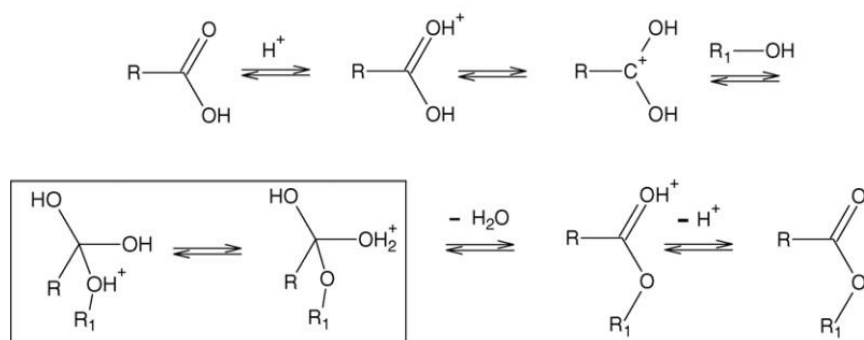


Figure 4.2 : Reaction mechanism of acid-catalyzed esterification reaction. Adopted from [140].

The reaction activity can be affected by the produced water. In the presence of water, the esterification kinetics will be low due to the reverse hydrolysis [141]. In order to minimize reverse hydrolysis, Dean-Stark trap was used to collect the produced water during the esterification reaction. However, the yield of ester (**M1**) obtained from this reaction was only 35%.

Attempts to vary the terminal unit, **X** on the naphthalene based monomer by replacing *p*-butoxyphenol group with *p*-cyanophenol and *p*-methoxyphenol (Figure 4.1) have been carried out using the same procedure, however no product was obtained. The effort of varying the terminal unit is to study the effect of electron withdrawing (cyano and methoxy) and electron donating (butoxy) group on mesomorphic behavior on the naphthalene based monomer and polymer. Due to failure to synthesize the target monomers, different types of monomers and polymers containing Schiff base ester in the mesogen have been synthesized to study their properties.

Monomers **M2** to **M9**, containing Schiff base and ester functionality as the central linkages has successfully synthesized. Two major reactions were involved in the formation of Schiff base and ester linkages (Figure 4.3). The condensation reaction between primary amine and aldehyde produced Schiff base linkage of the two aromatic rings. Meanwhile, the Steglich esterification reaction has been used to connect the

phenolic compound containing Schiff base linkage with synthesized benzoic acid namely as compound **4** and **5** (see section 3.2.2).

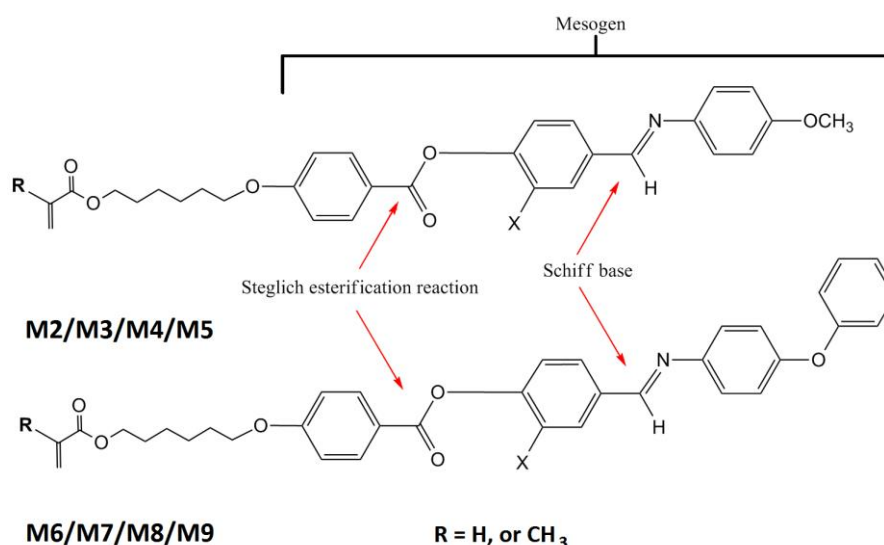


Figure 4.3 : Reaction involved in the preparation of monomers, **M2** to **M9**.

Schiff base formation

Schiff base is formed from nucleophilic addition reaction of an amine group with the carbonyl group of an aldehyde or ketone with acid catalyst to eliminate water. A weak acid (acetic acid) was used to catalyze the reaction. Mechanistically, the formation of Schiff base is shown in Figure 4.4. The amine nitrogen act as nucleophile and attack the electrophilic carbonyl carbon. Then, the nitrogen is deprotonated and the electrons from this N-H bond push the oxygen off the carbon forming the C=N bond and displaced a water molecule [142].

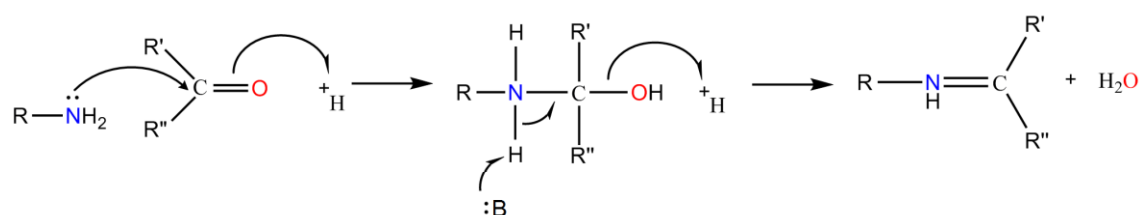
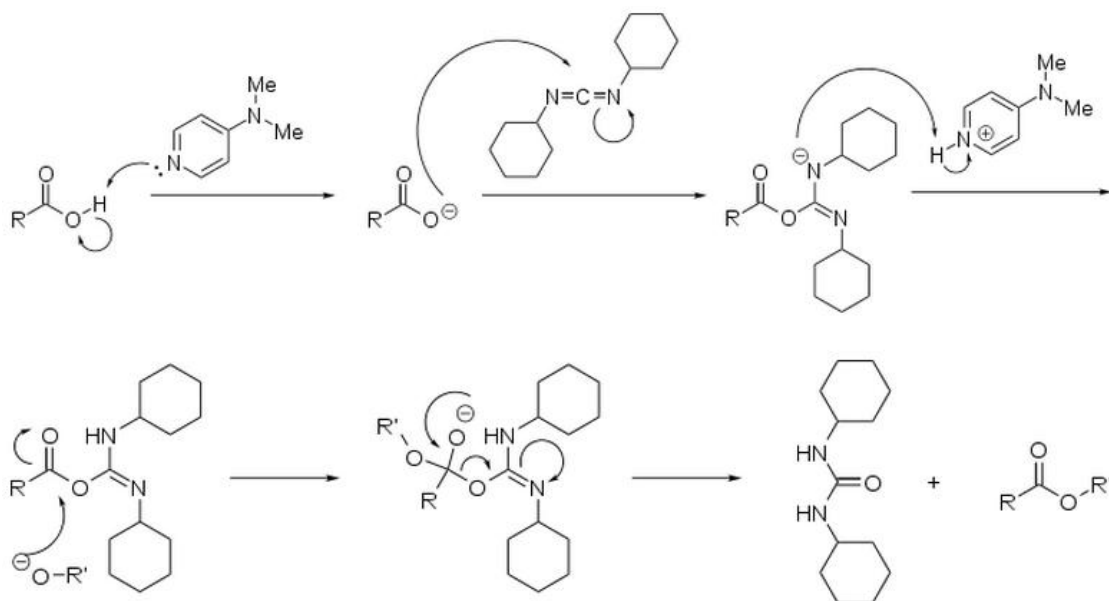


Figure 4.4: Reaction mechanism of Schiff base formation. Redrawn from [142].

Steglich esterification reaction

The ester linkage in the formation of Schiff base ester mesogen has been developed by Steglich esterification reaction by using *N,N'*-dicyclohexylcarbodiimide (DCC) as a coupling reagent and 4-dimethylaminopyridine (DMAP) as a catalyst. The reaction mechanism of the esterification is described in Figure 4.5.



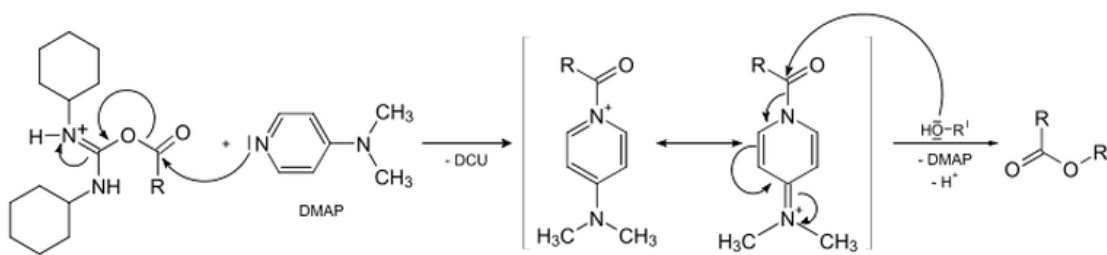
Where,

R = Compound 4 or 5

R' = Compound 6/7/8/9

Figure 4.5 : Reaction mechanism of Steglich esterification by DCC. Adopted from [143].

DCC and the carboxylic acid (compound 4 or 5) are able to form an *O*-acylisourea intermediate which is more reactive than the free acid. Then the phenol with Schiff base linkage attacks this intermediate forming the ester and *N,N'*-dicyclohexylurea (DHU) as the by-product. However, there is limitation with the use of DCC, that is the yield maybe variable and the *N*-acylureas produced are side-products which are unable to further react with the phenol. In order to suppress this reaction, DMAP is added to act as an acyl transfer reagent as shown in Figure 4.6.



Where,

R = Compound 4 or 5

R' = Compound 6/7/8/9

Figure 4.6 : Function of DMAP in the esterification reaction. Adopted from [143].

In this step, DMAP acts as a nucleophilic catalyst while the dimethylamino group acts as an electron donor substituent which increases both nucleophilicity and basicity of the pyridine nitrogen which then reacts with the *O*-acylisourea leading to a reactive amide (active ester). This intermediate cannot form intra-molecular side products but reacts rapidly with alcohols and gives the ester [144]. The yields of esters obtained from this reaction were almost 60% for all monomers.

4.2. SCLCPs

Table 4.2 shows the yields of SCLCPs synthesized by living ATRP using ethyl 2-bromoisobutyrate (EBriB), CuBr and N,N,N',N',N''-pentamethyldiethylenetriamine (PMDETA) as an initiator, catalyst and ligand respectively. The polymerization was carried out at 90°C for several hours in anisole solution to control the polydispersity and yield of the polymers. As shown in Table 4.2, the polymerization of polymers **PX1**, **PX2** and **PX3** did not give any yields as conducted for 3-4 hours reaction time. However, when the duration of the polymerization was extended to 7 hours, the yields of the polymers **HP1M1**, **HP2M1** and **HP3M1** were found to be around 28% to 35%. As the duration of polymerization was extended from 10 to 24 hours, the yields of the polymers **PX4-PX8** were decreased from 15% to 5%. According to Angiolini et al. [145], the yields and number average molecular weight of the polymers have a strong

dependence on the reaction time. The molecular weight of polymers **PX4-PX8** could not be measured due to small amount of polymers obtained.

Table 4.2 : SCLCPs synthesized by ATRP

| Polymer | Monomer (g) | CuBr (g) | PMDETA (g) | EBriB (g) | Anisole (ml) | Reaction time (h) | Yield (%) |
|--------------|-------------|----------|------------|-----------|--------------|-------------------|-----------|
| PX1 | 0.5 | 0.0068 | 0.0110 | 0.0062 | 2 | 3 | - |
| PX2 | 0.5 | 0.0053 | 0.0081 | 0.0041 | 2 | 3 | - |
| PX3 | 0.5 | 0.0040 | 0.0055 | 0.0031 | 2 | 4 | - |
| HP1M1 | 0.5 | 0.0068 | 0.0110 | 0.0062 | 2 | 7 | 30 |
| HP2M1 | 0.5 | 0.0053 | 0.0081 | 0.0041 | 2 | 7 | 35 |
| HP3M1 | 0.5 | 0.0040 | 0.0055 | 0.0031 | 2 | 7 | 28 |
| PX4 | 0.5 | 0.0065 | 0.0112 | 0.0065 | 2 | 10 | 15 |
| PX5 | 0.5 | 0.0055 | 0.0083 | 0.0045 | 2 | 12 | 12 |
| PX6 | 0.5 | 0.0041 | 0.0050 | 0.0032 | 2 | 12 | 10 |
| PX7 | 0.5 | 0.0066 | 0.0107 | 0.0060 | 2 | 24 | 7 |
| PX8 | 0.5 | 0.0053 | 0.0081 | 0.0041 | 2 | 24 | 5 |

However, other monomers (**M2** to **M9**) cannot be polymerized by ATRP technique. This is because ATRP does not work for monomers containing Schiff base group in their mesogen. Schiff base group is known as a multidentate nitrogen donor ligand [146] which easily form a metal complex with metal catalyst and produced side reactions. Hence, conventional radical chain polymerization was used to polymerize these monomers.

The polymerization was carried out in DMF solvent by using BPO as an initiator. A solvent was used in the polymerization because it acts as diluents and aids in the transfer of the heat of polymerization. It also allows easier stirring and thermally controllable compared to bulk polymerization [26]. Table 4.3 shows the yields of SCLCPs synthesized by radical chain polymerization.

Table 4.3 : SCLCPs synthesized by radical chain polymerization

| Polymer | Monomer (g) | BPO (g) | DMF (ml) | Reaction time (h) | Yield (%) |
|--------------|-------------|---------|----------|-------------------|-----------|
| HP1M2 | 0.5 | 0.30 | 3.5 | 3 | 35 |
| HP2M2 | 0.5 | 0.03 | 2.5 | 24 | 25 |
| HP1M3 | 0.5 | 0.30 | 3.5 | 3 | 30 |
| HP2M3 | 0.5 | 0.03 | 2.5 | 24 | 23 |
| HP1M5 | 0.5 | 0.30 | 3.5 | 3 | 33 |
| HP1M6 | 0.5 | 0.30 | 3.5 | 3 | 22 |
| HP2M6 | 0.5 | 0.03 | 2.5 | 24 | 31 |
| HP1M7 | 0.5 | 0.30 | 3.5 | 3 | 24 |
| HP2M7 | 0.5 | 0.03 | 2.5 | 24 | 30 |
| HP1M8 | 0.5 | 0.30 | 3.5 | 3 | 31 |
| HP1M9 | 0.5 | 0.30 | 3.5 | 3 | 29 |
| HP2M9 | 0.5 | 0.03 | 2.5 | 24 | 27 |

In this radical chain polymerization, different amounts of initiator have been used in order to get the polymers with high molecular weights. Polymers with **HP1** code were synthesized using 10 wt % of BPO for 3 hours reaction to prevent the polymer from gelling up with large amount of initiator. In addition, 3 hours reaction time has been chosen to control the polydispersity of the polymer since a very broad polydispersity may reduce the properties of the polymers. From the experiment, almost all monomers were successfully polymerized with large amount of initiator.

The polymers with **HP2** code were synthesized by using 5 wt % of BPO for 24 hours reaction to produce polymer with narrower polydispersity as summarized in Table 4.4. Monomer **M5** and monomer **M8** cannot be polymerized with this amount of initiator, this may be due to initiator efficiency produced in the homolysis reaction is not enough to initiate the polymer chains [26].

Molecular weight

Molecular weight distribution is one of the important characteristic of polymer because it affects polymer properties. Figure 4.7 shows the chromatogram for the synthesized polymer **HPIM6** that has an approximately molecular weight distribution which is typically similar for all synthesized polymer samples.

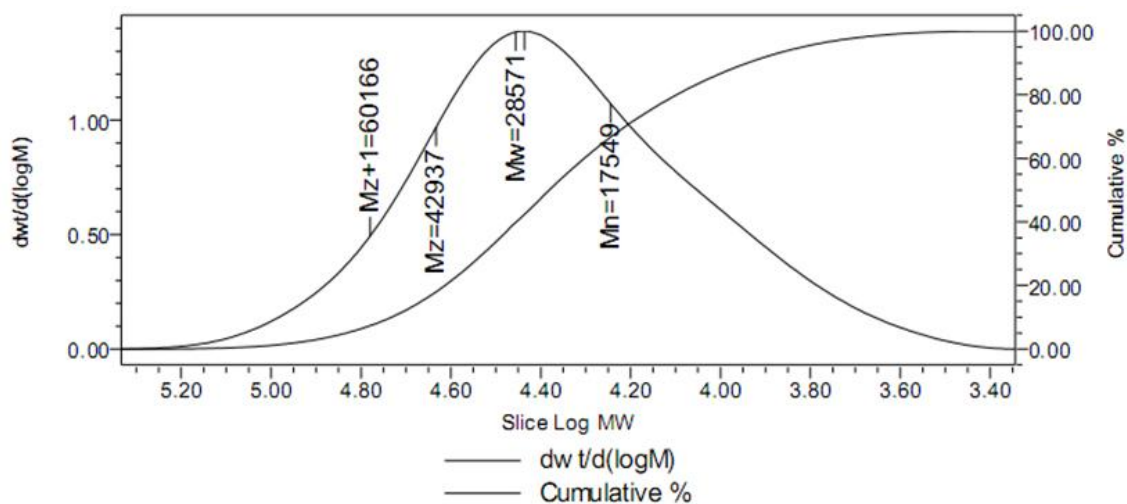


Figure 4.7 : GPC chromatograms of polymer **HP1M6**.

The GPC program gives a lot of information from the chromatograms: M_n , the number average molecular weight; M_w , the weight average molecular weight; M_z , the Z average molecular weight; and M_{z+1} , the Z + 1 average molecular weight. The M_w is probably the most useful as it fairly accounts for the contributions of different sized chains to the overall behavior of the polymer and correlates best with most of the physical properties of interest. The polydispersity index (PDI) of the polymer system is a measure of width of the molecular weight distribution for a polymer which is the M_w/M_n ratio of the two averages. A PDI value that is close to 1 implies a narrow distribution of molecular weights i.e., most of the molecules are of the same weight whereas a larger PDI value could arise from an unsymmetrical distribution such as small amounts of unreacted monomers and short polymer chains in the presence where the majority population are longer polymer chains.

Table 4.4 : GPC results of synthesized side chain liquid crystalline polymers

| Polymer | Polymerization technique | M_n | M_w | PDI |
|--------------|--------------------------|--------|---------|------|
| HP1M1 | ATRP | 9,000 | 10,500 | 1.17 |
| HP2M1 | ATRP | 8,800 | 10,100 | 1.16 |
| HP3M1 | ATRP | 11,000 | 12,800 | 1.16 |
| HP1M2 | RCP | 10,800 | 22,400 | 2.08 |
| HP2M2 | RCP | 9,800 | 17,700 | 1.80 |
| HP1M3 | RCP | 38,900 | 70,200 | 1.81 |
| HP2M3 | RCP | 17,000 | 50,000 | 1.80 |
| HP1M5 | RCP | 22,800 | 63,700 | 2.80 |
| HP1M6 | RCP | 26,500 | 53,200 | 2.00 |
| HP2M6 | RCP | 17,500 | 28,600 | 1.62 |
| HP1M7 | RCP | 47,300 | 122,500 | 2.59 |
| HP2M7 | RCP | 45,100 | 84,900 | 1.88 |
| HP1M8 | RCP | 20,500 | 43,900 | 2.13 |
| HP1M9 | RCP | 46,000 | 103,200 | 2.24 |
| HP2M9 | RCP | 46,400 | 85,800 | 1.84 |

* ATRP = Atom transfer radical polymerization

RCP = Radical chain polymerization

The M_n and M_w for all the synthesized SCLCPs determined by GPC as presented in Table 4.4 show that the PDI for the polymers synthesized by ATRP have a value close to 1. In ATRP, the radical is intermittently masked as a dormant species. The propagating radical is formed when the initiator (alkyl halide) interacts with an activator (a low oxidation state transition metal complex). The radical is quickly deactivated by a higher oxidation state transition metal complex and the dormant chain is created. All polymer chains grow at the same pace therefore well-defined molecular weight polymers with a narrow polydispersities can be achieved [39].

The PDI values for the polymers synthesized by radical chain polymerization have a value more than 2.0. This result indicates that the radical chain polymerization was terminated by disproportionation rather than combination as discuss earlier in Chapter 1

(section 1.6.1). Radical chain polymerization has fast, irreversible termination of the growing radicals through coupling and disproportionation reactions which precludes the synthesis of well-defined polymers with low polydispersities and complex architectures [147]. Generally, high molecular weight polymer forms very early in the reaction and in the most cases throughout the entire polymerization.

However, chains that are produced early in the reaction will have a different degree of polymerization (DP) compared to those which produced later in the reaction. This is due to the variations in reactant concentrations and rate constants. Hence, the molecular weight distribution of the final polymer will contain a wide range of DPs [35]. The radical chain ends also react with each other to terminate chains with either saturated alkane or sterically hindered alkene. This results in further transformation of the chain ends into other types of chemical groups or extension with other monomers [30].

4.3. Structural determination

4.3.1. ^1H NMR spectra

The chemical structures of all the synthesized monomers and polymers were characterized by ^1H NMR spectroscopy.

Figure 4.8(a) shows the ^1H NMR spectrum of monomer **M1** together with its molecular structure. The most de-shielded signals at chemical shift of δ 6.85-8.61 ppm are due to the protons on naphthalene and benzene ring (5, 6, 7, 8, 9, 10). The protons on an aromatic system are de-shielded due to the large anisotropic field which is generated by the circulation of the π electrons in the aromatic rings.

Two singlet signals at δ 5.46 and 6.03 ppm are attributed to the vinylic protons (13 and 14) of methacrylate backbone while the allylic protons on the methyl group (15) resonate at 1.87 ppm. These vinylic and allylic protons are de-shielded due to the

anisotropic field of the π electrons in the double bond. The effect is smaller for the allylic hydrogens because they are more distant from the double bonds.

The signals of the protons on the carbon attached to the single-bonded oxygen ($-\text{OCH}_2-$) resonate at 3.88–4.12 ppm (4, 11). They shifted to the downfield because of the electro-negativity of the oxygen atom. The signals in the range 1.40 to 1.85 ppm consist of methylene protons (2, 3 and 12) where the intense triplet signals at 0.89-0.94 ppm are due to the terminal methyl group (1).

After the polymerization, the characteristic vinylidene protons peaks of monomer located at $\delta = 6.03$ ppm and $\delta = 5.46$ ppm were completely disappeared (Figure 4.8(b)). At the same time, an additional chemical shift for methylene ($-\text{CH}_2-$) protons was observed at 1.03 ppm. The signal broadening with consistent chemical shifts was also observed in the polymer spectrum for the proposed polymers.

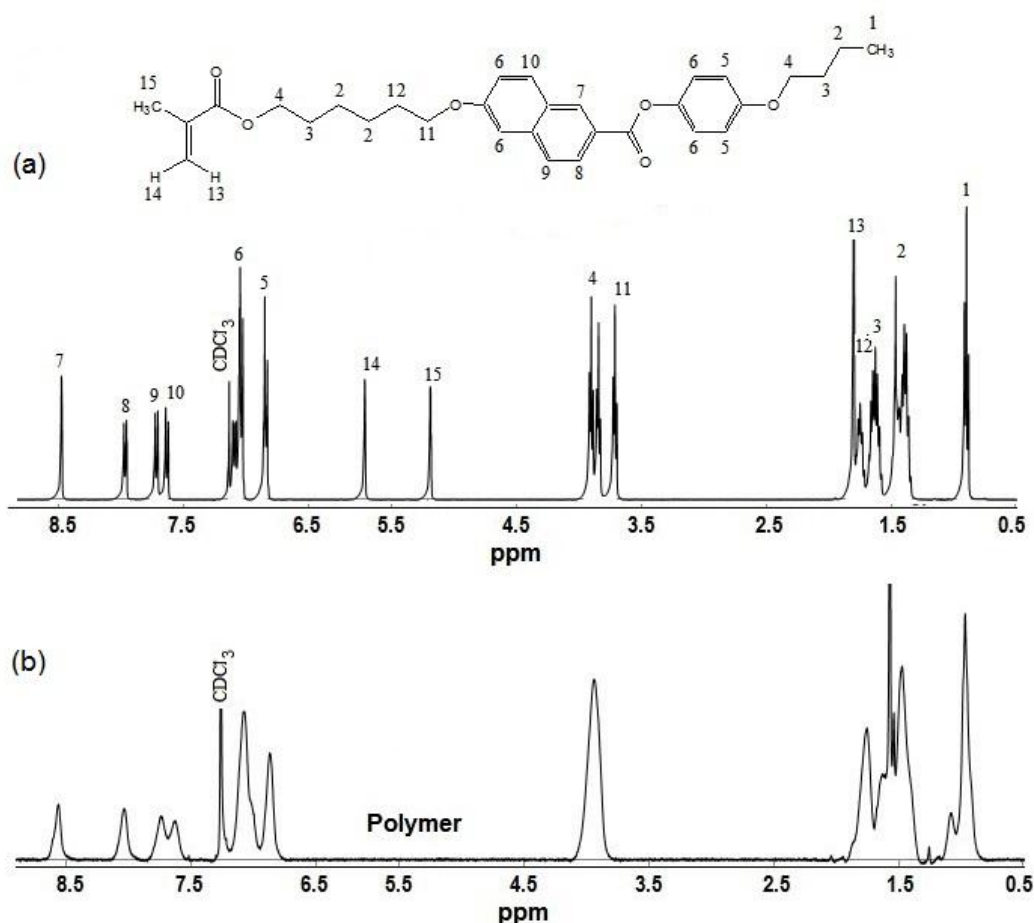


Figure 4.8: ^1H NMR spectrum of (a) monomer **M1** (b) polymer **HP1M1**.

Figure 4.9(a) shows the ^1H NMR spectrum of monomer **M3** together with its molecular structure. The most de-shielded singlet signal at chemical shift δ 8.72 ppm is due to the Schiff base group (4). The signal appeared as singlet is mainly because there are no adjacent protons. Existence of anisotropic field of the π electrons in the double bond and electron withdrawing effect of nitrogen atom shifted the proton to the most downfield [148].

The doublet signals appeared at δ 7.85–8.18 ppm, 7.32–7.56 ppm and 6.99–7.21 ppm are attributed to the aromatic protons on three phenyl rings linked by Schiff base and ester group. Two singlet signals at δ 5.71 and 6.07 ppm are attributed to the vinylic protons (12 and 13) of methacrylate backbone while the allylic protons on the methyl group (14) resonate at 1.89 ppm. The quartet signals of the protons on the carbon attached to the single-bonded oxygen ($-\text{OCH}_2-$) resonate at 4.08–4.19 ppm (9).

The intense singlet signal at 3.39 ppm is due to the terminal methoxy group attached to the phenyl ring (1). Methoxy is an electron donating group which increases the shielding of the hydrogens causing them to move upfield [148]. The signals in the range 1.39 to 1.73 ppm consist of methylene protons (10 and 11).

After the polymerization, the characteristic vinylidene proton peaks of the monomer located at $\delta = 5.72$ ppm and $\delta = 6.07$ ppm were completely disappeared (Figure 4.9(b)). At the same time, an additional chemical shift for methylene ($-\text{CH}_2-$) protons was also observed at 1.03 ppm. The signal broadening with consistent chemical shifts was also observed in the polymer spectrum for the proposed polymers structure.

As the monomer **M2** to **M5** and their polymers bear structural similarities except for the lateral unit in the mesogen, **M2**, **M4** and **M5** monomers (Chapter 3, section 3.2) and their polymers showed similar ^1H NMR spectral properties as described for monomer **M3**.

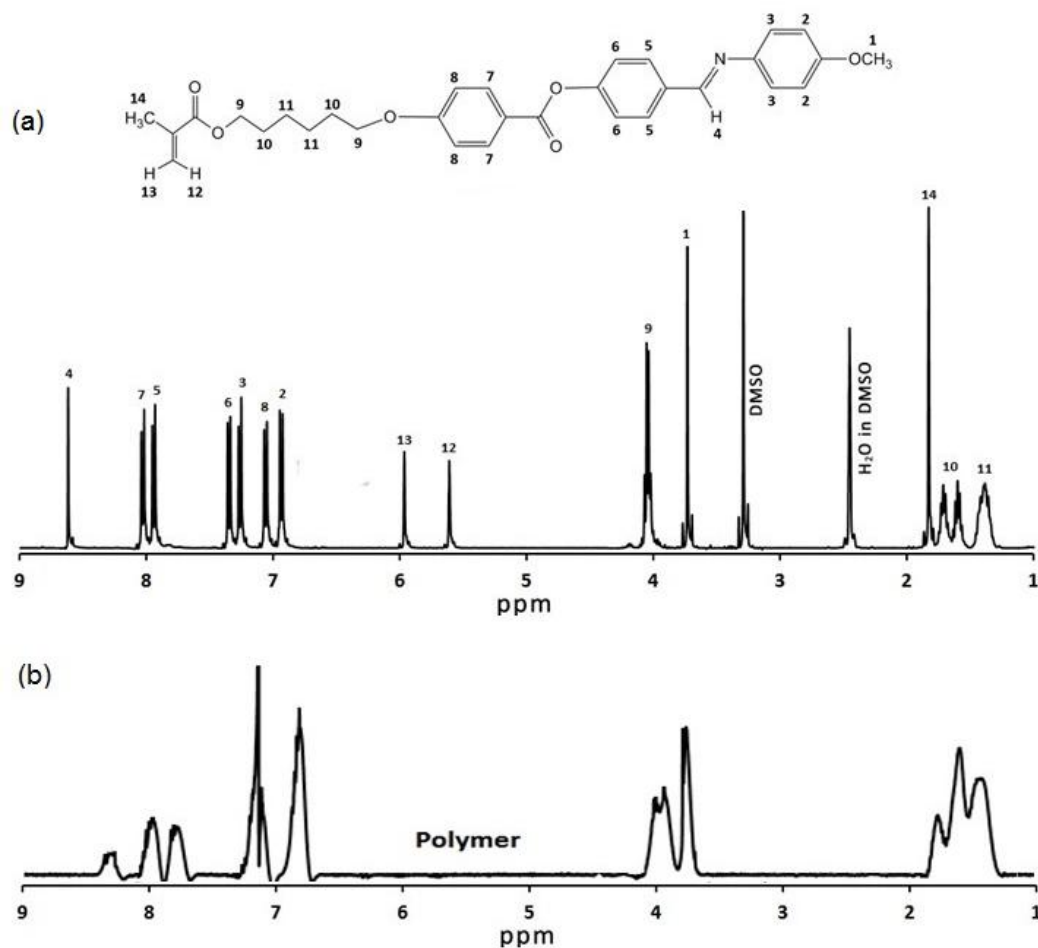


Figure 4.9 : ^1H NMR spectrum of (a) monomer **M3** (b) polymer **HP2M3**.

Figure 4.10(a) shows the ^1H NMR spectrum of monomer **M8** together with its molecular structure. The most de-shielded singlet signal at chemical shift δ 8.66 ppm is due to the Schiff base group (6). The signals appeared at 7.03–8.06 ppm region are mainly due to the presence of four aromatics rings linked by Schiff base and ester group. The doublet signals appeared at δ 8.04–8.06 ppm are attributed to the two aromatic protons on phenyl ring linked by ester group (11). An aromatic protons assigned as 8 appeared as a singlet signal at 7.72 ppm are due to the presence of Schiff base and methoxy group attached to the phenyl ring. The signal appeared as a singlet is mainly because there is no adjacent protons.

The signals of the vinylic protons on acrylate backbone resonate at a range of 5.91–6.33 ppm with different multiplicity of each proton. The two protons (16 and 17)

adjacent to the C=C double bond appeared as a doublet signals whereas proton (18) appeared as a doublet of doublets signals. Proton 16 and 17 are symmetry in-equivalent due to cis/trans relationships. The doublet of doublets signal pattern is observed because the proton 16 and proton 17 couple independently to the proton 18 where each proton splits the peak for proton 18 into a separate doublet. Generally, independent coupling occurs when protons are not freely rotating especially when the protons are attached to a double-bonded carbon [149].

The quartet signal of the protons on the $-\text{OCH}_2-$ of the ester and ether group (13) resonates at 4.08–4.12 ppm. The intense singlet signal at 3.8 ppm is due to the methoxy group (10) attached to the phenyl ring. The protons on this methoxy group are shifted to the higher field due to the de-shielding effect of the electronegative oxygen atom of the adjacent ester group. The signals in the range of 1.39 to 1.73 ppm consist of methylene protons (10 and 11) of the flexible groups attached to the rigid phenyl rings.

After polymerization, ^1H NMR spectra of the polymer showed an absence of vinyl peaks at a range between 5.92–6.33 ppm as shown in Figure 4.10(b) and an additional chemical shift for methylene ($-\text{CH}_2-$) protons at 1.03 ppm in ^1H NMR spectra of polymer. The broad and overlapped resonances of liquid crystal mesogens attached to polymeric back bones appeared at nearly the same positions also observed in all polymer spectra for the proposed polymers structure.

As the monomer **M6** to **M9** and their polymers bear structural similarities except for the lateral unit in the mesogen, **M6**, **M7** and **M9** monomers (Chapter 3, section 3.2) and their polymers showed similar ^1H NMR spectral properties as described for monomer **M8**.

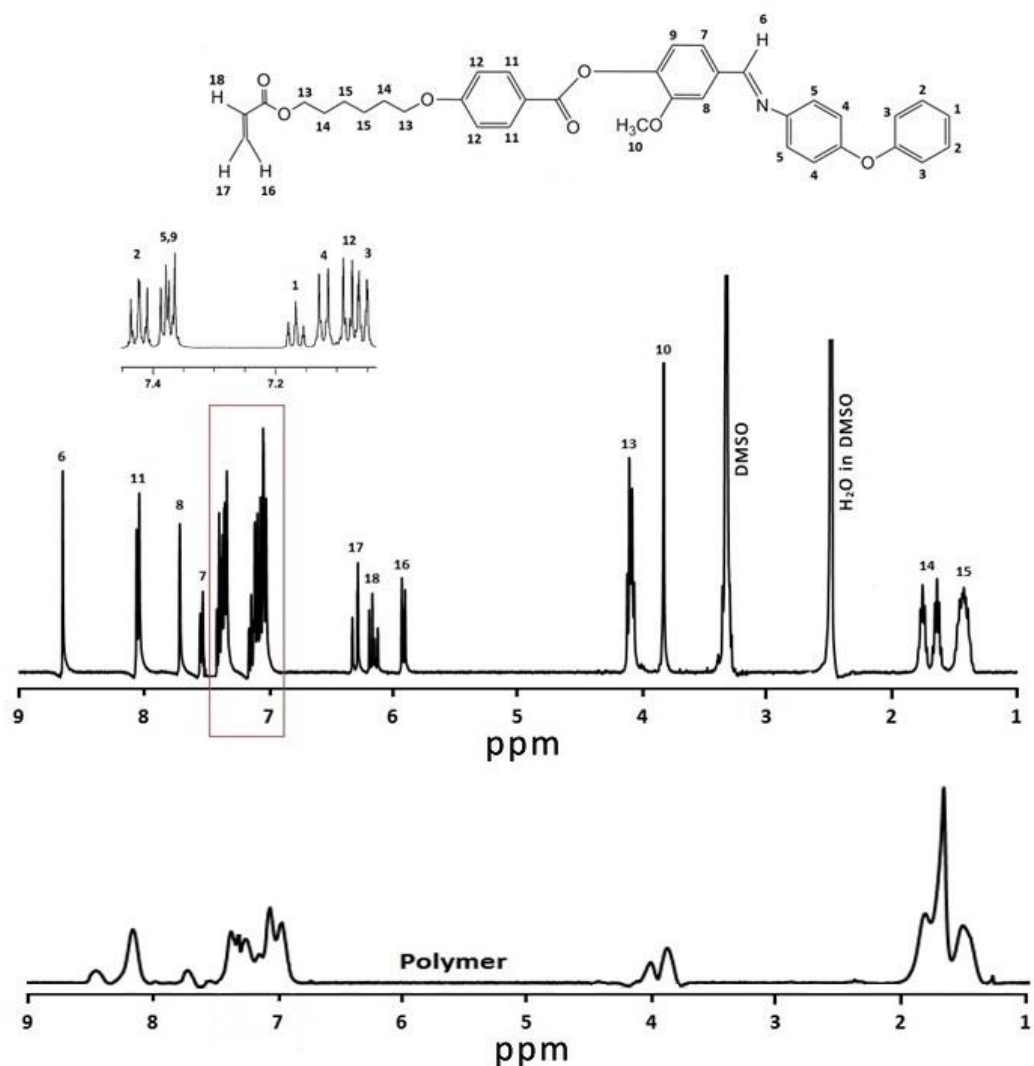


Figure 4.10 : ^1H NMR spectrum of (a) monomer **M8** (b) polymer **HP1M8**.

4.3.2. ^{13}C NMR and DEPT spectra

The proton decoupled ^{13}C NMR and the DEPT 135° spectrum of monomer **M1** are presented in Figure 4.11. The DEPT experiment differentiates between primary, secondary and tertiary carbon groups by variation of the selection angle parameter (the tip angle of the final ^1H pulse): $\theta = 45^\circ$ gives all carbons with attached protons in phase; $\theta = 90^\circ$ gives only methine groups, the others being suppressed; $\theta = 135^\circ$ gives all CH and CH_3 in a phase opposite to CH_2 . The signal that appears at the most downfield region, in the range of 167.0 to 144.5 ppm are assigned to quaternary carbons and other carbons with no attached protons which do not appear in the DEPT spectra. The signals

appeared at the low field region in between 115.4–137.7 ppm are attributed to the aromatic carbons.

The signals at 68.2 and 68.0 ppm are assigned to C₁₃ and C₄ which are carbons on a long alkyl chain attached to an oxygen atom and aromatic ring respectively. Therefore, these carbons were shifted to relatively low field as the oxygen atom acts as an electron withdrawing atom and diamagnetic anisotropy effect from the aromatic ring [148]. The C₁₇ carbon gave signal at 64.7 ppm which was slightly shifted to higher field compared to C₁₃ and C₄. This is because this carbon is only attached to an oxygen atom from the ester group which gives the electron withdrawing effect on that carbon. The signals that appeared at the most high field in the spectrum are the more shielded carbons. The signals of the carbon atoms that are attached to the alkyl chain appeared at 19.3–31.2 ppm. The methyl carbons (C₁ and C₁₉) resonated at 18.4 and 14.1 ppm.

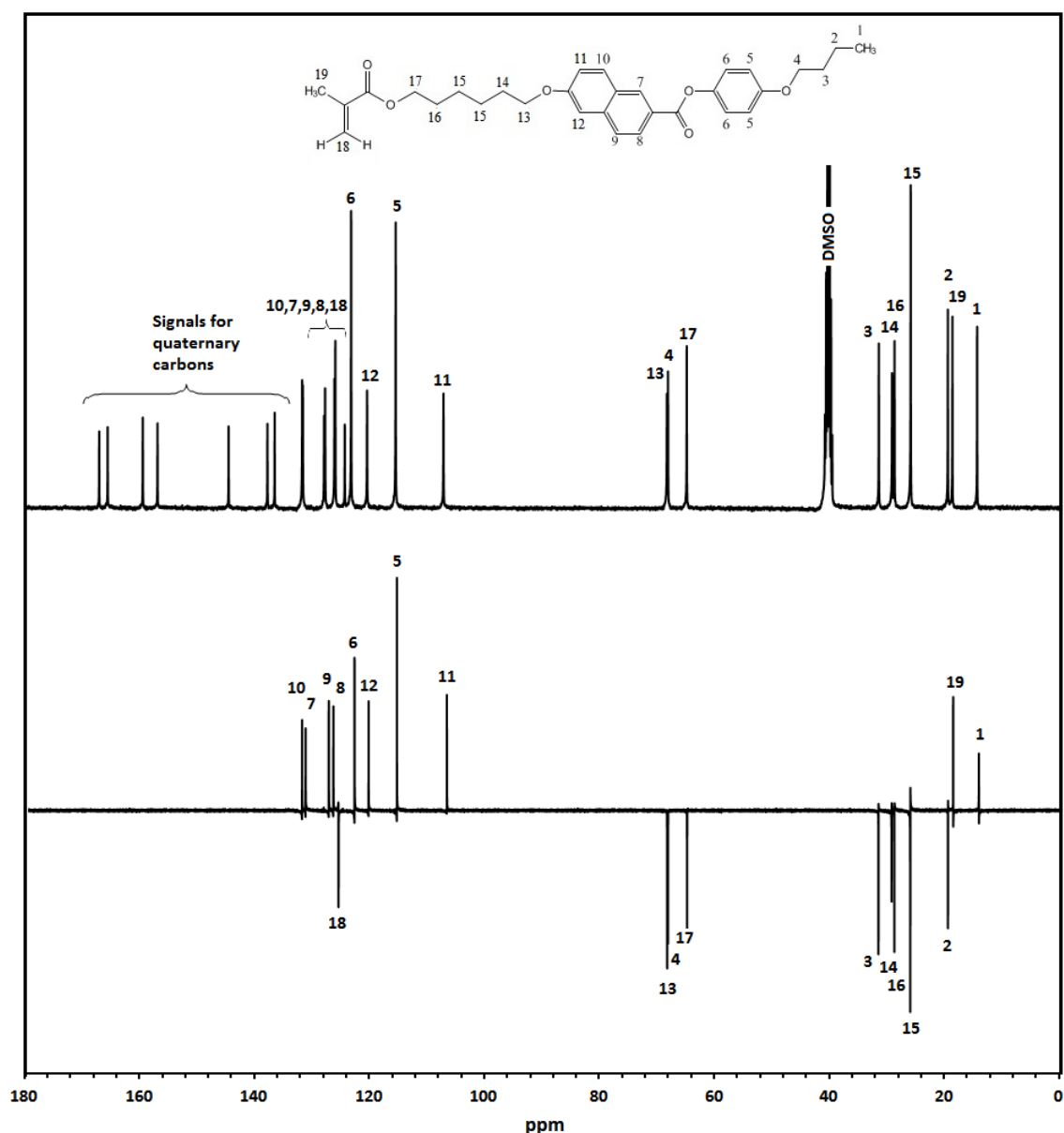


Figure 4.11: ^{13}C NMR and DEPT 135° spectra of monomer **M1**.

Figure 4.12 shows the ^{13}C NMR spectrum of monomer **M3** together with its molecular structure. The signals that appeared at the most downfield region at 165.8 ppm and 163.9 are due to the carbonyl groups, $-\text{OC}=\text{O}$, at C_{11} and C_{22} while that at 163.2 ppm is assigned to Schiff base carbon, $\text{CH}=\text{N}$ at C_6 . These carbons have the largest chemical shifts due to sp^2 hybridization effect of the double bond and to the fact that an electronegative oxygen and nitrogen is directly attached to the carbonyl carbon, de-shielding it even further [148]. The signals that appeared at the low field region in between 114.3–157.9 ppm are attributed to the aromatic carbons. The aromatic carbons

are mainly de-shielded due to sp^2 hybridization and diamagnetic anisotropy. Amongst all the aromatic carbons, C₂, C₅, C₇, C₁₀, C₁₂ and C₁₅ have the lowest intensity compared to the other aromatic carbons. This is because these carbons are *ipso* carbons where the substituent is directly attached. Thus, these six carbons have relatively weak signals due to a long relaxation time and a weak nuclear overhauser enhancement (NOE) effect. Other aromatic carbons, C₃, C₄, C₈, C₉, C₁₃, and C₁₄ have the highest intensity resulting from the two equivalent carbons. However, NOE effect also applied to this condition [148].

The signal at 67.8 ppm is assigned to C₁₆ which is carbon on a long alkyl chain attached to an oxygen atom and aromatic ring and C₂₁ carbon gave signal at 64.1 ppm. The signals of the carbon atoms that are attached to the alkyl chain appeared at 25.0–28.3 ppm. The long alkyl chain with the strongest intensity signal in that region is due to the NOE effect and the interaction of spin-spin dipoles that operates through space [148]. The methoxy carbon (C₁) resonated at 55.2 ppm while the methyl carbon (C₂₄) resonated at 17.9 ppm, showing that the carbon on methyl group is the most shielded carbon. The signal at low field observed on methoxy carbon compared to methyl carbon is due to the presence of electronegative oxygen atom that attracts a bonding pair of electrons from the carbon.

As the monomers **M2** to **M5** and their polymers bear structural similarities except for the lateral unit in the mesogen, **M2**, **M4** and **M5** monomers (Appendix B) and their polymers showed similar ¹³C NMR spectral properties as described for monomer **M3**.

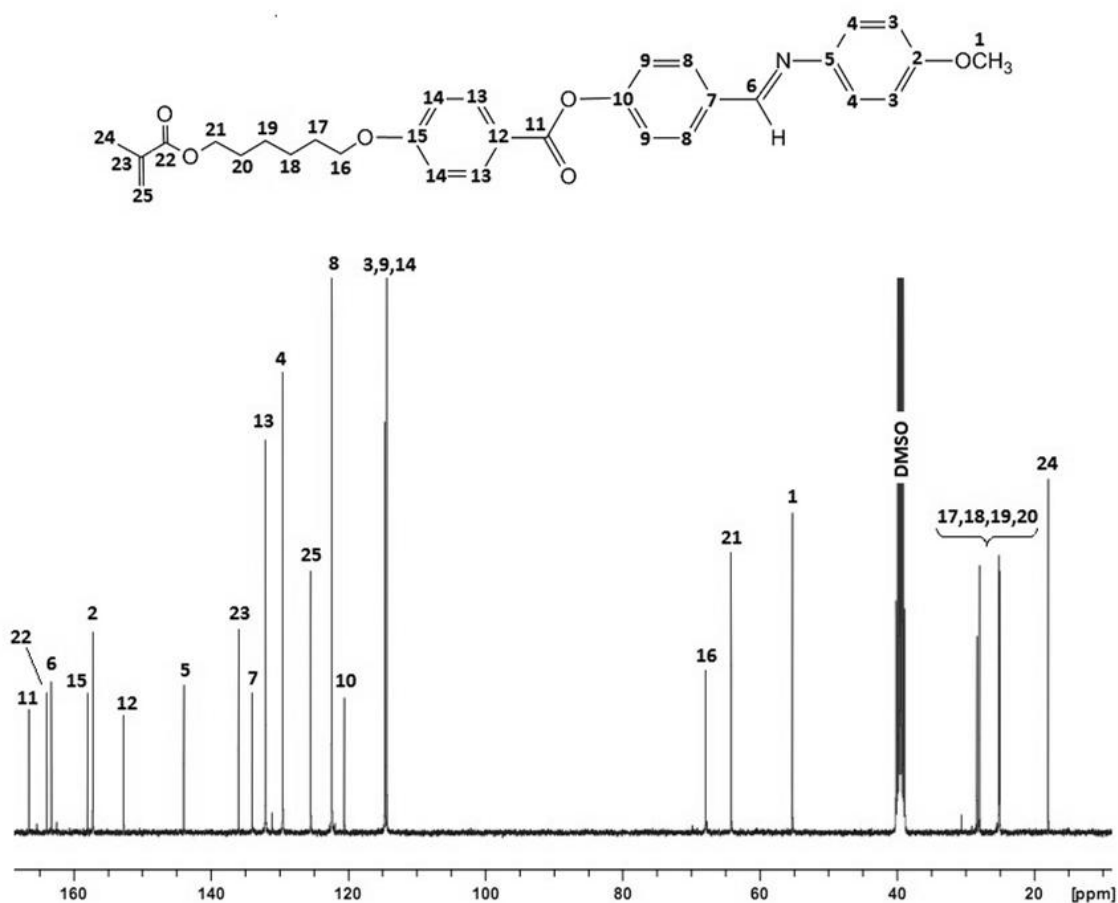


Figure 4.12 : ¹³C NMR spectrum of monomer **M3**.

Figure 4.13 shows the ¹³C NMR spectrum of monomer **M8** together with its molecular structure. The signals that appeared at the most low field region at 166.5 ppm and 163.4, are due to the carbonyl group, -OC=O at C₁₆ and C₂₇. The signal that appeared at 163.2 ppm is assigned to Schiff base carbon, CH=N at C₈. The signals between 111.1–159.1 ppm are attributed to the aromatic carbons while for aromatic carbons C₄ and C_{4'}, the signals are observed at 156.7 and 154.9 ppm respectively. These carbons are de-shielded due to presence of oxygen atom between the phenylene rings. The oxygen atom gives the electronegative effect on the carbons whereas the phenyl rings give the sp² hybridization and diamagnetic anisotropy effect hence bringing down the signal to the lower field. The electronegative effect of the oxygen atom on these carbons is high because there is no adjacent proton attached to it. However, aromatic carbon C₁₂ which is attached to the methoxy group gave signal at 151.3 ppm. This

signal shifted to the higher field because the effect of electronegative oxygen atom is reduced by three hydrogen atom on methoxy group.

The aromatic carbon C₇ showed signal at 146.6 ppm. This carbon is attached to the nitrogen atom of Schiff base group. As nitrogen has lower electro-negativity compared to oxygen, its electron-withdrawing effect on this carbon is weaker than oxygen and thus shifting the carbon to the lower field. Aromatic carbons assigned as C₂, C₃, C₅, C₆, C₁₃, C₁₈ and C₁₉ showed highest intensity due to the two equivalent carbons. Whereas other aromatic carbons show very low intensity due to NOE effect as discussed for monomer **M3**. The signal at 67.8 ppm is assigned to C₂₁ which is carbon on a long alkyl chain attached to an oxygen atom and aromatic ring. The C₂₆ carbon gave signal at 64.1 ppm which shifted slightly to higher field compared to C₂₁. The signals of the carbon atoms that are attached to the alkyl chain appeared at 25.0–28.3 ppm. The reason why these signals appeared with the corresponding chemical shifts has been discussed earlier.

As the monomers **M6** to **M9** and their polymers bear structural similarities except for the lateral unit in the mesogen, **M6**, **M7** and **M9** monomers (Appendix B) and their polymers showed similar ¹³C NMR spectral properties as described for monomer **M8**.

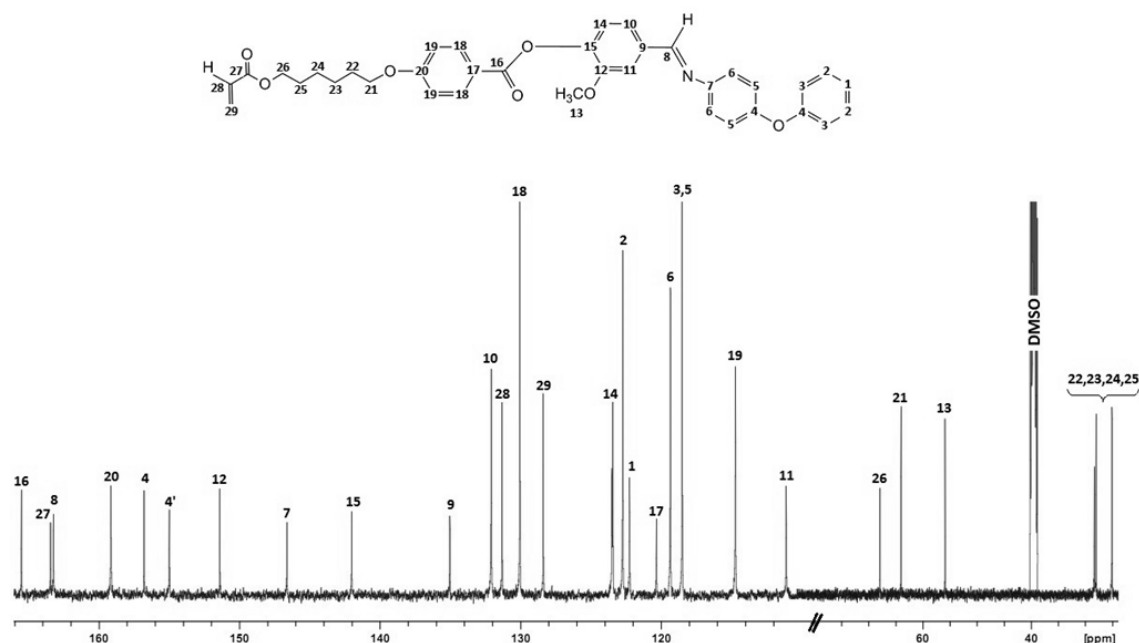


Figure 4.13 : ^{13}C NMR spectrum of monomer **M8** and the molecular structure.

4.3.3. Fourier Transform Infrared spectroscopy (FTIR)

The FTIR spectra of monomer **M3** and polymer **HP1M3** are shown in Figure 4.14. Although there are some slight variations in intensity of the peaks, generally, all the monomers and polymers exhibited the same characteristic FTIR peaks since the functional groups are similar. The peak observed at 3075 cm^{-1} is attributed to the aromatic unsaturated $=\text{C}-\text{H}$ stretching. The vibrations due to the asymmetrical and symmetrical $\text{C}-\text{H}$ stretchings of the methyl groups appeared at 2938 and 2857 cm^{-1} . A small stretching peak at 2849 cm^{-1} shows the presence of methoxy ($\text{O}-\text{CH}_3$) group. The ester carbonyl group is reflected from the very strong stretching frequencies at 1728 and 1708 cm^{-1} . The $\text{C}=\text{N}$ stretching due to Schiff base group showed signal at 1603 cm^{-1} . The peaks at 1578 and 1508 cm^{-1} are due to aromatic $\text{C}=\text{C}$ stretching. The $\text{C}-\text{O}$ link in the methacrylate and acrylate group appeared at 1201 cm^{-1} . The peaks at 1247 , 1160 and 1070 cm^{-1} are due to $\text{C}-\text{O}$ stretching. The out of plane bending vibrations of $\text{C}-\text{H}$ groups of benzene ring were observed at 836 and 756 cm^{-1} . The absorption band at 1623 cm^{-1} is assigned to the stretching vibration of vinyl $\text{C}=\text{C}$ and after the polymerization,

this band completely disappeared. The absorption bands at 1708 and 1728 cm^{-1} are due to the C=O stretching of the carbonyl groups. These bands shifted and appeared as one broad peak at 1724 cm^{-1} after polymerization. This shifting of vibrational frequency may be due to the reduced electron delocalization of the carbonyl double bond in the methacrylic group. All of these observations confirm that only the unsaturated methacrylic groups were involved in the polymerization process.

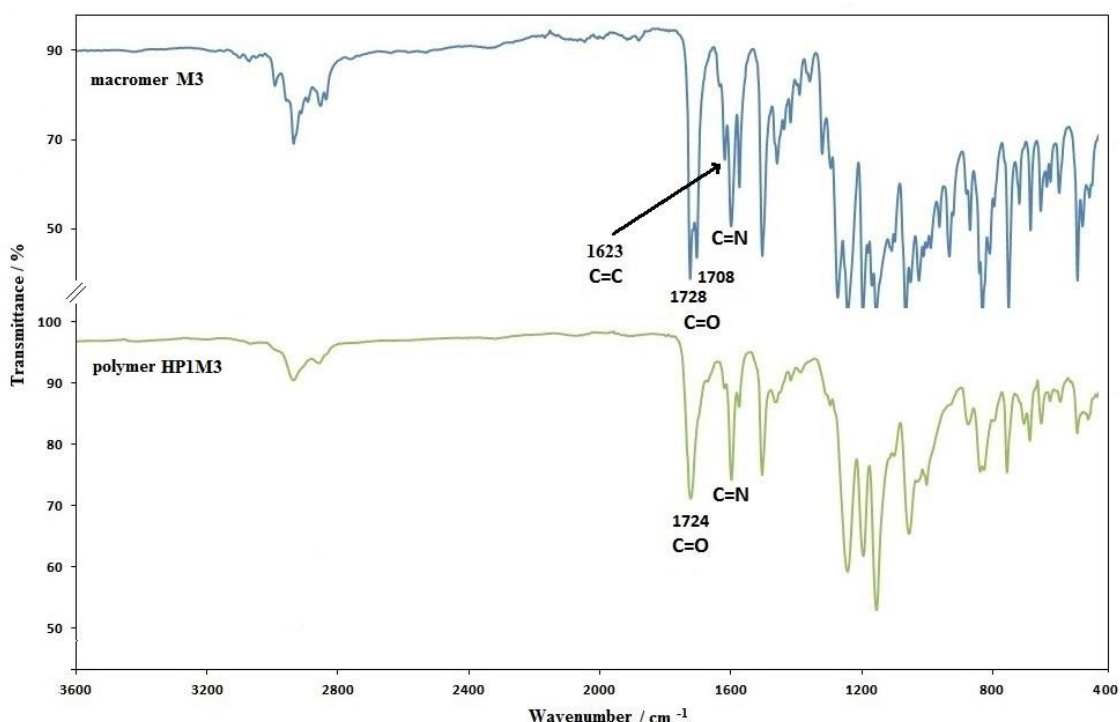


Figure 4.14 : FTIR spectra of monomer **M3** and polymer **HP1M3**.

4.4. Solubility behavior

The solubility tests for the monomers and polymers were done by immersing about 5 mg of the samples in 3 ml of solvents at room temperature. All the samples were readily soluble when immersed in solvents. The monomers and polymers had good solubility at room temperature in common organic solvents, such as tetrahydrofuran (THF), chloroform, *N,N*-dimethylformamide (DMF), dimethylsulfoxide (DMSO) and dichloromethane. The good solubilities of the monomers and polymers are attributed to

the presence of the polar ester linkages as well as aliphatic flexible spacer in the backbone which make the shape of the macromolecules to be far from a rigid mesogen [150].

4.5. Thermal properties and mesomorphic behavior of monomers

The thermal properties and the mesomorphic behavior of the monomers were studied by DSC, POM, SAXS and PXRD. Results of the thermal properties are summarized in Table 4.5. The phase transition temperatures and changes of enthalpy (ΔH) during the first cooling and the second heating cycles were obtained by DSC. The effect of mesogen structure, the effect of lateral substitution and the effect of polymerizable terminal group on the mesomorphic properties of the monomers will be discussed below.

Table 4.5 : Phase behavior and thermal properties of the monomers by Differential Scanning Calorimetry

| Monomer | Phase transitions($^{\circ}\text{C}$) ^{a,b} (corresponding enthalpy changes, J g^{-1}) | |
|-----------|-------------------------------------------------------------------------------------------------------------|-------------------------------------|
| | Heating | Cooling |
| M1 | S 86.8 (0.93) N 103.6 (1.23) I | I 102.3 (-1.21) N 85.5 (-0.92) S |
| M2 | N 217.68 (2.03) I | I 217.77 (-2.91) N |
| M3 | N 181.42 (1.35) I | I 180.08 (-5.28) N |
| M4 | N 126.84 (1.74) I | I 124.65 (-2.10) N |
| M5 | N 101.85 (1.30) I | I 99.47 (-1.57) N |
| M6 | S 108.70 (0.62) N 135.2 (1.63) I | I 133.45 (-1.21) N 106.96 (-0.92) S |
| M7 | S 105.84 (0.27) N 134.17 (0.28) I | I 131.48 (-0.14) N 103.16 (-0.11) S |
| M8 | N 49.84 (0.61) I | N 48.77 (-0.64) I |
| M9 | N 42.36 (0.68) I | N 40.25 (-0.71) I |

^aTransition temperatures ($^{\circ}\text{C}$) and enthalpies (in parentheses, J g^{-1}) were measured by DSC (at a heating and cooling rate of $10^{\circ}\text{C}/\text{min}$).

^bS= Smectic phase; N = nematic phase; I= isotropic phase.

4.5.1. Effect of mesogen structure

Thermotropic liquid crystals are highly sensitive to their molecular constitution. It is of prime importance to determine the effects of alterations in the mesogenic core on the mesomorphic behavior of a compound. The thermal stability and mesophase length as a measure of mesomorphism can be correlated with the molecular constitution of the compounds [151]. In this work, the monomers were designed with three types of mesogen structure consisting of: i) naphthalene ring (monomer **M1**), ii) three benzene rings (monomers **M2** to **M5**) and iii) four benzene rings (monomers **M6** to **M9**). In order to study the effect of mesogen structure on the mesomorphic behavior, monomers, **M1**, **M4** and **M8**, were chosen to represent other monomers.

Figure 4.15 shows the DSC thermograms of heating and cooling cycles of monomers, **M1**, **M4** and **M8**, at a rate 10°C/min. The glass transition (T_g) for these monomers were not detected by DSC. The thermal transitions for all monomers were enantiotropic where the liquid crystal phase existed upon heating and cooling. Monomer **M1** exhibited nematic and smectic mesophases which undergo isotropization at 103.6°C during second heating scan. Two peaks at 102.3°C and 85.5°C associated with the isotropic-nematic and nematic-smectic transitions respectively were observed during the cooling scan. Meanwhile, monomer **M4** and monomer **M8** exhibited nematic mesophase which undergo isotropization at 126.84°C and 49.84°C respectively during second heating scan. During cooling scan, the peak at 124.65°C and 48.77°C associated with the isotropic-nematic transition was observed for monomer **M4** and monomer **M8** respectively. Comparison among the three compounds reveals that monomer **M1** exhibited smectic and nematic mesophases whereas monomer **M4** and monomer **M8** exhibited only nematic mesophase. This result may be attributed to the fact that naphthalene derivatives exhibit rich mesomorphism [51].

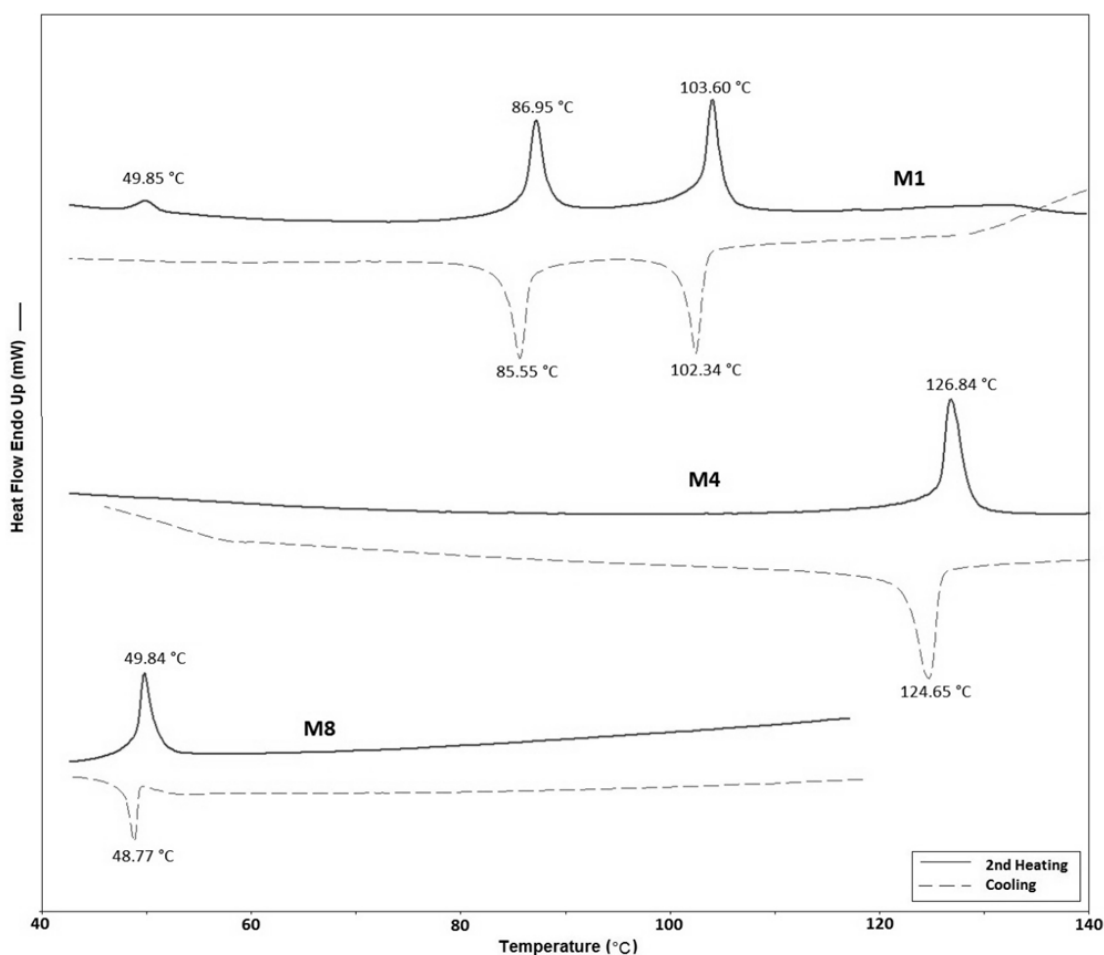


Figure 4.15 : DSC thermograms of **M1**, **M4** and **M8** monomers.

The phase transition temperature of monomer **M1** is lower by 22°C to 23°C as compared to monomer **M4**. The molecules of monomer **M1** and monomer **M4** differ on the linking unit and the rigid core structure. Monomer **M1** contains naphthalene and one phenyl ring in the mesogen linked by an ester group, whereas monomer **M4** has three phenyl rings linked by Schiff base and ester groups as shown in Figure 4.16. The naphthalene ring provides a crankshaft structure which restricts lamellar packing of the molecules, hence lower the phase transition temperature of monomer **M1** [152, 153]. However, the incorporation of Schiff base group as a linking unit increases the phase transition temperature of monomer **M4** compared to monomer **M1**. This Schiff base group provides a better stability and enables mesophase formation because it can maintain the molecular linearity of the molecules [1].

The phase transition temperature of monomer **M4** is higher by 77°C and 76°C as compared with monomer **M8**. The molecules of monomer **M4** and monomer **M8** differ only in the number of phenyl rings. Monomer **M4** has three phenyl rings, whereas monomer **M8** has four phenyl rings (Figure 4.16). According to Fornasieri et. al [69], increasing the number of aromatic rings in the core structure increases the phase transition temperatures. However, monomer **M4** showed higher thermal transition temperature compared to monomer **M8**. This is because the molecular length of monomer **M4** is longer than monomer **M8** as shown in Figure 4.16. Gray [8] and Ha et. al [55] suggested that the increase in the length of the molecule and resulting enhanced anisotropy of the polarizability, increases the intermolecular cohesive forces which leads to higher nematic phase transition temperatures as seen in monomer **M4** when compared to monomer **M8**.

In addition, the more stable nematic mesophase of monomer **M4** is influenced by its molecular geometry. As shown in Figure 4.16, monomer **M4** favors the formation of rod-like molecular geometry with large bent angle which enables more efficient packing of the molecules. In contrast, monomer **M8** favors the formation of bended molecular geometry with 86-93° bent angle. Monomer **M8** also has some flexibility in its mesogenic structure. Two of the phenylene rings in the mesogenic group are connected by a kinked unit, (-O-). The kinked unit served as separators to the phenylene rings hence the rotation of the rings becomes less hindered. The torsional barrier for this type of molecule is 10 kcal mol⁻¹ higher compared to the molecule with only one phenyl ring connected to oxygen atom. This may be due to the interaction between two phenyl rings. The most probable conformation for this type of molecule is found to be tilted at 40° [154]. Thus, this leads to destruction of linearity and increased the flexibility of the molecules [2]. In general, the compounds with kinked elements are no longer liquid crystals. However, monomer **M8** still shows nematic mesophase at about 50°C as the

mesogenic structure is still rigid due to the presence of the central Schiff base ester linkages [1, 4].

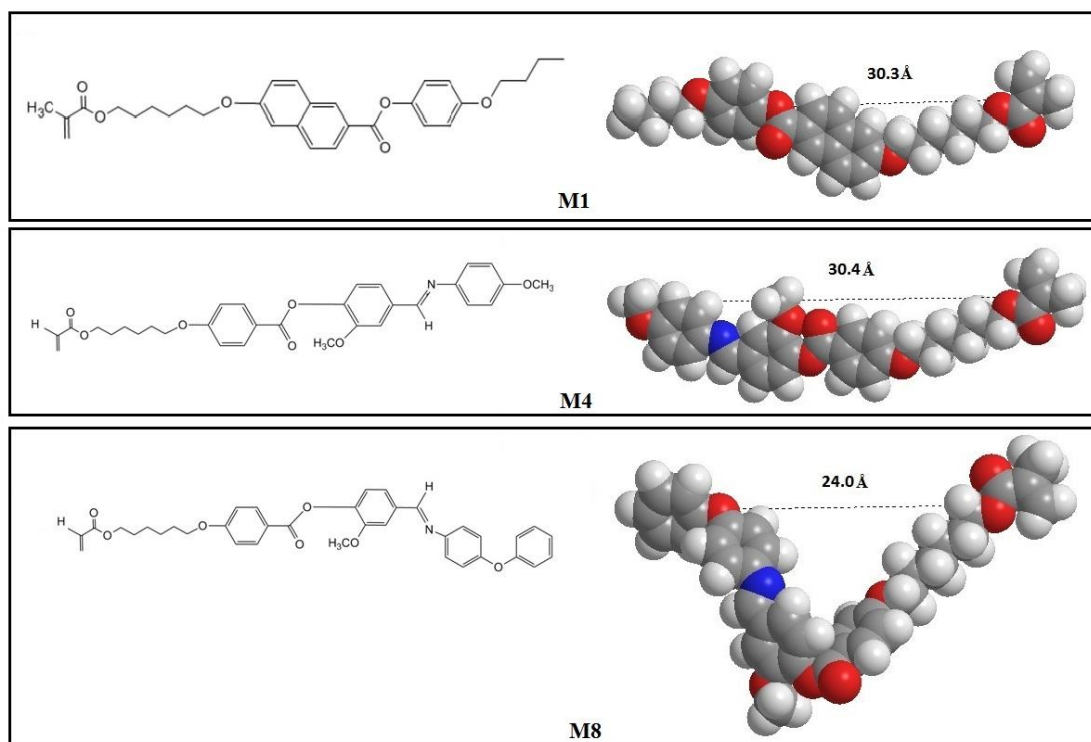


Figure 4.16 : Molecular structures and molecular lengths of the monomers (a) **M1** (b) **M4** (c) **M8**. The molecular lengths of the compounds were estimated from the most extended conformation with optimized energy level by energy-minimized space filling model (MM2 energy parameters derived from ChemBio3D Ultra 10.0 software).

Figure 4.17 shows the POM of monomer **M1** textures obtained at different temperatures. Upon cooling from isotropic melt, schlieren texture of nematic mesophase appeared at 101.9°C (Figure 4.17(a)). The transition from a nematic to a smectic mesophase was observed when the monomer was cooled to 85.1°C as shown in Figure 4.17(b). Certain region of focal conic fan texture which is characteristic of a smectic mesophase at 83.8°C became dark indicating the isotropic liquid area (Figure 4.17(c)). When the monomer was cooled to room temperature from its smectic state, it solidified and its crystalline phase appeared as lumber-like mosaic textures (Figure 4.17(d)). The mesophase temperature range was found to be very broad (49.85 – 103.66°C) which

might be attributed to the presence of crankshaft structure of the naphthalene that can decrease the freedom of movement of the molecule [152].

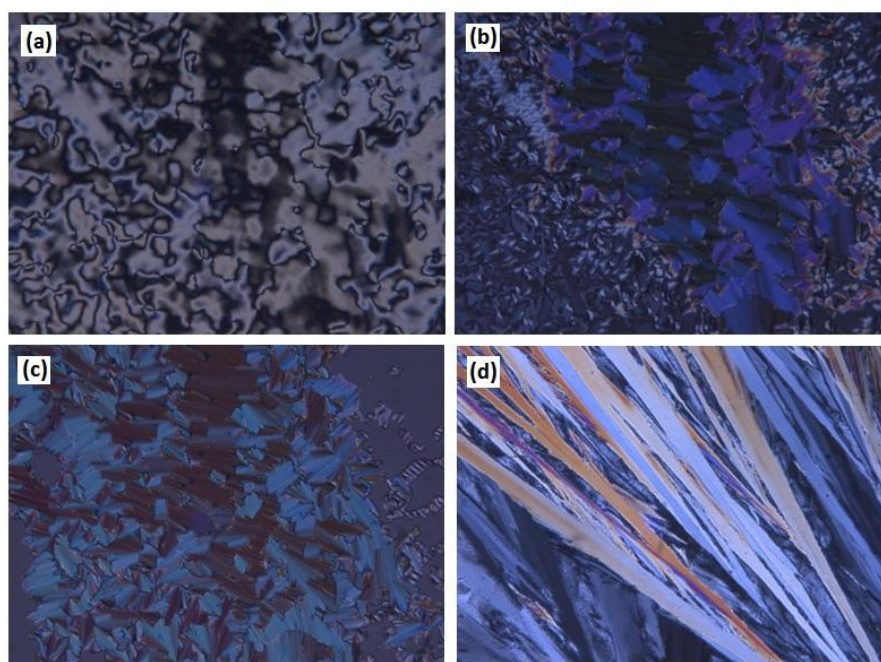


Figure 4.17 : POM textures of monomer **M1**. (a) 101.9°C (b) 85.1°C (c) 83.8°C (d) Crystalline at room temperature.

Figure 4.18 shows the POM of monomer **M4** textures obtained at different temperatures. The nematic droplets started to appear when the monomer was cooled to 108°C from the isotropic phase as shown in Figure 4.18(a). Upon cooling, the droplets became bigger to form schlieren nematic texture (Figure 4.18(b)). The droplets are characteristic of nematic mesophase because they occur nowhere else [155]. Upon cooling to 106°C, schlieren nematic texture was completely formed (Figure 4.18(c)) which exhibited characteristic sets of often curved dark brushes. At these directions, the director is parallel either to the polarizer or to the analyzer [156]. There are many point singularities with two dark brushes in the schlieren textures, which further confirm the nematic nature of the mesophase because such singularity is not compatible with the smectic C phase [157, 158]. As the monomer was heated slowly at a rate of 1°C/min from its crystal phase, the schlieren nematic texture with fourfold dark brushes was

observed at 106°C (Figure 4.18(d)). A closer look revealed that the brushes come together in a singular point to be fourfold brush.

Figure 4.19 shows the POM of monomer **M8** textures obtained at different temperatures. Monomer **M8** exhibited grayish multicolored droplets with a fine grain texture characteristic of nematic texture appearing when the monomer were cooled to 46°C from the isotropic phase (Figure 4.19(a)). Upon further cooling, the fine grain texture grew to form schlieren nematic texture (Figure 4.19(b)).

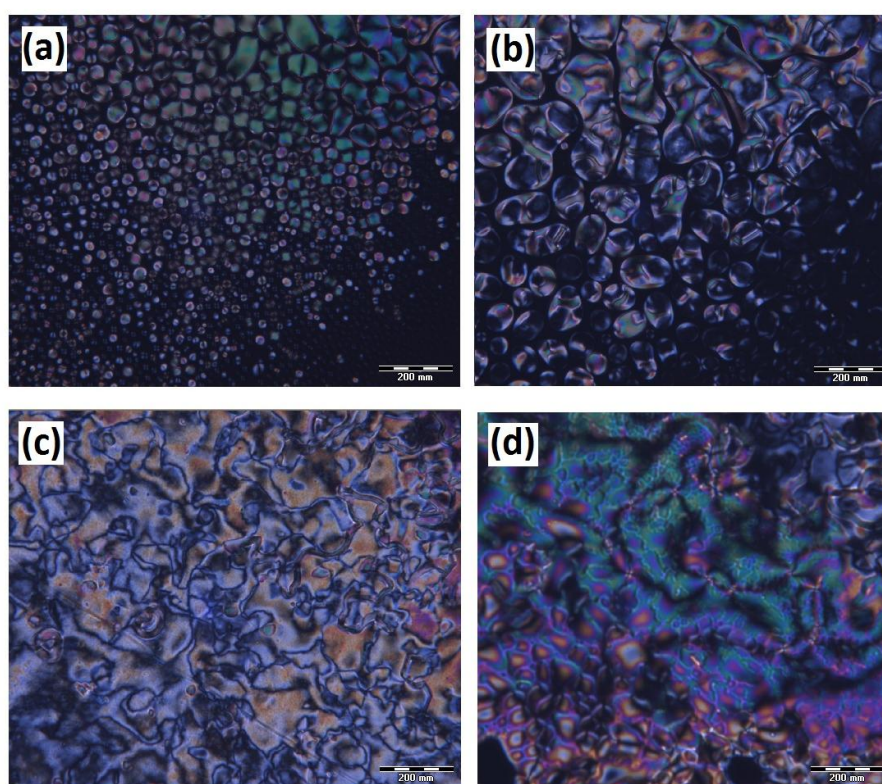


Figure 4.18 : POM textures of monomer **M4** at (a) 108°C (b) 106°C (c) 104°C (d) 106°C.

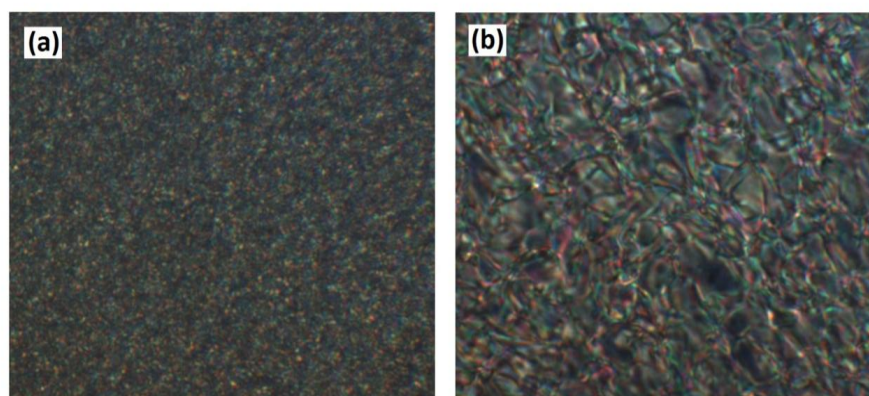


Figure 4.19 : POM textures of monomer **M8** at (a) 46°C (b) 40°C.

Although DSC and POM experiments provide very valuable information about the phase transitions of these monomers, they cannot elucidate concrete structural evolution. In order to illustrate the phase structures clearly, small angle x-ray (SAXS) was performed to identify the mesophase textures of monomer **M1** and powder X-ray diffraction (PXRD) experiments with varying temperatures were performed to identify the mesophase textures of monomer **M4** and monomer **M8**.

Figure 4.20 shows the SAXS intensity profiles of monomer **M1** at room temperature and 100°C. At room temperature, the sample showed a sharp scattering signal in the low q region (2.2 nm^{-1}) indicating a typical smectic phase texture and an intense broad peak in the higher q region (3.27 nm^{-1}) which indicates that only a short-range order existed in the molecular lateral packing [159]. The layer periodicities calculated for the first sharp peak was 2.86 nm and 1.92 nm for the broad peak. After heating at 100°C the sharp peak disappeared while the broad peak remained, indicating that the sample has entered the nematic phase. From the results of DSC, POM and SAXS, we can conclude that the transition from isotropic to nematic phase has occurred at higher temperature and that from nematic to smectic phase has occurred at lower temperature.

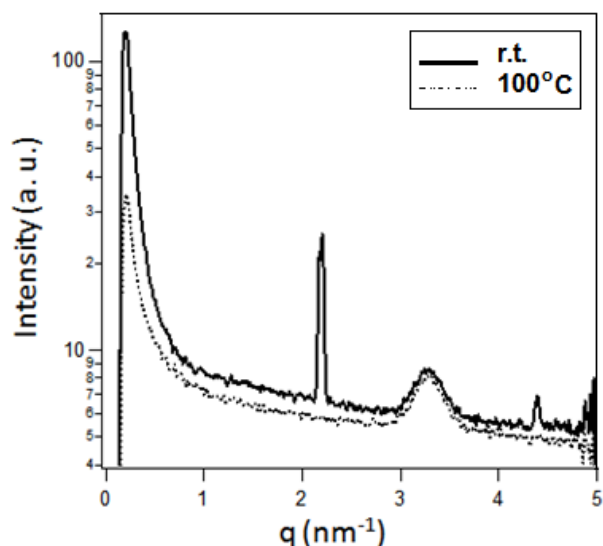


Figure 4.20 : Small angle X-ray scattering of monomer **M1**.

Figure 4.21(a) shows X-ray pattern of monomer **M4** during first heating. When the sample was heated to 100°C, high intensity of wide angle reflections was observed. This is because the attractive inter-chain interactions between the aromatic backbones are increased due to the flexibility of the aliphatic spacer [150]. After the temperature increased to 120°C, the wide angle reflections started to disappear and formed a broad halo in the region of $2\theta = 15\text{-}25^\circ$ with d -spacing of 3-5Å and small peaks. This behavior is related to a structural change accompanied by melting with disappearance of the long range order, indicating a nematic phase. The remaining weak peaks indicate the assembly of the mesogenic units in cybotactic groups into the nematic mesophase [150, 160]. These peaks disappeared completely when the sample was heated to 130°C indicating the isotropic phase of the monomer **M4**.

Figure 4.21(b) shows X-ray pattern of monomer **M8** during first heating. When the sample was heated to 60°C, a series of very sharp diffraction peaks were observed due to highly crystalline phase of the sample. At this temperature, the monomer still remain as a crystalline powder and immediately change to nematic mesophase as heated to 80°C with presence of broad peak in the region 12-25° and a d -spacing of 3-5Å. This

broad peak is classically due to lateral interference of the mesogenic cores of the monomer.

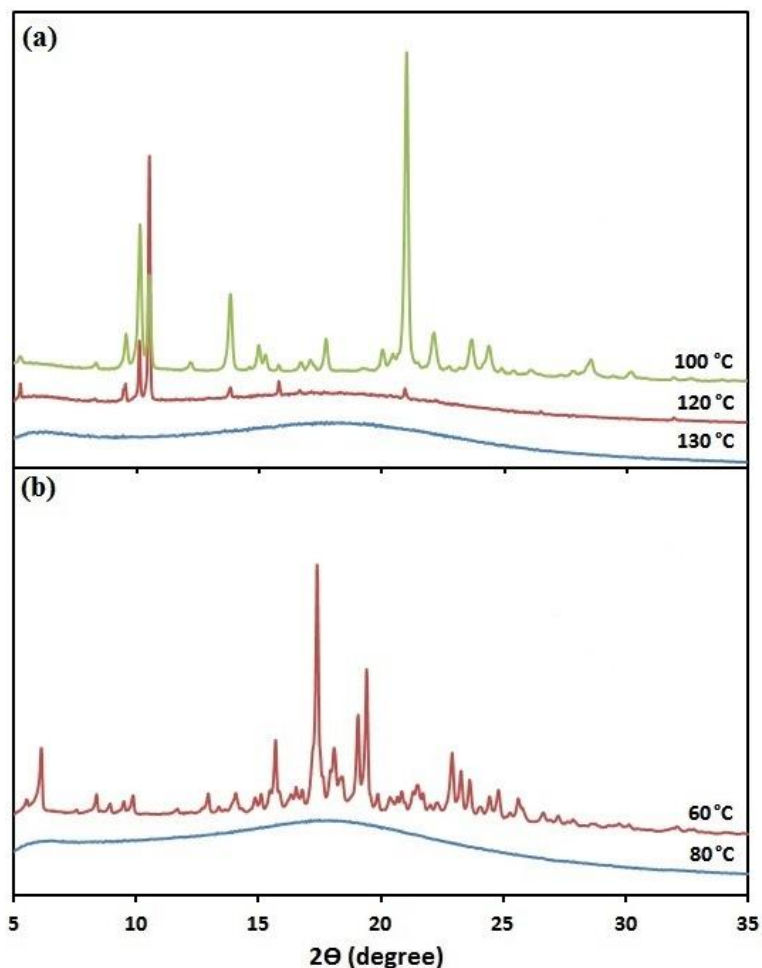


Figure 4.21 : PXRD patterns for monomers (a) **M4** and (b) **M8**.

4.5.2. Effect of lateral substitution on mesogenic unit

The modification of lateral substitutions could greatly effect of the mesophase behavior of low molar mass liquid crystals and liquid crystalline polymers [6, 17]. Therefore, the monomers with a lateral methoxy unit on the mesogen (monomers, **M4**, **M5**, **M8** and **M9**) and the monomers without a lateral substitution on the mesogen (monomers, **M2**, **M3**, **M6** and **M7**) were synthesized. In order to study the effect of

lateral substitution on the mesomorphic behavior of the monomers, monomer **M3** and monomer **M5** have been chosen to represent other monomers.

Figure 4.22 shows the DSC thermograms of heating and cooling cycles of monomer **M3** and monomer **M5** at a heating rate of 10°C/min. The T_g for these monomers were not detected by DSC. Both monomers exhibited a nematic mesophase which undergo isotropization at 181.42°C and 101.85°C for monomer **M3** and monomer **M5** respectively during the second heating scan. The thermal transitions were enantiotropic, where the liquid crystal phase existed upon heating and cooling. For the cooling scan, peaks at 180.08°C for monomer **M3** and at 99.47°C for monomer **M5** associated with the isotropic-nematic transition were observed.

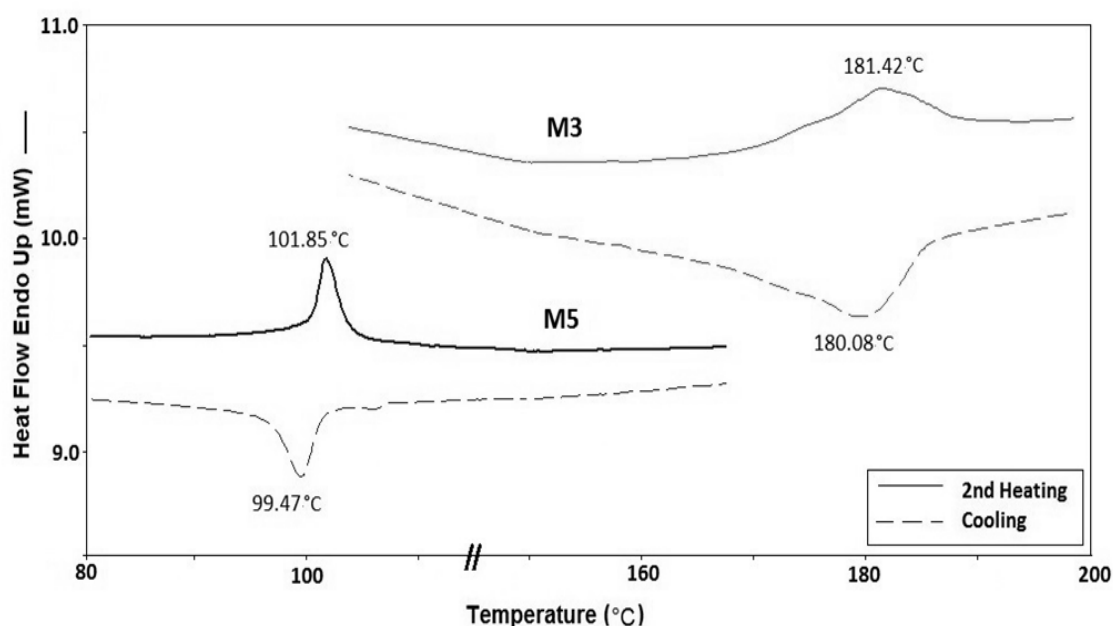


Figure 4.22 : DSC thermograms of monomer **M3** and monomer **M5**.

As can be seen in Figure 4.22, a higher nematic to isotropic transition temperature was found in monomer **M3** which has no substituent on the central ring. On the other hand, monomer **M5** exhibited a phase transition at a lower temperature due to the presence of a methoxy lateral unit. This observation was also reported in a similar work by Kaspar et al. [78]. It was suggested that the presence of a lateral methoxy group at

the *meta* position of monomer **M5** increased interactions among the molecules in the nematic phase. The methoxy group is an electron-donating group which, if present on a substituted aromatic ring, will increase the π -electron density of that ring, resulting in a reduction in the phase transition temperature.

In addition, the incorporation of a methoxy group as a lateral substitution increases the molecular breadth which reduces the length to breadth (L/B) ratio of monomer **M5** to 6.0 compared to 10.7 for monomer **M3** as shown in Figure 4.23. The increased of molecular breadth reduced the strength of the intermolecular lateral attraction thus the long narrow molecules will be forced further apart. The nematic mesophase is much more dependent on these cohesive forces to maintain the parallel orientations of the molecules. Therefore, substitution leading to an increase in molecular breadth will decrease the nematic thermal stabilities [8]. In this molecular system, where the monomer has a central carboxy group (-COO), the oxygen atom of the central carboxy group in the molecule will be in a position very close to the non-bonded side of the adjacent -H of the aromatic ring, thereby causing considerable strain on the molecule. This will cause some twisting around the C-O bond and force the benzene ring out of plane of the molecule hence broadening the molecule [54].

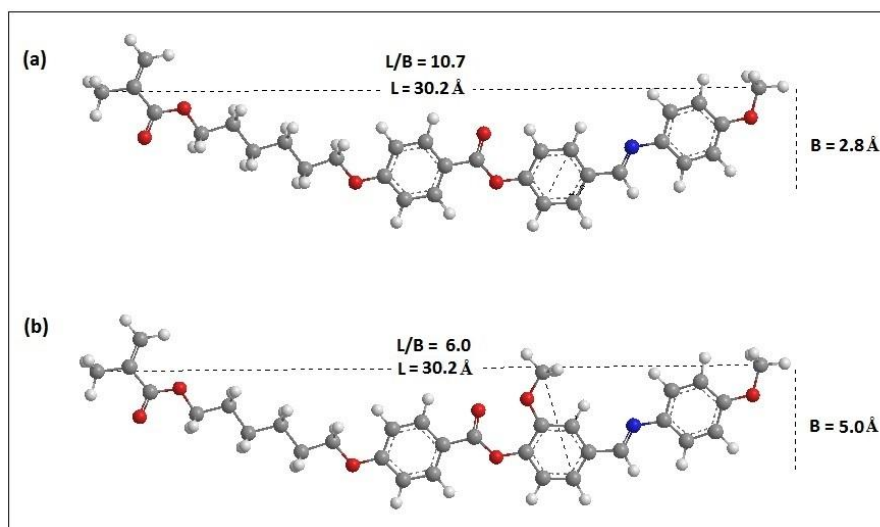


Figure 4.23: Molecular structures of monomers (a) **M3** and (b) **M5**.

The presence of a lateral methoxy group which is *ortho* to the –COO linkage not only increases the breadth of the molecule but also increases the acoplanarity in the system due to steric interaction. These two factors would eliminate the smectogenic tendencies as well as decrease the nematic mesophase range and the nematic to isotropic transition (N-I) temperature for monomer **M5** [51]. This finding is similar to that of Dave and Bhatt [81] who studied the effects of lateral methyl group on the mesomorphic behavior of liquid crystals. Additionally, the presence of the lateral unit in the mesogen structure not only gives a negative effect on thermal stabilities but also reduces the strength of the compound due to the thickening of the chain. It also lowers the crystallinity of the compound which leads to low mechanical property and heat deflection temperature [2]. All the negative aspects have to be considered when lateral substitution is used to bring down the melting points.

Figure 4.24 shows the POM of monomer **M3** textures obtained at different temperatures. The marble texture of a nematic mesophase started to appear when the monomer was cooled to 195.7°C from the isotropic temperature as shown in Figure 4.24(a). This is frequently observed in a natural nematic texture. Different colors of marble textures can be observed upon further cooling (Figure 4.24(b) to Figure 4.24(f)). The color alterations are due to a change in birefringence from in-plane and also out-of-plane variations of the director [156]. Upon further cooling to 53°C (Figure 4.24(g)), the nematic phase started to change conformation and crystallized when further cooled to room temperature (Figure 4.24(h)).

Figure 4.25 shows the POM of monomer **M5** textures obtained at different temperatures. The schlieren nematic texture appeared when the monomer was cooled to 94.5°C from the isotropic temperature as shown in Figure 4.25(a). When the monomer was cooled to room temperature from its nematic phase, its crystalline phase appeared as lumber-like mosaic textures (Figure 4.25(b)).

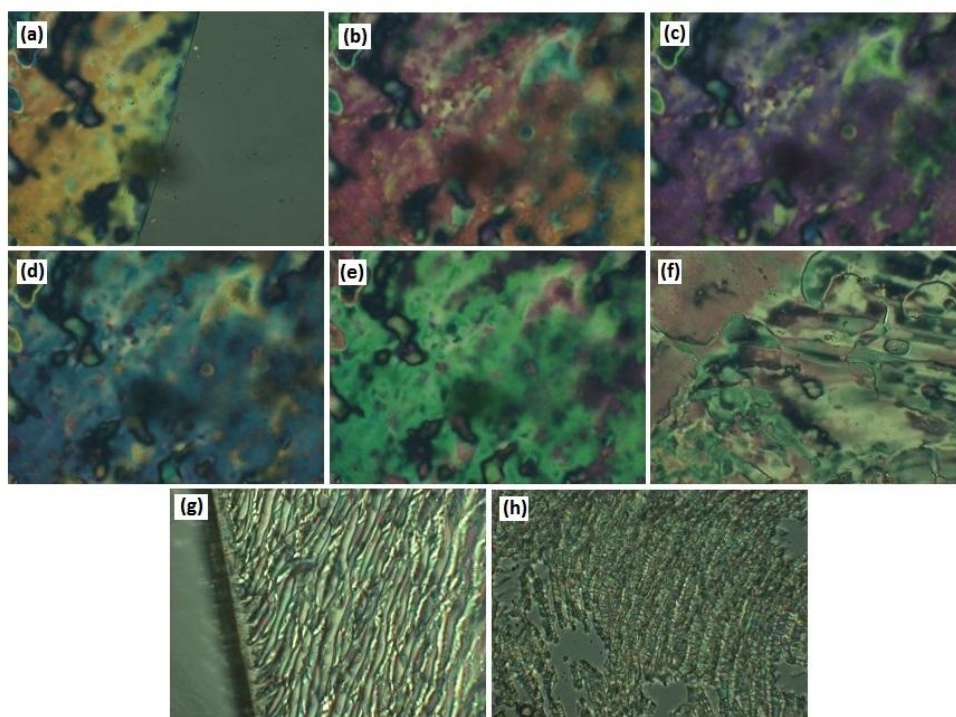


Figure 4.24: POM textures of monomer **M3**. (a) 195.7°C (b) 193.9°C (c) 192.5°C (d) 190.9°C (e) 186.6°C (f) 177.8°C (g) 53.1°C (h) crystalline at room temperature.

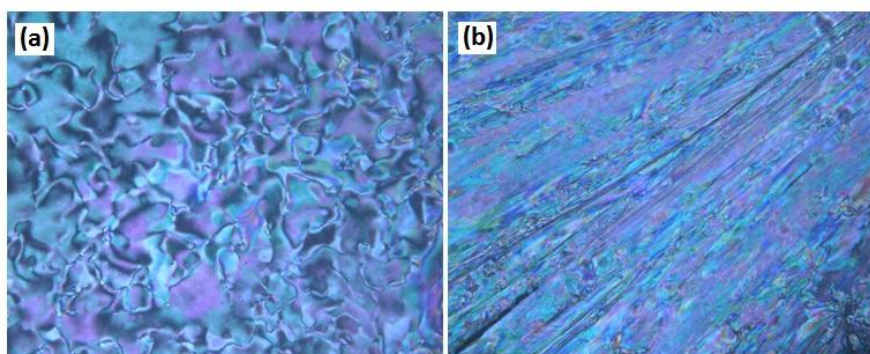


Figure 4.25: POM textures of monomer **M5**. (a) 94.5°C (b) crystalline at room temperature.

The identity of the nematic phase of these compounds was determined by powder X-ray diffraction (PXRD). PXRD patterns of monomer **M3** during first heating are shown in Figure 4.26(b). When the sample was heated to 70°C, a broad halo in the region $2\theta = 12-25^\circ$ with d -spacing of 4.3Å with small peaks was observed. This behavior is related to a structural change accompanied by melting with disappearance of the long range order, indicating a nematic phase [150]. As the temperature increased to 140°C, the small peaks disappeared and the intensity of the broad halo diminished. The intensity of the broad halo in a wide angle area ($2\theta = 18^\circ$) increased when the

temperature reached 160°C indicating that the nematic phase has formed again. At this temperature the liquid-like interactions among molten chains also appeared [161]. This phenomenon was also seen for the monomer **M5** when it was heated to 50°C, 70°C and 90°C as shown in Figure 4.26(b).

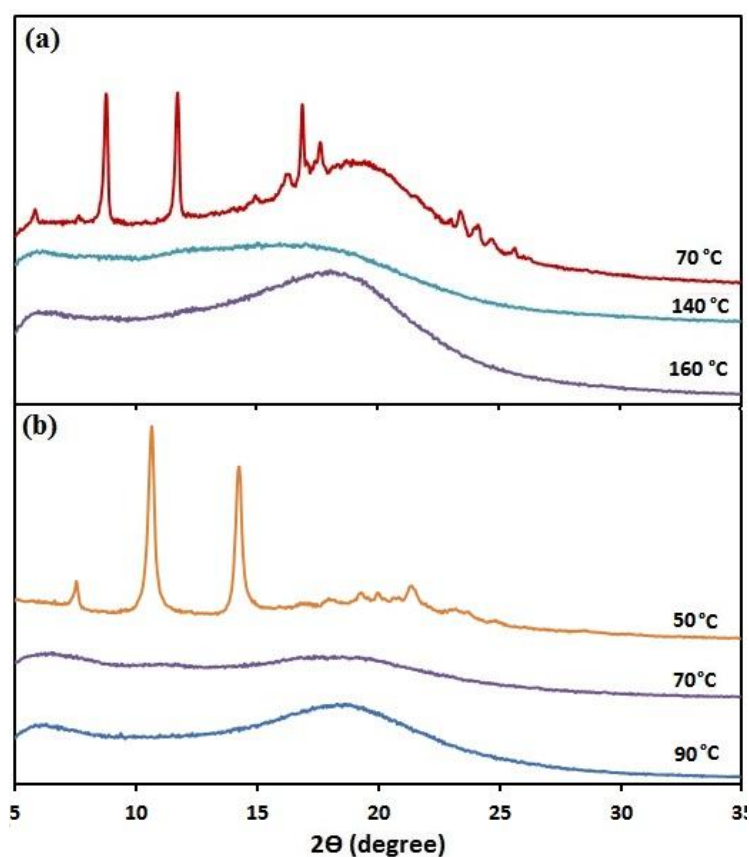


Figure 4.26 : PXRD spectra for monomers (a) **M3** and (b) **M5**.

4.5.3. Effect of polymerizable terminal group on the mesophase

Generally, most studies focus on the effect of terminal halogen, methoxy, methyl, or cyano on the mesomorphic properties of low molar mass liquid crystals. However, the effect of polymerizable terminal group on the mesophase is rarely been studied. In this work, monomers containing arylate (monomers, **M2**, **M4**, **M6** and **M8**) and methacrylate (monomers, **M3**, **M5**, **M7** and **M9**) terminal groups attached with the alkyl spacer have been synthesized. In order to study the effect of polymerizable terminal

group on the mesophase, monomer **M2** and monomer **M3** have been chosen to represent other monomers.

Figure 4.27 shows the DSC thermograms of heating and cooling cycles of monomer **M2** and monomer **M3** at a heating rate of 10°C/min. The T_g for these monomers were not detected by DSC. Both monomers exhibited a nematic mesophase which undergo isotropization at 217.68°C and 181.42°C for monomer **M2** and monomer **M3** respectively during the second heating scan. The thermal transitions were enantiotropic and the peaks observed at 217.77°C for monomer **M2** and at 180.08°C for monomer **M3** are associated to the isotropic-nematic transition.

The thermal transition temperature of monomer **M2** is higher by 36°C as compared to monomer **M3**. This is due to the presence of H group at the terminal in monomer **M2**, which gives the flexibility for the vinyl group to move easily. On the other hand, the presence of methyl group at the terminal in monomer **M3** restricts the movement of the vinyl group. The effect of this polymerizable terminal group is not so great because the thermal transition temperature is mainly affected by the mesogenic core structure.

Both monomers exhibited enantiotropic nematic mesophase with high thermal stabilities and broad mesophase range due to the presence of a methoxy group at the terminal position of the mesogenic core. It could be explained that, the lone pair of electrons on oxygen in the methoxy group is shielded by an insulator-like methyl group. The repulsive forces involving the oxygen lone pairs are thus significantly reduced and allow a close approach of the neighboring molecules hence increase the bonding forces [54]. This leads to a higher nematic to isotropic (N-I) transition temperature for both monomers.

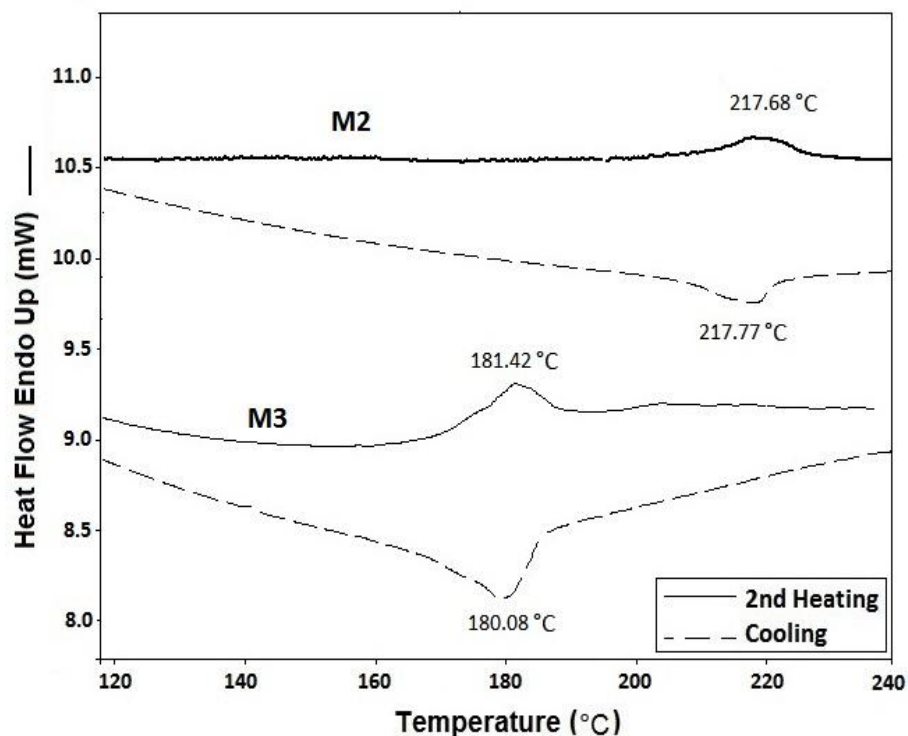


Figure 4.27 : DSC thermograms of monomer **M2** and monomer **M3**.

Figure 4.28 shows the POM of monomer **M2** textures obtained at different temperatures. The droplets and fourfold dark brushes of nematic textures appeared when the monomer was cooled to 207.9°C (Figure 4.28(a)). The droplets for nematic texture started to disappear when cooled to 66.5°C as shown in Figure 4.28(b) and the needle growth during direct crystallization from the isotropic melt without mesogenic behavior was observed at 61.8°C (Figure 4.28(c)). When the monomer was cooled to room temperature from this temperature, its crystalline phase appeared as spherulite textures (Figure 4.28(d)). This nematic texture has also been confirmed by the XRD results which showed a typical nematic characteristics of broad peak in the region of $2\theta = 17-30^\circ$ with d -spacing of 3-5 Å when heated at 200°C. The POM textures and XRD results of monomer **M3** have been discussed previously in section 4.5.2.

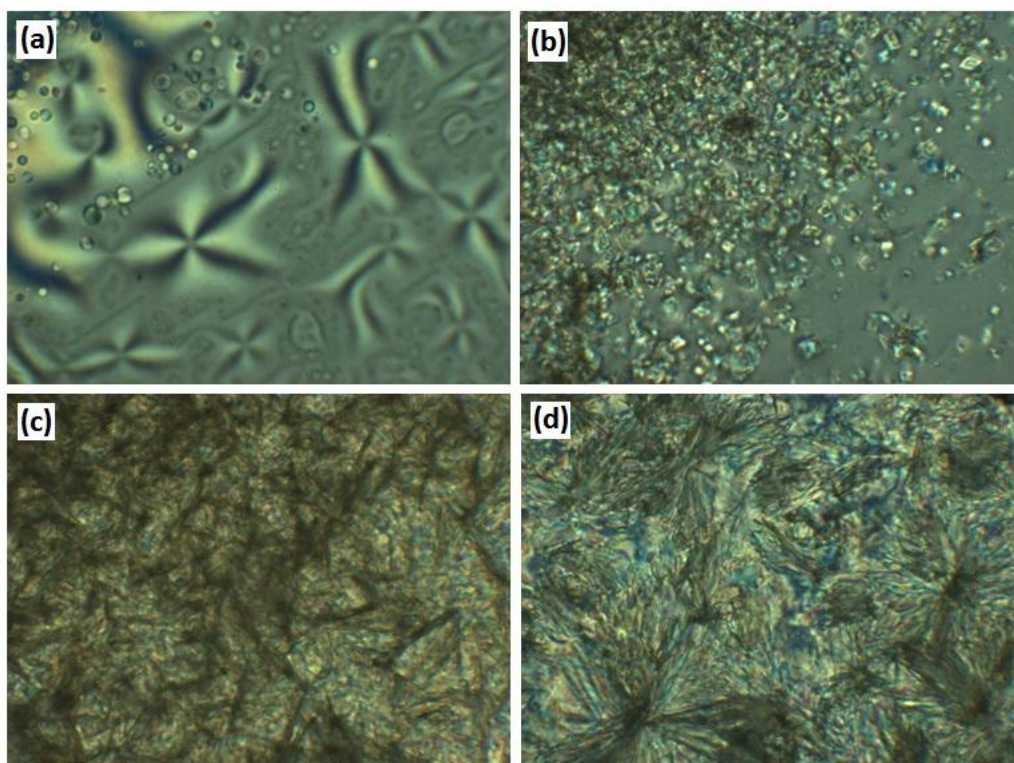


Figure 4.28 : POM textures of monomer **M2**. (a) 207.9°C (b) 66.5°C (c) 61.8°C (d) crystalline at room temperature.

4.6. Thermal properties and mesomorphic behavior of SCLCPs

The mesomorphic behavior of SCLCPs is determined by flexibility of the polymer backbone, mesogenic unit and the connecting moiety. The thermal properties and the mesomorphic behavior of the polymers were studied by DSC, POM and PXRD. Results of the thermal properties are summarized in Table 4.6. The glass transition temperatures and changes of enthalpy (ΔH) during the first cooling and the second heating cycles were obtained by DSC. The phase transition temperatures for the polymers however, can only be observed under POM.

Table 4.6 : Phase behavior and thermal properties of SCLCPs

| Polymers | Phase transitions(°C) ^{a,c} (corresponding enthalpy changes, J g ⁻¹) | | T _g (°C) |
|----------|-------------------------------------------------------------------------------------------|---------------------------------------|------------------------|
| | Heating | Cooling | |
| HP1M1 | S 149.4 (1.39) N 162.8 (2.48) I | I 161.6 (-2.27) N 148.2 (-1.24) S | 62.81 |
| HP2M1 | S 149.1 (1.41) N 162.6 (2.32) I | I 161.3 (-2.43) N 147.9 (-1.15) S | 62.63 |
| HP3M1 | S 150.6 (0.97) N 163.3 (1.82) I | I 162.01 (-2.08) N 149.3 (-1.44) S | 68.40 |
| HP1M2 | N 232.4 I ^b | - | 50.97 |
| HP2M2 | N 220.5 I ^b | - | 44.55 |
| HP1M3 | N 158.9 I ^b | - | 78.75 |
| HP2M3 | N 150.2 I ^b | - | 62.89 |
| HP1M5 | N 135.8 I ^b | - | 87.37 |
| HP1M6 | N 227.7 I ^b | - | 52.93 |
| HP2M6 | N 221.5 I ^b | - | 43.42 |
| HP1M7 | N 197.8 I ^b | - | 78.21 |
| HP2M7 | N 156.3 I ^b | - | 60.45 |
| HP1M8 | N 150.2 I ^b | - | 74.81 |
| HP1M9 | N 132.9 I ^b | - | 86.18 |
| HP2M9 | N 128.5 I ^b | - | 72.92 |

* Colored columns represent polymethacrylates SCLCPs

^aTransition temperatures (°C) and enthalpies (in parentheses, J g⁻¹) were measured by DSC (at a heating and cooling rate of 10 °C/min).

^bTransition temperatures (°C) and were determined by POM during heating

^cS= Smectic phase; N = nematic phase; I= isotropic phase.

4.6.1. Effect of the nature of polymer backbone

The nature of polymer backbone is a secondary factor in enhancing, altering or disrupting the natural ordering of the mesogenic side chains. In order to study this effect, SCLCPs with polyacrylate and polymethacrylate backbone have been synthesized from the earlier synthesized polymerizable monomers. The phase transitions and T_g values of these polymers are tabulated in Table 4.6.

In the liquid crystalline polymer system, T_g is associated to the freezing of segmental motions in which the liquid crystalline phases retain some mobility around the longitudinal axes of the mesogen. The T_g of polymers is closely related to the

flexibility of the chains in the sense that a high value of T_g is generally assumed to be connected to relatively high barriers of bond rotations. Other factors that also influence the barriers are the intermolecular constraint and supramolecular arrangement of the chains. For this reason, the T_g of the liquid crystalline phase can differ from the amorphous phase [162].

Table 4.6 shows that the T_g of liquid crystalline polyacrylates (polymers, **HP1M2**, **HP2M2**, **HP1M6**, **HP2M6**, and **HP1M8**) are lower (43-74°C) than those polymethacrylates (polymers, **HP1M1**, **HP2M1**, **HP3M1**, **HP1M3**, **HP2M3**, **HP1M5**, **HP1M7**, **HP2M7**, **HP1M9** and **HP2M9**) (60-87°C). This is because polyacrylate backbone is more flexible. Thus, less energy has been used by the side groups to get distorted and therefore this generates a more decoupled polymer system. The dynamics ordering of the side groups increases with higher flexibility and hence improves the ability of the polymer to form more ordered mesophases [163]. In contrast, the isotropization temperatures of polyacrylates are typically higher with backbone flexibility which facilitates the mesogen-mesogen interactions.

The T_g value is also influenced by the spacer group through plasticization of the polymer backbone by the side groups. The spacer group is a flexible segment connecting the polymeric backbone and the mesogenic unit and plays an important role to decouple the movements of the mesogens anisotropically from the polymer backbone which tend to adopt a random coil confirmation [163]. In this work, all polymers were designed with $-(CH_2)_6-$ spacer in order to produce liquid crystalline polymers as the liquid crystalline phases are favorable with intermediation by the spacers.

4.6.2. Effect of molecular weight and polydispersity

In the thermotropic system, the molecular weight also affects the thermotropic behavior, phase transition temperature, enthalpy and entropy changes at transitions, order parameter of liquid crystal as well as T_g value of the polymer. Generally, all these parameters increase with molecular weight and level off when the molecular weight becomes high enough and this is true for any side chain liquid crystalline polymers [2, 164]. As shown in Table 4.6, the thermal transition temperatures increase with molecular weight for all synthesized polymers. This observation is similar to those obtained by Percec and Tomazos [165] and they suggested that it is due to the greater dependence of isotropization on the degree of polymerization which leads to a greater decrease in entropy and increase in free energy of the isotropic liquid with increasing molecular weight compared to that of the more ordered phases. Stevens and co-workers [166] proposed that the increase in thermal transition temperature of the mesophase with molecular weight was attributed to denser packing of the mesogenic side group with a growing degree of polymerization.

In some cases, the temperature and the nature of mesophase depend not only on the degree of polymerization and molecular weight but also the polydispersity of the polymer. In this work, the SCLCPs prepared by ATRP (polymers, **HP1M1**, **HP2M1** and **HP3M1**) have narrow polydispersities while the SCLCPs prepared by radical chain polymerization (polymers, **HP1M2** to **HP2M9**) have broad polydispersity. The polydispersity indices (PDI) obtained by all synthesized polymers are summarized in Table 4.4.

As a result of narrow polydispersities, the phase transitions for the polymers synthesized from monomer **M1** (polymers, **HP1M1**, **HP2M1** and **HP3M1**) can be detected by DSC as shown in Figure 4.29. All polymers exhibited nematic and smectic mesophases which undergo isotropization at 163°C during the second heating scan. The

thermal transitions were enantiotropic and two peaks at 161°C and 148°C associated with the isotropic-nematic and nematic-smectic transitions respectively were observed during the cooling scan.

The phase transition temperatures and changes in enthalpy (ΔH) obtained during the first cooling and the second heating cycles are summarized in Table 4.6. The enthalpy changes observed are nearly independent of the molecular weights and this observation is in agreement with results obtained by Trimmel et. al [167]. They found that the polymers containing more than ten repeating units gave independent enthalpy changes to the molecular weight but were strongly dependent on spacer length, with a minimum $n=6$.

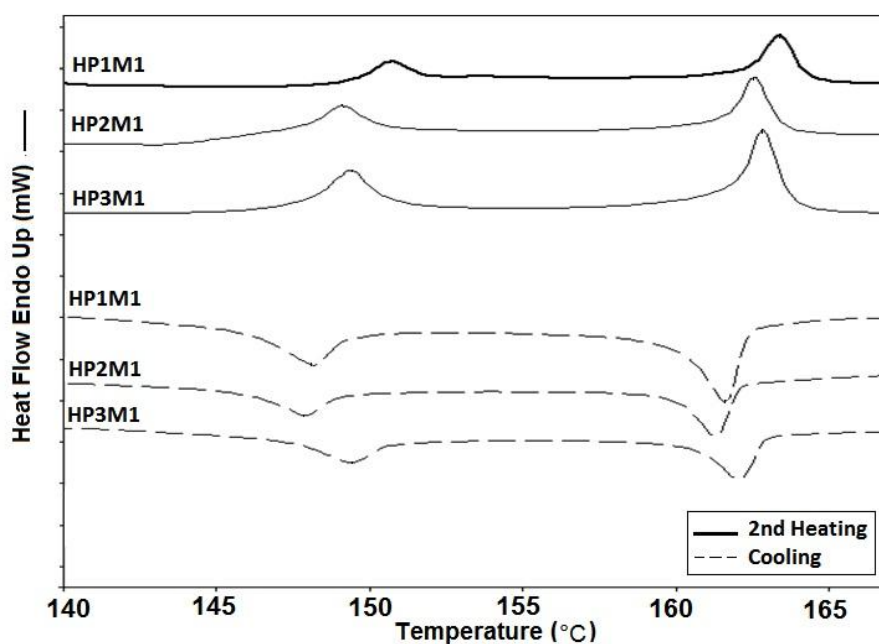


Figure 4.29 : DSC thermograms for the polymers, **HP1M1**, **HP2M1** and **HP3M1**.

Figure 4.30 represents the POM textures of the polymer **HP1M1** upon cooling from the isotropic point. The schlieren nematic textures appeared with droplets when the polymers were cooled to 165.7°C as shown in Figure 4.30(a). Upon cooling, coarse textures of disclination loops were formed (Figure 4.30(b)). The stripes of the textures disappeared upon heating and regenerated by cooling. When the polymers were cooled

to 108°C, the striped loops grew to striated feather textures of smectic mesophase (Figure 4.30(c)).

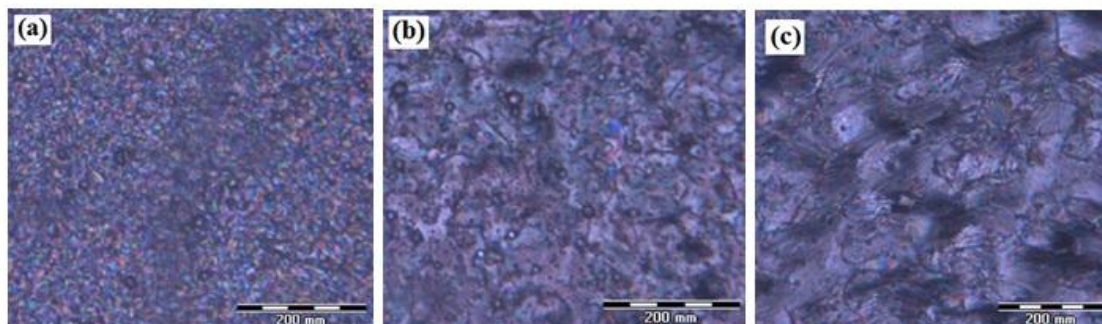


Figure 4.30 : POM textures of polymer **HP1M1**. (a) 165.7°C (b) 162°C (c) 108°C.

On the other hand, the phase transitions for the polymers with broad polydispersity values (polymers, **HP1M2** to **HP2M9**) were not detected by DSC. Heroguez and co-workers [168] also could not observe any thermal transition temperature for a polymer with broad polydispersity (PDI=1.9) by DSC; on the other hand they observed a clear thermal transition of a polymer with narrow polydispersity (PDI=1.2). The broad polydispersity is generally observed in a broad phase transition region. This may be due to the immiscibility of a mixture of different molecular architectures resulting from chain branching at the end of polymerization and entanglements [169].

All the synthesized polymers from monomers **M2** to **M9** show only a nematic mesophase at temperature range of 128°C to 232°C under POM during fast heating as shown in Table 4.6. As the temperature increased the viscosity of the polymers decreased. Marin et. al [150] suggested that this behavior could be the result of rotational motion of the alkyl chains whose flexibility increases with increase of thermal energy, favoring the self-assembly of the mesogen units.

Figure 4.31 shows the POM textures of some selected polymers. Polymer **HP2M2** exhibited a grainy texture of a nematic mesophase when it was cooled from the melt at 150°C as shown in Figure 4.31(a). This texture is also known as a tight texture, a dense

texture or a polydomain texture. Generally, this type of texture is observed for a high molecular weight thick film polymer at a low temperature. The domain size of this texture is difficult to observe by POM. Other researchers [170, 171] have been studying this texture under transmission electron microscopy and an assembly of ‘effective domain’ due to a particular arrangement of disclinations have been observed from its microstructure. The fine grains are believed to correspond to regions of uniform orientation correlation within the nematic structures bounded by disclinations as shown in Figure 4.32. Additionally, the coarsening of this nematic texture is related to the dynamics of disclinations. When a nematic phase is formed from its isotropic phase, its structure is dependent on the kinetics and mechanism of the phase transition.

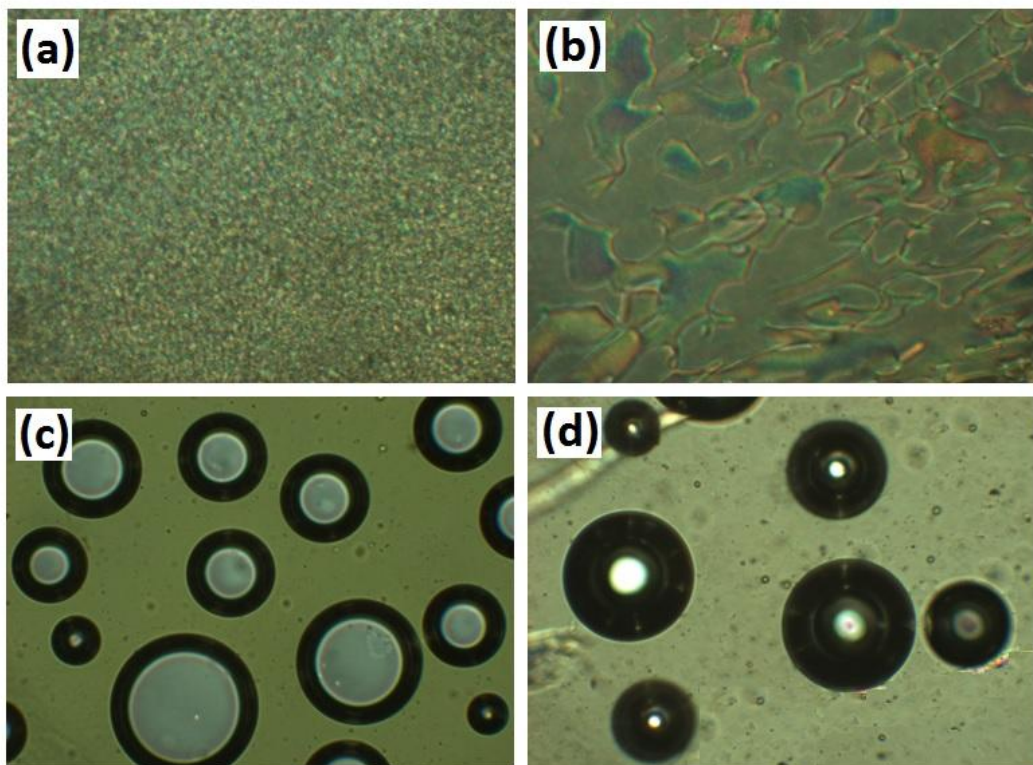


Figure 4.31 : POM textures of polymers. (a) **HP2M2** (b) **HP2M1** (c) **HP1M2** (d) **HP2M8**.

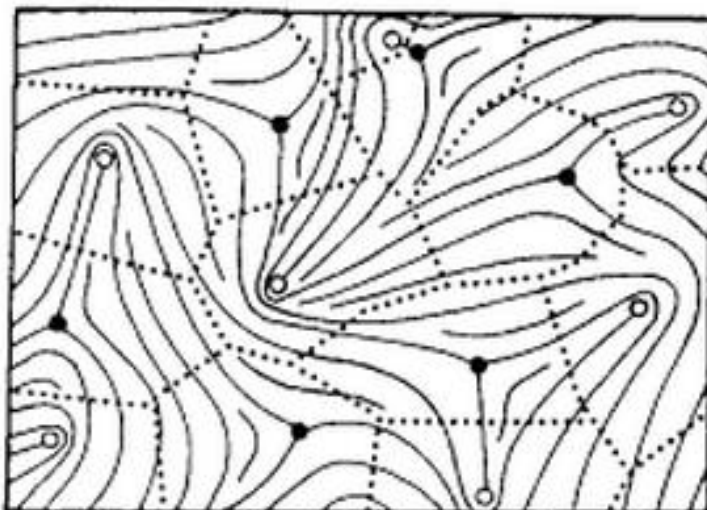


Figure 4.32 : Schematic representation of the polydomain structure produced by spatial distribution of disclination lines of $S=+1/2$ (open circles) and $S=-1/2$ (filled circles). Adopted from [171].

Polymer **HP2M1** exhibited a nematic tread like texture when it was cooled from the melt at 220°C as shown in Figure 4.31(b). This texture was attributed to the line disclinations of the nematic mesophase. Polymer **HP1M2** and polymer **HP2M8** exhibited a nematic droplet texture when cooled from the melt at 160°C and 130°C respectively as shown in Figure 4.31(c) and Figure 4.31(d). Most of the synthesized polymers exhibited this type of texture when cooled from their isotropic melt. Sakthivel and Kannan [172] explained that the nematic droplets structure is formed when the polymers tend to grow as large monodomains which can possibly be ascribed to significant segmental mobility and the mesogens taking maximum unidirectional alignment in the melt condition.

In order to further elucidate the structures of the mesophases, powder XRD measurements of the synthesized polymers were carried out. The polymer sample was heated to the temperature ranges of the mesophases and then quenched at room temperature. Figure 4.33 shows the XRD pattern of the representative polymers (polymers, **HP1M1** and **HP2M2**). All polymers showed a typical nematic characteristic of a broad peak around $2\theta = 20-25^{\circ}$, classically due to average intermolecular spacing

of approximately 3-5 Å at mesophases and no sharp Bragg peaks were observed for polymers in the lower angle regions ($2\theta < 5^\circ$). Zhang et. al [99] suggested that the absence of peaks at a lower angle regions indicated that the constituent molecules of the polymers did not regularly arrange within the two-dimensional order structure as a smectic mesophase. This was an evidence of nematic texture and the polymers' amorphous nature.

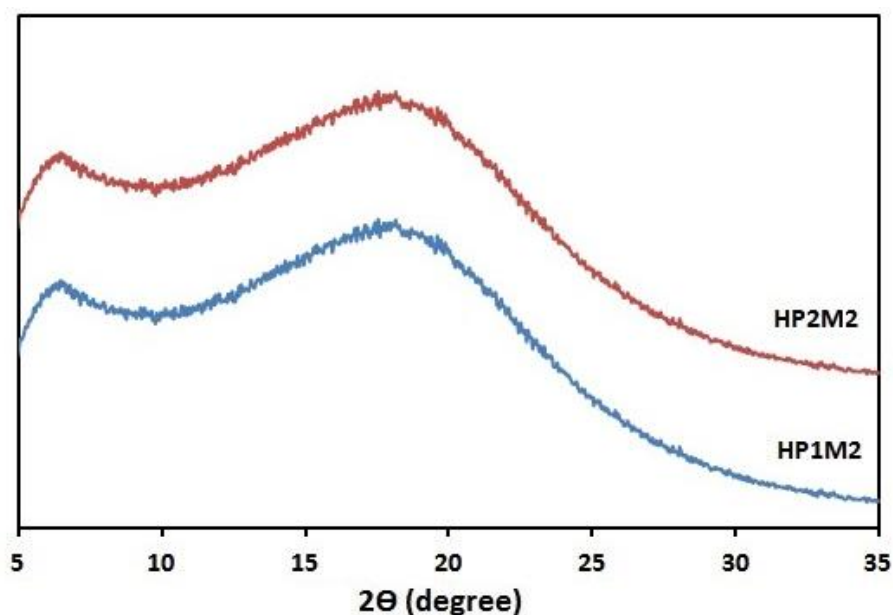


Figure 4.33 : PXR D patterns of representative polymers, **HP1M1** and **HP2M2**.

4.7. Thermal degradation properties of SCLCPs

TGA measurements were carried out to study the thermal stability of the synthesized polymers. The measurements were performed in a temperature range of 50-900°C in nitrogen atmosphere. Additionally, the thermal stability of these polymers is important since in organic LEDs much energy has been spent in non-radiative process and the heat produced instantaneously raises the temperature [173].

Figure 4.34 shows the thermogram of polymer **HP2M3** which is typically similar for all the other polymers. Table 4.7 shows the TGA data of the synthesized polymers. It can be deduced from both Figure 4.34 and Table 4.7 that onset decomposition

temperatures of all the polymers are above 280°C which indicate that all the polymers are thermally very stable. Figure 4.34 shows that all the polymers were decomposed through a single stage decomposition phenomenon. The first 5% weight loss, which is greater than 302°C, is due to the decomposition of aliphatic flexible segments. The results suggest that the existence of a longer mesogenic side chain might cause a strong interaction between the repeating units leading to the increase in thermal resistance. Obviously, the thermal stability of the material is adequate for the fabrication processes and other optoelectronic devices [173, 174]. This process is followed by the thermal cleavage of carbonyl groups or the scission of other C-O bonds [175] and decomposition of rigid mesogenic chain containing aromatic moiety for the remaining 95% weight loss. The ester linkages present in the mesogen are very stable due to its charge separated resonance form which makes it difficult to rotate around the carbon-oxygen single bond [176].

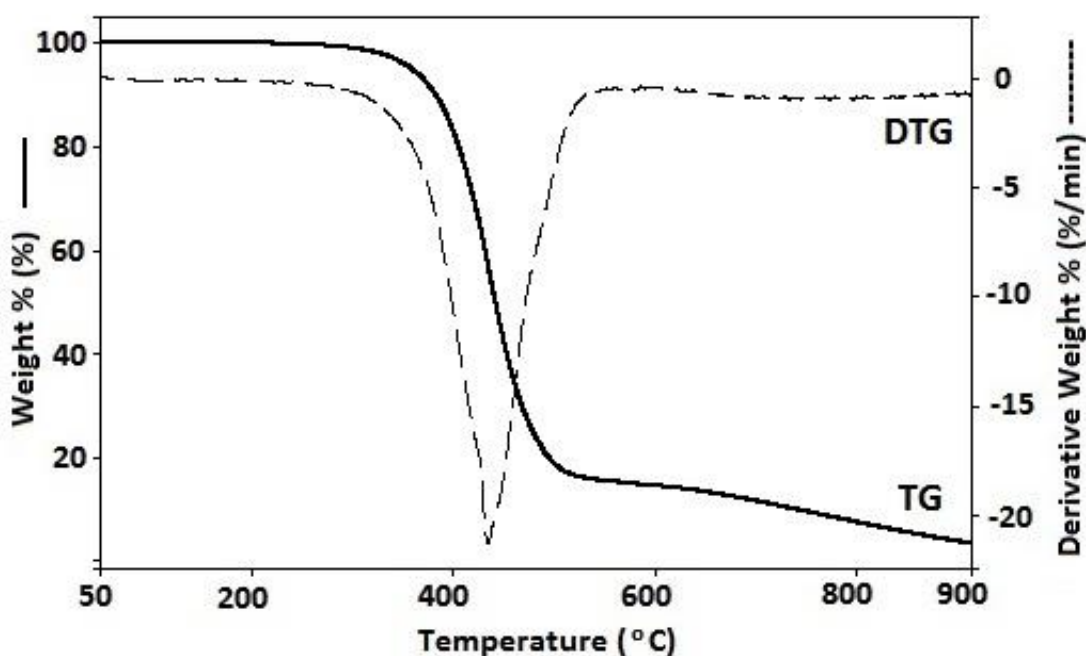


Figure 4.34 : TG and DTG traces of polymer **HP2M3**.

Table 4.7 : TGA data of polymers

| Polymers | Temperature (°C) corresponding to | | | | Char yield (%) at 600°C |
|--------------|-----------------------------------|------------|-------------|--------|----------------------------|
| | onset | 5% Wt loss | 50% Wt loss | DTp | |
| HP1M1 | 389.59 | 376.61 | 431.71 | 423.44 | 9.30 |
| HP2M1 | 386.01 | 376.45 | 424.39 | 423.44 | 6.05 |
| HP3M1 | 385.73 | 373.83 | 426.83 | 424.16 | 5.42 |
| HP1M2 | 280.75 | 304.60 | 429.86 | 431.79 | 18.4 |
| HP2M2 | 317.17 | 335.94 | 430.27 | 432.16 | 18.7 |
| HP1M3 | 283.72 | 307.13 | 432.51 | 434.31 | 19.25 |
| HP2M3 | 365.05 | 362.80 | 441.56 | 435.83 | 14.71 |
| HP1M5 | 331.34 | 312.01 | 446.73 | 441.04 | 19.96 |
| HP1M6 | 333.28 | 302.93 | 430.85 | 429.02 | 15.00 |
| HP2M6 | 310.05 | 330.64 | 426.31 | 433.20 | 17.08 |
| HP1M7 | 351.07 | 313.38 | 433.89 | 430.35 | 16.51 |
| HP2M7 | 383.31 | 366.28 | 430.77 | 423.60 | 15.03 |
| HP1M8 | 335.94 | 340.97 | 432.59 | 432.59 | 17.47 |
| HP1M9 | 319.73 | 323.12 | 429.31 | 433.03 | 17.75 |
| HP2M9 | 363.30 | 359.97 | 421.43 | 413.98 | 18.23 |

As shown in Table 4.7, the T_d 5% values of polymers containing naphthalene ring in the mesogen (polymers, **HP1M1-HP1M3**) are higher (373°C - 376°C) compared to the polymers containing Schiff base ester in the mesogen (polymers, **HP1M2-HP2M9**). This is due to the fact that naphthalene has better thermal stability and high heat resistance [177, 178]. The T_d 5% values of polymers **HP1M2**, **HP1M3**, **HP1M6** and **HP1M7** with the presence of an extra methoxy group in the *meta*-position of those polymers side groups make it more stable than polymers **HP1M5**, **HP1M8** and **HP1M9** due to higher bond energy values of this group. This may be explained by invoking bond energy values [179].

However, the results show that the T_d 50% and DT_p values for all polymers are almost the same which are higher than 421°C. It is suggested that at this stage, the thermal stability of the polymer is not affected by the presence of mesogenic group in the system. Liu and Yang [180] suggested that the existence of the longer side chain groups may cause a strong interaction between the repeating units and entanglement of the polymer chains. This interaction is expected to enhance interactions between the liquid crystal and the polymers, leading to an increase in the stabilization of liquid crystals inside the polymer matrix.

As a result of high decomposition temperature, these polymers have good thermal properties for industrial processing and for possible use in organic LEDs [173, 174]. Decomposition of the polymers was almost complete at around 900°C with no further weight loss observed after that. Char yield of the polymers are less than 20% which was measured at 600°C.

4.8. Optical properties of SCLCPs

The optical properties of SCLCPs were analyzed by UV-vis absorption and photoluminescence (PL) spectroscopies. UV-Vis and PL spectra of the synthesized polymers were acquired in dilute THF solvent at a concentration 1×10^{-6} M where the excitation wavelengths of PL were 365 nm, and the photophysical properties are summarized in Table 4.8.

Electronic absorption spectra of all synthesized polymers showed similar characteristics, i.e. two absorbance bands one with maximum (λ_{max}) located around 270 nm and a structured band at lower energies with the maximum in the range of 306-344 nm. It appeared only as shoulder due to its low intensity. According to Jaffe et al. [181] the band at around 260 nm results from a $\sigma \rightarrow \pi^*$ transition and the band at around 300 nm from a $\pi \rightarrow \pi^*$ transition. The $n \rightarrow \pi^*$ transition appears at 360 nm.

Table 4.8 : Absorption and PL emission spectral data of synthesized polymers in THF solutions

| Polymers | Absorption UV-Vis, λ_{\max} (nm) | PL emission, λ_{\max} (nm) | Stokes shift ^a (nm) |
|--------------|------------------------------------------|------------------------------------|--------------------------------|
| HP1M1 | 248, 306 | 414 | 108 |
| HP2M1 | 248, 307 | 413 | 106 |
| HP3M1 | 249, 306 | 409 | 103 |
| HP1M2 | 271, 334 | 429 | 95 |
| HP2M2 | 273, 335 | 428 | 93 |
| HP1M3 | 275, 337 | 379 | 42 |
| HP2M3 | 274, 336 | 390 | 54 |
| HP1M5 | 254, 330 | 421 | 91 |
| HP1M6 | 274, 341 | 418 | 77 |
| HP2M6 | 275, 343 | 419 | 76 |
| HP1M7 | 273, 342 | 415 | 73 |
| HP2M7 | 276, 344 | 418 | 74 |
| HP1M8 | 271, 328 | 419 | 91 |
| HP1M9 | 270, 329 | 417 | 88 |
| HP2M9 | 270, 328 | 418 | 90 |

^a Stokes shift = PL (nm) – UV (nm)

The first three polymers in the list of Table 4.8 (polymers, **HP1M1** – **HP3M1**) are the polymers containing naphthalene ring in the mesogenic core structure. The polymers exhibited intense absorption at 248 nm and weak absorption at 307 nm, corresponding to absorption of naphthalene moieties [182-184]. Meanwhile, the polymers containing Schiff base ester in the mesogenic core structure (polymers, **HP1M2** – **HP2M9**) exhibited intense absorption at 270-276 nm and weak absorption at 328-344 nm. Absorption bands at lower energies are due to inter-band transition between the $\pi \rightarrow \pi^*$ transition and $n \rightarrow \pi^*$ transition, derived from interaction of benzene and azomethine (Schiff base) π -orbitals, thus being characteristic for imine bonds [185].

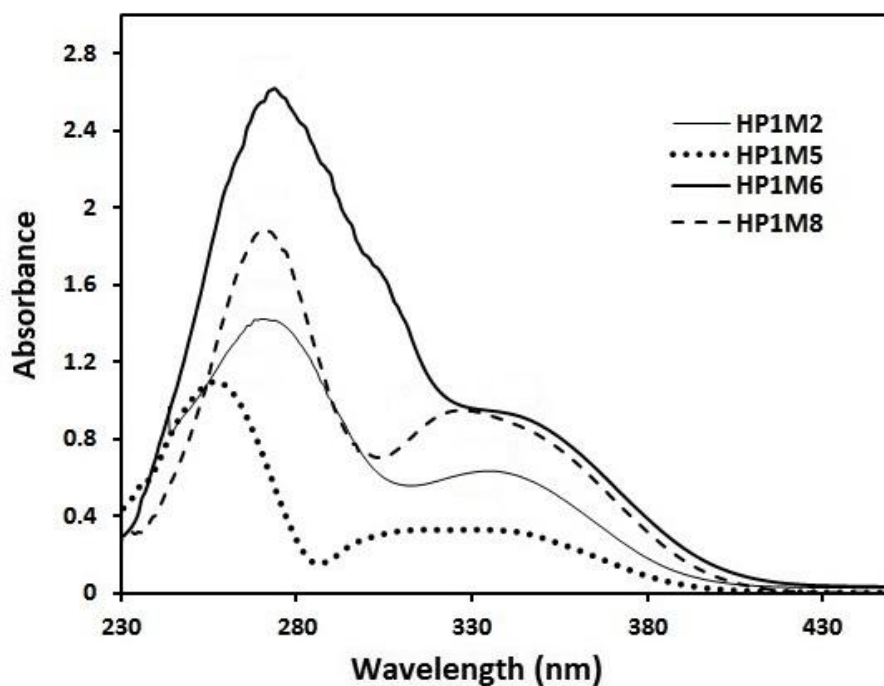


Figure 4.35 : UV-Vis absorption spectra of polymers, **HP1M2**, **HP1M5**, **HP1M6** and **HP1M8**.

Figure 4.35 shows the UV-vis absorption spectra of the selected polymers (**HP1M2**, **HP1M5**, **HP1M6** and **HP1M8**). The absorption bands are shifted to the lower wavelengths by the introduction of electron donating group, $-\text{OCH}_3$ in polymers, **HP1M2**, **HP1M5** and **HP1M8** as shown in Figure 4.35. The $\sigma \rightarrow \pi^*$ transition in the spectrum of polymer **HP1M2** (with one methoxy group) is shifted slightly to lower wavelengths compared to polymer **HP1M6** (without any substituent) and appears with decreased intensity at 271 nm. Polymer **HP1M5** contains two methoxy groups on its mesogenic core unit, and the $\sigma \rightarrow \pi^*$ transition is shifted to 254 nm with decreased intensity. This is due to the negative inductive effect of the methoxy group as reported by Knopke et al. [186].

The bands of the $\pi \rightarrow \pi^*$ transitions are also shifted to lower wavelength by the introduction of methoxy group in the polymer side group. The polymers that have one methoxy group on the benzene ring (polymer **HP1M2** and polymer **HP1M8**) are blue shifted by ~ 20 nm, whereas the polymer that with two methoxy groups on the benzene rings (polymer **HP1M5**) is blue shifted by ~ 40 nm compared to the corresponding un-

substituted polymer **HP1M6**. This blue-shift may be caused by perturbation of the $\pi \rightarrow \pi^*$ transition due to the electronic effects of two methoxy groups on the π -electrons of both phenyl and aniline rings [186]. According to Luo et al. [187], this blue-shift may be attributed to the steric effect of the methoxy group at the central benzene ring in the polymer system, which results in less co-planarity of the molecule. However, the shift was only a few nanometres which are mainly due to the absence of strong donor-acceptor pairs in the emission chromophores. Oxygen atoms in the methoxy group are not strong donors even though they have unshared electron pairs. In addition, the polymer molecules are not easily surrounded by solvents as small molecules are. Thus, made the absorption spectra less shifted. The phenomenon is in agreement with Sun [188].

Table 4.8 shows the PL data of all synthesized polymers. Upon excitation of the polymers at 365 nm, all polymers show emission in the range of 380-560 nm with emission maximum at a range 379-429 nm. This reveals that these polymers may have the ability to emit bluish light throughout the visible region of electromagnetic spectrum. All the polymers had pure PL spectra without other shoulder peaks due to possession of only one kind of emission chromophore, therefore, the degree of polymerization had no effect on the width of the PL spectra.

Figure 4.36 shows the PL emission spectra of the selected polymers (**HP1M2**, **HP1M5**, **HP1M6** and **HP1M8**). The polymers **HP1M6** and **HP1M8** exhibited a blue shift of the emission maxima compared to other polymers due to the extension conjugation with an additional phenyl ring, resulting in good π -electrons delocalized along azomethine-phenylene core, which is a p - π conjugated system. This observation was also reported by Marin et al. [150] and they suggested that the emission wavelength was controlled by the conjugation length which leads to the shifting of the emission bands. It can be seen that the PL intensity of the investigated polymers increase with the

molecular weight of the polymers which is in agreement with results obtained by Zhang et. al [189] and Zhao et. al [183]. They suggested that the increase in PL intensity with molecular weight of polymers may be assigned to the chromophore–chromophore interactions in the intramolecular system due to the increase of side chain length. Polymer **HP1M2** exhibited highest emission intensity compared to the other polymers (**HP1M5**, **HP1M6** and **HP1M8**) (Figure 4.36) which could originated from the efficient intermolecular charge transfer in the excited state [190].

Table 4.8 also shows stokes shift values of the synthesized polymers where stokes shift is the difference between PL and UV/Vis absorption peaks. The small value of stokes shift will result in overlapping of the emission and absorption spectra. Then the emitting light will be self-absorbed and the luminescence efficiency will decrease in the devices. Polymers **HP1M1**, **HP2M1** and **HP3M1** exhibited large stokes shift compared to the other polymers, thus, they are the best candidate for organic LEDs.

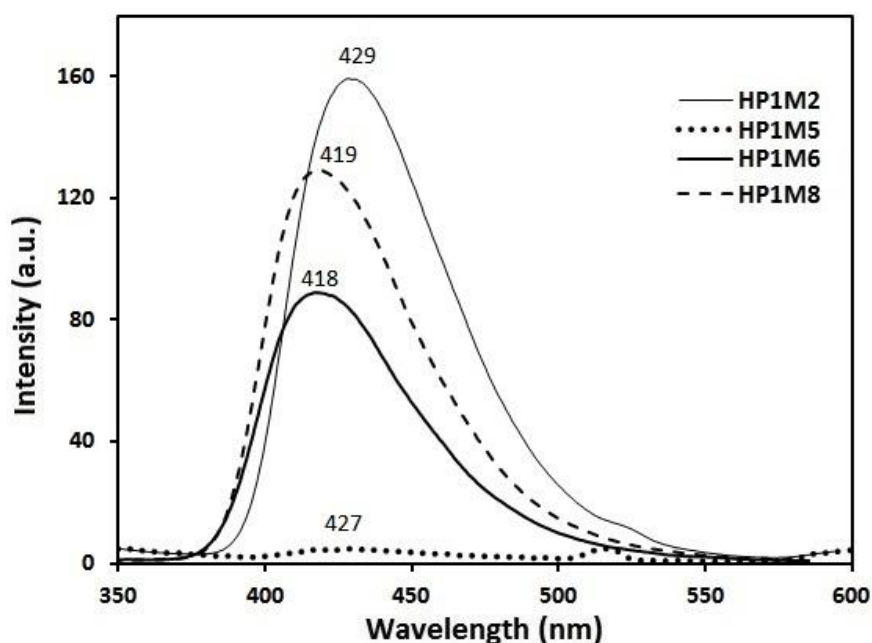


Figure 4.36 : Photoluminescence spectra of polymers, **HP1M2**, **HP1M5**, **HP1M6** and **HP1M8**.

4.9. Electrochemical properties

Based on the optical properties results, the selected polymers (polymers, **HP1M2**, **HP1M5**, **HP1M6** and **HP1M8**) have been used to study their electrochemical properties. The electrochemical properties were investigated using cyclic voltammetry (CV) in chloroform solution containing 0.1 M tetrabutylammonium perchlorate (Bu_4NClO_4) as the supporting electrolyte at a scanning rate of 50 mV/s. Figure 4.38 shows the parent CV curve which is typically similar for all the polymers. No reduction processes have been found in the available potential range. The lack of reduction of the azomethines was also observed for the other compounds with imine linkages as described in the literature [185, 191]. It shows the robustness of the azomethine bond [174].

Optical band gap values could be obtained by the following equation:

$$E_g = \frac{hc}{\lambda_{onset}} \quad \text{Eq 4.1}$$

where h is plank constant, c is speed of light and λ_{onset} is the onset wavelength which can be determined by intersection of two tangents on the absorption edges as shown in Figure 4.37. λ_{onset} also indicates the electronic transition start wavelength [192].

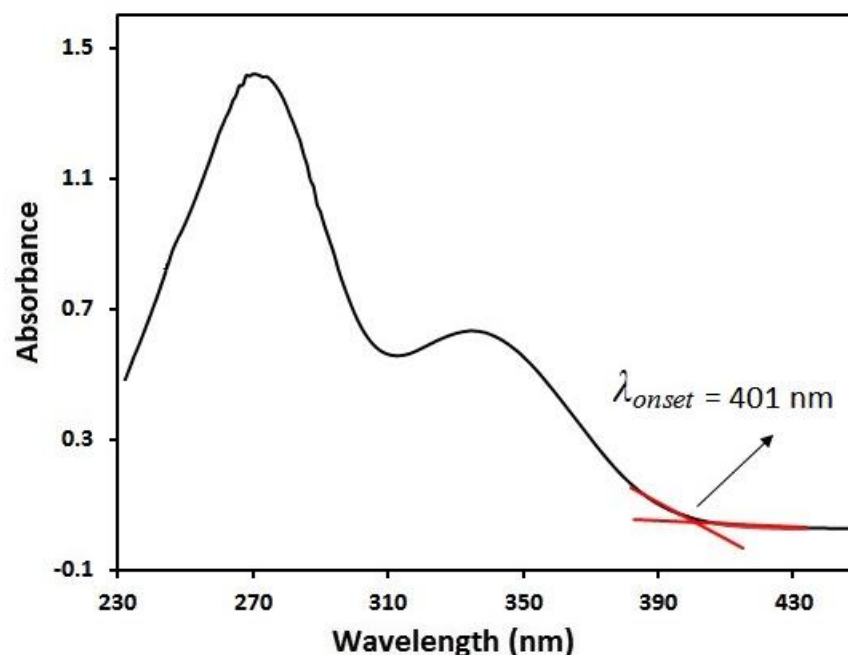


Figure 4.37 : UV-vis spectrum of polymer **HP1M2** in THF solution.

The highest occupied molecular orbital (HOMO) and the lowest unoccupied molecular orbital (LUMO) energy level can be estimated by using ferrocene ionization potential value of 4.8 eV as standard. The HOMO energy levels can be calculated from the onset oxidation potential based on the reference energy level of ferrocene by using the following equation:

$$HOMO (eV) = -[(E_{OX}(onset) + 4.8 - E_{FOC})] eV \quad \text{Eq 4.2}$$

where E_{ox} is the onset oxidation potential and E_{FOC} is the external standard potential of the ferrocene/ferricinium ion couple. The E_{FOC} was estimated under the same experimental condition and the value was located at 0.31 V to the Ag/AgCl electrode. The onset oxidation potentials of the polymers were calculated from the intersection of two tangents drawn at the rising and background currents of the CV as shown in Figure 4.38. Since no reduction of the polymers was observed under the experimental conditions, the electrochemically calculated HOMO level and spectroscopically

measured band gap were used to calculate the LUMO energy level according to the following equation:

$$LUMO (eV) = HOMO + E_g(opt.) \quad \text{Eq 4.3}$$

The LUMO levels estimated by this method do not give an accurate account of the electron affinity, but nevertheless allow for a qualitative trend to be established and provide some information to help in selecting suitable combinations with electron acceptors in devices [185].

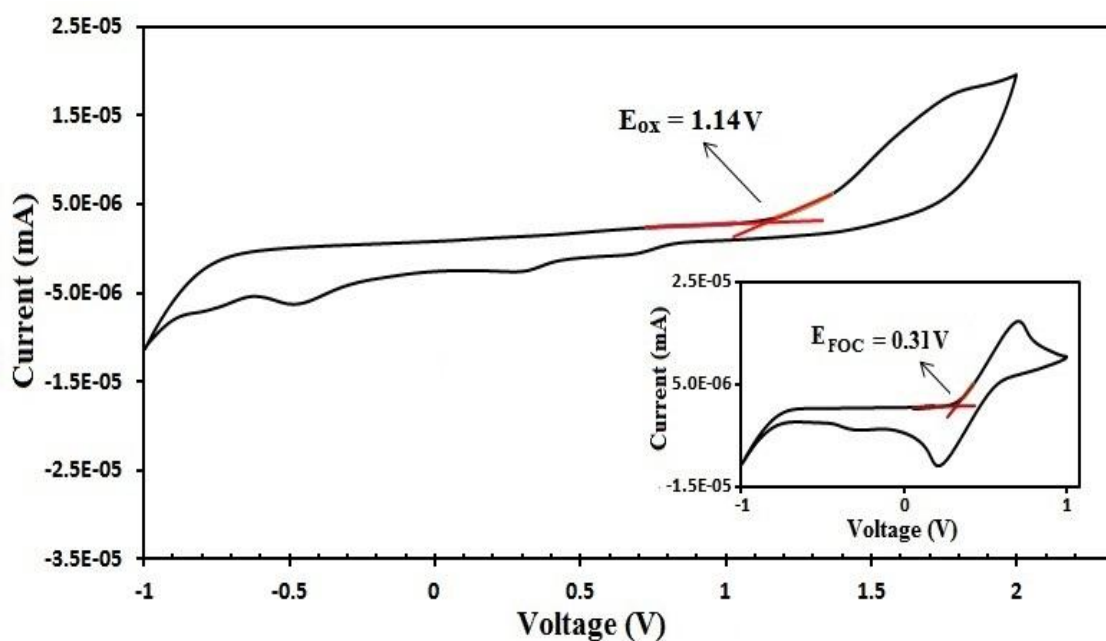


Figure 4.38 : CV of polymer **HP1M2** in chloroform solution. The inset is the CV curve of ferrocene standard, swept in the same conditions as that for polymer **HP1M2**.

Table 4.9 : Electrochemical data of selected polymers

| Polymers | UV-Vis, λ_{max} (nm) | UV-Vis, λ_{onset} (nm) | PL, λ_{max} (nm) | E_g (opt.) (eV) | E_{ox} (onset) (V) | HOMO (eV) | LUMO (eV) |
|--------------|------------------------------------|--------------------------------------|--------------------------------|----------------------|-------------------------|--------------|--------------|
| HP1M2 | 271, 334 | 401 | 429 | 3.15 | 1.14 | -5.63 | -2.48 |
| HP1M5 | 254, 330 | 390 | 421 | 3.18 | 1.18 | -5.67 | -2.49 |
| HP1M6 | 274, 341 | 410 | 418 | 3.20 | 1.10 | -5.59 | -2.39 |
| HP1M8 | 271, 328 | 404 | 419 | 3.21 | 1.31 | -5.80 | -2.59 |

HOMO and LUMO energies of the polymers and their corresponding band gap values are summarized in Table 4.9. From this table, it can be seen that the incorporation of methoxy substituent at the *para*- and *ortho*-position of the benzene rings had a significant effect on the electrochemical properties of the polymers. The polymers with two methoxy substituent at the *ortho*- and *para*-position of two benzene rings (polymer **HP1M5**) showed the smallest E_g value followed by the polymers with a methoxy substituent at the *para*-position of benzene ring (polymer **HP1M2** and polymer **HP1M8**) as compared to the unsubstituted polymer (polymer **HP1M6**).

This shows that the introduction of an electron-donating group ($-\text{OCH}_3$) into the terminal and lateral benzene rings of the polymers results in a decrease in the E_g s of the polymers. This is due to the increment of electron density of *ortho*- and *para*-positions of the aromatic ring as reported by Kaya and Kamaci [193]. The electron donating group may extend the conjugation of the polymers hence lower the energy levels between HOMO and LUMO. Similar observation has been reported by Liu et al. [194]. They found that the E_g s of diarylethenes bearing an electron-withdrawing group were much higher than those of diarylethenes bearing an electron-donating group.

The obtained HOMO and LUMO values of polymers are around -5.59 eV and -2.59 eV respectively. These results indicate that the newly synthesized SCLCPs are conjugated *p*-type polymers and may exhibit electron transporting properties [195]. HOMO levels obtained (-5.59 to -5.80 eV) for these polymers also are close to that of the materials currently use in hole-transporting layers [185, 196].

4.10. Rheological properties of SCLCPs

Rheological properties of liquid crystalline polymers are rather complex due to the anisotropy of the material. Thus, amplitude sweep and frequency sweep experiments were carried out to study the dynamic viscoelastic properties of SCLCPs in the smectic, nematic and isotropic mesophases.

Dynamics in the nematic and smectic mesophases

The amplitude sweep is an oscillatory test to measure elastic and loss moduli with variable amplitude and constant frequency values. The storage modulus, G' is a measure of the deformation energy that is stored in the sample during the shear and recovered after the load is removed by shearing in the opposite direction or releasing stress while the loss modulus, G'' is a measure of the energy that is dissipated in the sample during the shear process. Figure 4.39 shows the strain dependence of storage (G') and loss (G'') moduli of the polymers at 170°C with $\omega = 10$ rad/s by strain amplitude sweep experiments. Both polymers (polymer **HP2M1** and polymer **HP3M1**) show linear viscoelastic behavior at small strain amplitudes. It can be seen that G'' is greater than G' in both polymers and largely insensitive to strain amplitude. As such, the polymers do not form a viscoelastic gel.

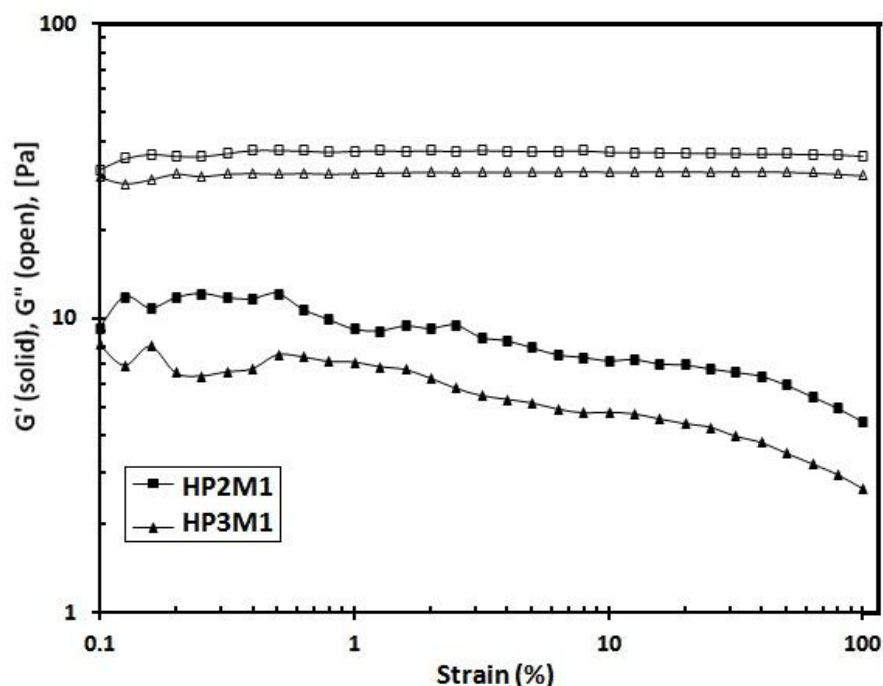


Figure 4.39 : Strain amplitude sweep of polymer **HP2M1** and polymer **HP3M1** at 170°C.

Figure 4.40 represents the plots of $\log \eta$ vs $\log \dot{\gamma}$ for polymers **HP2M1** and **HP3M1** over the temperature range of the phase transitions. Both polymers exhibit Bingham body-like flow behavior at 100°C and 110°C which shows “three region flow curves” as characterized by Onogi and Asada [197, 198]. At low values of shear rate ($\dot{\gamma} < 1 \text{ s}^{-1}$), both polymers exhibit a shear thinning behavior and the viscosity decreases. A Newtonian behavior appears at intermediate values of shear rate ($1 \text{ s}^{-1} < \dot{\gamma} < 10 \text{ s}^{-1}$), where the domains appear to decrease in size with increasing shear rate. At this stage the viscosity is relatively insensitive to shear rate. At higher values of ($\dot{\gamma} > 10 \text{ s}^{-1}$), a strong thinning behavior appears where the domain structure is not evident at this stage [197]. These results are in agreement with the results of Kannan et al. [199] and Dan et al. [200] which suggested that the large amplitude oscillatory shear orientated the SCLCPs.

However, as the temperature is increased from 120°C to 150°C, the polymers exhibit shear thinning behavior where the particles rearranged resulting in reduced flow resistance and consequently lower the viscosity of the polymers with increase in shear

rate. The polymers exhibit Newtonian behavior at low shear rate, followed by strain hardening behavior at higher shear rate at 160°C and 170°C which are in the isotropic region for both polymers. Rubin et al. [201] reported that the strain hardening behavior is probably due to the tendency of the mesogens to orient perpendicular to the backbone of the SCLCPs. The mesogens which are attached to a strand may be forced to adopt an intermediate orientation between the backbone segment and local orientation of the director.

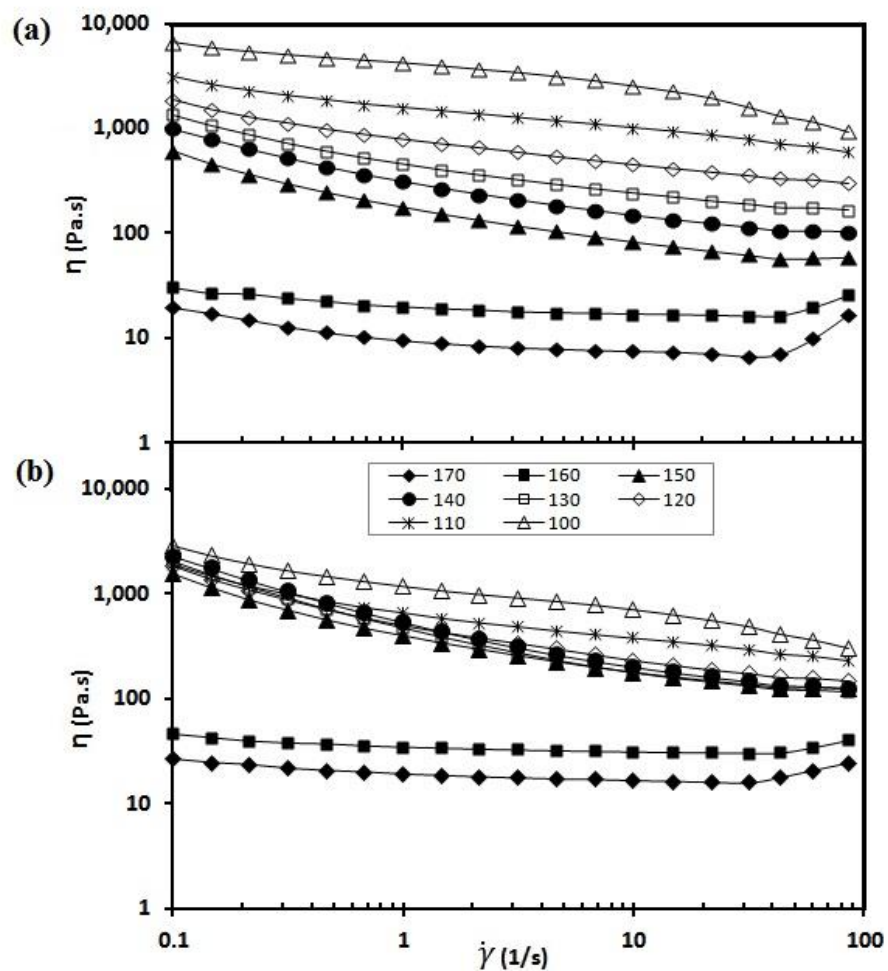


Figure 4.40 : Plots of $\log \eta$ vs $\log \dot{\gamma}$ for polymer **HP2M1** and polymer **HP3M1** at various temperatures.

Figure 4.41 shows plots of $\log G'$ vs $\log \omega$ and plots of $\log G''$ vs $\log \omega$ for polymer **HP2M1** at 100°C to 150°C in the smectic region and 160°C in the nematic region. The values of G' and G'' in the smectic region are much higher than those in the

nematic region, attributing to the 3-dimensional textures in smectic textures and 1-dimensional textures in the nematic phase. This finding is similar to that of Kim and Han [202] who studied the effect of bulkiness of pendant side group of semi-flexible main chain liquid crystal polymers (MCLCPs).

At low frequency values, both G' and G'' tend to level off and do not follow the typical terminal behavior where $G' \propto \omega^2$ and $G'' \propto \omega^2$. The slope of G' in the terminal region decreases from 0.73 to 0.56 as the temperature increases from 100°C to 150°C. As the temperature increases from 100°C to 150°C the slope of the loss modulus G'' decreases from 0.69 to 0.62. From this observation, the polymer exhibits solid-like behavior when $T \leq 150^\circ\text{C}$. The slopes of G' and G'' are subsequently increased to 0.97 and 0.94 respectively when the temperature increases to 160°C. At this temperature, the polymer exhibits liquid-like behavior. The general trends resemble the un-shifted linear viscoelastic data as reported by Auad et al. [203] for the smectic SCLCPs. The changes in the linear viscoelastic response are a common signature of ordering transitions.

In the isotropic phase, molecular weight of a polymer has a strong influence on the rheology where an entanglement plateau emerges. Nevertheless, the polymer, **HP2M1**, has a low molecular weight which is less than the molar mass of entanglement and also the smectic phase rheology is dominated by the layer structure and is comparatively insensitive to the molecular weight. Therefore, it is not expected to have a plateau in the terminal region. Similar trend of behavior are also obtained for **HP3M1** polymer.

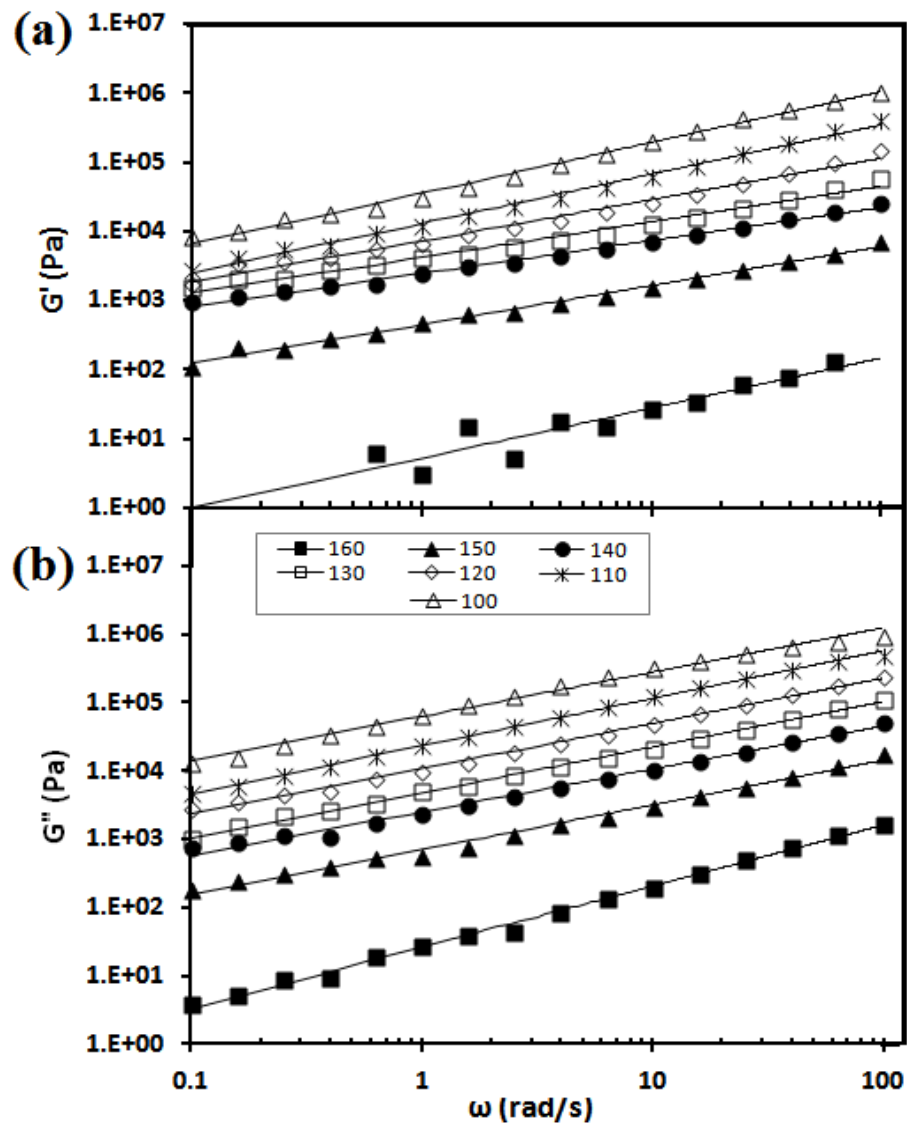


Figure 4.41 : Plots of $\log G'$ vs $\log \omega$ and $\log G''$ vs $\log \omega$ for polymer **HP2M1** at various temperatures.

Figure 4.42 shows a plot of $\log |\eta^*|$ vs $\log \omega$ for polymer **HP2M1** at various temperatures, where $|\eta^*|$ is the complex viscosity defined by $|\eta^*| = [((G'/\omega)^2 + ((G''/\omega)^2)]^{1/2}$. As the temperature increases from 100°C to 150°C, the polymer enters the smectic phase which exhibits a strong frequency dependence of $|\eta^*|$ at low angular frequencies and consequently Newtonian behavior is observed at 160°C. At this temperature, the polymer enters the nematic phase which exhibits weak frequency dependence over the entire range of angular frequencies tested. The abrupt decrease of $|\eta^*|$ values is due to the breakdown of 3-dimensional smectic order to 1-dimensional nematic order where, in the nematic phase the molecules would exhibit preferential

orientation during shear flow. A similar observation has been reported by Lee and Han [204] for their SCLCPs.

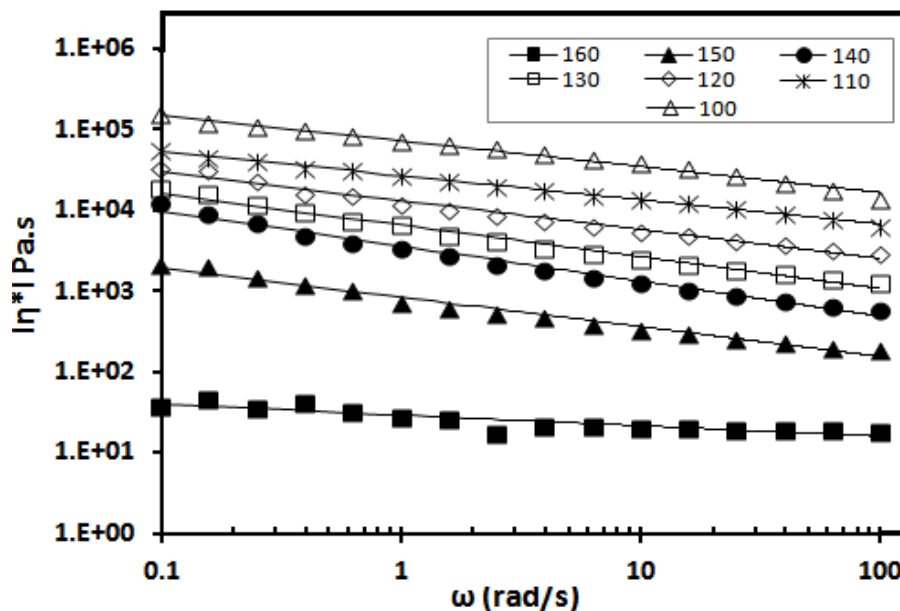


Figure 4.42 : Plots of $\log |\eta^*|$ vs $\log \omega$ for polymer **HP2M1** at various temperatures.

Dynamics in the isotropic and nematic mesophases

Determination of linear viscoelastic (LVE) region of materials is important in performing dynamic rheological characterizations which are independent of the applied strains. Figure 4.43 shows the strain dependence of storage (G') and loss (G'') moduli of the polymer **HP1M5** at 160°C with $\omega=10$ rad/s by strain amplitude sweep experiments. The polymer shows linear viscoelastic behavior at small strain amplitudes and G'' is greater than G' . It can be seen that both moduli are decreased when the strain amplitude overcomes the limit of linear viscoelasticity at the strain amplitudes larger than 100.

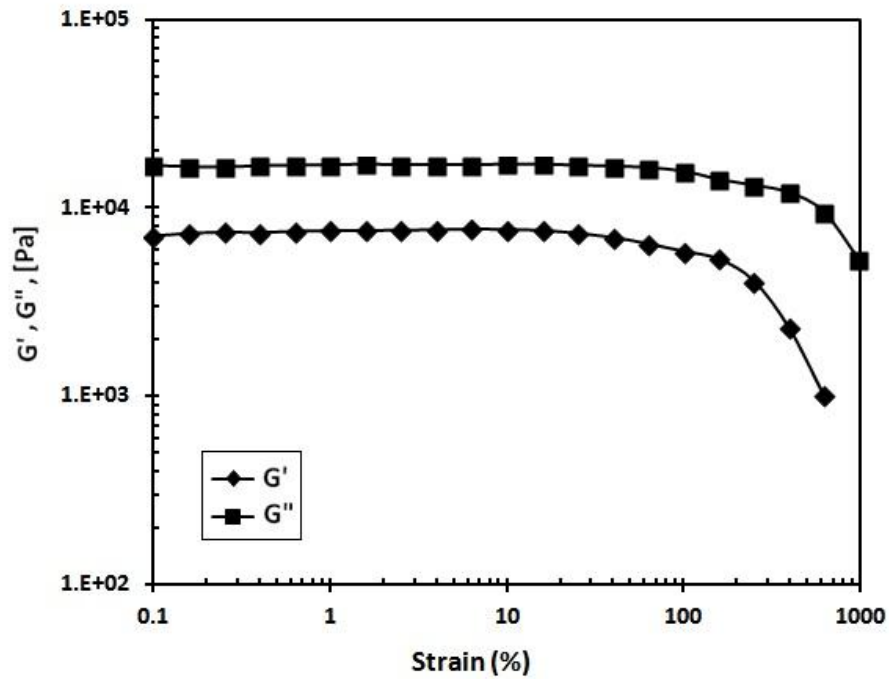


Figure 4.43 : Strain amplitude sweep of polymer **HP1M5** at 160°C.

Onogi and Asada [197] postulated that liquid crystalline polymers exhibit three regions of steady shear flow. Region I is classified by shear thinning at low shear rates and the flow behavior is dominated by defect. Region II has a viscosity plateau and texture refinement while Region III has a second shear thinning region where a monodomain is reached at higher shear rates. Figure 4.44 shows plots of $\log \eta$ vs $\log \dot{\gamma}$ for polymer **HP1M5** at various temperatures. The polymer shows a shear thinning behavior over the entire range of shear rate, $\dot{\gamma}$ tested. This behavior shows that this polymer exhibits region I followed by region III without having region II. The strong shear thinning usually shows yield behavior which is attributed to the nematic liquid crystalline domain upon start-up of steady shear flow, resulting from shear-induced rapid orientation of the molecules. Such steady state behavior has also been observed in MCLCPs [202, 205] micro-phase separated block copolymers and highly molten polymers [206].

Figure 4.44 also shows that the shear viscosity decreases as the applied temperature increases. This finding is similar to that of Zhou [207] who studied the rheology of combined main chain and side chain liquid crystalline polymers (MCSCCLCPs). The viscosity decreases upon transition from the isotropic to the nematic state. It can be well understood by the solid-nematic phase transition where the stiff solid molecules are aligned preferentially along the shear direction and liquid is positionally disordered but orientationally ordered [208].

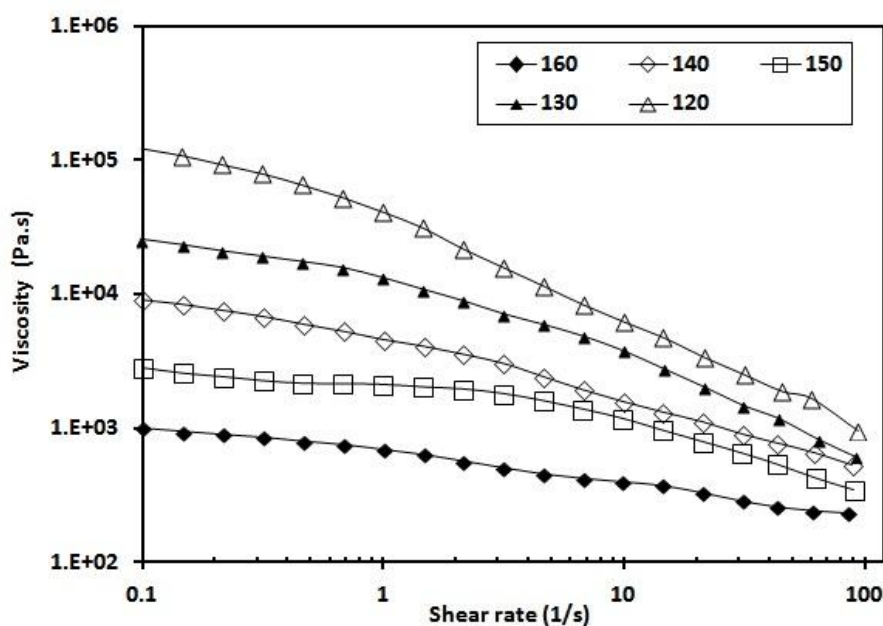


Figure 4.44 : Plots of $\log \eta$ vs $\log \dot{\gamma}$ for polymer **HP1M5** at various temperatures.

Figure 4.45(a) shows plots of $\log G'$, G'' and $|\eta^*|$ vs $\log \omega$ for polymer **HP1M5** at 110°C. The complex viscosity shows an upward concavity over the frequency range investigated. It can be seen that only a terminal regime was detected with a viscous response ($G'' > G'$) being prevalent in the whole frequency region investigated (0.1-100 rad/s). This trend is similar to Rodrun 3000 co-polyester at 250°C as reported by Somma et. al [209]. The storage modulus, G' , levels off at low frequencies indicating a solid like elasticity in the sample. According to Somma et. al [209] this behaviour is associated to a macrostructure which enhanced the material elasticity. Guskey and

Winter [210] suggested that the levelling off of G' could be attributed to an array of disclinations related to the polydomain structure.

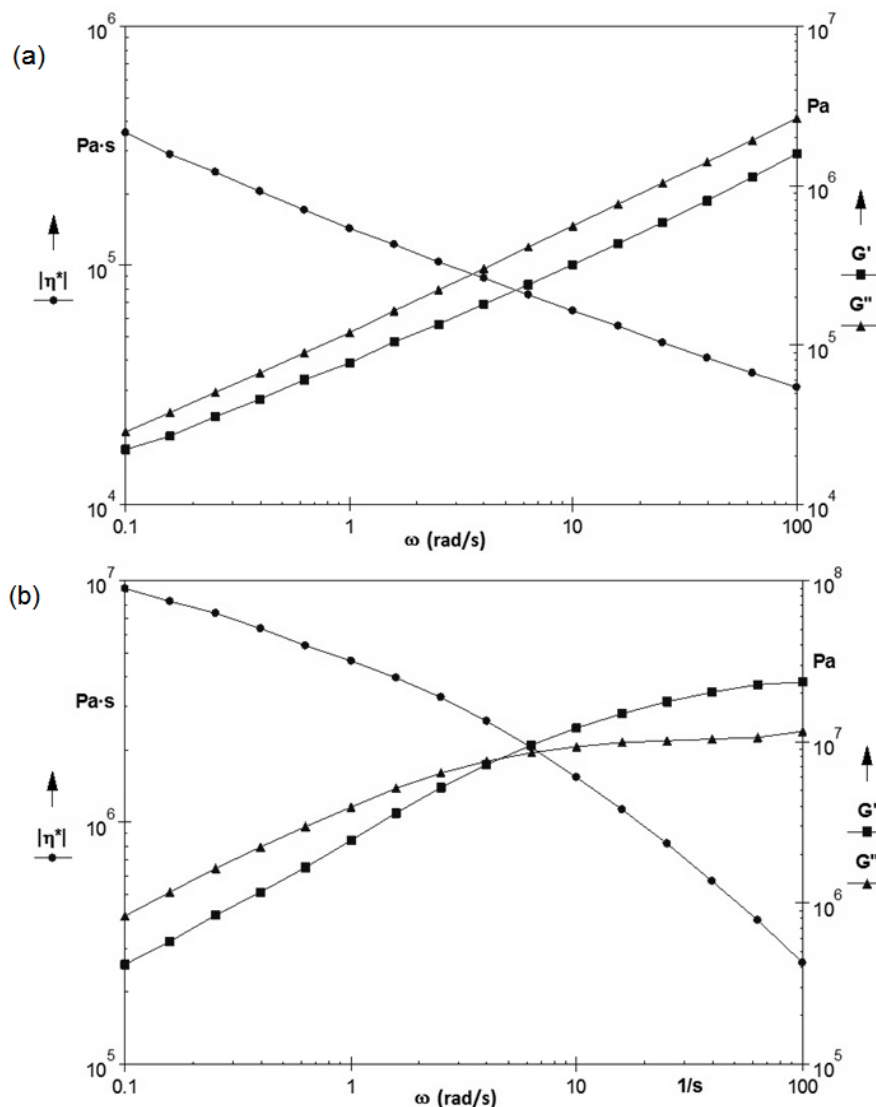


Figure 4.45 : Plots of $\log G'$, G'' and $|\eta^*|$ vs $\log \omega$ for polymer **HP1M5** at (a) 110°C (b) 90°C.

As the sample was cooled to 90°C, different behavior of the sample can be observed as shown in Figure 4.45(b). The complex viscosity shows an upward convexity over the frequency range investigated. At high frequencies, the G' and G'' profiles show an essentially solid like behavior ($G' > G''$). The moduli crossover is observed at $\omega_c = 4.6$ rad/s where $G' = G'' = 7.9 \times 10^6$ Pa. At low frequencies, the G' and G'' profiles show an essentially liquid like behavior ($G' < G''$). Materials that exhibit

solid like at high frequency and liquid like at low frequency are known as thixotropic [211]. Huang et al. [212] hypothesized that the viscous behavior of the polymer is due to the grafted polymers from one rod, which is in contact with another rod, can sufficiently rearrange their configurations thus allowing the rods to move with respect to each other. On the other hand, the polymer is unable to relax on a shorter time scale and thus the network of rods behaves like a soft solid.

Figure 4.46 shows plots of $\log G'$ vs $\log \omega$ and plots of $\log G''$ vs $\log \omega$ for polymer **HP1M5** at various temperatures. As shown in Figure 4.46(a), the slope of G' over the entire range of frequency tested remains less than 2 at the temperatures 140°C and below whereas the slope in the terminal region becomes 2 when the temperature is increased to 150°C and higher. The above observations shows that the frequency dependence of G' at temperatures below 150°C makes sense, because it is in an anisotropic state forming the nematic phase. At temperatures above 150°C, it will become a homogeneous liquid, and thus it is expected to exhibit a liquid like behavior in the terminal region. The frequency dependence of G' for this polymer has never been observed in ordinary flexible linear polymers. Similar observation has been reported by Lee and Han [213] during their study on rheological behavior of nematic SCLCPs.

On the other hand, G'' exhibits a liquid like behavior over the entire range of temperature tested as shown in Figure 4.46(b). The dynamic loss modulus, G'' is not as sensitive as the dynamic storage modulus, G' to a variation in the morphological state from the nematic to isotropic phase as the temperature is increased [213]. The frequency dependence of G'' for polymer **HP1M5** is consistent with the observation by Colby et. al [214] who studied the dynamic linear viscoelastic properties of the SCLCPs in nematic and isotropic states. They also concluded that the dynamic linear viscoelastic properties of the SCLCPs were qualitatively similar to ordinary flexible linear polymers.

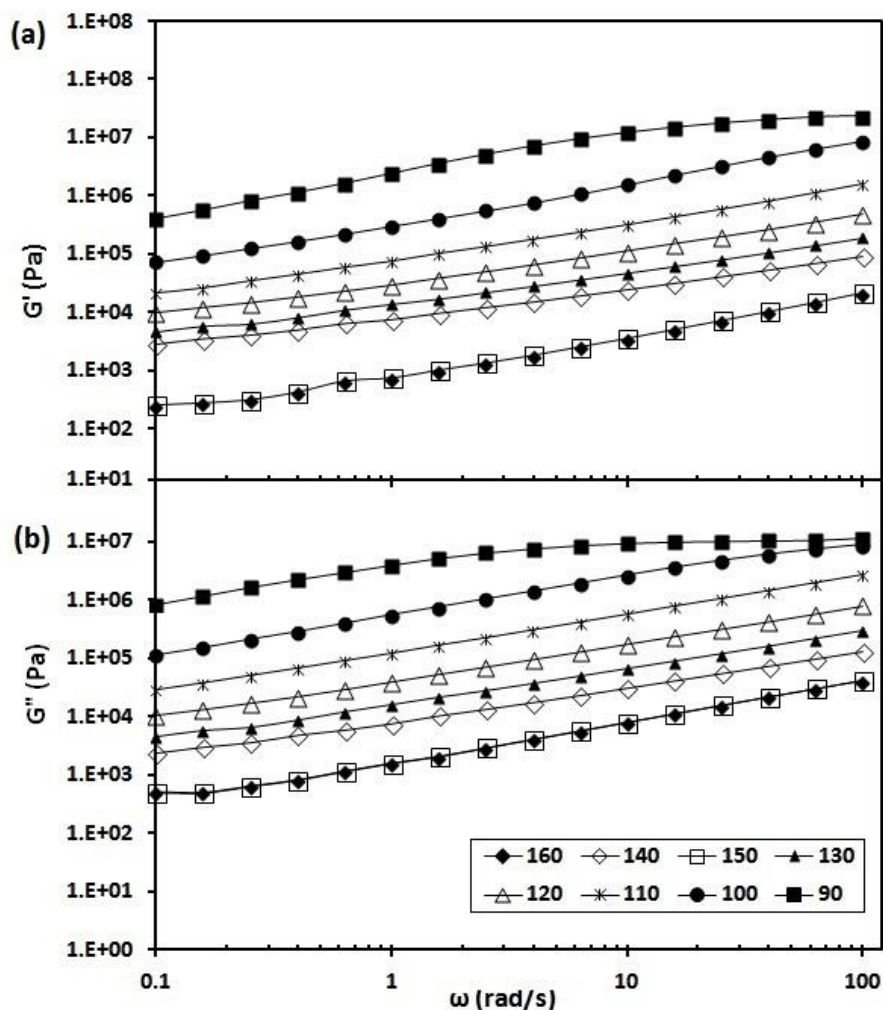


Figure 4.46 : Plots of $\log G'$ vs $\log \omega$ and $\log G''$ vs $\log \omega$ for polymer **HP1M5** at various temperatures.

Figure 4.47 shows a plot of $\log |\eta^*|$ vs $\log \omega$ for polymer **HP1M5** at various temperatures. The $|\eta^*|$ of the polymer at 90°C exhibits a shear-thinning behavior over the entire range of angular frequencies tested. As the temperature increases to 160°C the shear-thinning behavior becomes weaker. A smooth transition takes place from weak frequency dependence in the nematic state to frequency independence in the isotropic state. Note that in the nematic region the angular frequency dependence of $|\eta^*|$ in oscillatory shear flow (Figure 4.47) is very similar qualitatively to the shear rate dependence of η in steady shear flow (Figure 4.44).

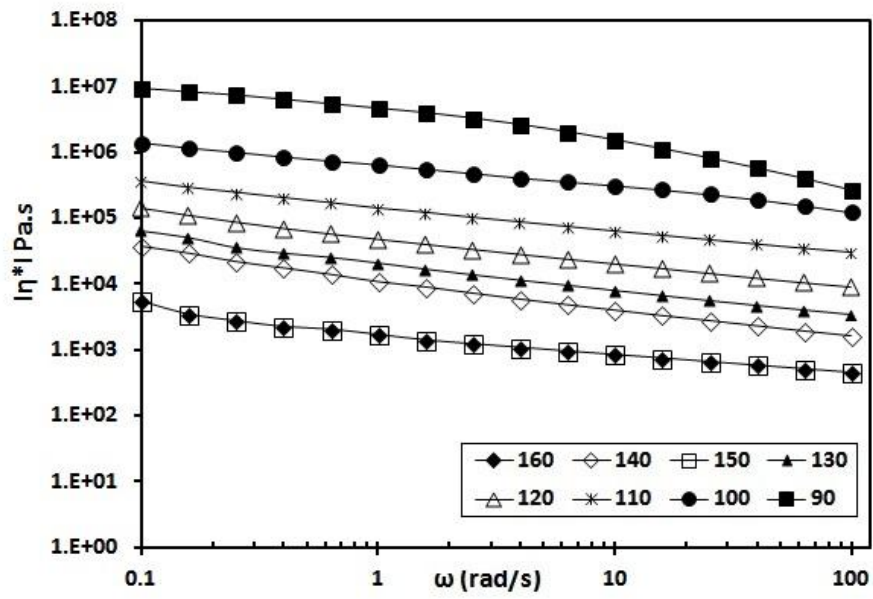


Figure 4.47 : Plots of $\log |\eta^*|$ vs $\log \omega$ for polymer **HP1M5** at various temperatures.

CHAPTER 5 : CONCLUSIONS & SUGGESTIONS FOR FUTURE STUDIES

5.1. Conclusions

New types of polymerizable liquid crystal monomers have been designed and have been successfully synthesized. The structures of the monomers have been identified by ^1H NMR, ^{13}C NMR and FTIR. The synthesized monomers were used to synthesize side chain liquid crystalline polymers (SCLCPs) via radical chain polymerization and atom transfer radical polymerization (ATRP). The molecular weights of the polymers as measured by GPC were higher when synthesized by radical chain polymerization than those synthesized by ATRP. Polydispersity indices for the polymers synthesized by radical chain polymerization suggest a strong tendency for chain termination by disproportionation. The polymers synthesized by ATRP showed narrow polydispersity index and resulted in well-defined polymers.

The monomer with naphthalene and one phenyl ring in the mesogen linked by an ester group (**M1**) showed lower thermal transition temperature compared to the monomer with three phenyl rings linked by Schiff base and ester groups (**M4**). The naphthalene ring provides a crankshaft structure which restricts lamellar packing of the molecules whereas the Schiff base group provides a better stability and enables mesophase formation.

Monomer with three phenyl rings linked by Schiff base and ester groups (**M4**) showed higher thermal transition temperature compared to the monomer with four phenyl rings linked by Schiff base and ester groups (**M8**). This is because the molecular length of M4 is greater than M8 therefore increases the intermolecular cohesive forces of the molecules which lead the higher thermal transitions temperatures of **M4** compared to **M8**.

The monomers with the presence of a lateral methoxy group on the mesogenic structure showed lower thermal transition temperatures compared to the monomers without a presence of a lateral methoxy group. The lateral methoxy group increases the breadth of the molecule and increases the acoplanarity in the system due to steric interaction. Hence, decrease the nematic mesophase range and the N-I transition temperature of the monomers.

The monomers with acrylate terminal group showed broader nematic mesophase range compared to the monomers with methacrylate terminal group. The hydrogen on the acrylate group promotes flexibility of the vinyl group where the methyl on the methacrylate restricts the movement of the vinyl group. The monomers also have a methoxy terminal group at their mesogenic structure which promotes broad nematic mesophase range of the monomers.

SCLCPs with narrow polydispersity exhibited both smectic and nematic mesophases whereas SCLCPs with broad polydispersity exhibited only nematic mesophase. This is due to the immiscibility of a mixture of different molecular architectures resulting from chain branching at the end of polymerization and entanglements. Generally, the thermal transition temperature of the SCLCPs increased as increase in molecular weight. All SCLCPs with polyacrylates backbone showed lower T_g values compared to the SCLCPs with polymethacrylates backbone. However, the isotropization temperatures of SCLCPs with polyacrylates backbone are typically higher compared to the SCLCPs with polymethacrylates backbone.

The polymers exhibited one stage decomposition with very high thermal stability which is really good for practical processing or for possible use in devices. The absorption peaks from UV-Vis spectroscopy of these polymers varied from 300 to 400 nm, while the fluorescence peaks varied from 380 to 560 nm. The bands of $\sigma \rightarrow \pi^*$ and $\pi \rightarrow \pi^*$ transitions are shifted to lower wavelength by the introduction of electron

donating group, $-\text{OCH}_3$ in the polymer side group. All polymers have the characteristic of emissive polymers. The band gaps of polymers were slightly shifted toward lower energy by the influence of the electron donating group in the side chain. The introduction of an electron-donating group ($-\text{OCH}_3$) into the terminal and lateral benzene rings of the studied polymers resulted in a decrease in the electrochemical band gap of the polymers. The band gap values of polymers (3.03-3.18 eV) revealed that the newly synthesized SCLCPs could be potential candidate in photovoltaic applications.

The rheological properties of the polymers carried out in smectic to nematic regions showed that the frequency behavior of the polymers in a smectic phase is characterized by the leveling off in the storage modulus, G' at low frequencies. Complex viscosities, $|\eta^*|$ of the smectic phase exhibited a shear thinning behavior over the shear rates investigated. In the nematic region, the angular frequency dependence of $|\eta^*|$ in oscillatory shear flow is found to be very similar qualitatively to the shear rate dependence of η in steady shear flow.

5.2. Suggestions for future studies

The polymers synthesized by ATRP in this work only possess low molecular weights. Further investigation is required on the successful ATRP system to produce high molecular weight with narrow polydispersity SCLCPs. High molecular weight SCLCPs will present higher thermal stability and very good mechanical properties. The logical continuation of this work would be to scale up the production of the monomers and polymers for various practical applications.

It is also interesting to synthesize block copolymers by adding styrene to the synthesized monomers to explore the novel mesomorphic and optical properties of the block copolymers. The block copolymers could be polymerized by using normal ATRP technique or reverse ATRP such as Activator Generated by Electron Transfer (AGET) ATRP, Initiators for Continuous Activator Regeneration (ICAR) ATRP and Activator Regenerated by Electron Transfer (ARGET) ATRP. These polymerization techniques would be possible to produce high molecular weight with narrow polydispersity block copolymers.

REFERENCES

1. Collings P.J. and Hird M., *Introduction to liquid crystals: Chemistry and physics*. Liquid crystals book series. 1997, US: CRC Press, Taylor and Francis.
2. Wang X., Zhou Q., and Zhou Q., *Liquid crystalline polymers*. 2004, Singapore: World Scientific Publishing Co. Pte. Ltd.
3. Kumar S., *Chemistry of discotic liquid crystals: From monomers to polymers*. Liquid crystals book series. 2011, New York: CRC Press, Taylor and Francis.
4. Singh S. and Dunmur D., *Liquid crystals: Fundamentals*. 2002: World Scientific Pub Co Inc.
5. Meier G., Sackmann E., and Grabmaier J.G., *Applications of liquid crystals*. 1975, New York: Springer.
6. Demus D., Goodby J., Gray G.W., W S.H., and Vill V., *Handbook of liquid crystals, fundamentals*. Vol. 1. 1998, New York: John Wiley & Sons.
7. Sluckin T.J., Dunmur D.A., and Stegemeyer H., *Crystals that flow: Classic papers from the history of liquid crystals*. 2004, New York: Taylor & Francis.
8. Gray G.W., *Molecular structure and the properties of liquid crystals*. 1962, London: Academic Press.
9. Stegemeyer H., "Professor horst sackmann, 1921 – 1993". *Liquid Crystals Today*, 1994. **4**(1): p. 1-2.
10. Gray G.W. and Winsor P.A., *Liquid crystals & plastic crystals*. Vol. 1. 1974, Chichester: Ellis Horwood.
11. Hilsom C., *Technology of chemicals and materials for electronics*, E.R. Howells, Editor. 1991, Ellis Horwood: Chichester.
12. Eidenschink R., Erdmann D., Krause J., and Pohl L., *Substituted phenylcyclohexanes—a new class of liquid crystalline compounds*. *Angewandte Chemie International Edition in English*, 1977. **16**(2): p. 100-100.
13. Boller A., Cereghetti M., Schadt M., and Scherrer H., *Synthesis and some physical properties of phenylpyrimidines*. *Molecular Crystals and Liquid Crystals*, 1977. **42**(1): p. 215-231.
14. De Gennes P. and Prost J., *The physics of liquid crystals* 2nd ed. 1993, Oxford: Oxford University Press.
15. Khoo I.C., *Liquid crystals*. 2007, New Jersey: John Wiley & Sons.
16. Chandrasekhar S., *Liquid crystals*. 1992, New York: Cambridge University Press.

17. Collings P., *Liquid crystals: Nature's delicate phase of matter*. 2nd ed. 2002, New Jersey: Princeton Univ. Press. 204.
18. *Soft matter : Liquid crystal*. 2011 [cited 2013 May 11]; Available from: [http://www.matdl.org/matdlwiki/index.php/softmatter:Liquid Crystal](http://www.matdl.org/matdlwiki/index.php/softmatter:Liquid_Crystal).
19. Sainsbury L. *Centre of molecular materials for photonics and electronics*. Materials - Introduction to liquid crystals 2003 [cited 2013 June 26]; Available from: <http://www-g.eng.cam.ac.uk/CMMPE/index.html>.
20. Fernsler J. *Liquid crystals*. [cited 2013 May 12]; Available from: <http://www.calpoly.edu/~jfernsl/Research/Liquid%20Crystals/LCResearch.html>.
21. Ritter O., Silveira N., and Merlo A., *Synthesis and mesomorphic properties of side chain liquid-crystalline biphenyl-phenyl polyacrylates*. Journal of the Brazilian Chemical Society, 2006. **17**: p. 348-356.
22. Craig A.A., Winchester I., Madden P., Larcey P., Hamley I., and Imrie C., *Synthesis, thermal characterization and rheological properties of a homologous series of polymethacrylate-based side-chain liquid crystal polymers*. Polymer, 1998. **39**(5): p. 1197-1205.
23. Braunecker W.A. and Matyjaszewski K., *Controlled/living radical polymerization: Features, developments, and perspectives*. Progress in Polymer Science, 2007. **32**(1): p. 93-146.
24. Matyjaszewski K., *Controlled radical polymerization*. Current Opinion in Solid State and Materials Science, 1996. **1**(6): p. 769-776.
25. McGrath J.E., *Chain reaction polymerization*. Journal of Chemical Education, 1981. **58**(11): p. 844.
26. Odian G., *Principles of polymerization*. 3rd ed. 2007, New Jersey: John Wiley & Sons.
27. Matyjaszewski K. and P.Davis T., *The kinetics of free-radical polymerization*, in *Handbook of radical polymerization*, Christopher Barner-Kowollik, Philipp Vana, and T. P.Davis, Editors. 2003, John Wiley & Sons: New York. p. 187-261.
28. Patten T. and Matyjaszewski K., *Atom transfer radical polymerization and the synthesis of polymeric materials*. Advanced Materials, 1998. **10**(12): p. 901-915.
29. Coessens V., Pintauer T., and Matyjaszewski K., *Functional polymers by atom transfer radical polymerization*. Progress in Polymer Science, 2001. **26**(3): p. 337-377.
30. Matyjaszewski K. and Xia J., *Atom transfer radical polymerization*. Chemical Reviews, 2001. **101**(9): p. 2921-2990.
31. Ayres N., *Atom transfer radical polymerization: A robust and versatile route for polymer synthesis*. Polymer Reviews, 2011. **51**(2): p. 138-162.

32. Pintauer T. and Matyjaszewski K., *Structural and mechanistic aspects of copper catalyzed atom transfer radical polymerization*. 2011, Springer Berlin / Heidelberg. p. 1-31.
33. Al-Harathi M., Sardashti A., Soares J.B.P., and Simon L.C., *Atom transfer radical polymerization (atrp) of styrene and acrylonitrile with monofunctional and bifunctional initiators*. *Polymer*, 2007. **48**(7): p. 1954-1961.
34. Beers K.L. and Matyjaszewski K., *The atom transfer radical polymerization of lauryl acrylate*. *Journal of Macromolecular Science, Part A: Pure and Applied Chemistry*, 2001. **38**(7): p. 731 - 739.
35. Shipp D.A., *Living radical polymerization: Controlling molecular size and chemical functionality in vinyl polymers*. *Journal of Macromolecular Science, Part C: Polymer Reviews*, 2005. **45**(2): p. 171-194.
36. Li M., Min K., and Matyjaszewski K., *Atrp in waterborne miniemulsion via a simultaneous reverse and normal initiation process*. *Macromolecules*, 2004. **37**(6): p. 2106-2112.
37. Matyjaszewski K., *Mechanistic and synthetic aspects of atom transfer radical polymerization*. *Journal of Macromolecular Science, Part A: Pure and Applied Chemistry*, 1997. **34**(10): p. 1785 - 1801.
38. Matyjaszewski K. *Atrp : The chemistry*. Kinetic studies on ATRP [cited 2013 June 27]; Available from: <http://www.cmu.edu/maty/chem/catalyst-development/kinetic-studies.html>.
39. Coessens V. and Matyjaszewski K., *Fundamentals of atom transfer radical polymerization*. *Journal of Chemical Education*, 2010. **87**(9): p. 916–919.
40. Jackson W.J., *Liquid crystalline polymers. 5. Liquid crystalline polyesters containing naphthalene rings*. *Macromolecules*, 1983. **16**(7): p. 1027-1033.
41. Leube H.F. and Finkelmann H., *New liquid-crystalline side-chain polymers with large transversal polarizability*. *Die Makromolekulare Chemie*, 1990. **191**(11): p. 2707-2715.
42. Leube H.F. and Finkelmann H., *Optical investigations on a liquid-crystalline side-chain polymer with biaxial nematic and biaxial smectic a phase*. *Die Makromolekulare Chemie*, 1991. **192**(6): p. 1317-1328.
43. Simionescu C., Grigoras M., Cianga I., and Olaru N., *Synthesis of new conjugated polymers with schiff base structure containing pyrrolyl and naphthalene moieties and hmo study of the monomers reactivity*. *European Polymer Journal*, 1998. **34**(7): p. 891-898.
44. Sapich B., Stumpe J., Kricheldorf H.R., Fritz A., and Schönhals A., *Synthesis, dielectric, and photochemical study of liquid crystalline main chain poly (ester imide) s containing cinnamoyl moieties*. *Macromolecules*, 2001. **34**(16): p. 5694-5701.

45. Sung H.H. and Lin H.C., *Effect of polar substituents on the properties of 1, 3, 4-oxadiazole-based liquid crystalline materials containing asymmetric cores*. *Liquid Crystals* 2004. **31**(6): p. 831-840.
46. Kozmík V., Kuchař M., Svoboda J., Novotná V., Glogarová M., Baumeister U., Diele S., and Pelzl G., *Laterally substituted naphthalene-2, 7-diol-based bent-shaped liquid crystals*. *Liquid Crystals*, 2005. **32**(9): p. 1151-1160.
47. Lee S.K., Naito Y., Shi L., Tokita M., Takezoe H., and Watanabe J., *Mesomorphic behaviour in bent-shaped molecules with side wings at different positions of a central naphthalene core*. *Liquid Crystals*, 2007. **34**(8): p. 935-943.
48. Mori T. and Kijima M., *Synthesis and optical properties of luminescent naphthalene-based liquid crystals*. *Molecular Crystals and Liquid Crystals*, 2008. **489**(1): p. 246-256.
49. Prajapati A. and Pandya H., *Effect of a lateral chloro group on azomesogens containing the naphthalene moiety*. *Molecular Crystals and Liquid Crystals*, 2003. **393**(1): p. 31-39.
50. Prajapati A., *Effect of a lateral methyl group on azo-mesogens containing the naphthalene moiety*. *Liquid Crystals*, 2000. **27**(8): p. 1017-1020.
51. Prajapati A., Pandya H., and Bonde N., *Naphthyl azomesogens with lateral chloro groups*. *Journal of Chemical Sciences*, 2004. **116**(4): p. 227-233.
52. Prajapati A., Thakkar V., and Bonde N., *New mesogenic homologous series of schiff base cinnamates comprising naphthalene moiety*. *Molecular Crystals and Liquid Crystals*, 2003. **393**(1): p. 41-48.
53. Kelker H. and Scheurle B., *A liquid-crystalline (nematic) phase with a particularly low solidification point*. *Angewandte Chemie International Edition in English*, 1969. **8**(11): p. 884-885.
54. Thaker B., Kanojiya J., and Tandel R., *Effects of different terminal substituents on the mesomorphic behavior of some azo-schiff base and azo-ester-based liquid crystals*. *Molecular Crystals and Liquid Crystals*, 2010. **528**(1): p. 120-137.
55. Ha S.T., Ong L.K., Wong J.P.W., Yeap G.Y., Lin H.C., Ong S.T., and Koh T.M., *Mesogenic schiff's base ether with dimethylamino end group*. *Phase Transitions*, 2009. **82**(5): p. 387-397.
56. Ha S.T., Ng M.Y., Subramaniam R.T., Ito M.M., Saito A., Watanabe M., Lee S.L., and Bonde N.L., *Mesogenic azomethine esters with different end groups: Synthesis and thermotropic properties*. *International Journal of Physical Sciences*, 2010. **5**: p. 1256-1262.
57. Mihai I., Ivanoiu M., Vacareanu L., and Grigoras M., *Polyazomethines with triphenylamine groups synthesized by suzuki polycondensation reactions*. *Designed Monomers and Polymers*, 2012. **15**(1): p. 41-52.

58. Hussein M.A., Abdel-Rahman M.A., Asiri A.M., Alamry K.A., and Aly K.I., *Review on: Liquid crystalline polyazomethines polymers. Basics, syntheses and characterization*. Designed Monomers and Polymers, 2012. **15**(5): p. 431-463.
59. Jin J.I., Kim H.S., Chung J.W.S.B.Y., and Jo B.W., *Synthesis and liquid crystalline properties of the compounds consisting of a schiff base type mesogen and a dyad type aromatic ester structure interconnected through the central hexamethylene spacer*. Bulletin of The Korean Chemical Society, 1990. **11**(3): p. 209-214.
60. Yeap G.Y., Ooi W.S., Nakamura Y., and Cheng Z., *Synthesis and mesomorphic properties of schiff base esters p-n-octadecanoyloxybenzylidene-p-cyano-, p-hydroxy-, p-nitro-, and p-carboxyanilines*. Molecular Crystals and Liquid Crystals, 2002. **381**(1): p. 169-178.
61. Yeap G.Y., Ha S.T., Lim P.L., Boey P.L., Mahmood W.A.K., Ito M.M., and Sanehisa S., *Synthesis and mesomorphic properties of schiff base esters ortho-hydroxy-para-alkyloxybenzylidene-para-substituted anilines*. Molecular Crystals and Liquid Crystals, 2004. **423**(1): p. 73-84.
62. Yeap G.Y., Ha S.T., Lim P.L., Boey P.L., Ito M.M., Sanehisa S., and Vill V., *Nematic and smectic a phases in ortho-hydroxy-para-hexadecanoyloxybenzylidene-para-substituted anilines*. Molecular Crystals and Liquid Crystals, 2006. **452**(1): p. 63-72.
63. Yeap G.Y., Ha S.T., Boey P.L., Mahmood W.A.K., Ito M.M., and Youhei Y., *Synthesis and characterization of some new mesogenic schiff base esters n-[4-(4-n-hexadecanoyloxybenzoyloxy)-benzylidene]-4-substituted anilines*. Molecular Crystals and Liquid Crystals, 2006. **452**(1): p. 73-90.
64. Yeap G.Y., Ha S.T., Lim P.L., Boey P.L., Ito M.M., Sanehisa S., and Youhei Y., *Synthesis, physical and mesomorphic properties of schiff's base esters containing ortho-, meta-and para-substituents in benzylidene-4'-alkanoyloxyanilines*. Liquid Crystals, 2006. **33**(2): p. 205-211.
65. Ha S.T., Lee T., Win Y., Lee S., and Yeap G., *Synthesis and characterization of new thermotropic liquid crystals derived from 4-hydroxybenzaldehyde*. World Academy of Science, Engineering and Technology 2011. **81**: p. 575-579.
66. Ha S.T., Lee T.L., and Yeap G.Y., *Synthesis of new homologous series of schiff base liquid crystals with iodo terminal group*, in *14th International Electronic Conference on Synthetic Organic Chemistry (ECSOC-14)*. J.A.S.M.P. Vázquez-Tato, Editor. 2010, MDPI: University of Santiago de Compostela, Spain.
67. Ha S.T., Ong L.K., Sivasothy Y., Yeap G.Y., Lin H.C., Lee S.L., Boey P.L., and Bonde N.L., *Mesogenic schiff base esters with terminal chloro group: Synthesis, thermotropic properties and x-ray diffraction studies*. International Journal of Physical Sciences, 2010. **5**(5): p. 564-575.
68. Ha S.T., Win Y.F., Lee S.L., Ito M.M., Abe K., Oonishi H., and Yeap G.Y., *Synthesis, spectral studies of 4-[(3-substitutedphenyl) imino] methyl-3-hydroxyphenyl octadecanoate and effect of meta substituents on mesomorphic properties*. International Journal of the Physical Sciences 2011. **6**(10): p. 2507-2517.

69. Fornasieri G., Guittard F., and G ribaldi S., *Influence of the structure of the mesogenic core on the thermotropic properties of ω -unsaturated fluorinated liquid crystals*. *Liquid Crystals*, 2003. **30**(2): p. 251-257.
70. Mori A., Itoh T., Taya H., Kubo K., Ujiie S., Baumeister U., Diele S., and Tschierske C., *Mesomorphic property of 2,5-dibenzoyloxy-, 5-benzoylamino-2-benzoyloxy-, and 2,5-dibenzoylamino-tropones with mono-, di-, and tri-alkoxyl groups on the benzoyl groups and their benzenoid derivatives*. *Liquid Crystals*, 2010. **37**(4): p. 355 - 368.
71. Chia W.L., Li C.L., and Lin C.H., *Synthesis and mesomorphic studies on the series of 2-(4-alkoxyphenyl)-5-phenylpyridines and 2-(6-alkoxynaphthalen-2-yl)-5-phenylpyridines*. *Liquid Crystals*, 2010. **37**(1): p. 23 - 30.
72. Matsunaga Y., Echizen T., Hashimoto K., and Nakamura S., *Effects of terminal substituents on mesomorphic properties. 4-(4-x-substituted benzylideneamino) phenyl 4-y-substituted benzoates*. *Molecular Crystals and Liquid Crystals Science and Technology. Section A. Molecular Crystals and Liquid Crystals*, 1998. **325**(1): p. 197-207.
73. Neubert M.E., Abdallah D.G., Keast S.S., Kim J.M., Lee S., Stayshich R.M., Walsh M.E., Petschek R.G., and Wu S.-T., *The effect of olefinic terminal chains on the mesomorphic properties of 4,4'-disubstituted diphenyldiacetylenes*. *Liquid Crystals*, 2003. **30**(6): p. 711-731.
74. Neubert M.E., Fisch M.R., Keast S.S., Kim J.M., Lohman M.C., Murray R.S., Miller K.J., Shenoy R.A., Smith M.J., Stayshich R.M., Walsh M.E., Petschek R.G., Lorenzo G.A., Burrows D.C., and Oliver S.M., *The effect of terminal chain modifications on the mesomorphic properties of 4,4'-disubstituted diphenyldiacetylenes*. *Liquid Crystals*, 2004. **31**(7): p. 941-963.
75. Neubert M.E., Keast S.S., Kim J.M., Norton A.G., Whyde M.J., Smith M.J., Stayshich R.M., Walsh M.E., and Abdallah D.G., *The effect on mesomorphic properties of a triple bond in a terminal chain of 4,4'-disubstituted phenyl benzoates and phenyl thiobenzoates*. *Liquid Crystals*, 2005. **32**(2): p. 247-266.
76. Karim M.R., Sheikh M.R.K., M Salleh N., Yahya R., Hassan A., and Hoque M.A., *Synthesis and characterization of azo benzothiazole chromophore based liquid crystal monomers: Effects of substituents on benzothiazole ring and terminal group on mesomorphic, thermal and optical properties*. *Materials Chemistry and Physics*, 2013. **140**: p. 543-552.
77. Kařpar M., Svereny k H., Hamplov  V., Glogarov  M., Pakhomov S.A., Van k P., and Trunda B., *The effect of a lateral methoxy group on the mesomorphic properties of ferroelectric liquid crystals*. *Liquid Crystals*, 1995. **19**(6): p. 775-778.
78. Kaspar M., Hamplova V., Pakhomov S.A., Stibor I., Sverenyak H., Bubnov A.M., Glogarova M., and Vanek P., *The effect of a lateral substituent on the mesomorphic properties in a series of ferroelectric liquid crystals with a 2-alkoxypropionate unit*. *Liquid Crystals*, 1997. **22**(5): p. 557-561.

79. Kašpar M., Bubnov A., Hamplová V., Málková Z., Pirkl S., and Glogarová M., *Effect of lateral substitution by fluorine and bromine atoms in ferroelectric liquid crystalline materials containing a 2-alkoxypropanoate unit*. *Liquid Crystals*, 2007. **34**(10): p. 1185-1192.
80. Chang C.Y., Chien S.Y., Hsu C.S., Gauza S., and Wu S.T., *Synthesis of laterally substituted *a*-methylstilbene-tolane liquid crystals*. *Liquid Crystals*, 2007. **35**(1): p. 1-9.
81. Dave J.S. and Bhatt H.S., *Synthesis of liquid crystals with lateral methyl group and study of their mesomorphic properties*. *Molecular Crystals and Liquid Crystals*, 2012. **562**(1): p. 1-9.
82. Dave J.S., Upasani C., and Patel P.D., *Effect of lateral substitution on mesogenic properties of fluoro aniline derivatives*. *Molecular Crystals and Liquid Crystals*, 2010. **533**(1): p. 73-81.
83. Doshi A. and Ganatra K. *Synthesis of new mesogens: 4 (4'-*n*-alkoxy benzoyloxy)-phenyl-azo-4 "-methyl benzenes*. in *Proceedings of the Indian Academy of Sciences-Chemical Sciences*. 1999: Springer.
84. Finkelmann H. and Rehage G., *Liquid crystal side chain polymers* *Advances in Polymer Science* 1984. **60/61**: p. 99-172.
85. Akiyama E., Nagase Y., Koide N., and Araki K., *New side chain liquid crystalline polymers: Synthesis and thermal properties of side chain polyacrylates having segmented spacers*. *Liquid Crystals*, 1999. **26**(7): p. 1029-1037.
86. Akiyama E., Matsui N., and Nagase Y., *A new synthetic approach to side-chain liquid crystalline polyacrylates containing siloxane spacers and their thermal behaviours*. *Liquid Crystals*, 1997. **23**(3): p. 425-438.
87. Akiyama E., Takamura Y., and Nagase Y., *Side-chain liquid-crystalline polymers containing the siloxane spacer v. Syntheses and thermal properties of copolymethacrylates with different spacer structures*. *Polymer Journal*, 1994. **26**(11): p. 1277-1285.
88. Akiyama E., Yamazaki M., Takamura Y., and Nagase Y., *Side chain liquid crystalline polymers containing siloxane spacer, 4. Introduction of trisiloxane unit into the spacer component*. *Macromolecular Rapid Communications*, 1994. **15**(2): p. 161-167.
89. De Tang X., Gao L.C., Fan X.H., and Zhou Q.F., *Effect of spacer length on the liquid crystalline property of azobenzene-containing aba-type triblock copolymers via atrp*. *Chinese Chemical Letters*, 2007. **18**(9): p. 1129-1132.
90. Palani T., Saravanan C., and Kannan P., *Pendant triazole ring assisted mesogen containing side chain liquid crystalline polymethacrylates: Synthesis and characterization*. *Journal of Chemical Sciences*, 2011: p. 1-9.
91. Craig A.A. and Imrie C.T., *Effect of backbone flexibility on the thermal properties of side-group liquid-crystal polymers*. *Macromolecules*, 1999. **32**(19): p. 6215-6220.

92. Crivello J.V., Deptolla M., and Ringsdorf H., *The synthesis and characterization of side-chain liquid crystal polymers based on polystyrene and poly-*a*-methystyrene* Liquid crystals 1988. **3**(2): p. 235-247.
93. Kong X. and Tang B.Z., *Synthesis and novel mesomorphic properties of the side-chain liquid crystalline polyacetylenes containing phenyl benzoate mesogens with cyano and methoxy tails*. Chemistry of Materials, 1998. **10**(11): p. 3352-3363.
94. Portugall M., Ringsdorf H., and Zentel R., *Synthesis and phase behaviour of liquid crystalline polyacrylates*. Macromolecular Chemistry and Physics 1982. **183**(10): p. 2311 -2321
95. Reck B. and Ringsdorf H., *Synthesis and phase behaviour of liquid-crystalline side group polyesters*. Liquid Crystals, 1990. **8**(2): p. 247-262.
96. Zentel R. and Ringsdorf H., *Synthesis and phase behaviour of liquid crystalline polymers from chloroacrylates and methacrylates*. Macromolecular Rapid Communications, 1984. **5**(7): p. 393 -398.
97. Yuichiro Haramoto and Masato Nanasawa, *New side chain liquid crystalline polysiloxanes containing 1,3-dithiane or 1,3-dioxane rings as mesogenic side groups*. Liquid Crystals,, 1997. **23**(2): p. 263-267.
98. Lorenz R., *Liquid-crystalline side-chain polyacrylates and polymethacrylates i. Variation of the terminal group*. Liquid Crystals, 1989. **6**(6): p. 667-674.
99. Zhang B.Y., Zhi J.G., and Meng F.B., *Synthesis and mesomorphic behaviour of novel chiral nematic side chain liquid crystalline polysiloxanes*. Liquid Crystals, 2003. **30**(9): p. 1007-1014.
100. Wang L.Y., Li K.C., and Lin H.C., *Synthesis and characterization of side-chain liquid-crystalline block-copolymers containing laterally attached photoluminescent quinquphenyl units via atp*. Polymer, 2010. **51**(1): p. 75-83.
101. Hsu and Shu C., *The application of side-chain liquid-crystalline polymers*. Progress in Polymer Science, 1997. **22**(4): p. 829-871.
102. Shibaev V.P., Kozlovsky M.V., Beresnev L.A., Blinov L.M., and Platé N.A., *Thermotropic liquid crystalline polymers*. Polymer Bulletin, 1984. **12**(4): p. 299-301.
103. Androozzi L., Faetti M., Giordano M., Zulli F., and Galli G., *A trap model description of enthalpy relaxation in a side chain liquid crystal polymethacrylate*. Molecular Crystals and Liquid Crystals, 2005. **429**(1): p. 289-299.
104. Brown D., Natansohn A., and Rochon P., *Azo polymers for reversible optical storage. 5. Orientation and dipolar interactions of azobenzene side groups in copolymers and blends containing methyl methacrylate structural units*. Macromolecules, 1995. **28**(18): p. 6116-6123.

105. Gindre D., Boeglin A., Fort A., Mager L., and Dorkenoo K.D., *Rewritable optical data storage in azobenzene copolymers*. *Optics Express* 2006. **14**(21): p. 9896-9901.
106. Hagen R. and Bieringer T., *Photoaddressable polymers for optical data storage*. *Advanced Materials*, 2001. **13**(23): p. 1805-1810.
107. Ikeda T. and Tsutsumi O., *Optical switching and image storage by means of azobenzene liquid-crystal films*. *Science*, 1995: p. 1873-1873.
108. McArdle C.B., *Side chain liquid crystal polymers*. 1989, New York: Springer.
109. Ho M.S., Natansohn A., Barrett C., and Rochon P., *Azo polymers for reversible optical storage. 8. The effect of polarity of the azobenzene groups*. *Canadian Journal of Chemistry*, 1995. **73**(11): p. 1773-1778.
110. Hvilsted S., Pedersen M., Holme N., and Ramanujan P., *Azobenzene side-chain liquid crystalline polyesters with outstanding optical storage properties*. *Turkish Journal of Chemistry*, 1998. **22**: p. 33-46.
111. Mandal B.K., Chen Y., Jeng R., Takahashi T., Huang J., Kumar J., and Tripathy S., *Thin film processing of nlo materials—i. Studies on relaxation behaviour of corona poled aromatic dipolar molecules in a polymer matrix*. *European Polymer Journal*, 1991. **27**(7): p. 735-741.
112. Mandal B.K., Jeng R.J., Kumar J., and Tripathy S.K., *New photocrosslinkable polymers for second order nonlinear optical processes*. *Macromolecular Chemistry Rapid Communications*, 1991. **12**(11): p. 607-612.
113. Mandal B.K., Takahashi T., Maeda M., Kumar S., and Blumstein A., *Comb-like polymers containing nlo active pendant groups*. 1990, DTIC Document.
114. Kumar J. and Tripathy S., *Organic polymeric electro-optic materials: Synthesis, processing and device applications*. 1993, DTIC Document.
115. Janini G.M., Laub R.J., and Shaw T.J., *Synthesis and properties of high temperature mesomorphic polysiloxane (mepsil) solvents. Amide, ester and schiff's base linked systems*. *Macromolecular Chemistry Rapid Communications*, 1985. **6**(2): p. 57-63.
116. Janini G., Laub R., Pluyter J., and Shaw T., *Probe-solute study of mesomorphic polysiloxane (mepsil) solvents. Synthesis and characterization of some ester-linked copolymer mepsil stationary phases*. *Molecular Crystals and Liquid Crystals*, 1987. **153**(1): p. 479-489.
117. Janini G., Muschik G., and Fox S., *Comparison of the gas-chromatographic properties of mesomorphic polymeric stationary phases*. *Chromatographia*, 1989. **27**(9-10): p. 436-440.
118. Bradshaw J.S., Schregenberger C., Chang K.H.-C., Markides K.E., and Lee M.L., *Synthesis and chromatographic properties of polysiloxane stationary phases containing biphenylcarboxylate ester liquid-crystalline side groups*. *Journal of Chromatography A*, 1986. **358**: p. 95-106.

119. Lin J.L. and Hsu C.S., *Synthesis of high temperature mesomorphic polysiloxanes and their use as stationary phases for high resolution gas chromatography*. Polymer Journal, 1993. **25**(2): p. 153-167.
120. Nishioka M., Jones B., Tarbet B., Bradshaw J., and Lee M., *Gas chromatographic retention behavior of polycyclic aromatic compounds on smectic liquid-crystalline polysiloxane stationary phases*. Journal of Chromatography A, 1986. **357**: p. 79-91.
121. Naikwadi K., McGovern A., and Karasek F., *Prospectives of polymeric liquid crystal stationary phases for capillary column gas chromatographic separations*. Canadian Journal of Chemistry, 1987. **65**(5): p. 970-975.
122. Markides K.E., Nishioka M., Tarbet B.J., Bradshaw J.S., and Lee M.L., *Smectic biphenylcarboxylate ester liquid crystalline polysiloxane stationary phase for capillary gas chromatography*. Analytical chemistry, 1985. **57**(7): p. 1296-1299.
123. Fang P.F., Zeng Z.R., Fan J.H., and Chen Y.Y., *Synthesis and characteristics of [60] fullerene polysiloxane stationary phase for capillary gas chromatography*. Journal of Chromatography A, 2000. **867**(1): p. 177-185.
124. Zeng Z.R., Ye H.Y., Liu Y., and Chen Y.Y., *[60] fulleropyrrolidine functionalized polysiloxane as a stationary phase for capillary gas chromatography*. Chromatographia, 1999. **49**(5-6): p. 293-298.
125. Tran C.D. and Challa S., *Fullerene-impregnated ionic liquid stationary phases for gas chromatography*. Analyst, 2008. **133**(4): p. 455-464.
126. Fan J.H., Zeng Z.R., Fang P.F., Chen Y.Y., and Cheng J.K., *Synthesis and characteristics of new high temperature stationary phase [60] fullerene polysiloxane for capillary gas chromatography [j]*. Chemical Research In Chinese Universities, 2000. **9**.
127. Pesek J.J. and Williamsen E.J., *The potential uses of bonded liquid crystal materials in high-performance liquid chromatography and supercritical-fluid chromatography*. Trends in Analytical Chemistry, 1992. **11**(7): p. 259-266.
128. Chang H.K., Markides K., Bradshaw J., and Lee M., *Selectivity enhancement for petroleum hydrocarbons using a smectic liquid crystalline stationary phase in supercritical fluid chromatography*. Journal of Chromatographic Science, 1988. **26**(6): p. 280-289.
129. Luffer D.R. and Novotny M., *Thermodynamic study of solute retention on a smectic liquid-crystalline phase in supercritical fluid chromatography*. Journal of Physical Chemistry, 1990. **94**(7): p. 3161-3166.
130. Schurig V., *Separation of enantiomers by gas chromatography on chiral stationary phases*, in *Chiral separation methods for pharmaceutical and biotechnological products*, S. Ahuja, Editor. 2011, John Wiley and Sons: New Jersey. p. 251-297.

131. Gritti F., Felix G., Achard M.-F., and Hardouin F., *Laterally attached liquid-crystalline polymers as stationary phases. Effect of temperature in rp hplc and comparison with a commercial c18 stationary phase*. *Chromatographia*, 2002. **56**(1-2): p. 9-17.
132. Saito Y., Jinno K., Pesek J.J., Chen Y.-L., Luehr G., Archer J., Fetzer J., and Biggs W., *Molecular shape recognition capability of liquid-crystal bonded phases in reversed-phase high performance liquid chromatography*. *Chromatographia*, 1994. **38**(5-6): p. 295-303.
133. Klein B.H. and Springer J., *Thermotropic liquid crystalline side group polymers as stationary phases in high performance liquid chromatography. I. The temperature dependence*. *Journal of Liquid Chromatography*, 1991. **14**(8): p. 1519-1538.
134. Gray G.W. and Kelly S.M., *Liquid crystals for twisted nematic display devices*. *Journal of Materials Chemistry*, 1999. **9**(9): p. 2037-2050.
135. Nakamura T., Ueno T., and Tani C., *Application of side chain type liquid crystal polymer for display and recording devices*. *Molecular Crystals and Liquid Crystals Incorporating Nonlinear Optics*, 1989. **169**: p. 167-192.
136. Finkelmann H. and Price A., *Liquid crystalline side-chain polymers [and discussion]*. *Philosophical Transactions of the Royal Society of London. Series A, Mathematical and Physical Sciences*, 1983. **309**(1507): p. 105-114.
137. Svensson M., Helgee B., Skarp K., Andersson G., *Influence of molar mass parameters on electro-optical switching in ferroelectric liquid crystalline polysiloxanes*. *Macromolecular Chemistry and Physics*, 1998. **199**: p. 535-541.
138. Smith I.C.P. and Blandford D.E., *Nuclear magnetic resonance spectroscopy*. *Analytical chemistry*, 1995. **67**(12): p. 509-518.
139. Otera J. and Nishikido J., *Reaction of alcohols with carboxylic acids and their derivatives*, in *Esterification: Methods, reactions, and applications*. 2010, Wiley VCH-Verlag: New York. p. 3-144.
140. Liu Y., Lotero E., and Goodwin Jr J.G., *Effect of water on sulfuric acid catalyzed esterification*. *Journal of Molecular Catalysis A: Chemical*, 2006. **245**(1): p. 132-140.
141. Roomana A., Rahman M.A., and Subhash B., *Kinetics of esterification of palmitic acid with isopropanol using p-toluene sulfonic acid and zinc ethanoate supported over silica gel as catalysts*. *Journal of Chemical Technology and Biotechnology*, 2004. **79**(10): p. 1127-1134.
142. Soderberg T., *Nucleophilic carbonyl addition reactions*, in *Organic Chemistry With a Biological Emphasis* [cited 2013 March 29], UC Davis GeoWiki: United State Available from: [http://chemwiki.ucdavis.edu/Organic_Chemistry/Organic_Chemistry_With_a_Biological_Emphasis/Chapter_11%3a_Nucleophilic_carbonyl_addition_reactions/Section_11.6%3a_Imine_\(Schiff_base\)_formation](http://chemwiki.ucdavis.edu/Organic_Chemistry/Organic_Chemistry_With_a_Biological_Emphasis/Chapter_11%3a_Nucleophilic_carbonyl_addition_reactions/Section_11.6%3a_Imine_(Schiff_base)_formation).

143. *Steglich esterification*. [cited 2013 March 29]; Available from: http://en.wikipedia.org/wiki/Steglich_esterification.
144. Neises B. and Steglich W., *Simple method for the esterification of carboxylic acids*. *Angewandte Chemie International Edition in English*, 1978. **17**(7): p. 522-524.
145. Angiolini L., Benelli T., Giorgini L., Paris F., Salatelli E., Fontana M.P., and Camorani P., *Synthesis by atp and effects of molecular weight on photomechanical properties of liquid crystalline polymers containing side-chain azobenzene chromophores*. *European Polymer Journal*, 2008. **44**: p. 3231-3238.
146. Krzysztof Matyjaszewski T.P.D., *Handbook of radical polymerization* 2003, New York: John Wiley & Sons.
147. Wang T.L., Liu Y.Z., Jeng B.C., and Cai Y.C., *The effect of initiators and reaction conditions on the polymer syntheses by atom transfer radical polymerization*. *Journal of Polymer Research*, 2005. **12**(2): p. 67-75.
148. Pavia D.L., G.M. L., G.S. K., and J.R. V., *Introduction to spectroscopy*. 4th ed. 2009, Canada: Brooks Cole Publishing Company.
149. Anderson R.J., Bendell D.J., and Groundwater P.W., *Organic spectroscopic analysis*. 2004, Royal Society of Chemistry: UK.
150. Marin L., Damaceanu M.D., and Timpu D., *New thermotropic liquid crystalline polyazomethines containing luminescent mesogens*. *Soft Materials*, 2009. **7**(1): p. 1-20.
151. Prajapati A.K. and Modi V., *Mesogenic quinazolone derivatives: Synthesis and characterisation*. *Liquid Crystals*, 2010. **37**(10): p. 1281 - 1288.
152. Chen B.K., S.Y. Tsay, and Chen J.Y., *Synthesis and properties of liquid crystalline polymers with low tm and broad mesophase temperature ranges*. *Polymer* 2005. **46**(20): p. 8624–8633
153. Chauhan B.C. and Doshi A.V., *Synthesis and mesomorphism of novel liquid crystalline: 4-(4'-n-alkoxy benzyloxy)-naphthylazo-4"-chlorobenzenes*. *Molecular Crystals and Liquid Crystals*, 2011. **552**(1): p. 16-23.
154. Ciferri A., *Liquid crystallinity in polymers : Principles and fundamental properties*. 1991, New york: VCH Publishers.
155. Kong X. and Tang B. Z., *Synthesis and novel mesomorphic properties of the side-chain liquid crystalline polyacetylenes containing phenyl benzoate mesogens with cyano and methoxy tails*. *Chemistry of Materials*, 1998. **10**(11): p. 3352-3363.
156. Dierking I., *Textures of liquid crystals*. 2003, German: Wiley-VCH Verlag.
157. Demus D., *Physical properties of liquid crystals*, ed. J.G. D. Demus, G.W. Gray, H. W. Spiess, V. Vill. 1999, Germany: John Wiley & Sons.
158. Stegemeyer H., *Phase types, structures and chemistry in liquid crystals*, in *Liquid crystals*. 1994, Springer: Germany. p. 1-50.

159. Wang Q., Yang C.-a., Xie H., Wang X., and Zhang H., *Effect of mesogenic density on liquid-crystalline behaviours of polymethacrylates bearing azobenzene mesogen*. *Liquid Crystals*, 2010. **37**(4): p. 435 - 443.
160. Hu T., Xie H., Xiao J., Zhang H., and Chen E., *Design, synthesis, and characterization of a combined main-chain/side-chain liquid-crystalline polymer based on ethyl cellulose*. *Cellulose*, 2010. **17**(3): p. 547-558.
161. Marin L., Perju E., and Damaceanu M.D., *Designing thermotropic liquid crystalline polyazomethines based on fluorene and/or oxadiazole chromophores*. *European Polymer Journal*, 2011. **47**(6): p. 1284-1299.
162. Fernández-Blázquez J.P., Bello A., and Pérez E., *Observation of two glass transitions in a thermotropic liquid-crystalline polymer*. *Macromolecules*, 2004. **37**(24): p. 9018-9026.
163. Demus D., Goodby J.W., Gray G.W., Spiess H.W., and Vill V., *Handbook of liquid crystals, high molecular weight liquid crystals*. 2008, Germany: John Wiley & Sons.
164. Zhang H., Yu Z., Wan X., Zhou Q.F., and Woo E.M., *Effects of molecular weight on liquid-crystalline behavior of a mesogen-jacketed liquid crystal polymer synthesized by atom transfer radical polymerization*. *Polymer*, 2002. **43**(8): p. 2357-2361.
165. Percec V. and Tomazos D., *Molecular engineering of side chain liquid crystalline polymers*, in *Advances in new materials*, J.C. Salamone and J. Riffle, Editors. 1992, Springer US. p. 247-268.
166. Stevens H., Rehage G., and Finkelmann H., *Phase transformations of liquid crystalline side-chain oligomers*. *Macromolecules*, 1984. **17**(4): p. 851-856.
167. Trimmel G., Riegler S., Fuchs G., Slugovc C., and Stelzer F., *Liquid crystalline polymers by metathesis polymerization*, in *Adv. Polym. Sci.* . 2005. p. 43-87.
168. Heroguez V., Schappacher M., Papon E., and Deffieux A., *Synthesis and characterization of poly(vinylether)s with pendant mesogenic groups*. *Polymer Bulletin*, 1991. **25**(3): p. 307-314.
169. Kasko A.M., Heintz A.M., and Pugh C., *The effect of molecular architecture on the thermotropic behavior of poly[11-(4'-cyanophenyl-4''-phenoxy)undecyl acrylate] and its relation to polydispersity*. *Macromolecules*, 1998. **31**(2): p. 256-271.
170. Wood B.A. and Thomas E.L., *Are domains in liquid crystalline polymers arrays of disclinations?* *Nature*, 1986. **324**(6098): p. 655-657.
171. Shiwaku T., Nakai A., Hasegawa H., and Hashimoto T., *Ordered structure of thermotropic liquid-crystal polymer. 1. Characterization of liquid-crystal domain texture*. *Macromolecules*, 1990. **23**(6): p. 1590-1599.
172. Sakthivel P. and Kannan P., *Thermotropic main-chain liquid-crystalline photodimerizable poly(vanillylidenealkyloxy alkylphosphate ester)s containing a cyclopentanone moiety*. *Polymer International*, 2005. **54**(11): p. 1490-1497.

173. Radhakrishnan S., Subramanian V., and Somanathan N., *Structure–optical, thermal properties studies on thiophene containing benzothiazole groups*. *Organic Electronics*, 2004. **5**(5): p. 227-235.
174. Pérez Guarín S.A. and Skene W., *Thermal, photophysical, and electrochemical characterization of a conjugated polyazomethine prepared by anodic electropolymerization of a thiophenoazomethine co-monomer*. *Materials Letters*, 2007. **61**(29): p. 5102-5106.
175. Liu J.H., Wang Y.K., Chen C.C., Yang P.C., Hsieh F.M., and Chiu Y.H., *Synthesis and characterization of optically active liquid crystalline polyacrylates containing mesogenic phenylbenzoate groups*. *Polymer*, 2008. **49**(18): p. 3938-3949.
176. Komiya Z. and Schrock R., *Synthesis of side chain liquid crystal polymers by living ring-opening metathesis polymerization. 5. Influence of mesogenic group and interconnecting group on the thermotropic behavior of the resulting polymers*. *Macromolecules*, 1993. **26**(6): p. 1393-1401.
177. Chen B.K., Tsay S.Y., and Shih I.C., *Synthesis of copolyimide containing fluorine and naphthalene with synergizing effect on dielectric constants*. *Polymer Bulletin*, 2005. **54**(1): p. 39-46.
178. Pan G., Du Z., Zhang C., Li C., Yang X., and Li H., *Synthesis, characterization, and properties of novel novolac epoxy resin containing naphthalene moiety*. *Polymer*, 2007. **48**(13): p. 3686-3693.
179. Blanksby S.J. and Ellison G.B., *Bond dissociation energies of organic molecules*. *Accounts of Chemical Research*, 2003. **36**(4): p. 255-263.
180. Liu J.H. and Yang P.C., *Synthesis and characterization of novel monomers and polymers containing chiral (–)-menthyl groups*. *Polymer*, 2006. **47**(14): p. 4925-4935.
181. Jaffe H., Yeh S.J., and Gardner R., *The electronic spectra of azobenzene derivatives and their conjugate acids*. *Journal of Molecular Spectroscopy*, 1958. **2**(1): p. 120-136.
182. Han K.L. and Zhao G.J., *Hydrogen bonding and transfer in the excited state*. 2011, UK: John Wiley & Sons.
183. Zhao K., Cheng Z., Zhang Z., Zhu J., and Zhu X., *Synthesis of fluorescent poly (methyl methacrylate) via aget atp*. *Polymer Bulletin*, 2009. **63**(3): p. 355-364.
184. Anuragudom P., El-daye J., Chinwangso P., Advincula R.C., Phanichphant S., and Lee T.R., *New light-emitting poly {(9, 9-di-n-octylfluorenediyl vinylene)-alt-[1, 5-(2, 6-dioctyloxy) naphthalene vinylene]}*. *Polymer International*, 2011. **60** (4):p. 660-665
185. Sek D., Grucela-Zajac M., Krompiec M., Janeczek H., and Schab-Balcerzak E., *New glass forming triarylamine based azomethines as a hole transport materials: Thermal, optical and electrochemical properties*. *Optical Materials*, 2012. **34**(8): p. 1333-1346.

186. Knöpke L.R., Spannenberg A., Brückner A., and Bentrup U., *The influence of substituent effects on spectroscopic properties examined on benzylidene aniline-type imines*. *Spectrochimica Acta Part A: Molecular and Biomolecular Spectroscopy*, 2012. **95**: p. 18-24.
187. Luo Z., Shi H., Zhu H., Song G., and Liu Y., *A new blue light-emitting terphenyl-bridged bisbenzimidazolium salts: Synthesis, crystal structure, and photophysical properties*. *Dyes and Pigments*, 2012. **92**(1): p. 596-602.
188. Sun Y.M., *Synthesis and optical properties of novel blue light-emitting polymers with electron affinitive oxadiazole*. *Polymer*, 2001. **42**(23): p. 9495-9504.
189. Zhang W., Zhu X., Zhou D., Wang X., and Zhu J., *Reversible addition-fragmentation chain transfer polymerization of 2-naphthyl acrylate with 2-cyanoprop-2-yl 1-dithionaphthalate as a chain-transfer agent*. *Journal of Polymer Science Part A: Polymer Chemistry*, 2005. **43**(12): p. 2632-2642.
190. Hohnholz D., Schweikart K.-H., Subramanian L., Wedel A., Wischert W., and Hanack M., *Synthesis and studies on luminescent biphenyl compounds*. *Synthetic Metals*, 2000. **110**(2): p. 141-152.
191. Sek D., Jarzabek B., Grabiec E., Kaczmarczyk B., Janeczek H., Sikora A., Hreniak A., Palewicz M., Lapkowski M., and Karon K., *A study of thermal, optical and electrical properties of new branched triphenylamine-based polyazomethines*. *Synthetic Metals*, 2010. **160**(19): p. 2065-2076.
192. Bilici A., Kaya İ., and Yildirim M., *A comparative study of 9, 9-bis (4-aminophenyl) fluorene polymers prepared by catalytic and non-catalytic oxidative polymerisation methods*. *European Polymer Journal*, 2011. **47**(5): p. 1005-1017.
193. Kaya İ. and Kamacı M., *Synthesis, optical, electrochemical, and thermal stability properties of poly(azomethine-urethane)s*. *Progress in Organic Coatings*, 2012. **74**(1): p. 204-214.
194. Liu G., Pu S., Wang X., Liu W., and Yang T., *Effects of substitution on the optoelectronic properties of photochromic diarylethenes bearing a pyrrole moiety*. *Dyes and Pigments*, 2011. **90**(1): p. 71-81.
195. Manjunatha M., Adhikari A.V., Hegde P.K., Sandeep C.S., and Philip R., *Synthesis and characterization of a new nlo-active donor-acceptor-type conjugated polymer derived from 3, 4-diphenylthiophene*. *Journal of Polymer Research*, 2010. **17**(4): p. 495-502.
196. Wang Y.J., Sheu H.S., and Lai C.K., *New star-shaped triarylamine: Synthesis, mesomorphic behavior, and photophysical properties*. *Tetrahedron*, 2007. **63**(7): p. 1695-1705.
197. Onogi S. and Asada T., eds. *Rheology and rheo-optics of polymer liquid crystals in rheology*. ed. G. Astarita, G. Marrucci, and L. Nicolais. Vol. 1. 1988, Plenum Press: New York.
198. Lee H. and Denn M., *Polymer blends with a liquid crystalline polymer dispersed phase*. *Korea-Australia Rheology Journal*, 1999. **11**(4): p. 269-273.

199. Kannan R.M., Kornfield J.A., Schwenk N., and Boeffel C., *Rheology of side-group liquid-crystalline polymers: Effect of isotropic-nematic transition and evidence of flow alignment*. *Macromolecules*, 1993. **26**(8): p. 2050-2056.
200. Dan K., Kim B., and Han Y., *The physical properties of thermotropic side-chain triblock copolymers of n-butyl acrylate and a comonomer with azobenzene group*. *Macromolecular Research*, 2009. **17**(5): p. 313-318.
201. Rubin S.F., Kannan R.M., Kornfield J.A., and Boeffel C., *Effect of mesophase order and molecular weight on the dynamics of nematic and smectic side-group liquid-crystalline polymers*. *Macromolecules*, 1995. **28**(10): p. 3521-3530.
202. Kim D. and Han C., *Effect of bulkiness of pendent side groups on the rheology of semiflexible main-chain thermotropic liquid-crystalline polymers*. *Macromolecules*, 2000. **33**(9): p. 3349-3358.
203. Auad M.L., Kempe M.D., Kornfield J.A., Rendon S., Burghardt W.R., and Yoon K., *Effect of mesophase order on the dynamics of side group liquid crystalline polymers*. *Macromolecules*, 2005. **38**(16): p. 6946-6953.
204. Lee K.M. and Han C.D., *Effect of flexible spacer length on the rheology of side-chain liquid-crystalline polymers*. *Macromolecules*, 2003. **36**(23): p. 8796-8810.
205. Lee K.M. and Han C.D., *Rheology of nematic side-chain liquid-crystalline polymer: Comparison with main-chain liquid-crystalline polymer*. *Macromolecules*, 2002. **35**(16): p. 6263-6273.
206. Dae Han C. and Kim J.K., *On the use of time-temperature superposition in multicomponent/multiphase polymer systems*. *Polymer*, 1993. **34**(12): p. 2533-2539.
207. Zhou M., *Synthesis, phase transition, morphology, and rheology of combined main-chain and side-chain liquid-crystalline polymers in both thermotropic and lyotropic states*, in *The Graduate Faculty*. 2006, The University of Akron
208. Fan Y., Dai S., and Tanner R.I., *Rheological properties of some thermotropic liquid crystalline polymers*. *Korea-Australia Rheology Journal*, 2003. **15**(3): p. 109-115.
209. Somma E., Iervolino R., and Nobile M.R., *The viscoelasticity of thermotropic liquid crystalline polymers: Effects of the chemical composition*. *Rheologica acta*, 2006. **45**(4): p. 486-496.
210. Guskey S.M. and Winter H.H., *Transient shear behaviour of a thermotropic liquid crystalline polymer in the nematic state*. *Journal of Rheology*, 1991. **35**: p. 1191-1207.
211. Barnes H.A., *Thixotropy—a review*. *Journal of Non-Newtonian Fluid Mechanics*, 1997. **70**(1): p. 1-33.
212. Huang F., Rotstein R., Fraden S., Kasza K.E., and Flynn N.T., *Phase behavior and rheology of attractive rod-like particles*. *Soft Matter*, 2009. **5**(14): p. 2766-2771.

213. Lee K. and Han C., *Rheology of nematic side-chain liquid-crystalline polymer: Comparison with main-chain liquid-crystalline polymer*. *Macromolecules*, 2002. **35**(16): p. 6263-6273.
214. Colby R.H., Gillmor J.R., Galli G., Laus M., Ober C.K., and Hall E., *Linear viscoelasticity of side chain liquid crystal polymer*. *Liquid Crystals* 1993. **13**(2): p. 233-245.

APPENDICES

APPENDIX A : ^1H NMR Figures

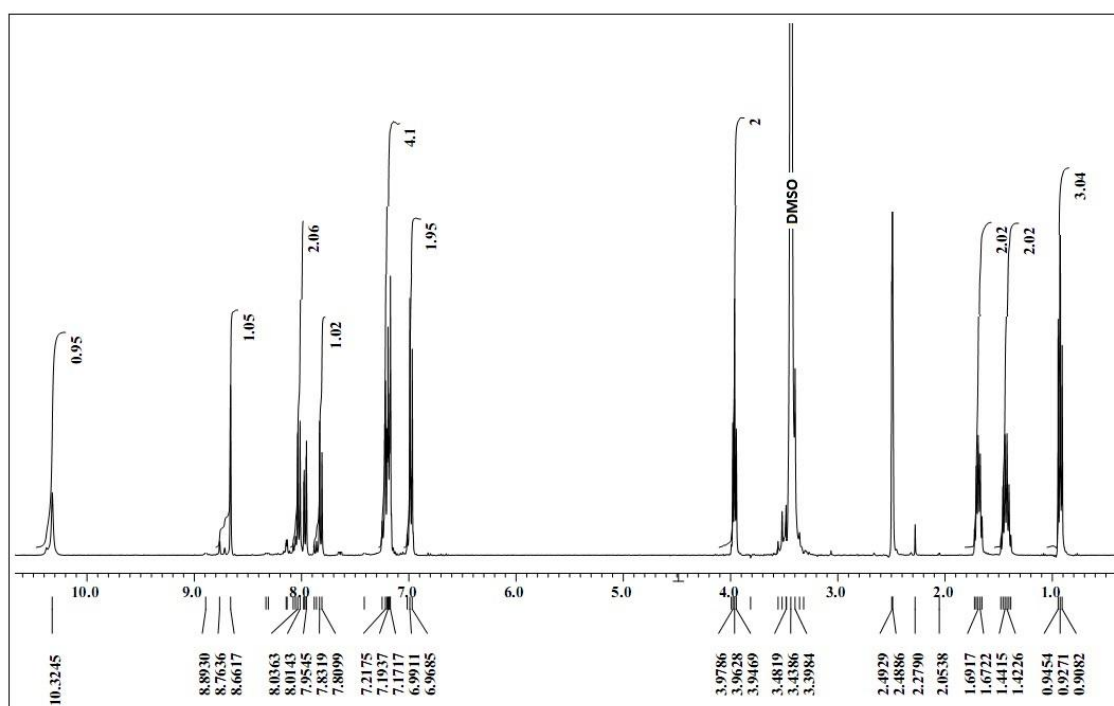


Figure A1: Compound 1

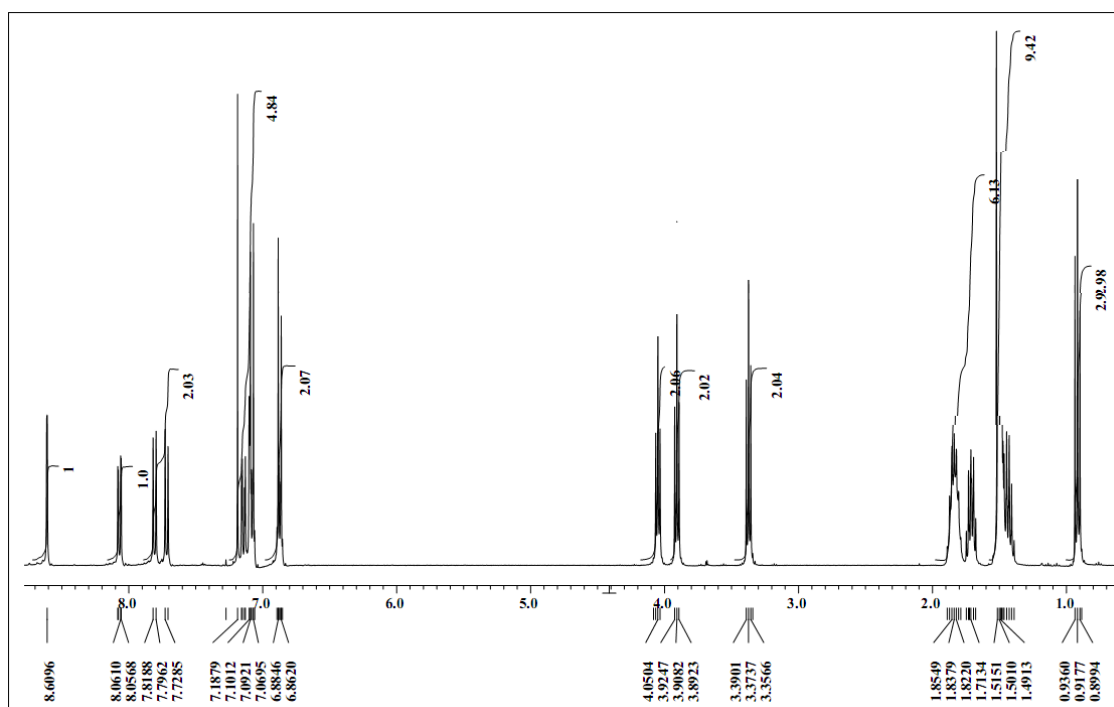


Figure A1: Compound 2

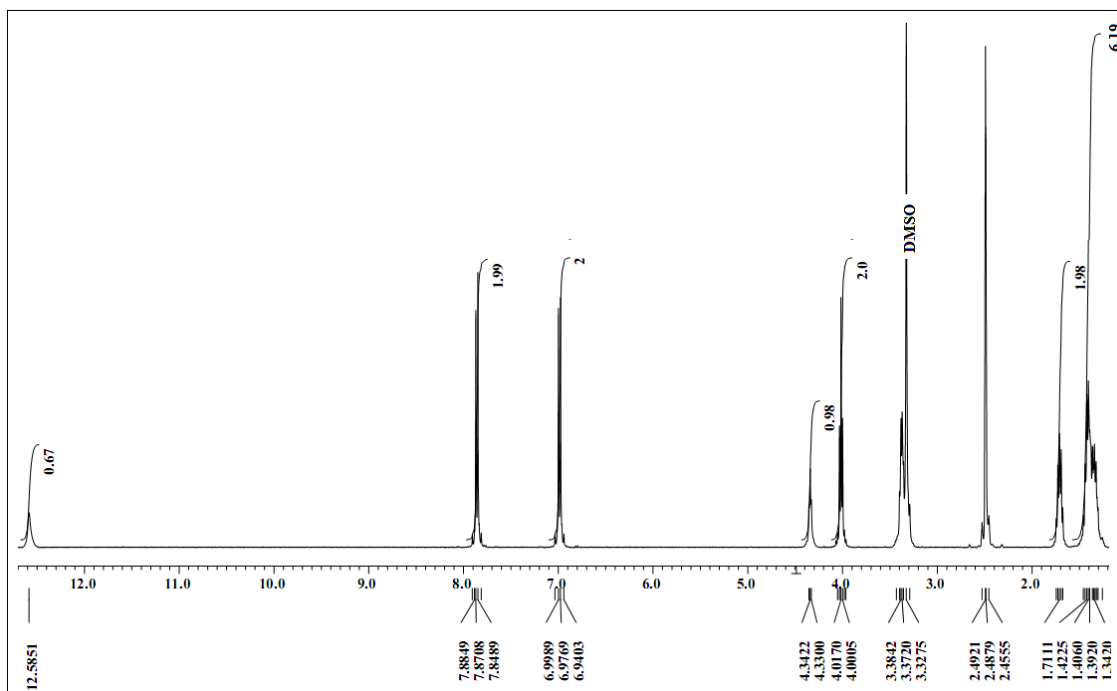


Figure A1: Compound 3

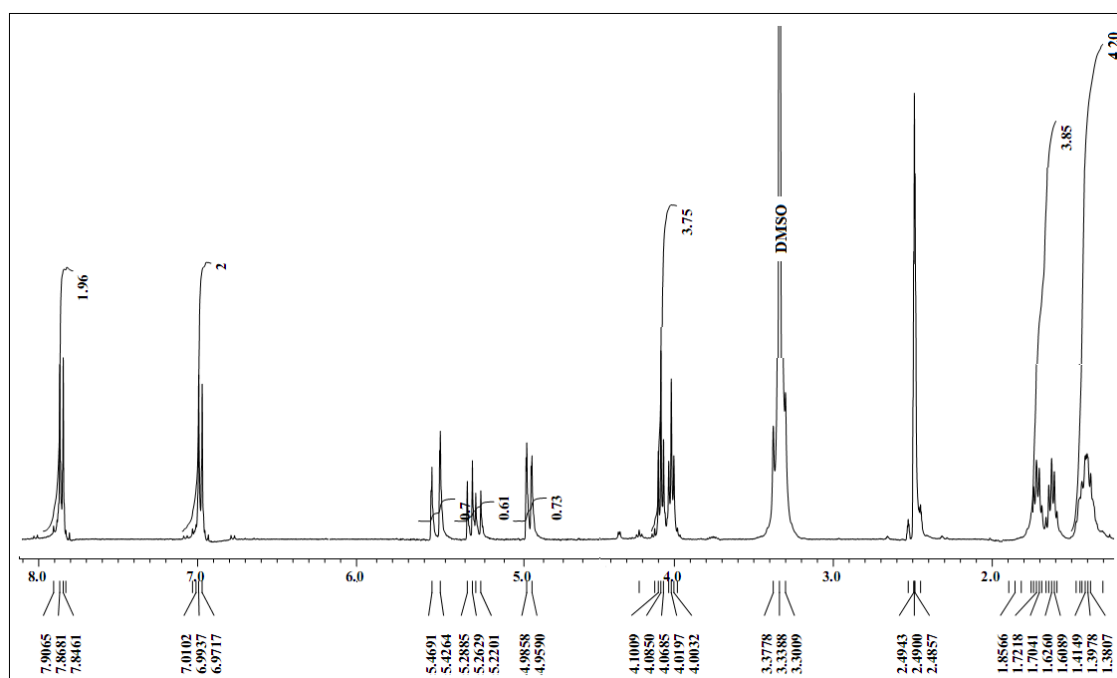


Figure A1: Compound 4

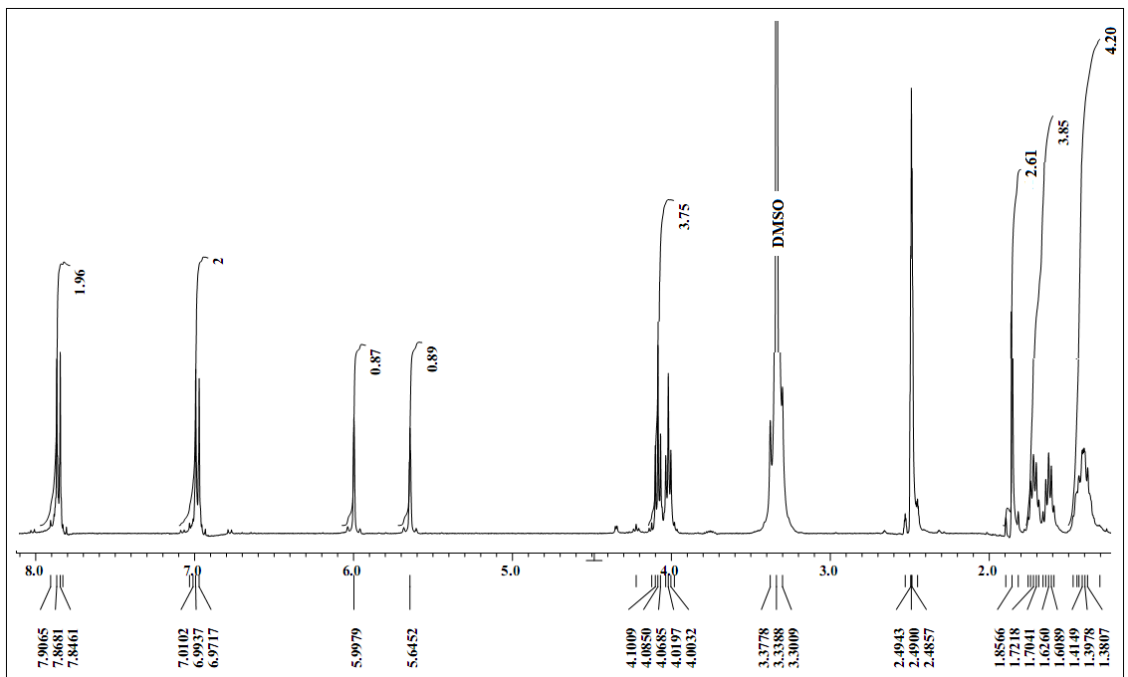


Figure A1: Compound 5

APPENDIX B : ^{13}C NMR Figures

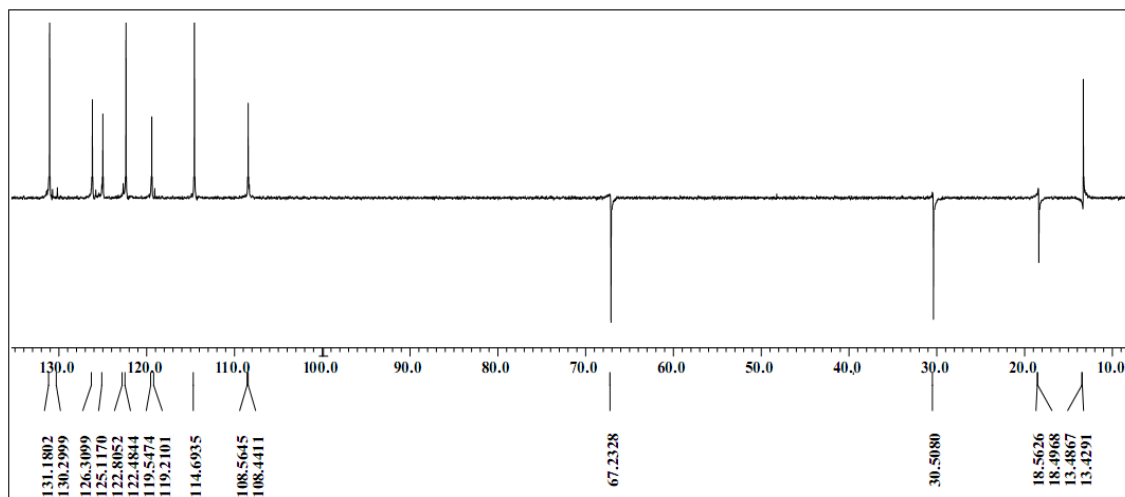


Figure B1: Compound 1

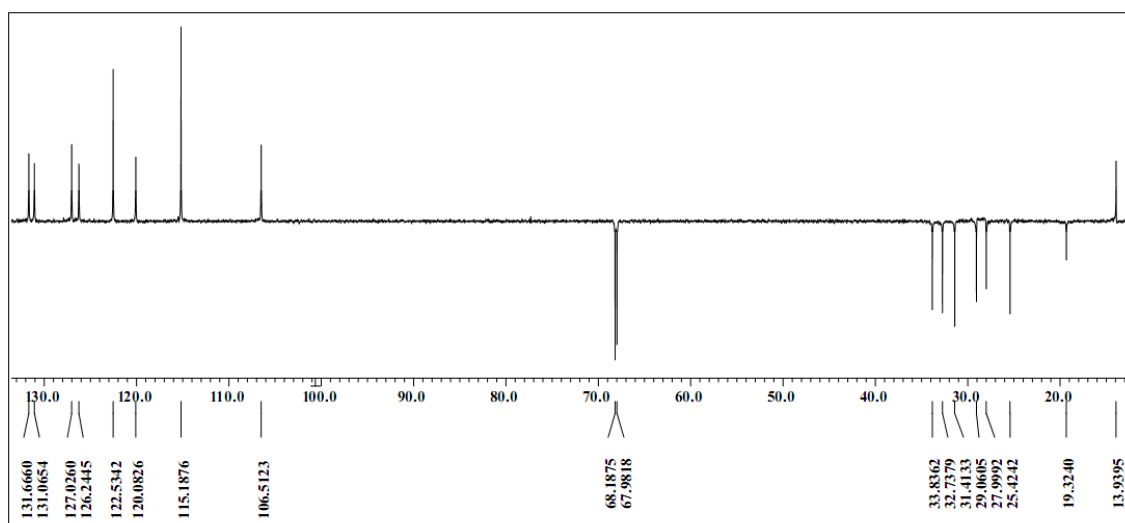


Figure B2: Compound 2

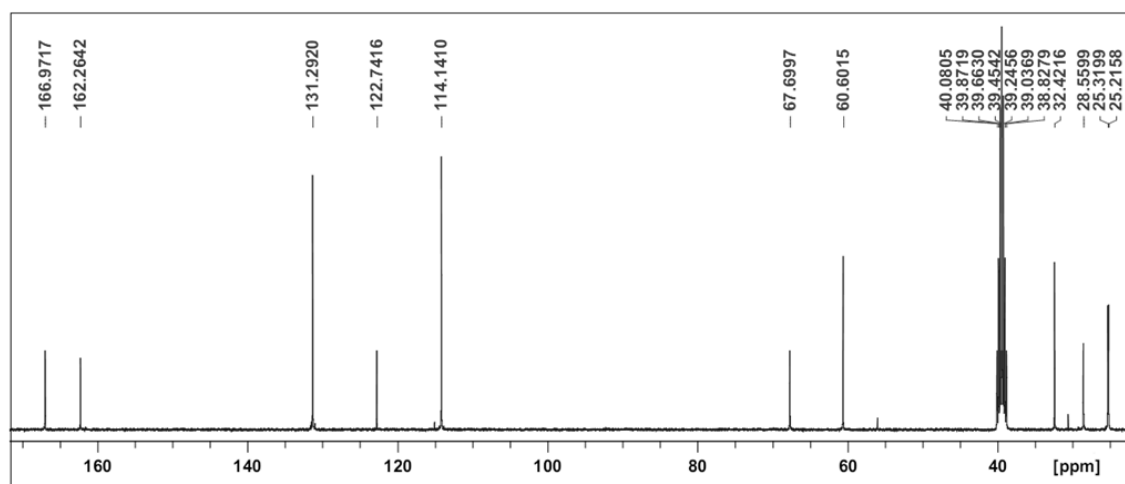


Figure B3: Compound 3

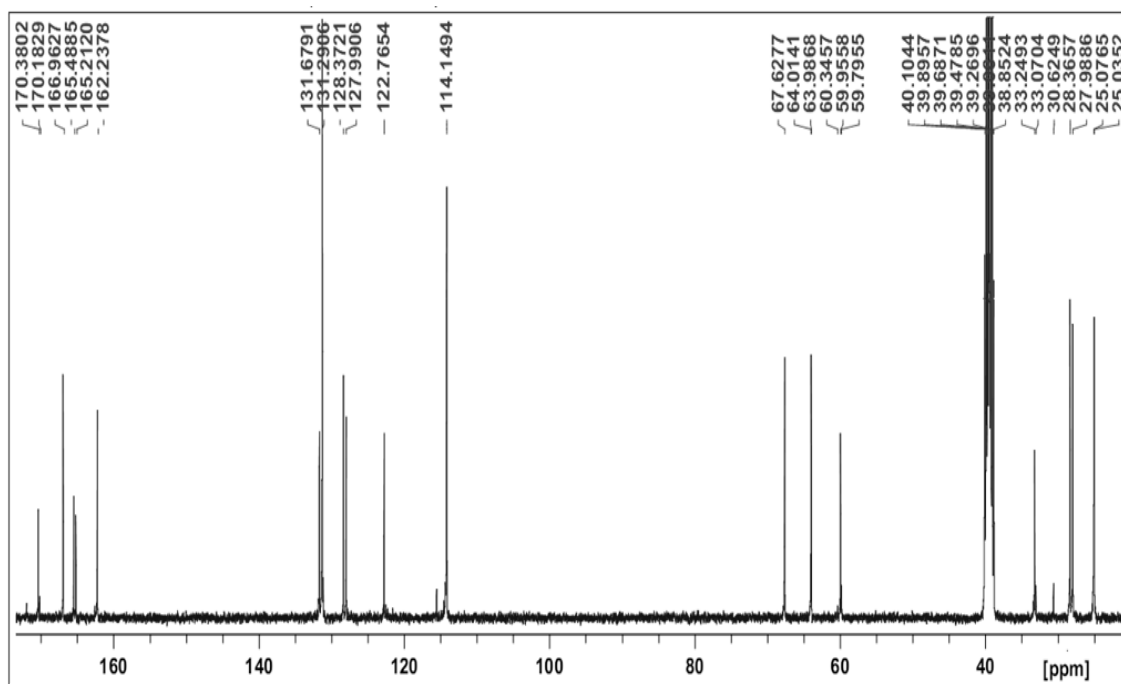


Figure B4: Compound 4

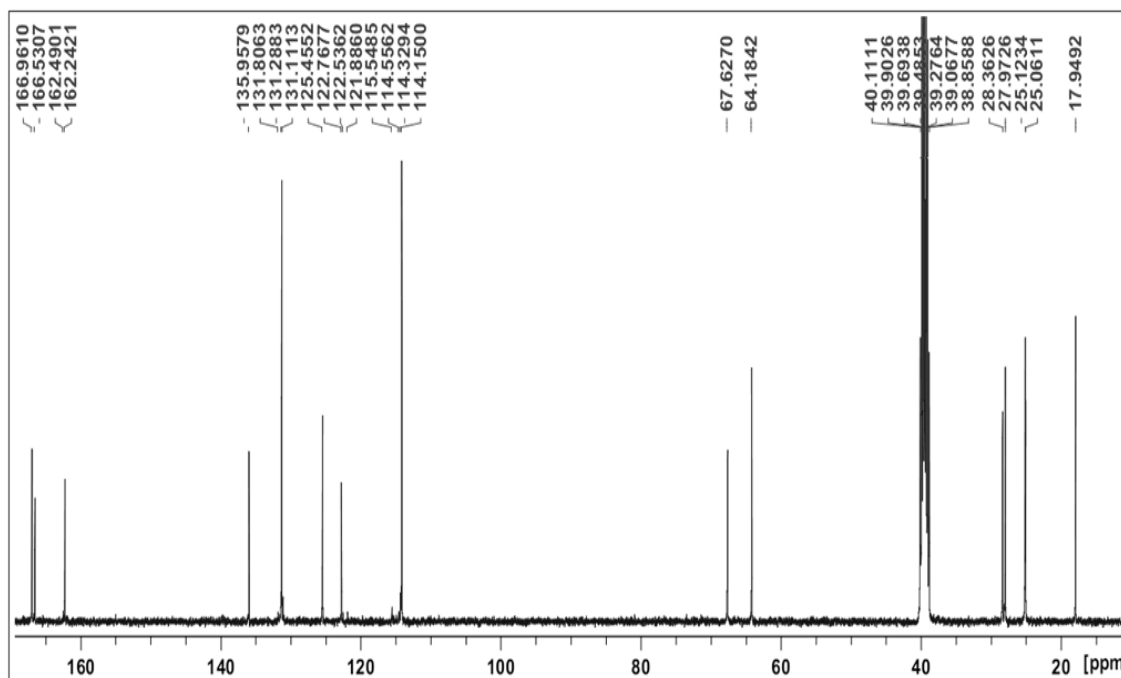


Figure B5: Compound 5

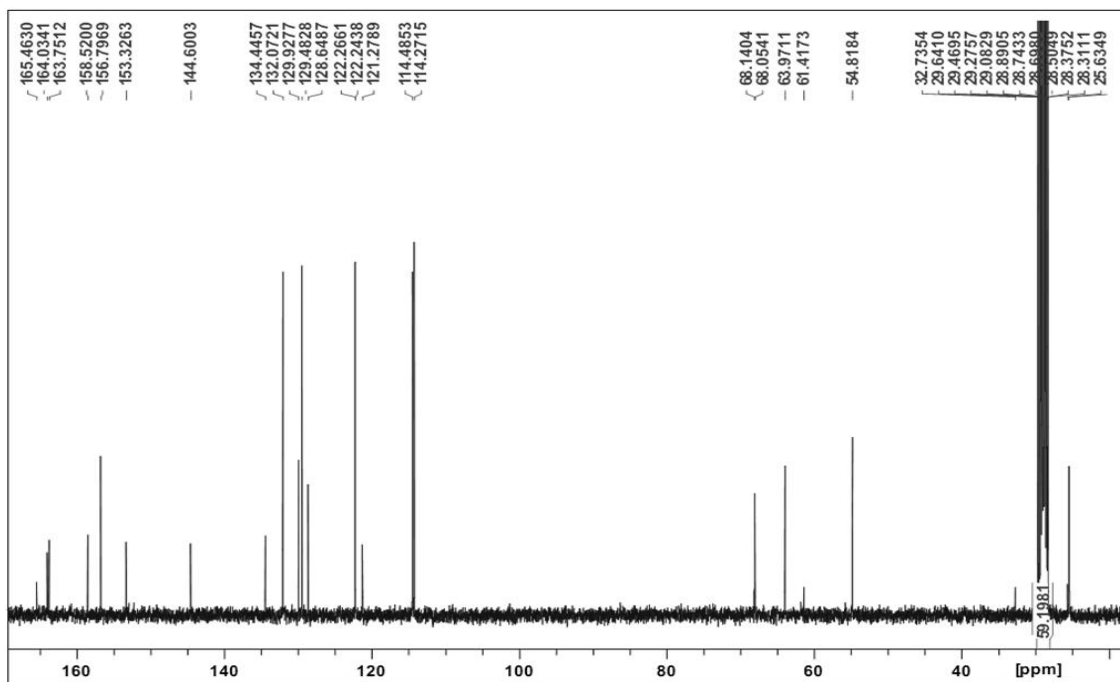


Figure B6: Monomer **M2**

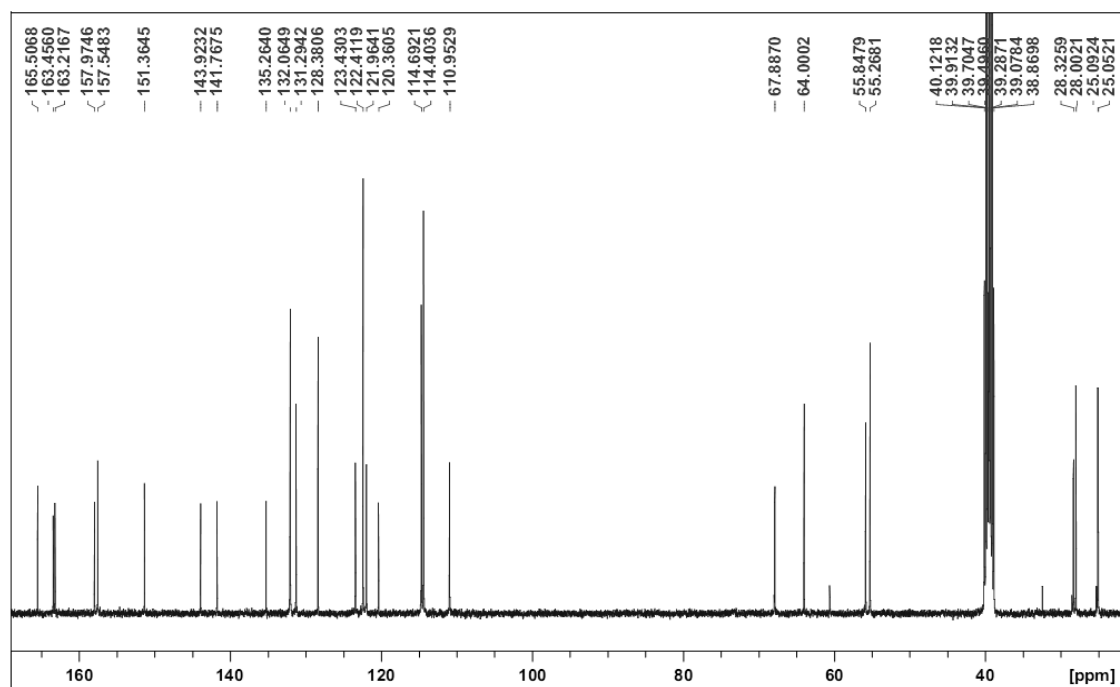


Figure B7: Monomer **M4**

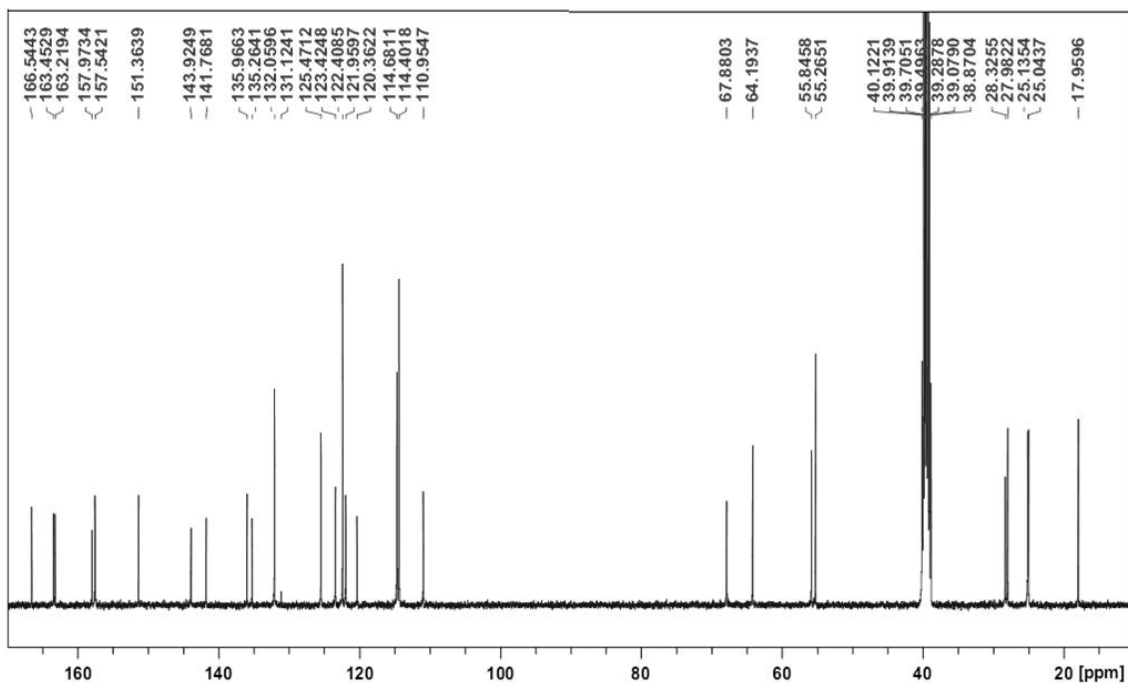


Figure B8: Monomer M5

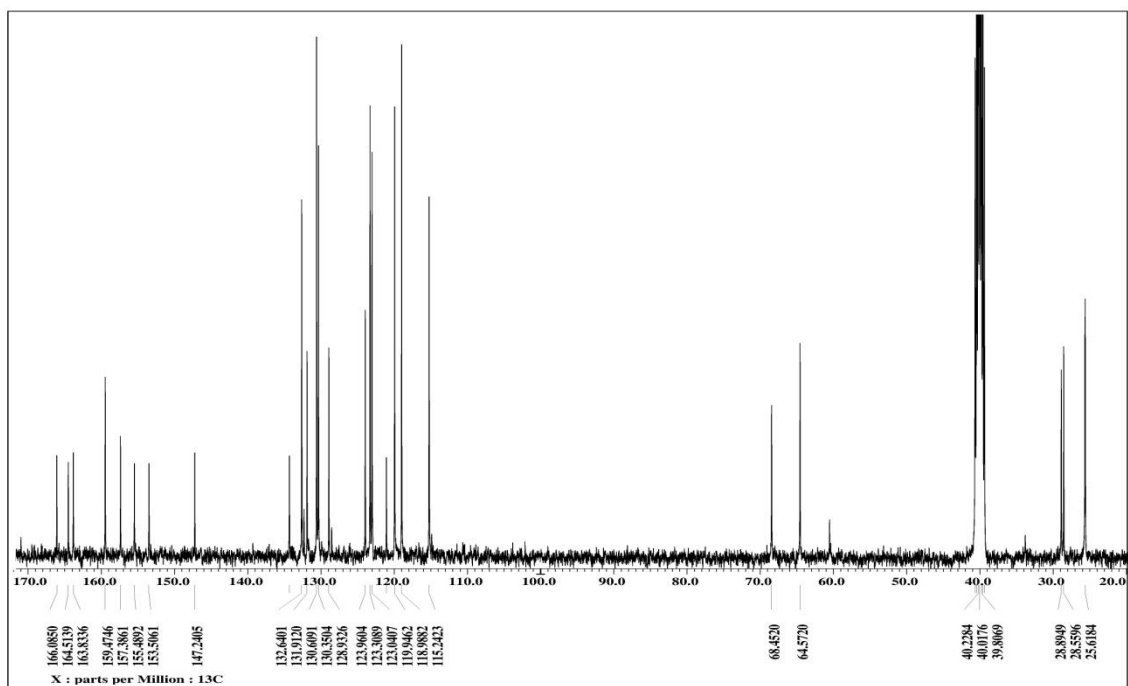


Figure B9: Monomer M6

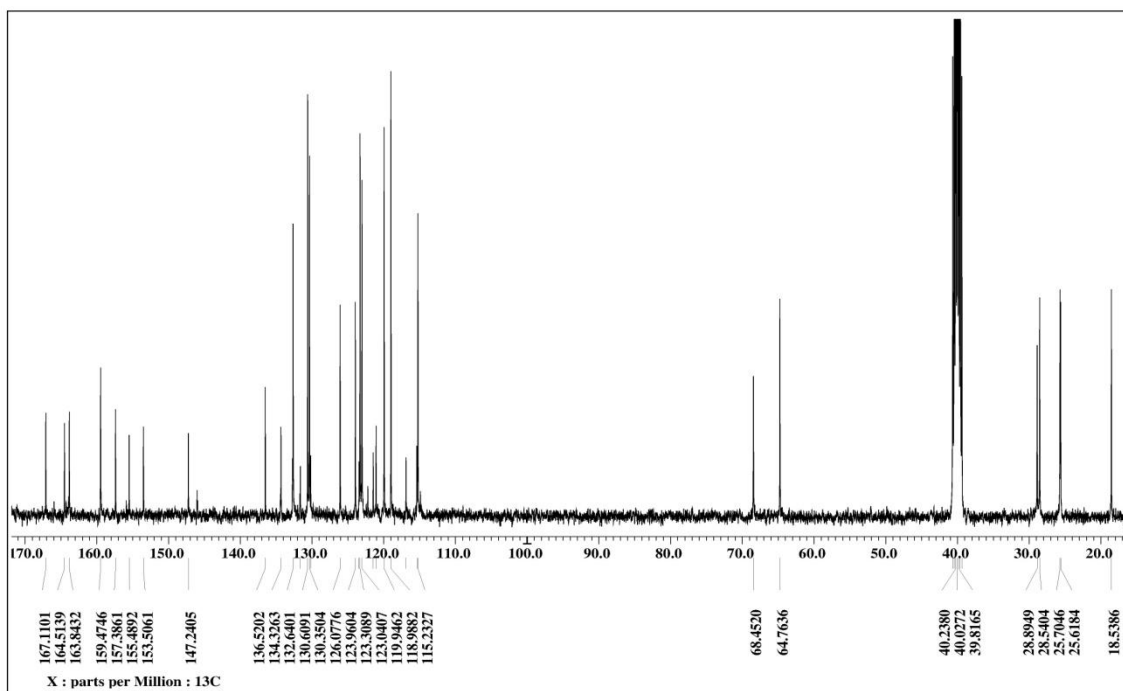


Figure B10: Monomer M7

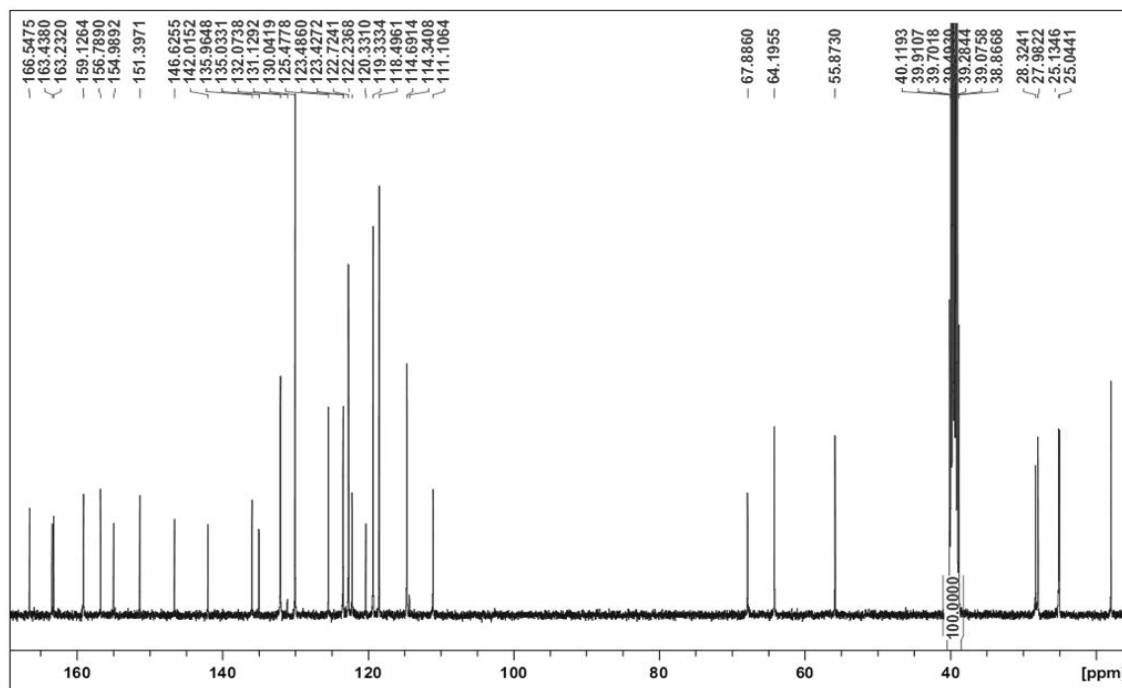


Figure B11: Monomer M8

APPENDIX C : DSC Figures

Figure C1 is a compilation of raw thermograms for the synthesized polymers.

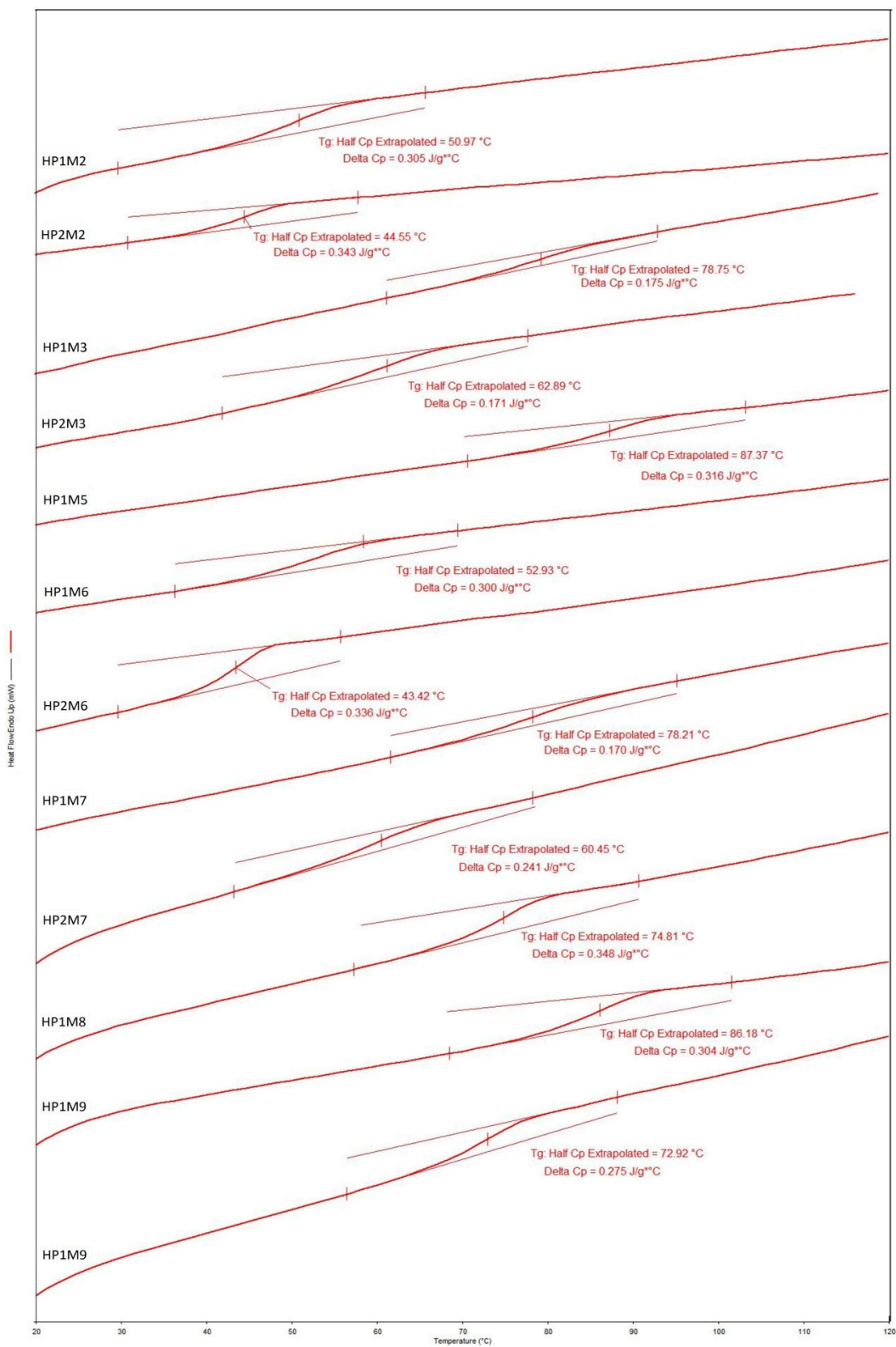


Figure C1

APPENDIX D : GPC Figures

Figure D1 is a typical example of the processed chromatogram output of the GPC software. The results of all the samples have been summarized in Table 4.4 of Chapter 4.

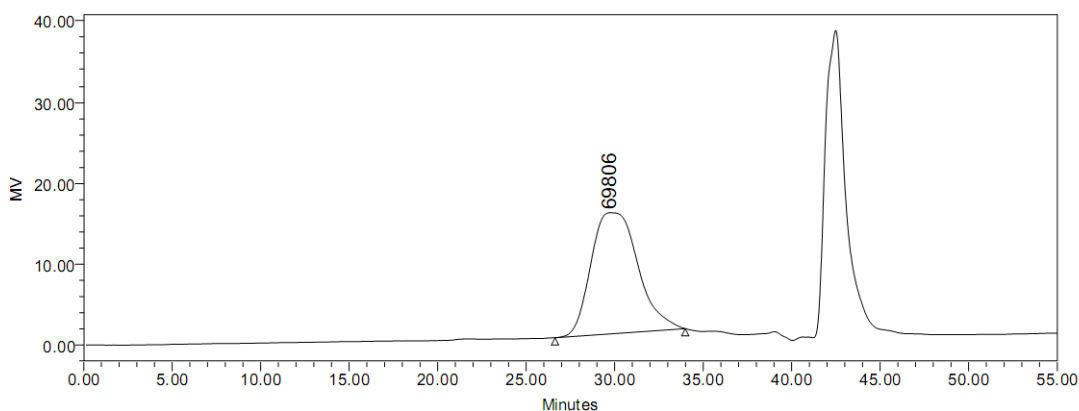


GPC Report

Reported by User: System

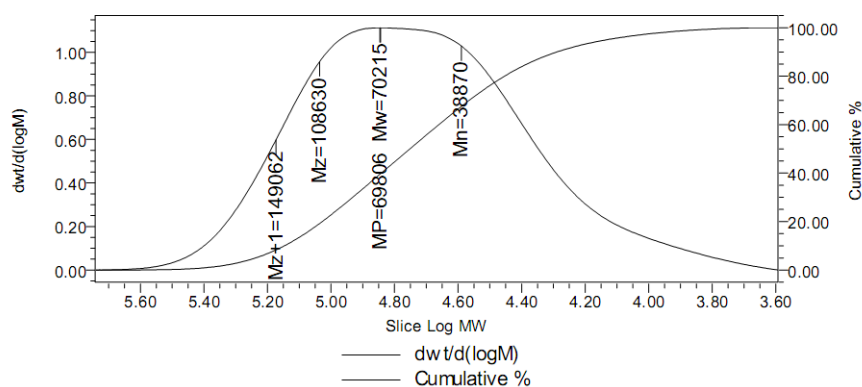
Project Name: UM_GPC1

| SAMPLE INFORMATION | | | |
|--------------------|---------------|---------------------|--------------------------|
| Sample Name: | HP1M3 | Acquired By: | System |
| Sample Type: | Broad Unknown | Date Acquired: | 1/21/2013 1:44:32 PM MYT |
| Vial: | 3 | Acq. Method Set: | GPC |
| Injection #: | 1 | Date Processed: | 1/22/2013 3:26:31 PM MYT |
| Injection Volume: | 100.00 ul | Processing Method: | GPC 2013_01_16_1st Order |
| Run Time: | 55.0 Minutes | Channel Name: | 410 |
| Sample Set Name: | dini21012013 | Proc. Chnl. Descr.: | |



GPC Results

| | Mn | Mw | MP | Mz | Mz+1 | Mv | Poly dispersity |
|---|-------|-------|-------|--------|--------|----|-----------------|
| 1 | 38870 | 70215 | 69806 | 108630 | 149062 | | 1.806408 |



Report Method: GPC Report

Printed 3:34:22 PM As 1/22/2013

Page: 1 of 1

Figure D1

APPENDIX E : TGA Figures

Figure E1 is typical example of the raw thermogram output of the TGA software.

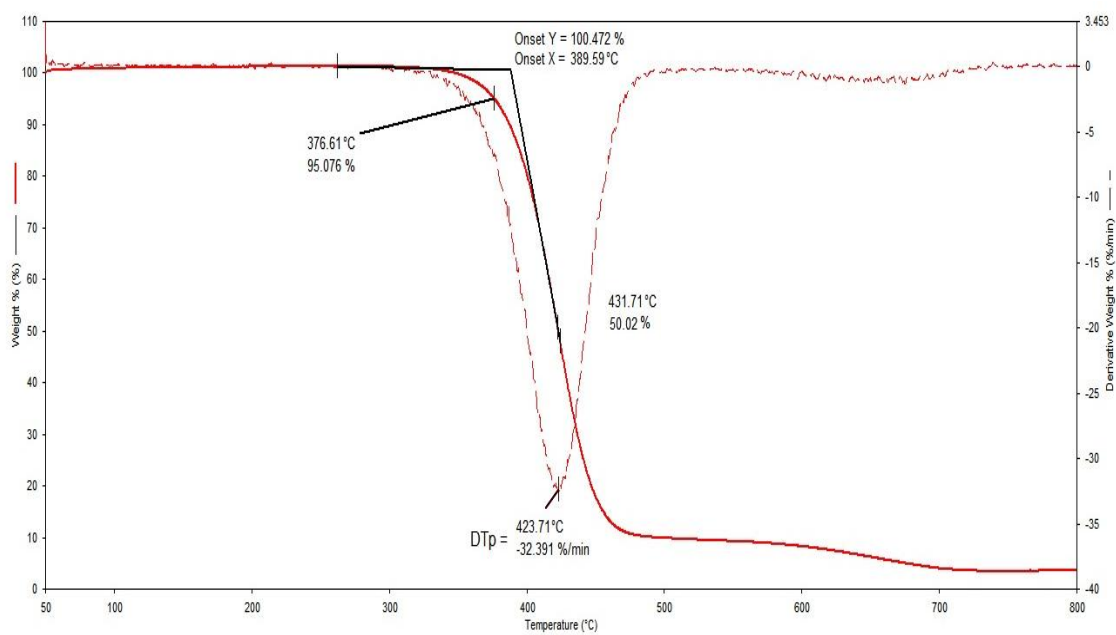


Figure E1

APPENDIX F : Research Output

Publications:

NM Salleh, MRK Sheikh, R. Yahya, MR Karim, Aziz Hassan, Naphthalene group containing side chain liquid crystalline polymers and their rheological behavior, Journal of Polymer Research (2013)20:131-140 (*ISI-Cited Publication*)

NM Salleh, MRK Sheikh, MR Karim, R Yahya, AD Azzahari, Aziz Hassan, Effect of the lateral substituent on the mesomorphic behavior of side chain liquid crystalline polymers containing a Schiff base ester, Journal of Polymer Research (2013)20:296 (*ISI-Cited Publication*)